

# The Mimetic Spectral Element Method

## A discretization of Geometry and Physics

DRAFT January 9, 2013

ter verkrijging van de graad van doctor  
aan de Technische Universiteit Delft,  
op gezag van de Rector Magnificus Prof. ir. K.C.A.M. Luyben,  
voorzitter van het College voor Promoties,  
in het openbaar te verdedigen  
op woensdag, 27 januari 2010 om 10.00 uur  
door

Jasper Jonas KREEFT

ingenieur luchtvaart- en ruimtevaart techniek  
geboren te Hoorn.

---

Dit proefschrift is goedgekeurd door de promotor:

Prof. dr. ir. drs. H. Bijl

Copromotor:

Dr. M.I. Gerritsma

Samenstelling promotiecommissie:

Rector Magnificus	voorzitter
Prof. dr. ir. drs. H. Bijl	Technische Universiteit Delft, promotor
Dr. M.I. Gerritsma	Technische Universiteit Delft, copromotor
Prof. dr. ir. B. Koren	Technische Universiteit Eindhoven
Prof. dr. ir. H. van Brummelen	Technische Universiteit Eindhoven
Prof. dr. J.J.W. van der Vegt	Universiteit Twente
Prof. dr. A. Bossavit	????
Dr. P. Bochev	Sandia National Laboratories
Prof. dr. R. Hiptmair	Eidgenössische Technische Hochschule Zürich
Prof. dr. J.B. Perot	University of Massachusetts Amherst
Prof. dr. B. de Pagter	Technische Universiteit Delft

Printed by [Proefschriftenmaken.nl](#), Oisterwijk, The Netherlands  
Copyright © 2012 by J.J. Kreeft

All rights reserved. No part of the material protected by this copyright notice may be reproduced or utilized in any form or by any means, electronic or mechanical, including photocopying, recording or by any information storage and retrieval system, without the prior permission of the author.

ISBN [978-90-8891-146-0](#)

Cover design by [Jasper Kreeft](#).  
Typeset with the L<sup>A</sup>T<sub>E</sub>X Documentation System.  
Author email: [j.j.kreeft@gmail.com](mailto:j.j.kreeft@gmail.com)

# Contents

<b>I</b>	<b>Introduction, motivation and philosophy</b>	<b>1</b>
<b>1</b>	<b>Introduction</b>	<b>3</b>
1.1	Motivation . . . . .	3
1.2	Topology and metric . . . . .	5
1.3	Introduction JCPsp2012 . . . . .	5
1.3.1	Reduction and reconstruction . . . . .	6
1.3.2	Geometry and orientation . . . . .	7
1.3.3	Mimetic framework . . . . .	9
1.4	Prior and related work . . . . .	11
1.5	Introduction MARC ECCOMAS . . . . .	14
1.6	Aim and Objective . . . . .	14
1.7	Thesis outline . . . . .	15
<b>2</b>	<b>Structures in fluid dynamics</b>	<b>19</b>
2.1	Notation . . . . .	20
2.2	Balance laws in unsteady incompressible Navier-Stokes . . . . .	20
2.3	Stokes problem and geometry . . . . .	24
2.4	Topology vs Metric . . . . .	27
2.5	Summary . . . . .	30
<b>3</b>	<b>Consistency, stability and convergence</b>	<b>31</b>
3.1	Introduction . . . . .	31
3.2	Abstract linear problem . . . . .	32
<b>II</b>	<b>Mimetic Framework for Elliptic Problems</b>	<b>37</b>
<b>4</b>	<b>Differential Geometry</b>	<b>39</b>
4.1	Manifolds . . . . .	40
4.2	Orientation . . . . .	44
4.3	Differential forms . . . . .	47
4.4	Differential forms under mappings . . . . .	49

---

4.5	Differential forms and orientation . . . . .	51
4.6	Exterior derivative . . . . .	53
4.7	Hodge star operator, inner product and Hilbert spaces . . . . .	56
4.8	Codifferential and Hodge-Laplacian . . . . .	60
4.9	Hodge decomposition . . . . .	61
<b>5</b>	<b>Algebraic Topology</b>	<b>69</b>
5.1	Finite dimensional topology . . . . .	70
5.1.1	Cell complex and boundary operator . . . . .	70
5.1.2	$k$ -Chains . . . . .	72
5.1.3	Topological Hodge decomposition . . . . .	76
5.1.4	Chain map . . . . .	78
5.2	Degrees of freedom . . . . .	79
5.2.1	Cochains and coboundary operator . . . . .	79
5.2.2	Cochain space decomposition . . . . .	82
5.2.3	Cochain map . . . . .	83
5.3	Dual complexes . . . . .	84
5.4	The boundary of cell complexes . . . . .	86
<b>6</b>	<b>Mimetic Operators</b>	<b>91</b>
6.1	Reduction, reconstruction and projection operator . . . . .	92
6.2	Discrete operators . . . . .	100
6.2.1	The wedge product . . . . .	100
6.2.2	The pullback . . . . .	101
6.2.3	The exterior derivative . . . . .	102
6.2.4	The discrete inner product . . . . .	103
6.2.5	The Hodge star operator . . . . .	104
6.2.6	The codifferential . . . . .	105
6.3	$L^2$ -bounded projection operator . . . . .	105
6.4	Discrete Hodge decomposition . . . . .	106
6.5	Discussion . . . . .	110
<b>7</b>	<b>Mimetic Spectral Elements</b>	<b>111</b>
7.1	Domain partitioning . . . . .	112
7.2	Reconstruction, mimetic basis functions and projections . . . . .	112
7.2.1	Projection $\pi_h$ using $D$ . . . . .	113
7.2.2	Bounded projections . . . . .	117
7.2.3	Tensor product interpolation functions . . . . .	120
7.2.4	Projection $\tilde{\pi}_h$ using $\tilde{D}$ . . . . .	121
7.2.5	The coprojections $\pi_h^*$ and $\tilde{\pi}_h^*$ . . . . .	122
7.3	Applications of discrete operators . . . . .	123
7.4	Mimetic B-splines . . . . .	129
7.5	Discussion . . . . .	134

---

<b>III Application of Mimetic Discretization</b>	<b>137</b>
<b>8 Hodge-Laplace problems</b>	<b>139</b>
8.1 Scalar Hodge-Laplace problems . . . . .	140
8.1.1 Staggered grid approach . . . . .	140
8.1.2 Single grid approach . . . . .	147
8.1.3 Numerical results scalar Poisson problem . . . . .	148
8.1.4 Darcy flows . . . . .	150
8.1.5 Numerical test cases Darcy flow . . . . .	152
8.1.6 Harmonic forms . . . . .	154
8.2 Abstract Hodge-Laplacian problem . . . . .	154
8.2.1 Abstract Hodge-Laplacian . . . . .	154
8.2.2 Mixed formulation . . . . .	155
8.2.3 Numerical stability . . . . .	158
8.2.4 Numerical test cases . . . . .	159
8.3 Eigenvalue problem . . . . .	163
8.3.1 Maxwell eigenvalue problem . . . . .	163
8.3.2 Numerical test cases . . . . .	166
8.3.3 Remarks on conditioning . . . . .	171
<b>9 Mixed Mimetic Spectral Element Method for Stokes problem</b>	<b>173</b>
9.1 Introduction . . . . .	173
9.2 Stokes problem in terms of differential forms . . . . .	175
9.2.1 Hodge decomposition of the VVP Stokes problem . . . . .	180
9.3 Mixed formulation . . . . .	181
9.3.1 Mixed formulation of the Stokes problem . . . . .	181
9.3.2 Well-posedness of mixed formulation . . . . .	182
9.3.3 Influence of boundary terms . . . . .	184
9.4 Issues on discretization and implementation . . . . .	185
9.4.1 Pointwise divergence-free discretization . . . . .	185
9.4.2 Implementation . . . . .	186
9.5 Numerical stability . . . . .	186
9.6 Numerical Results I . . . . .	187
9.6.1 Manufactured solution . . . . .	188
9.6.2 Lid-driven cavity Stokes . . . . .	190
9.6.3 Flow over a cylinder . . . . .	192
9.7 A priori error estimates for all admissible boundary conditions . . . . .	195
9.8 Numerical Results II . . . . .	199
9.9 Conclusions and future aspects . . . . .	201
9.10 Concluding remark . . . . .	201
<b>IV Towards full Navier-Stokes</b>	<b>205</b>
<b>10 Structure-Preserving Convection</b>	<b>207</b>
10.1 Notes Evans . . . . .	207
10.2 Introduction . . . . .	207

---

10.3	Convection in differential geometry . . . . .	208
10.3.1	Vector field . . . . .	208
10.3.2	Interior product . . . . .	209
10.3.3	Lie derivative . . . . .	210
10.3.4	Space-time notation . . . . .	212
10.4	Skew-symmetric formulation . . . . .	213
10.5	Incompressible Euler flow . . . . .	214
10.5.1	Adjoint operators . . . . .	214
10.5.2	Euler problem . . . . .	214
10.5.3	Advection of vorticity . . . . .	215
10.6	Discretization of Lie-derivative . . . . .	216
10.7	Numerical Results . . . . .	216
10.7.1	Testproblem 1 . . . . .	216
10.7.2	Testproblem 2 . . . . .	216
10.7.3	Incompressible Euler flow through advection of vorticity . . . . .	216
10.8	Conclusions and future aspects . . . . .	217
10.8.1	Curved meshes . . . . .	217
<b>11</b>	<b>Discretization of Covector-Valued Differential Forms</b>	<b>219</b>
11.1	Calculus on (co)vector-valued differential $k$ -forms . . . . .	219
11.1.1	Covariant derivative . . . . .	220
11.1.2	$L^2$ -inner product . . . . .	221
11.1.3	Cohomology (Hodge decomposition) . . . . .	221
11.1.4	Pullback . . . . .	221
11.1.5	Lie-derivative . . . . .	221
11.2	Inclusion and Trace . . . . .	221
11.2.1	Discretization . . . . .	222
11.3	Velocity . . . . .	223
11.4	Conclusion . . . . .	224
11.4.1	Velocity and momentum . . . . .	224
11.5	Mail Marc . . . . .	226
11.6	mathoverflow . . . . .	226
<b>V</b>	<b>Conclusions, Recommendations and Outlook</b>	<b>229</b>
<b>VI</b>	<b>Appendices</b>	<b>231</b>
<b>A</b>	<b>From vectors and covectors to differential forms</b>	<b>233</b>
A.1	FORMS AND VECTORS . . . . .	233
A.1.1	Tangent vectors and vector fields . . . . .	233
A.1.2	Covectors and 1-forms . . . . .	234

---

<b>B Polynomial Expansions</b>	<b>239</b>
B.1 Modal expansion . . . . .	239
B.2 Interpolatory polynomials . . . . .	242
B.3 Numerical integration . . . . .	245
<b>Bibliography</b>	<b>249</b>
<b>List of publications</b>	<b>263</b>
<b>Stellingen / Proposition</b>	<b>265</b>



## Part I

# Introduction, motivation and philosophy



# Chapter 1

## Introduction

*Waves follow our boat as we meander across the lake, and turbulent air currents follow our flight in a modern jet. Mathematicians and physicists believe that an explanation for and the prediction of both the breeze and the turbulence can be found through an understanding of solutions to the Navier-Stokes equations. Although these equations were written down in the 19<sup>th</sup> Century, our understanding of them remains minimal. The challenge is to make substantial progress toward a mathematical theory which will unlock the secrets hidden in the Navier-Stokes equations.*

The Navier-Stokes equations Millennium Prize Problem,  
Clay mathematics Institute, 2000.

### 1.1 Motivation

At the start of the 20<sup>th</sup> century, David Hilbert published the list of Hilbert's problems, [91], a list of unresolved mathematical problems. One of them is to expand the limited theoretical understanding of the motion of fluids described by the Navier-Stokes equations. Especially the riddle of turbulent flows gives rise to more questions than answers. After a century without satisfactory answer on the Navier-Stokes problem, at the start of the new millennium, the Clay Mathematics Institute stated the millennium prize problems, [102], a list of seven unresolved problems in mathematics, among which again the Navier-Stokes problem, as is cited above. The same problem was also stated in the list of Smale's problems, [166], which was published at the same time. Both lists of problems were inspired by Hilbert's list.

Although the Navier-Stokes equations were formulated in the 19<sup>th</sup> century, they still are not well understood. Since we encounter fluid flows in our daily live, a decent knowledge of fluid dynamics is desired. As long as we lack theoretical understanding of fluid flows, we try to find some answers using experimental and numerical techniques. In that sence, we try to increase our knowledge by simplification and approximation of the problem.

---

In computational fluid dynamics we try to solve the Navier-Stokes equations with a finite set of unknowns, the degrees of freedom, as approximation of the behaviour of the infinitely accurate solution. How to approximate is a topic of research that lasts already for almost a century, and broad a wide variety of different numerical methods, ranging from the continuum methods like the classical finite difference, finite volume and finite element methods to particle methods like smooth particle hydrodynamics and lattice Boltzmann methods.

In this thesis we present a *mimetic framework* and constitute from this framework the *mimetic spectral element method*. This method distinguishes from other mentioned continuum numerical methods in that it will have a strong emphasis on mimicking *both* physical and geometrical structures that appear in the full problem.

It is the authors belief that understanding not only the physical, but also the geometric structures, will give a significant avantage in the construction and understanding of physical and geometric compatible numerical schemes. Already in the 19th century Maxwell, [125], was wondering whether geometry could be the unifying concept which is responsible for the fact, despite the differences in physics, that all mathematical models are so similar:

*“But it is evident that all analogies of this kind depend on principles of a more fundamental nature; and that, if we had a true mathematical classification of quantities, we should be able at once to detect the analogy between any system of quantities presented to us and other systems of quantities in known sciences, so that we should lose no time in availing ourselves of the mathematical labours of those who had already solved problems essentially the same. [...] At the same time, I think that the progress of science, both in the way of discovery, and in the way of diffusion, would be greatly aided if more attention were paid in a direct way to the classification of quantities”.*

As Maxwell mentions, understanding the underlying structure which explains the analogies between physical systems is important for understanding the system and to teach analogous physical systems. Almost 100 years later Nobelprize winner Feynman, [68], remarks:

*“Why are the equations from different phenomena so similar?” We might say: “It is the underlying unity of nature.” But what does that mean? What could such a statement mean? It could mean simply that the equations are similar for different phenomena; but then, of course, we have given no explanation. The underlying unity might mean that everything is made out of the same stuff, and therefore obeys the same equations. That sounds like a good explanation, but let us think. The electrostatic potential, the diffusion of neutrons, heat flow - are we really dealing with the same stuff? Can we really imagine that the electrostatic potential is physically identical to the temperature, or to the density of particles? Certainly is not exactly the same as the thermal energy of particles. The displacement of a membrane is certainly not like a temperature. Why, then, is there “an underlying unity”? [...] Is it possible that this is the clue? That the thing which is common to all the phenomena is the space the framework into which the physics is put?*

---

So, also Feynman comes to the conclusion that space or geometry itself is responsible for the fact that vastly different physical phenomena are described by identical equations. It was Tonti in 1972, [174], who rigorously made the classification for a very large number of physical theories based on geometry. Tonti provided the ‘classification of quantities’ which Maxwell referred to.

Field models like fluid dynamics, electromagnetism, heat problems, etc. contain many physical and geometrical structures, expressed in the form of primary and secondary conservation or balance laws, symmetries, invariants, topological and symplectic structures. Unlike mathematical numerical issues like inaccuracy, inconsistency and instability, which are usually recognized straight away, the violation of these physical and geometrical structures not always causes direct failure of the numerical method. As a result, physically incorrect numerical solutions can potentially go unnoticed. Especially in complex physical systems, like turbulent or multiphase flows, fluid-structure interaction or magnetohydrodynamics, it becomes more and more difficult to check the physical correctness of the numerical solution. Therefore, in our mimetic framework, we try to incorporate as much as possible the physical and geometrical structures. This significantly differs from approaches based on minimization principles, where certain residuals are minimal, but all physical and geometrical structures might be lost. Despite of the differences in approach, we will show that the mimetic framework has a strong analogy with (staggered) finite volume and (mixed) finite element methods.

In the following sections we will motivate some basic considerations that formed the starting point of the development of the mimetic framework.

## 1.2 Topology and metric

In line with the distinction between geometry and physics is the distinction between topology and metric.

Mimetic methods aim to preserve essential physical/mathematical structures in a discrete setting. Many of such structures are *topological*, i.e. independent of metric. They involve connectivity relations from a geometric point of view, and integral relations from a physics point of view.

Pure topology relations make no distinction between Cartesian and curvilinear grids, but solely depends on the grid connectivity. This has many practical advantages. For example when dealing with moving grids in fluid-structure interaction simulations.

## 1.3 Introduction JCPsp2012

Mimetic methods aim to preserve essential physical/mathematical structures in a discrete setting. Many of such structures are *topological*, i.e. independent of metric, and involve *integral relations*. Since integration will play an important role and integration of differential forms is a metric-free operation, we will work with differential forms. Formally, differential forms are linear functionals on multi-vectors, but Flanders, [?, p.1], refers to them as ‘*things which occur under integral signs*’. Such would not be

the case if we were to use vectors, because integration of vector quantities is a metric operation. The same holds for vector operations; the grad, curl and div are metric-dependent operators, whereas the exterior derivative, which plays a similar role for differential forms, is metric-free. The important difference between vectors and forms will be explicitly addressed in this paper.

Commuting relations between the discretization (mimetic projection) and operations at the continuous and discrete level will play an important role in order to ensure that the ‘discrete system behaves just like the continuous system’.

Throughout this paper the basic idea will be highlighted by putting statements in a box and the main idea of this paper is:

A discrete representation of a physical system will display the same structure/dynamics when when discrete operators and the continuous operators commute with the projection of the infinite dimensional space onto the discrete space.

### 1.3.1 Reduction and reconstruction

The starting point of physics is the science of measurable, quantifiable objects and the relation among these objects. Any measurable quantity is associated with a spatial and a temporal geometric object. For instance, the measurement of velocity in air flow can be performed by particle image velocimetry (PIV), where tracer particles are released in the flow, two pictures are taken at consecutive time instants and the average velocity is calculated from the distance a particle has traveled divided by the time interval between the two snapshots. Velocity, measured in this way, is therefore associated with a curve in space (the trajectory of the particle between the two time instants) and a time interval (the time interval between the two snapshots). This association of velocity with a curve and a time interval does not depend on the particular way in which the measurement of velocity is performed. Strictly speaking, what we measure is not the average velocity, but the *integrated* velocity,

$$\int_{t^1}^{t^2} \vec{v} dt = \int_{t^1}^{t^2} \frac{d\vec{r}}{dt} dt = \vec{r}(t^2) - \vec{r}(t^1) .$$

This is an *exact* relation between the velocity in the time interval  $[t^1, t^2]$  and the position of the tracer particles at  $t^1$  and  $t^2$ , irrespective of the particular path traced out by the particle. So, if we could measure these two positions with infinite accuracy, we obtain the time integral of the velocity. The approximation enters into the measurement by *assuming* that the particle moves at a constant velocity in a straight line from  $\vec{r}(t^1)$  to  $\vec{r}(t^2)$ , which allows us to equate the velocity in the interval  $[t^1, t^2]$  to

$$\vec{v}(t) \approx \frac{1}{t^2 - t^1} \int_{t^1}^{t^2} \vec{v} dt = \frac{\vec{r}(t^2) - \vec{r}(t^1)}{t^2 - t^1} , \quad t \in [t^1, t^2] .$$

We can decompose this velocity measurement in two consecutive steps: 1.) A reduction step, where we sample the position of the tracer particles at discrete time instants. Although the reduction step is exact, we loose information, because we take a finite

---

number of samples from an infinitely large set. 2.) A reconstruction map, where we *assume* a certain behaviour of the particles between the consecutive time instants. In computational science, we often assume a piecewise polynomial behaviour.

These two steps, reduction and reconstruction, which implicitly play an important role in any measurement, will also turn out to be the two key ingredients in setting up mimetic discretizations.

So, the velocity obtained in the PIV experiment is only the time-averaged velocity. Only by assuming that the trajectory of the tracer particle is sufficiently smooth as a function of time, we can reduce the time interval such that we can quite accurately determine ‘the velocity’ at a given position and at a given time instant.

The same reasoning also holds in computational science. Whereas we want to know what the value of density and velocity is in a certain point at a certain moment in time, we only work with a finite dimensional mesh. This mesh consists of various kinds of geometric objects, i.e. points, lines, surfaces and volumes, on which we can associate integral values. This means that we consider mass The values in a certain point at a certain moment in time are only obtained through interpolation of the integral values by means of some assumed relation between the individual integral values.

### 1.3.2 Geometry and orientation

**Marc ECCOMAS:** The relation between physics and geometry is intriguing. Before the 20th century physics was assumed to ‘take place’ in space and time. In the 20th century space and time became physical variables themselves in special and general relativity.

Ultimately, in many physical theories, one takes the limit for all lengths and time intervals to zero, which enables physicists and engineers to talk about the velocity *in a point* at a *certain time instant*,  $\vec{v}(\mathbf{x}, t)$ . Any connection with a distance and a time interval is lost after this limiting process. Similarly, consider a mass contained in a volume,  $\mathcal{V}$ . The average density is the mass divided by the volume. By taking the limit for  $\mathcal{V} \rightarrow 0$  we obtain the density in a point,  $\rho(\mathbf{x}, t)$ . Again, the connection with the volume is lost after taking this limit. The same holds for physical models, like Navier-Stokes and Maxwell equations, that describe phenomena in terms of fields acting on (space-time) manifolds. These are usually derived as integral equations. Their corresponding PDEs are subsequently obtained by extracting geometry from the integral equations. These limiting processes are purely mathematical. Field quantities are mathematical abstractions that are intrinsically associated to geometric objects.

If we consider the PIV experiment again to measure the local velocity, we always need a finite time interval in order to evaluate the average velocity. In other words, in experimental techniques we do not measure fields, but rather obtain a set of integral values. If we would reduce the time interval to zero, no velocity measurement could be made. So despite the fact that we can accurately determine the velocity in a flow at a certain location and at a certain time, this measured velocity will always be connected to a time interval and the displacement along a curve. So all our measured quantities are associated to oriented geometric objects (points, lines, surfaces, volumes or hyper-volumes).

---

The association of physical variables with spatial and temporal geometric elements can be done for all physical variables. This is, however, beyond the scope of this thesis, but the interested reader is referred to the work of [27, 122, 174] and especially the forthcoming book by Tonti, [175].

Once we acknowledge that there is such an association between physical variables and geometric objects, we need to take orientation of the geometric object into account. Physical variables are associated to geometric objects and geometric objects have an orientation. Whereas the physical quantity is *independent of the orientation of the associated geometric object*, its integrated value does depend on the orientation. If we choose the direction of time to be positive when pointing in the past, the integral value of the velocity changes sign

$$+ \int_{t^2}^{t^1} \mathbf{v} dt = - \int_{t^1}^{t^2} \mathbf{v} dt .$$

Sommige variabelen veranderen van teken als de orientatie verandert, anderen niet. Dit is het verschil tussen real forms and pseudo forms. Volgens mij is dit wat wij aanduiden met inner- en outer-orientation. Voorbeelden: Massa (outer) en arbeid (inner) flux (outer). So integral values (the ones that are measurable) are intimately connected to the orientation of geometry, while average values – and in the limit densities – are insensitive to the orientation of space and time, because

$$\frac{1}{t^1 - t^2} \int_{t^2}^{t^1} \mathbf{v} dt = \frac{1}{t^2 - t^1} \int_{t^1}^{t^2} \mathbf{v} dt .$$

We distinguish between two types of orientation: *inner*- and *outer* orientation. With *inner* orientation, we mean the orientation *in* the geometric object such as for instance the electric current *in* a wire or the rotation *in* a plane, whereas *outer* refers to the orientation *outside* the geometric object such as the Biot-Savart law *around* the wire and or the flux *through* the plane. The inner and outer orientations can be seen as generalizations of the concept of tangential and normal in vector calculus, respectively.

It turns out that the association with oriented geometric objects is a vital ingredient in the description of physics and when we perform the limiting process to define all physical quantities in points and at time instants without reference to the associated geometric objects much of this rich structure of the physical model will be lost.

In a three dimensional space we distinguish between four types of submanifolds, that is, points, lines, surfaces and volumes, and two types of orientation, namely, outer- and inner-orientation. This geometric structure will form the backbone of the mimetic method to be discussed in this thesis. It will reappear throughout the thesis in various guises. Examples of outer- and inner-oriented submanifolds in  $\mathbb{R}^3$  are shown in Figure 1.1.

**JCPsp2012:** When integrals over  $k$ -dimensional geometric objects are considered, the orientation of these  $k$ -dimensional objects need to be taken into account. If we change the orientation of a point, curve, surface or volume, some integral values change sign, whereas others do not. For instance the work  $W_{AB}$  of a conservative force along a curve  $\gamma$  connecting the points  $A$  and  $B$  is equal to  $-W_{BA}$ , i.e. the work of the same force in the opposite direction along the curve. So the physical quantity

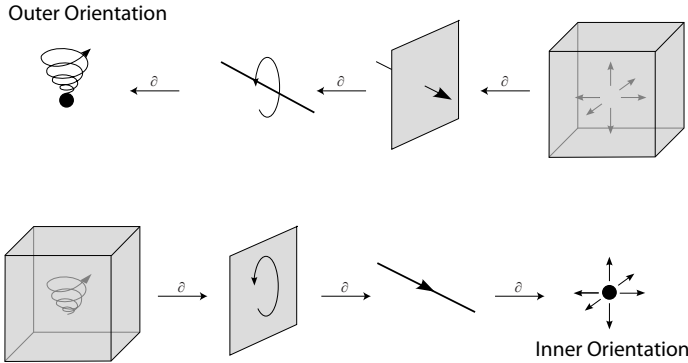


Figure 1.1: The four geometric objects possible in  $\mathbb{R}^3$ , point, line, surface and volume, with outer- (above) and inner- (below) orientation. The boundary operator,  $\partial$ , maps  $k$ -dimensional objects to  $(k - 1)$ -dimensional objects.

work changes sign when we change the orientation of the curve. Mass, on the other hand, which is the integral of mass density over a volume, does not change sign when we change the orientation.

Therefore, we need to consider two distinct types of differential forms: Those that do not change sign when orientation is reversed, the *true forms* and those that do change sign, the *pseudo-forms*. The operator which switches between forms and pseudo-forms is called the *Hodge- $\star$  operator*. This operator depends explicitly on the metric.

Integrals and integral relations can be represented without error in terms of duality pairing between chains and cochains. The distinction between integrals of true forms and pseudo-forms requires in principle two grids: One on which we represent the integral of a true form and the other grid on which we represent the integral of a pseudo-form. The formulation obtained by employing two dual grids resembles staggered finite volume methods.

An alternative way to implement the action of the Hodge- $\star$  operator is to make use of an inner product. In this approach only one grid is required. The formulation based on a single grid approach leads to a finite element method.

### 1.3.3 Mimetic framework

In the section above it has been revealed that geometry plays an important role in physics. In computational engineering one usually works with fields and densities, i.e. the variables obtained after the limiting process. The main reason fields have emerged as the preferred way of encoding physics is because physical laws can then be stated in terms of differential equations. This is nice when examining model characteristics, but of less use when considering experiments or numerics.

An alternative description is in terms of integral equations. The appeal of an integral approach lies in the fact that the physical laws can be stated without any limiting process involved, rendering them closer to the physical measurement process and more suited for a discrete treatment. Integration can be interpreted as duality

pairing between geometry and variables connected to this geometry.

In this thesis, therefore, we want to set up a framework in which we *mimic* the association of physical variables with oriented geometric objects for computational analysis. The aim is to develop families of numerical discretizations which work on general quadrilateral and hexahedral meshes of arbitrary order. By ‘families’ we mean that we first formulate the basic requirements a numerical discretization needs to possess in order to be *compatible* with its associated geometry. The most evident example, which plays a fundamental role throughout this thesis, is the relation between taking the boundary of an oriented geometric object and the discrete representations of the gradient, curl and divergence operators, by means of the Newton-Leibniz, Stokes’ circulation and Gauss divergence theorems, see also Figure 1.2,

$$\int_{\partial l} \phi = \int_l \text{grad } \phi \, dl, \quad \int_{\partial S} \vec{u} \cdot \vec{t} \, dl = \int_S \text{curl } \vec{u} \times \vec{n} \, dS, \quad \int_{\partial V} \vec{q} \cdot \vec{n} \, dS = \int_V \text{div } \vec{q} \, dV.$$

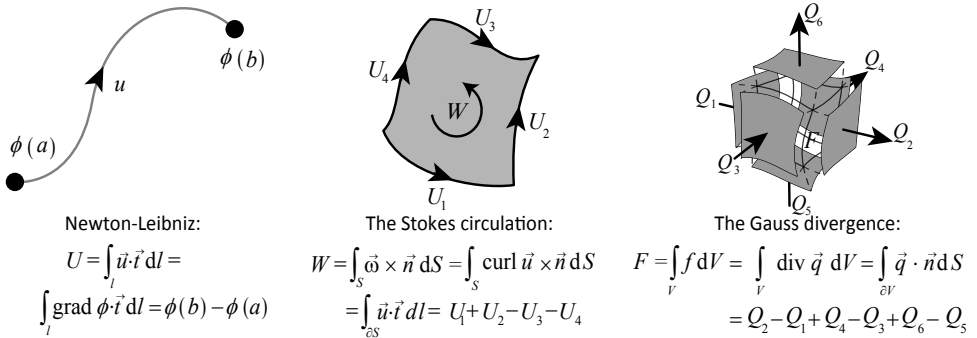


Figure 1.2: Illustrations of Newton-Leibniz, Stokes circulation and Gauss divergence theorems.

By creating a quadrilateral or hexahedral mesh, we divide the physical domain in a large number of these geometric objects, and to each geometric object we associate a discrete unknown. This implies that these discrete unknowns are *integral quantities*. Since the mentioned theorems are integral equations, obeying geometry and orientation will result in satisfying exactly the mentioned theorems, and consequently performing the vector operators exactly in a finite dimensional setting. For example taking a divergence in a volume is equivalent to taking the sum of the integral quantities associated to the surrounding surface elements, i.e. the fluxes. So using integral quantities as degrees of freedom to perform a vector operation like grad, curl or div, is equivalent to taking the sum of the degrees of freedom located at its boundary. As a result the continuous differential operators, grad, curl and div, are exactly mimicked at the discrete level. The action of the boundary operator is indicated by the horizontal connections between the geometric objects in Figure 1.1. They form a topological sequence or complex. This sequence is fundamental. It has a direct connection with the de Rham complex, chain complex and cochain complex, describing relations of the underlying PDEs, the computational mesh and the discretization of the PDEs.

The vertical connections – not shown in Figure 1.1 –, are strongly related to the discrete representation of the constitutive relations in physics. This is where metric

---

dependent parts are introduced. Constitutive relations are ‘man made’ extractions from physics acting on a much smaller scale. Since these relations are already approximations of material characteristics, this is where our numerical approximations come into play.

The mimetic structure that will be introduced in this thesis ensures that the reduced physical model behaves in the same way as the full infinite dimensional system as much as possible. Let  $A$  and  $B$  be two physical quantities and  $T$  a continuous operator which maps  $A$  onto  $B$ ,  $T(A) = B$ , then the following diagram should commute

$$\begin{array}{ccc} A & \xrightarrow{T} & B \\ \pi \downarrow & & \pi \downarrow \\ A_h & \xrightarrow{T} & B_h \end{array}$$

Here is  $\pi$  a suitably constructed projection operator, that consists of a reduction and reconstruction step, which maps continuous variables into finite dimensional representations. So  $\pi \circ T = T \circ \pi$ , i.e. we can perform the operation  $T$  at the continuous level and then discretize or first discretize and then apply the operator  $T$ . In that sense, operations at the discrete level truly mimic the behaviour of the operators at the continuous level. This implies, among others, and most importantly that incompressible Navier-Stokes and Stokes flow are guaranteed to be pointwise divergence-free, because the projection operator commutes with the divergence operator, see Chapter 9.

The grad, curl and div can be generalized into the exterior derivative from the language of differential geometry, which is the formal adjoint of the boundary operator through the three mentioned theorems. This allows one to uniquely decompose the space of variables (differential forms) into a direct sum of sub-spaces. This *Hodge decomposition* generalizes the classical Helmholtz decomposition for non-contractible domains. This is one of the fundamental structures that must be preserved both at the topological and discrete level.

The new framework requires a new set of reconstruction functions. In the finite element context also known as basis functions. We derive mimetic spectral element interpolation functions that are tensor product based interpolants. In every coordinate direction either a nodal or an edge interpolation function is used. By using tensor products, we are able to interpolate points, lines, surfaces, volumes, hyper-volumes and higher degree cubes. The mimetic spectral elements belong to the class of compatible finite elements. The development of the mimetic spectral elements can be seen as the closure of the mimetic framework.

## 1.4 Prior and related work

Over the years numerical analysts have developed numerical schemes which preserve some of the structure of the differential models they aim to approximate, so in that respect the whole mimetic idea is not new. A recent development is that the proper language in which to encode these structures/symmetries is the language of differential geometry. In contrast to vector calculus, it puts emphasis on the geometry on which physical variables are acting. It makes a clear distinction between purely

---

topological relations, which are completely metric-free and independent of a chosen coordinate system, and purely metric-dependent relations. The same distinction is recognized in physics. Whereas the relations that are obtained from physics, like conservation or balance laws, and symplectic structures like symmetries and invariants, are independent of metric and coordinate systems, the ‘man made’ constitutive relations are completely metric dependent. A novel aspect of mimetic discretizations is the identification of the metric-free part of the differential models, which can be conveniently described discretely in terms of algebraic topology, which is the discrete counterpart of the topology part of differential geometry.

Dissecting physical models into metric-free and metric dependent part was already proposed by Danzigt [?, ?] in case of Maxwell equations. The similarities between differential geometry and algebraic topology in physical theories were first described by Tonti, [174]. Around the same time Dodziuk, [58], set up a finite difference framework for harmonic functions based on Hodge theory. Both Tonti and Dodziuk introduce differential forms (continuous variables) and cochains (discrete variables) as the building blocks for their theory. Differential forms and cochains are fields that, when integrated over a corresponding oriented geometric object, returns the measured quantity. The relation between differential forms and cochains is established by the Whitney map ( $k$ -cochains  $\rightarrow$   $k$ -forms) and the De Rham map ( $k$ -forms  $\rightarrow$   $k$ -cochains). The interpolation of cochains to differential forms on a triangular grid was already established by Whitney, [185]. These interpolatory forms are now known as the *Whitney forms*, see also [153].

Hyman and Scovel, [99], initiated a discrete mimetic framework in terms of cochains, which are the natural building blocks of finite volume methods. Later Bochev and Hyman, [18], extended this work and derived mimetic discrete operators such as the discrete wedge product, the discrete codifferential, the discrete inner product, etc. These operators are all cochain operators. A major extension of the mimetic framework was provided by Kreeft, Palha and Gerritsma, [115], and resembles the second part of this thesis.

In a finite difference/volume context Robidoux, Hyman, Steinberg and Shashkov, [98, 100, 101, 155, 156, 164, 168, 169] used symmetry considerations to discretize diffusion problems on rough grids and with non-smooth non-isotropic diffusion coefficients. In a recent paper by Robidoux and Steinberg [158] a discrete vector calculus in a finite difference setting is presented. It satisfies the discrete differential operators grad, curl and div exactly and the numerical approximations are all contained in the constitutive relations, which are already polluted by modeling and experimental error. This paper also contains an extensive list of references to mimetic methods. For mimetic finite differences, see also Brezzi et al., [33, 34].

The two types of orientation, inner and outer, will result in a staggered grid configuration, one for the outer-oriented degrees of freedom, as in the top row of Figure 1.1, and one for the inner-oriented degrees of freedom, as in the bottom row of Figure 1.1. Staggered grids were first introduced by Harlow and Welch, [82] ook in de Yee-scheme, in their Marker and Cell scheme. This scheme provides a mass-, momentum- and energy-conserving discretization on Cartesian meshes. Extensions to higher-order and non-uniform meshes are found in the work of Wesseling [181, 182] and Verstappen and Veldman [179, 180]. The application of mimetic ideas to

---

unstructured staggered grids has been extensively studied by Perot, [142, 143, 145, 146, 172, 188]. Especially the recent paper, [144], lucidly describes the rationale of preserving symmetries in numerical algorithms.

The reduction of physical variables onto  $k$ -dimensional submanifolds results in discrete unknowns representing *integral quantities*. This is one of the major differences with related methods as the Harlow and Welch staggered grid method [82] and the lowest-order Raviart-Thomas and Nédélec compatible finite elements [133, 154], where use is made of averaged quantities.

Mattiussi, [121, 122, 124] puts the geometric ideas proposed by Tonti in an finite difference, finite volume and finite element context. The idea of switching between cochains and differential forms is also prominent in the work of Hiptmair, for instance [92]. This work also displays the close connection between finite volume methods and finite element methods.

Mimetic methods show a clear connection between the variables (differential forms) and the geometry in which these variables are defined. The most ‘geometric approach’ is described in the work by Desbrun et al., [55, 56, 61, 131, 141] and the thesis by Hirani, [95].

An excellent introduction and motivation for the use of [geometric structures and](#) differential forms in the description of physics and the use in numerical modeling can be found in the ‘Japanese papers’ by Bossavit, [26, 27]. The field of application is electromagnetism, but these papers are sufficiently general to extend all concepts to other fields of expertise.

A framework, closely related to the mentioned mimetic framework, is the finite element exterior calculus framework, described in two extensive papers by Arnold, Falk and Winther [6, 8]. Just like in this thesis, Arnold, Falk and Winther consider methods of arbitrary order, only then for simplices. Higher order methods are also described by Rapetti, [152, 153] and Hiptmair, [94].

We make use of spectral element interpolation functions as basis functions. In the past nodal spectral elements were mostly used in combination with Galerkin (GSEM), [13, 106], and least-squares formulations (LSSEM), [148, 149, 150]. The GSEM satisfies the Ladyshenskaya-Babuška-Brezzi (LBB) compatibility condition, that appears in mixed and constrained formulations, like in incompressible flow and elasticity problems, by lowering the polynomial degree of the pressure by two with respect to the velocity. This results in a method that is only weakly divergence-free, meaning that the divergence of the velocity field only converges to zero with mesh refinement. The LSSEM circumvents the LBB condition in order to be able to use equal order polynomials. The drawback of this method is the poor mass conservation property, [107, 151].

The present study uses mimetic spectral element interpolation or basis functions on curvilinear quadrilaterals and hexahedrals of arbitrary order as initially described in Gerritsma [73] and are described more extensively in [115] and in Part II of this thesis. Independently, for the one-dimensional case, these elements were derived by Robidoux, [157]. The mixed mimetic spectral element method (MMSEM), as described in Part III, satisfies the LBB condition and gives a pointwise divergence-free solution for all mesh sizes and for deformed meshes.

Although mimetic spectral elements are used here in combination with the mimetic

---

framework, alternative compatible/mimetic reconstruction functions could be used in combination with the mimetic framework without much change, e.g., compatible B-splines by Buffa et. al., [39, 40], which are extensively used in [65], and mimetic B-splines described in [10, 90].

Based on the Raviart-Thomas and Nédélec compatible finite elements, many  $H(\text{curl})$ - and  $H(\text{div})$ -conforming finite elements for quadrilaterals and hexahedrals have been derived, [4, 24, 36, 35]. However, these elements are unsuitable for curvilinear mappings and some types of boundary conditions (like no-slip) and suffer from high condition numbers in case of higher-order, due to their monomial construction.

Applications of mimetic spectral element methods can be found in this thesis as well as in [30, 76, 111, 113, 114, 139].

Although this thesis only considers space (space-time) discretizations, structure-preserving techniques are also found for time integrators when using the method of lines principle, see [131, 160] and the references therein.

Although the cited literature is far from complete, the above references serve as excellent introduction into the field of mimetic discretization techniques.

## 1.5 Introduction MARC ECCOMAS

The relation between physics and geometry is intriguing. Before the 20th century physics was assumed to ‘take place’ in space and time. In the 20th century space and time became physical variables themselves in special and general relativity.

Reading Tonti is a fascinating experience, because his work sheds a completely new light on how we perceive physical equations. The analogies between different physical theories become selfevident, because the underlying geometric structure is the same. Mattiussi, [13], wrote in 2000 a very clear paper based on Tonti’s work. Mattiussi relates he geometric concepts to numerical methods. Bossavit explains the whole geometric structure underlying the Maxwell equations in a series of papers, [1]. The above cited references, Tonti, Mattiussi and Bossavit, serve as an excellent introduction into the relation between physical models, partial differential equations, numerical methods and the underlying geometrical structure. Understanding the geometry associated with physical variables also has profound implications for numerical methods. If one faithfully respects the underlying geometrical structure, then some of the discrete relations become exact. This exactness is preserved under a large class of transformations, it is independent of the numerical method employed and independent of the basis functions. It is therefore a basic structure one wants to preserve in a numerical scheme. CONTINUE PAPER

## 1.6 Aim and Objective

The overall goal of this research is to develop a framework for mimetic discretization on quadrilaterals and hexahedrals of physics and geometry. With mimetic we mean that the discretization technique is based on (mimics) the structures that appear in physics and geometry. The method should:

- 
- obey the physical structures, expressed in terms of, for example, balance laws,
  - perform exact discretization of the most fundamental properties,
  - be applicable on Cartesian as well as curvilinear meshes. In other words, it should allow for all diffeomorphisms, i.e. affine as well as isoparametric/transfinite/isogeometric mappings,
  - hold for arbitrary order of approximation (not only lowest or high order),
  - be numerically stable without additional contributions, like penalty or stabilization terms,
  - optimally converging, for all sufficiently smooth meshes and all sufficiently smooth imposed data,
  - work on both structured and unstructured grids.

Note that to make this list complete we would like to have that the numerical problems can be solved efficiently. However, this is beyond the scope of this thesis.

In order to obtain these requirements, in Part II we aim at

1. developing a topological and discrete structure that mimics the structures found in differential geometry,
2. developing a set of mimetic operators that connects algebraic topology with differential geometry,
3. developing mimetic spectral element interpolation functions that satisfy the definitions of the mimetic operators.

Once we obtain the mimetic framework, we aim at

4. deriving and proving a physically sound, stable and converging variational formulation for the discretization of a wide variety of elliptic problems,
5. extending the mimetic framework with the Lie-derivative and covector-valued differential forms for the formulation and discretization of incompressible Navier-Stokes equations.

To proof that our numerical method satisfies the listed properties, not only proof by example, but also theoretical proofs are given.

## 1.7 Thesis outline

Nog niet af, mag je overslaan

### Part I

---

**Part II** Part II describes the mimetic framework for the discretization of elliptic problems. If we want to incorporate geometry into our physical description, differential geometry is a concise and potent way to do so. Therefore, in Chapter 4 a brief introduction into differential geometry will be presented. Although this material can be found in any book on differential geometry, [41, 69, 71], we include this chapter to introduce our notation and in the remainder of the thesis we want to highlight which properties from differential geometry are retained at the discrete level.

Despite the fact that physics requires metric concepts like length, angles and area, many structures in physics are completely independent of the metric. These non-metric concepts are called *topological*. In Chapter 5 elements from algebraic topology will be discussed which are required for the development of the mimetic spectral element framework. It will be shown that the structure of algebraic topology resembles the structure of differential geometry and therefore algebraic topology could serve as the discrete setting for our numerical framework.

In Chapter 6 the connection between algebraic topology and differential geometry will be established. Based on the existence of a suitable reduction map,  $\mathcal{R}$ , which maps  $k$ -forms onto  $k$ -cochains and a reconstruction map,  $\mathcal{I}$ , which converts  $k$ -cochains to  $k$ -forms, a general mimetic framework will be set up using the projection operator  $\pi_h = \mathcal{I} \circ \mathcal{R}$ , which maps the space of differential forms,  $\Lambda^k$ , to a finite dimensional space of differential forms,  $\Lambda_h^k$ . This chapter continues the work by Bochev and Hyman, [18], but the main difference is that in Chapter 6 the finite dimensional discrete space consists of differential forms while Bochev and Hyman take the cochains as their discrete variables.

In Chapter 7 the construction of compatible reconstruction maps, called mimetic spectral elements, are presented which satisfy the requirements described in Chapter 6. Their composition forms a bounded linear projection as proven in this chapter.

Although this outline suggests a collection of seemingly unrelated scientific fields, several ideas/concepts permeate throughout this thesis. Ultimately, all concepts contribute to mimetic, numerical concepts:

1. The exterior derivative  $\rightarrow$  coboundary operator  $\rightarrow$  discrete gradient, curl and divergence;
2. The Hodge decomposition  $\rightarrow$  cohomology group  $\rightarrow$  discrete Helmholtz decomposition;
3. The wedge product  $\rightarrow$  tensor products  $\rightarrow$  basis functions on quadrilateral elements;
4. The behaviour under mappings: the pullback operator  $\rightarrow$  the cochain map  $\rightarrow$  mimetic discretization on highly deformed meshes;
5. Inner- and outer orientation  $\rightarrow$  the double De Rham complex  $\rightarrow$  mimetic spectral element method on a staggered grid;
6. The generalized Stokes Theorem  $\rightarrow$  discrete generalized Stokes  $\rightarrow$  exact conservation and existence of scalar and vector potentials.

---

**Part III** In part III we apply the mimetic framework to some sample elliptic problems. In Chapter 8 we consider abstract Hodge Laplace problems, also called generalized Poisson problems. We start with the simplest sample problem, the scalar Poisson problem. This problems serves as an excellent toy problem to introduce staggered grid and single grid discretization using mimetic spectral elements. This chapter continues with the motivation and derivation of the mixed formulation for the generalized Poisson problem. This section is accompanied with some functional analysis statements. Special attention is for the resonant cavity or curl-curl eigenvalue problem as appears in electromagnetism, which is used to test the operator convergence. This chapter contains numerical examples showing the performance of the mimetic spectral element method and, in some cases, how it outperforms alternative compatible mixed finite elements.

Chapter 9, the second chapter in this part, is about the Stokes problem written in a vorticity-velocity-pressure formulation. It shows among others that the solution for velocity is pointwise divergence-free up to machine precision. Next, a priori error estimates are derived that hold for all admissible types of boundary conditions.

## Part IV

**Part V** In Chapter ?? we will review the tools developed in this thesis and look back to the introduction and see how this approach may enable us to faithfully simulate problems in physical sciences. Furthermore, potential future directions will be identified.

As a final remark, this thesis is accompanied with many illustrations and examples to illustrate and exemplify the topic of interest.

*In learning the sciences examples are of more use than precepts.*

Isaac Newton, *Arithmetica Universalis*, 1707.



# Chapter 2

## Structures in fluid dynamics

*Stability, consistency and convergence are the mathematical concepts that are typically used to analyze numerical methods for partial differential equations (PDEs). These important tools quantify how well the mathematics of a PDE is represented, but they fail to say anything about how well the physics of the system is represented by a particular numerical method. In practice, physical fidelity of a numerical solution can be just as important (perhaps even more important to a physicist) as these more mathematical concepts. A numerical solution that violates the underlying physics (destroying mass or kinetic energy, for example) is in many respects just as flawed as an unstable solution. Therefore, it is better to address the issue of physical fidelity at the numerical method design level. In fluid dynamics the physics of the system is often discussed in terms of conservation laws or balance laws. In this section we discuss the derivation of primary and secondary balance laws, and indicate what consequences this should have on the design of numerical methods.*

*Primary balance laws are usually satisfied either globally or locally in most numerical methods for computational fluid dynamics. Therefore, primary variables like mass and momentum are usually conserved. In contrast, secondary balance laws involve the balance of derived quantities, such as kinetic energy, vorticity, enstrophy, helicity and enstrophy, which are not directly variables of the PDE model. They are an indirect indication that a numerical method is well formulated to capture the physics of the system. Unlike primary balance laws, secondary balance laws cannot be directly imposed during the construction of the numerical method. Satisfying secondary balance laws can further improve physical fidelity and often enhance the accuracy of a numerical solution, but it is typically much harder to achieve.*

J. Blair Perot, *Annual Review of Fluid Mechanics*, 2011.

Our main interest in this thesis is to create discretization techniques that are capable of simulating fluid flows in a physically correct way. With physically correctness we mean to what extend the discretization is capable of obeying the invariants and symmetries of the fluid flow models, see [81], and, more importantly, to what extend they satisfy the various conservation or balance laws of a model.

---

In this section we make a break down, starting with the tensorial unsteady Navier-Stokes equations, followed by the vectorial Stokes equations, and ending up with the scalar heat problem. The section on Navier-Stokes focusses on the derivation of primary and secondary balance laws, while the section on Stokes flow puts emphasise on geometric considerations, and finally in the section on the heat equation we concentrate on the distinction between topology and metric.

## 2.1 Notation

In this chapter we consider equations from fluid dynamics of different rank. We distinguish scalar, vector and tensor equations, and so we make a distinction between vector and tensor operations:

- Vectors are indicated using a small arrow, for example the velocity field  $\vec{u}$ . Vector operators  $\cdot$ , grad, curl and div represent the dot product between two vectors, the gradient applied to a scalar and the curl and divergence operators applied to vectors. In two-dimensions we make a distinction between two types of rotations, i.e., curl applied to a scalar and rot applied to a vector.
- Bold symbols, like the stress tensor  $\boldsymbol{\sigma}$ , indicate rank two tensors. Tensor operators  $\otimes$ ,  $\cdot$ ,  $\nabla$  and  $\nabla \cdot$  represent the tensor product between two vectors, the component-wise product between two tensors, the gradient applied to a vector and the divergence applied to a tensor.

## 2.2 Balance laws in unsteady incompressible Navier-Stokes

The derivation of balance laws for Navier-Stokes is largely based on [65, 136, 144]. Consider the unsteady incompressible Navier-Stokes equations on a three-dimensional periodic domain  $\Omega = [-1, 1]^3$ , with coordinates  $\mathbf{x}$ . Then conservation of momentum  $\vec{m} = \rho\vec{u}$  is given by

$$\frac{\partial \vec{m}}{\partial t} + \nabla \cdot [(\vec{u} \otimes \vec{m}) - \boldsymbol{\sigma}] = \vec{f}, \quad \text{in } \Omega \times \mathbb{R}^+, \quad (2.2.1)$$

with initial condition  $\vec{m}(\mathbf{x}, t) = \vec{m}_0(\mathbf{x})$ . Above,  $\rho$  denotes the constant density of the fluid,  $\vec{u}$  the convective velocity vector of the flow,  $\boldsymbol{\sigma}$  the stress tensor acting on the fluid and  $\vec{f} = \text{grad } \phi$  a conservative body force with potential  $\phi$ . Conservation of mass in incompressible flow reduces to the a divergence-free constraint on the velocity field,

$$\text{div } \vec{u} = 0 \quad \text{in } \Omega \times \mathbb{R}^+. \quad (2.2.2)$$

The stress tensor consists of normal stresses due to pressure  $p$  and normal and shear stresses  $\boldsymbol{\tau}$  due to viscosity,

$$\boldsymbol{\sigma} = -pI + \boldsymbol{\tau}, \quad (2.2.3)$$

where  $I$  denotes the identity tensor. The system is closed by introducing a model relation for the viscous stress. The most common closure is that of a Newtonian fluid, so

$$\boldsymbol{\tau} = \mu \nabla \vec{u} \quad \text{or} \quad \boldsymbol{\tau} = \mu \nabla \left( \frac{1}{\rho} \vec{m} \right), \quad (2.2.4)$$

where  $\mu$  is the dynamic viscosity. Note that in incompressible flow the velocity gradient tensor is sometimes split into a rate of strain tensor and a rotation tensor,  $\nabla \vec{u} = \boldsymbol{\varepsilon} + \boldsymbol{\omega}$ , where  $\boldsymbol{\varepsilon} = \frac{1}{2}(\nabla \vec{u} + \nabla \vec{u}^T)$  and  $\boldsymbol{\omega} = \frac{1}{2}(\nabla \vec{u} - \nabla \vec{u}^T)$ . Because the skew-symmetric part is zero, i.e.  $\boldsymbol{\omega} = 0$ , (WHY??) the viscous stress can be also written as  $\boldsymbol{\tau} = 2\nu\boldsymbol{\varepsilon}$ .

Substitution of the described relations in (2.2.1) and (2.2.2) and divide by the constant density we obtain the more familiar expression for Newtonian incompressible Navier-Stokes flow:

$$\frac{\partial \vec{u}}{\partial t} + \nabla \cdot (\vec{u} \otimes \vec{u}) - \nabla \cdot (\nu \nabla \vec{u}) + \text{grad } \bar{p} = \vec{f} \quad \text{in } \Omega \times \mathbb{R}^+, \quad (2.2.5)$$

$$\text{div } \vec{u} = 0 \quad \text{in } \Omega \times \mathbb{R}^+, \quad (2.2.6)$$

$$\vec{u}(\mathbf{x}, t=0) = \vec{u}_0(\mathbf{x}) \quad \text{in } \Omega, \quad (2.2.7)$$

with  $\nu = \mu/\rho$  the kinematic viscosity and  $\bar{p} = p/\rho$ .

**Balance of mass** The balance laws we derive give global statements of the behavior of the incompressible Navier-Stokes model. Starting with a global balance of mass. Mass is automatically conserved because we consider incompressible flow, which results in an assumed constant mass density distribution.

**Balance of linear momentum** Next consider the global balance of linear momentum. Integrate (2.2.1) over  $\Omega$ . Since the domain  $\Omega$  inherits periodic boundary conditions and since  $\vec{f} = \nabla \cdot (\phi I)$  is conservative, by Gauss divergence theorem we obtain the expression for a *global balance of linear momentum*:

$$\frac{d}{dt} \int_{\Omega} \vec{m} d\Omega = 0. \quad (2.2.8)$$

**Balance of angular momentum** Angular momentum  $\vec{r} \times \vec{m}$ . HOE??

**Balance of kinetic energy** The expression for kinetic energy of the fluid is,  $k = \frac{1}{2} \vec{m} \cdot \vec{u} = \frac{1}{2} \rho |\vec{u}|^2$ . To obtain a balance for kinetic energy, multiply (2.2.1) by the velocity vector  $\vec{u}$  and integrate over  $\Omega$ . This gives,

$$\frac{d}{dt} \int_{\Omega} k d\Omega + \int_{\Omega} \vec{u} \cdot [\nabla \cdot (\vec{u} \otimes \vec{m})] d\Omega + \int_{\Omega} \vec{u} \cdot [-\nabla \cdot (\mu \nabla \vec{u})] d\Omega + \int_{\Omega} \vec{u} \cdot (\text{grad } p - \vec{f}) d\Omega = 0.$$

The second integral can be rewritten as

$$\int_{\Omega} \vec{u} \cdot [\nabla \cdot (\vec{u} \otimes \vec{m})] d\Omega = \int_{\Omega} (\text{div } (\vec{u}k) + k \text{div } \vec{u}) d\Omega,$$

which is zero by Gauss divergence theorem and the incompressibility constraint. For the third and fourth integral we apply integration by parts,

$$\int_{\Omega} \vec{u} \cdot \left[ -\nabla \cdot (\mu \nabla \vec{u}) + \vec{u} \cdot (\text{grad } p - \vec{f}) \right] d\Omega = \int_{\Omega} (\mu |\nabla \vec{u}|^2 - (p - \phi) \text{div } \vec{u}) d\Omega.$$

The last term vanishes due to the incompressibility constraint. Therefore the *global balance of kinetic energy* becomes:

$$\frac{d}{dt} \int_{\Omega} k d\Omega = - \int_{\Omega} \mu |\nabla \vec{u}|^2 d\Omega \leq 0. \quad (2.2.9)$$

Hence, the total amount of kinetic energy is dissipated in time. Note that the incompressibility constraint is applied twice in order to obtain (2.2.9). So to have a numerical scheme that satisfies both the balance of momentum and balance of kinetic energy, it must have a *pointwise divergence-free discretization* of the incompressibility constraint.

Numerical schemes that are energy conserving in the limit of zero viscosity are free of numerical dissipation. This is especially important in DNS and LES where a proper treatment of viscous effects result in a correct energy spectrum. In the limit of high-Reynolds number incompressible flow (turbulence), the dissipation term is extremely small and the kinetic energy is almost conserved. Artificial dissipation, if it exists, is a problem because it is likely to completely overwhelm the small physical dissipation. Kinetic energy conservation can usually be achieved by using a discrete approximation for the skew-symmetric form of the advection term (Feiereisen et al. 1981). For incompressible flow, where  $\text{div } \vec{m} = 0$ , the skew-symmetric form is given by  $\frac{1}{2} \nabla \cdot (\vec{u} \otimes \vec{m}) + \frac{1}{2} (\vec{u} \cdot \nabla) \vec{m}$ . This is identical to the conservative form  $\nabla(\vec{u} \otimes \vec{m})$  used in (2.2.1) and the advective form  $(\vec{u} \cdot \nabla) \vec{m}$ . Numerically these three variants are only the same once we obtain a pointwise divergence-free velocity field. Staggered mesh methods are interesting because they can conserve both momentum and kinetic energy. Proofs were provided in [118, 143, 188] for a variety of meshes.

**Balance of Vorticity** Instead of expressing the flow dynamics in terms of momentum or velocity and pressure, it can be written in terms of vorticity and velocity. Vorticity is defined as  $\vec{\omega} = \text{curl } \vec{u}$  and is a measure for the local angular rate of rotation of the flow field. The vorticity equation is obtained by applying the curl to the momentum equation (2.2.5). Since  $\text{curl grad } p$  is always zeros, the pressure drops out of the system. Moreover, since we assumed constant viscosity, we can write  $\text{curl}(-\nabla \cdot (\mu \nabla \vec{u})) = -\nabla \cdot (\mu \nabla \vec{\omega})$ . This results in the following expression for the vorticity equation,

$$\frac{\partial \vec{\omega}}{\partial t} + \nabla \cdot (\vec{u} \otimes \vec{\omega} - \vec{\omega} \otimes \vec{u}) = \nabla \cdot (\mu \nabla \vec{\omega}). \quad (2.2.10)$$

Note that the body force disappeared in the same way as the pressure. Similarly, since  $\text{div curl } \vec{u} = 0$  the vorticity-velocity system is closed with the following solenoidal constraint,

$$\text{div } \vec{\omega} = 0. \quad (2.2.11)$$

---

Then the *global balance of vorticity* is obtained by integrating (2.2.10) over the periodic domain  $\Omega$  and by applying Gauss divergence theorem,

$$\frac{d}{dt} \int_{\Omega} \vec{\omega} d\Omega = 0. \quad (2.2.12)$$

So the total amount of vorticity is conserved in time. Discretely, this is only obtained in case the identities  $\operatorname{curl} \operatorname{grad} = 0$  and  $\operatorname{div} \operatorname{curl} = 0$  are preserved in the discretization.

**Balance of Enstrophy** The enstrophy density of a fluid is denoted as  $\eta = \frac{1}{2}|\vec{\omega}|^2$ . Multiply (2.2.10) by  $\vec{\omega}$  and integrate over  $\Omega$ . This gives,

$$\frac{d}{dt} \int_{\Omega} \eta d\Omega = \int_{\Omega} \vec{\omega} \cdot \left( \nabla \cdot (\vec{\omega} \otimes \vec{u} - \vec{u} \otimes \vec{\omega}) + \nabla \cdot (\mu \nabla \vec{\omega}) \right) d\Omega.$$

Due to the incompressibility constraint and a solenoidal vorticity, the first term on the right hand side can be rewritten as the product of the rate of strain tensor and the vorticity vector,

$$\vec{\omega} \cdot \nabla \cdot (\vec{\omega} \otimes \vec{u}) = \vec{\omega}^T (\nabla \vec{u}) \vec{\omega} = \vec{\omega}^T \boldsymbol{\varepsilon} \vec{\omega}.$$

Note that  $\boldsymbol{\varepsilon} \vec{\omega}$  expresses the vortex stretching in a three-dimensional flow. The term  $\vec{\omega}^T \boldsymbol{\varepsilon} \vec{\omega}$  represents the enstrophy production and is related to vortex stretching. Since  $\operatorname{Tr} \boldsymbol{\varepsilon} = \operatorname{div} \vec{u} = 0$ , the eigenvalues of the strain-rate tensor can be both positive and negative, the total amount of enstrophy can both increase and decrease.

For the second term we again substitute the incompressibility constraint and apply the Gauss divergence theorem to get,

$$\int_{\Omega} \vec{\omega} \cdot (\nabla \cdot (\vec{u} \otimes \vec{\omega})) d\Omega = \int_{\Omega} \operatorname{div} (\vec{u} \eta) d\Omega = 0.$$

The integral of the product of vorticity with vorticity diffusion can be rewritten using integration by parts with vanishing boundary integral,

$$\int_{\Omega} \vec{\omega} \cdot \nabla \cdot (\mu \nabla \vec{\omega}) d\Omega = - \int_{\Omega} \mu |\nabla \vec{\omega}|^2 d\Omega \leq 0.$$

Then the *global balance of enstrophy* becomes,

$$\frac{d}{dt} \int_{\Omega} \eta d\Omega = - \int_{\Omega} \mu |\nabla \vec{\omega}|^2 d\Omega + \int_{\Omega} \vec{\omega}^T \boldsymbol{\varepsilon} \vec{\omega} d\Omega. \quad (2.2.13)$$

Vortex stretching is a three-dimensional phenomenon. Therefore, the second term does not appear in two-dimensional flow. So in two dimensions, enstrophy is conserved when considering inviscid flows (incompressible Euler) and is strictly decreasing in viscous flows. For three-dimensional flows the production of enstrophy can be positive. Therefore, the global amount of enstrophy could also increase despite of the dissipation term.

---

**Balance of Helicity** The last structure that is relevant to mention is helicity, [128]. Helicity density is defined as  $h = \vec{u} \cdot \vec{\omega}$ . Helicity describes the linkage and tanglement of vortex tubes in the flow. The balance of helicity is critical in the flow structure development and is the basis for the cascade of helicity (joint with energy) through the inertial range [44, 136].

To obtain a balance of helicity, multiply (2.2.5) by the vorticity vector  $\vec{\omega}$  and integrate over  $\Omega$ , and multiply (2.2.10) by the velocity vector  $\vec{u}$  and integrate over  $\Omega$ . Adding the two gives,

$$\begin{aligned} \frac{d}{dt} \int_{\Omega} h d\Omega &= \int_{\Omega} \left( \vec{\omega} \cdot \nabla \cdot (\vec{u} \otimes \vec{u}) + \vec{u} \cdot \nabla \cdot (\vec{u} \otimes \vec{\omega} - \vec{\omega} \otimes \vec{\omega}) \right) d\Omega \\ &\quad - \int_{\Omega} \left( \vec{\omega} \nabla \cdot (\mu \nabla \vec{u}) + \vec{u} \cdot \nabla \cdot (\mu \nabla \vec{\omega}) \right) d\Omega \\ &\quad + \int_{\Omega} \vec{\omega} \cdot (\operatorname{grad} p - \vec{f}) d\Omega. \end{aligned} \quad (2.2.14)$$

From integration by parts and periodic boundary conditions we obtain

$$\int_{\Omega} \vec{u} \cdot \nabla \cdot (\vec{u} \otimes \vec{\omega}) d\Omega = - \int_{\Omega} \vec{\omega} \cdot \nabla \cdot (\vec{u} \otimes \vec{u}) d\Omega.$$

Using the incompressibility constraint and Gauss divergence theorem we find that

$$\int_{\Omega} \vec{u} \cdot \nabla \cdot (\vec{\omega} \otimes \vec{u}) d\Omega = \int_{\Omega} \operatorname{div}(\vec{u} h) d\Omega = 0.$$

Applying integration by parts to the last two integrals of (2.2.14) and substitute the solenoidal constraint of vorticity, we find

$$\int_{\Omega} -\left( \vec{\omega} \nabla \cdot (\mu \nabla \vec{u}) + \vec{u} \cdot \nabla \cdot (\mu \nabla \vec{\omega}) \right) + \int_{\Omega} \vec{\omega} \cdot (\operatorname{grad} p - \vec{f}) d\Omega = - \int_{\Omega} 2\mu(\nabla \vec{u}) : (\nabla \vec{\omega}) d\Omega \leq 0.$$

So the *balance of global helicity* becomes

$$\frac{d}{dt} \int_{\Omega} h d\Omega = - \int_{\Omega} 2\mu(\nabla \vec{u}) : (\nabla \vec{\omega}) d\Omega. \quad (2.2.15)$$

Like global kinetic energy, global helicity is strictly decreasing and is conserved in absence of viscosity. From a numerical point of view, a proper balance of helicity can only be obtained once we numerically obtain a pointwise divergence-free velocity and vorticity solution and we satisfy the vector identities  $\operatorname{curl} \operatorname{grad} = 0$  and  $\operatorname{div} \operatorname{curl} = 0$ .

## 2.3 Stokes problem and geometry

Next we reduce the complexity of the flow model by neglecting the convective term. Then by assuming constant viscosity, we are allowed to rewrite the Stokes problem in terms of vector operations only. This allows us to emphasize on the relation between the Stokes problem, the vector operations and geometry.

---

Let  $\Omega \subset \mathbb{R}^n$ ,  $n = 2, 3$ , be a bounded  $n$ -dimensional domain with boundary  $\partial\Omega$ . On this domain we consider the Stokes problem, consisting of a momentum equation and the incompressibility constraint, resulting from the conservation of mass. The Stokes problem is given by

$$\nabla \cdot \boldsymbol{\sigma} = \vec{f} \quad \text{on } \Omega, \tag{2.3.1a}$$

$$\operatorname{div} \vec{u} = 0 \quad \text{on } \Omega, \tag{2.3.1b}$$

where the stress tensor  $\boldsymbol{\sigma}$  is given by

$$\boldsymbol{\sigma} = -pI + \nu \nabla \vec{u}, \tag{2.3.2}$$

with  $\vec{u}$  the velocity vector,  $p$  the pressure,  $\vec{f}$  the forcing term and  $\nu$  the kinematic viscosity. For the geometrical interpretations and consequences we like to present here and in Chapter 9, we restrict ourselves to vector operations only. Therefore, instead of considering the divergence of a stress tensor,  $\nabla \cdot (\nu \nabla \vec{u})$ , we write this as  $\nu \Delta \vec{u}$  by considering constant viscosity. Then the following vector identity is used for the vector Laplacian,  $-\Delta \vec{u} = \operatorname{curl} \operatorname{curl} \vec{u} - \operatorname{grad} \operatorname{div} \vec{u}$ . The *vorticity-velocity-pressure* (VVP) formulation is obtained by introducing vorticity as auxiliary variable,  $\vec{\omega} = \operatorname{curl} \vec{u}$ . In terms of vector operations only, the Stokes problem becomes

$$\vec{\omega} - \operatorname{curl} \vec{u} = 0 \quad \text{on } \Omega, \tag{2.3.3a}$$

$$\operatorname{curl} \vec{\omega} + \operatorname{grad} p = \vec{f} \quad \text{on } \Omega, \tag{2.3.3b}$$

$$\operatorname{div} \vec{u} = 0 \quad \text{on } \Omega. \tag{2.3.3c}$$

Since these PDEs should hold on a certain physical domain, we will include geometry by means of integration. In that case we can relate every physical quantity to a geometric object. Starting with the incompressibility constraint (2.3.3c) we have due to Gauss' divergence theorem,

$$\int_V \operatorname{div} \vec{u} dV = \int_{\partial V} \vec{u} \cdot \vec{n} dS = 0,$$

and by means of Stokes' circulation theorem the relation (2.3.3a) can be written as

$$\int_S \vec{\omega} \times \vec{n} dS = \int_S \operatorname{curl} \vec{u} \times \vec{n} dS = \int_{\partial S} \vec{u} \cdot \vec{t} dl.$$

From the first relation it follows that  $\operatorname{div} \vec{u}$  is associated to volumes. The association to a geometric object for velocity  $\vec{u}$  itself is less clear. In fact it can be associated to two different types of geometric objects. In the incompressibility constraint velocity denotes a flux *through* a surface that bounds a volume, while in the circulation relation velocity is defined *along* a line that bounds the surface. We will call the velocity vector *through* a surface *outer-oriented* and the velocity *along* a line segment *inner-oriented*. Similarly, vorticity has two different representations, either as the rotation *in* a plane as Stokes' circulation theorem above suggests, or the Biot-Savart description of rotation *around* a line. In the former case  $\vec{\omega}$  is *inner-oriented* whereas in the latter case  $\vec{\omega}$  is *outer-oriented*, see also Figure 1.1. In fact both the velocity vector  $\vec{u}$  and

the vorticity vector  $\vec{\omega}$  itself do not have a connection with geometry. Therefore, it are the terms  $\vec{u} \cdot \vec{t} dl$ ,  $\vec{u} \cdot \vec{n} dS$ ,  $\vec{\omega} \times \vec{n} dS$  and  $\vec{\omega} \times \vec{t} dl$  that are *more useful variables* when considering Stokes problem on a physical domain.

The last equation to be considered is (2.3.3b). This equation shows that classical Newton-Leibniz, Stokes circulation and Gauss divergence theorems tell only half the story. From the perspective of the classical Newton-Leibniz theorem, the gradient acting on the pressure relates line values to their corresponding end point, while the Stokes circulation theorem shows that the curl acting on the vorticity vector relates surface values to the line segment enclosing it. So how does this fit into one equation? In fact there exists two gradients, two curls and two divergence operators. One of each related to the mentioned theorems as explained above. The others are formal Hilbert adjoint operators, so the second gradient is the Hilbert adjoint of a divergence that is related to Gauss divergence theorem, the second curl is the Hilbert adjoint of the curl related to Stokes circulation theorem and the second divergence is the Hilbert adjoint of the gradient related to the classical Newton-Leibniz theorem. Let grad, curl and div be the original differential operators associated to the mentioned theorems, then the formal Hilbert adjoint operators  $\text{grad}^*$ ,  $\text{curl}^*$  and  $\text{div}^*$  are defined as,

$$(\vec{a}, -\text{grad}^* b) := (\text{div } \vec{a}, b), \quad (\vec{a}, \text{curl}^* \vec{b}) := (\text{curl } \vec{a}, \vec{b}), \quad (a, -\text{div}^* \vec{b}) := (\text{grad } a, \vec{b}). \quad (2.3.4)$$

The adjoint operators relate geometric operators in opposite direction. Where div relates a vector quantity associated to surfaces to a scalar quantity associated to a volume enclosed by these surfaces. Its adjoint operator,  $\text{grad}^*$ , relates a scalar quantity associated with a volume to a vector quantity associated with its surrounding surfaces. This is illustrated in Figure 2.1. Following Figure 2.1, the adjoint operators consist of three consecutive steps: First, switch to the other type of orientation (inner  $\rightarrow$  outer or outer  $\rightarrow$  inner), then take the derivative and finally switch the result back to its original orientation.

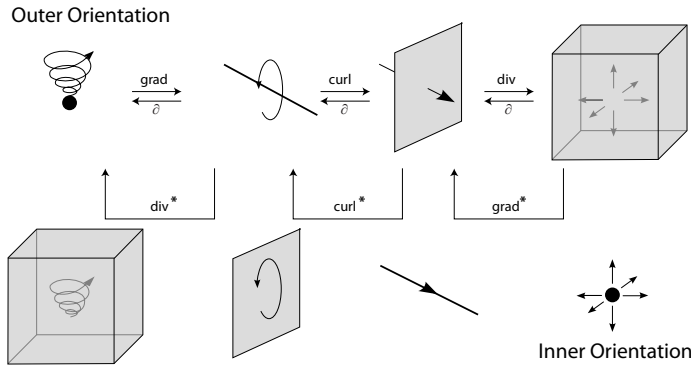


Figure 2.1: Geometric interpretation of the action of the boundary operators, vector differential operators and their formal Hilbert adjoint operators.

So (2.3.3b) could then either be associated to an inner-oriented line segment by rewriting it as

$$\text{curl}^* \vec{\omega} + \text{grad } p = \vec{f},$$

---

or be associated to an outer-oriented surface by rewriting it as

$$\operatorname{curl} \vec{\omega} + \operatorname{grad}^* p = \vec{f}.$$

Without geometric considerations we could never make a distinction between  $\operatorname{grad}$ ,  $\operatorname{curl}$  and  $\operatorname{div}$  and their associated Hilbert adjoints  $\operatorname{div}^*$ ,  $\operatorname{curl}^*$  and  $\operatorname{grad}^*$ . Vector calculus does not make this distinction.

Since in Chapter 9 the main focus is on obtaining a pointwise divergence-free result, use is made of a formulation associated to outer-oriented geometric objects. Then the Stokes problem becomes,

$$\vec{\omega} - \operatorname{curl}^* \vec{u} = 0, \tag{2.3.5a}$$

$$\operatorname{curl} \vec{\omega} + \operatorname{grad}^* p = \vec{f}, \tag{2.3.5b}$$

$$\operatorname{div} \vec{u} = 0, \tag{2.3.5c}$$

where the first equation is associated to line segments, the second to surfaces and the third to volumes. In [16, 17] the same velocity-vorticity-pressure formulation is given in terms of  $\operatorname{grad}$ ,  $\operatorname{curl}$ ,  $\operatorname{div}$  and  $\operatorname{grad}^*$ ,  $\operatorname{curl}^*$  and  $\operatorname{div}^*$ .

For a valid equation, the mathematical objects should be the same; we can only add vectors with vectors and scalars with scalars, but not scalars with vectors. But now we add that equations also need to be *geometrically compatible*. We can only add quantities associated with the same kind of geometry and with the same type of orientation. This lack of geometric notion in vector calculus is what motivates many to use the language of differential geometry instead, [6, 8, 10, 18, 26, 27, 40, 55, 71, 99, 111, 115, 174]. Other advantages of using differential geometry over vector calculus are that it possesses a clear distinction between variables associated with inner- and outer-orientation and it makes a clear distinction between topological and metric-dependent operations. All horizontal relations in Figure 2.1 are topological. Any detour along geometric objects with the other type of orientation introduces metric in the equation. In differential geometry these structures are intrinsically embedded. It naturally leads to a discretization technique that can be seen as a hybrid between the finite volumes (topological part) and finite elements (metric part).

## 2.4 Topology vs Metric

In this section we zoom in on the implications of a geometric and orientation compatible discretization, with emphasise on the distinction between the topological and metric dependent structure of PDEs and corresponding exact discretization and approximation. A simple, but relevant problem in many fields of physics is the Poisson equation. This could be a model for full potential flow, but here we consider the heat equation,

$$-\operatorname{div} (k \operatorname{grad} T) = f. \tag{2.4.1}$$

with temperature  $T$ , heat source  $f$  and thermal conductivity  $k$ . Tonti [174, 175] suggests to break up the PDE into three smaller relations,

$$\text{balance law :} \quad \operatorname{div} \vec{q} = f, \quad (2.4.2a)$$

$$\text{kinematic equation :} \quad \vec{u} = \operatorname{grad} T, \quad (2.4.2b)$$

$$\text{constitutive relation :} \quad \vec{q} = -k\vec{u}, \quad (2.4.2c)$$

where  $\vec{u}$  is the temperature gradient and  $\vec{q}$  the heat flux. The balance law and kinematic equation result purely from physical and mathematical considerations. In contrast, the constitutive relation, known as the Fourier's law, is a 'man made' approximation of the material characteristics. The three relations can be illustrated in a socalled 'Tonti diagram' as

$$\begin{array}{ccc} \vec{q} & \xrightarrow{\operatorname{div}} & f \\ -k \uparrow & & \\ \vec{u} & \xleftarrow[\operatorname{grad}]{} & T \end{array}$$

Similar diagrams for a wide variety of physics is found in [174]. The example of the heat equation to motivate a geometric compatible discretization, sometimes called 'discrete calculus methods', can also be found in [122, 123, 145, 146, 172].

In numerical methods, equations (2.4.2a)-(2.4.2c) need to be translated in a finite dimensional setting. This is done by means of reduction and reconstruction (integration and interpolation), similar to the PIV measurement in Section 1.3.1. Figure 2.2 shows examples of the location of the discrete unknowns. Observe that the balance law and kinematic equation are discretized on two different grids, that are topologically dual with respect to each other. Reducing (2.4.2a) and (2.4.2b) gives the following relations,

$$\begin{aligned} F_e &= \int_{V_e} f \, dV = \int_{V_e} \operatorname{div} \vec{q} \, dV = \int_{\partial V_e} \vec{q} \cdot \vec{n} \, dS \\ &= Q_{S_3} - Q_{S_1} + Q_{S_4} - Q_{S_2}, \end{aligned} \quad (2.4.3)$$

$$U_{l_1} = \int_{l_1} \operatorname{grad} T \cdot \vec{t} \, dl = \int_{\partial l_1} T = T_3 - T_2, \quad (2.4.4)$$

$$U_{l_2} = \int_{l_2} \operatorname{grad} T \cdot \vec{t} \, dl = \int_{\partial l_2} T = T_3 - T_1. \quad (2.4.5)$$

These relations show that the discrete representations of the vector operators  $\operatorname{grad}$  and  $\operatorname{div}$  reduce to topological relations between integral values (the discrete unknowns). The matrix representations of the gradient and divergence only contains -1, 0 and 1, referring to the connectivity at the topological level. Whereas the integral quantities in (2.4.3) are outer-oriented, the integral quantities in (2.4.4)-(2.4.5) are inner oriented. The meshes shown in Figure 2.2 are Cartesian, but with the same ease we could have chosen curvilinear meshes without affecting equations (2.4.3)-(2.4.5). Because the two meshes are each others topological dual, the discrete gradient and divergence matrices are each others transpose (or adjoint) matrix. A formal construction of

the topological structures in mimetic numerical methods are well described by the language of algebraic topology in Chapter 5.

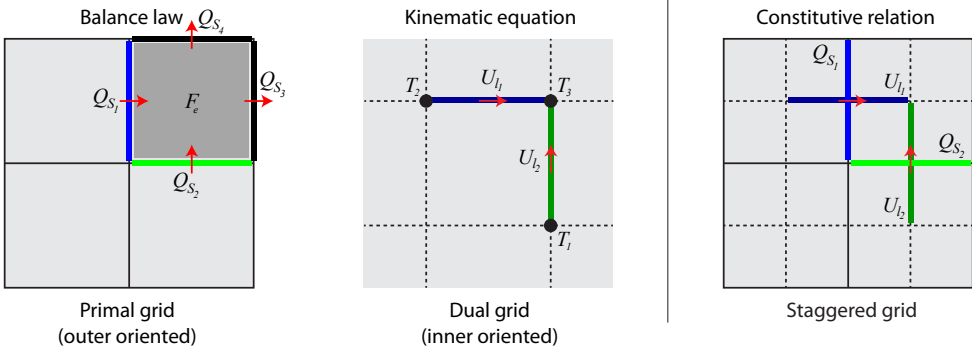


Figure 2.2: From left to right: the primal outer-oriented mesh with examples of discrete unknowns of heat flux and heat source corresponding to the discrete balance law; the dual inner-oriented mesh with examples of the discrete unknowns of the temperature and temperature gradient corresponding to the discrete kinematic equation; the staggered mesh indicating the discrete constitutive relation.

The right figure in Figure 2.2 shows the staggered mesh. Here a connection is made between the discrete heat fluxes on the primal grid (outer) and discrete temperature gradients on the dual grid (inner). Half a century ago Lilly [118] already noticed that staggered mesh methods also automatically satisfy secondary balance laws as well. Although the type of orientation and location of both unknowns  $U_{l_i}$  and  $Q_{S_i}$ , for  $i = 1, 2$ , differ, the direction of their orientation is the same. Since the constitutive relation is already an approximation of physics, it is therefore consistent to place also all the numerical approximation in the same place as the physical approximation. The precise nature of the approximation determines if the method has the flavor of a finite difference method, a finite volume method or a finite element method. As an example, we give the most straight forward, second-order approximation,

$$Q_{S_1} \approx -k \frac{\Delta y}{\Delta x} U_{l_1}, \quad Q_{S_2} \approx -k \frac{\Delta x}{\Delta y} U_{l_2}. \quad (2.4.6)$$

The matrix relating all line integral unknowns  $U_{l_i}$  with all surface integral unknowns  $Q_{S_i}$  is called a Hodge star matrix and is in this case a diagonal matrix. Relations like (2.4.6) depend on the metric characteristics of the meshes. In this thesis we extend this to higher-order and curvilinear meshes, resulting in a fuller matrix.

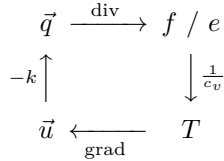
Returning for a moment to the experimental environment. Although we are interested in the temperature field, we cannot measure temperature in a point, but instead we measure the amount of heat in a small volume. The relation between temperature and amount of heat can be described up to subatomic level, but this is much too detailed for field models. Instead one uses averaged material properties relating the two, e.g.  $e = c_v T$ , where  $c_v$  is the heat capacity at constant volume. Relations containing material dependent approximations are known as *constitutive relations*.

---

The heat equation (2.4.1) can alternatively be written as

$$-\operatorname{div} \left( k \operatorname{grad} \left( \frac{1}{c_v} e \right) \right) = f. \quad (2.4.7)$$

The corresponding Tonti diagram becomes,



From a discrete point of view, the diagram starts and ends with variables associated with volumes (surface in 2D). Let  $E_e = \int_{\mathcal{V}_e} e \, dV$  be the amount of heat in a subvolume  $\mathcal{V}_e$  on the primal grid. From a discretization point of view, it is evident that temperature point  $T_3$  is its corresponding dual on the dual grid. Then the most straight forward metric relation approximating the relation between temperature and internal heat becomes,

$$T_3 \approx \frac{1}{c_v} \frac{1}{\Delta x \Delta y} E_e. \quad (2.4.8)$$

In single grid methods, like (mixed) finite elements, only variables of the primal grid are considered. In case of (2.4.7), these are  $\vec{q}$  and  $\vec{e}$ . The constitutive relations are then treated by the bilinear forms (weighted inner products) and the gradient is rewritten into a divergence using integration by parts. Similar as in the previous section. This is the approach that is taken in Part III.

Observe that although a single grid approach is taken, it still contains a staggered grid structure underneath, and therefore satisfies the secondary conservation laws, [118].

## 2.5 Summary

This section showed a number of structures that appear in physics and geometry, like primary and secondary balance laws, association with inner- and outer-oriented geometric objects and the distinction between topology and metric. A good mimetic method should obey all these structures also at the discrete level. Mathematical languages that are better capable in recognizing and treating these structures are differential geometry at the continuous level and algebraic topology at the discrete level. These will be discussed in the next part of this thesis.

# Chapter 3

## Consistency, stability and convergence

*There are certain classes of phenomena, as I have said, in which a small error in the data only introduces a small error in the result. Such are, among others, the larger phenomena of the Solar System, and those in which the more elementary laws in Dynamics contribute the greater part of the result. The course of events in these cases is stable.*

James C. Maxwell, 1873. *The Life of Maxwell*, 1882.

### 3.1 Introduction

Although the driving issues for the derivation of the mimetic discretization methods are geometrical and physical consistency, and not mathematical issues like mathematical consistency, stability and convergence, these issues can not be left unnoticed when developing a numerical method. The three mathematical issues are related through the celebrated *Lax equivalence theorem*, [117], that says that,

$$\text{consistency} + \text{stability} = \text{convergence}. \quad (3.1.1)$$

Let us write a linear PDE describing some physical problem and acting on certain manifold  $\mathcal{M}$  in its most general form,

$$Lu = f, \quad (3.1.2)$$

with  $u \in U$ , where  $U$  is an infinitely dimensional space. Discretizing the general problem gives

$$L_h u_h = f_h, \quad (3.1.3)$$

---

with  $u_h \in U_h$ . Here  $h$  denotes a small positive parameter, typically a reference meshsize. Then the dimension of the finite dimensional space  $U_h$  is proportional to  $h^{-1}$ .

Stability in this context means that the finite dimensional operator  $L_h$  is well-posed, that is, it has a bounded inverse with respect to some norm. In other words, the system matrix resulting from the discretization of the PDEs is invertible. In numerical schemes where a clear separation between topology and metric can be made, stability tells you that purely topological structures, like conservation and symmetries, are captured well, [14].

Consistency on the other hand tells us that the finite dimensional operator  $L_h$  approaches continuous operator  $L$  with grid refinement, again with respect to some norm. It refers to the approximation of the physical quantities, which is a metric dependent quality.

So only if both topological and metric relations are modeled well, we find a convergent method. Consistency and stability are automatically satisfied when considering compatible subspaces, i.e.  $U_h \subset U$  and  $L \circ \pi_h = \pi_h \circ L$ , for some linear operator  $L$  and conforming projection operator  $\pi_h : U \rightarrow U_h$ . As a consequence if  $f_h$  is close to  $f$  then also  $u_h$  is close to  $u$  and  $u_h$  convergence to  $u$  on grid refinement.

A more elaborate describtion of consistency, stability and convergence follows below.

## 3.2 Abstract linear problem

**Abstract variational problem** Consider again the abstract linear problem (3.1.2). There exists an abstract variational problem that is equivalent to this original problem. For that let  $U$  and  $V$  be Hilbert spaces<sup>1</sup>,  $V'$  the dual space of  $V$ , let  $B : U \times V \rightarrow \mathbb{R}$  be a bounded linear form and  $F : V \rightarrow \mathbb{R}$  a bounded linear form, i.e. there exists constants  $c_B, c_F > 0$  such that

$$\begin{aligned} |B(u, v)| &\leq c_B \|u\|_U \|v\|_V, & \forall u \in U, \forall v \in V, \\ |F(v)| &\leq c_F \|v\|_V, & \forall v \in V. \end{aligned}$$

The bilinear form is isomorphic to the operator  $L : U \rightarrow V'$  by duality pairing,  $\langle Lu, v \rangle = B(u, v)$ . The variational problem now reads: find  $u \in U$ , with given data  $f \in V'$ , such that

$$B(u, v) = F(v), \quad \forall v \in V. \tag{3.2.1}$$

The isomorphism between the operator  $L$  and the bilinear form  $B$  ensures that there exists a unique solution for every  $f \in V'$ . This well-posedness is formally formulated in the generalized Lax-Milgram Theorem<sup>2</sup> as follows.

**Theorem 1 (Well-posedness).** [9, 32, 63] Let  $B$  be defined as above. Then there

---

<sup>1</sup>The analysis also holds for Banach spaces, see [9, 63], but throughout the thesis we restrict ourselves to Hilbert spaces.

<sup>2</sup>Also called Banach-Nečas-Babuška Theorem in the more general Banach setting, [63].

---

exists a unique solution if and only if there exists a positive constant  $\beta$  such that<sup>3</sup>

$$\inf_{0 \neq u \in U} \sup_{0 \neq v \in V} \frac{B(u, v)}{\|u\|_U \|v\|_V} \geq \beta > 0, \quad (3.2.2a)$$

$$\sup_{u \in U} B(u, v) > 0, \quad \forall v \in V, v \neq 0. \quad (3.2.2b)$$

Condition (3.2.2a) is better known as the *inf-sup* condition and condition (3.2.2b) is the *dense range* condition. These are both necessary and sufficient for well-posedness. The constants  $c_B$  and  $\beta$  are called the continuity and inf-sup constants, respectively, and can be seen as the upper and lower bound of the bilinear form,

$$\beta \|u\|_U \|v\|_V \leq |B(u, v)| \leq c_B \|u\|_U \|v\|_V.$$

**Generalized Galerkin method** Next consider the *generalized Galerkin method*, where we introduce a finite dimensional trial space  $U_h$  and finite dimensional test space  $V_h$ , such that

$$\lim_{h \rightarrow 0} \inf_{w_h \in U_h} \|u - w_h\|_U = 0. \quad (3.2.3)$$

Similar *approximation property* should hold for the restricted space  $V_h$  with respect to the space  $V$ . Although not necessary, if possible we choose  $U_h$  and  $V_h$  to be conforming subspaces of  $U$  and  $V$ . Suppose there exists conforming projections  $\pi_h$  from the spaces  $U$  and  $V$  to their corresponding subspaces, which satisfies the approximation property,

$$\lim_{h \rightarrow 0} \|u - \pi_h u\|_U = 0 \quad \text{and} \quad \|u - \pi_h u\|_U \leq C \inf_{w_h \in U_h} \|u - w_h\|_U. \quad (3.2.4)$$

Then the finite dimensional variational problem reads, find  $u_h \in U_h$ , with given data  $f_h = \pi_h f \in V'_h$ , such that

$$B(u_h, v_h) = F(v_h), \quad \forall v_h \in V_h. \quad (3.2.5)$$

Remark that in (3.2.5) we assumed that the linear and bilinear forms are consistent, i.e.,  $B_h(u, v) \rightarrow B(u, v)$  and  $F_h(v) \rightarrow F(v)$  as  $h \rightarrow 0$ , and that the error in evaluating the linear and bilinear forms are neglectable with respect to the other errors made in the numerical scheme. The evaluation of the linear and bilinear forms are usually performed by Gauss or Gauss-Lobatto quadrature. These can even be made exact for polynomial evaluations.

Expression (3.2.5) is again equivalent to the following strong problem,

$$L_h u_h = f_h. \quad (3.2.6)$$

This discretization is consistent if  $L_h$  and  $f_h$  are sufficiently near  $L$  and  $f$ .

**A priori error estimate** Our next objective is to obtain an a priori error estimate of the approximation error  $u - u_h$ , by means of stability and consistency arguments. This will proof convergence as  $h \rightarrow 0$ . Since the approximate solution is sought in a

---

<sup>3</sup>From now on we ommit mentioning that 0 must be excluded when using infimums or supremums.

finite-dimensional space, we use the projection operator  $\pi_h$  to split the approximation error into an interpolation error and a discretization error,

$$\underbrace{u - u_h}_{\text{approximation error}} = \underbrace{u - \pi_h u}_{\text{interpolation error}} + \underbrace{\pi_h u - u_h}_{\text{discretization error}}. \quad (3.2.7)$$

From a suitable choice of  $\pi_h$ , it follows that the interpolation error decreases when the subspace  $U_h$  approaches  $U$ , as given in (3.2.4). In finite element methods, this is usually done by decreasing the meshsize  $h$  or by increasing polynomial order. The discretization error is directly related to the consistency error,  $L_h \pi_h u - f_h$ , by

$$\pi_h u - u_h = L_h^{-1} (L_h \pi_h u - f_h).$$

If the finite-dimensional problem is nonsingular, we find a stable solution, with as stability constant the norm of the discrete solution operator,  $\|L_h^{-1}\|_{\mathcal{L}(V'_h, U_h)}$ . Therefore, the norm of the discretization error is bounded by the product of the stability constant and the consistency error,

$$\|\pi_h u - u_h\|_U = \|L_h^{-1}\|_{\mathcal{L}(V'_h, U_h)} \|L_h \pi_h u - f_h\|_{V'}. \quad (3.2.8)$$

The stability constant is directly related to the well-posedness of the bilinear form as was given in Theorem 1. Then

$$\|L_h^{-1}\|_{\mathcal{L}(V'_h, U_h)}^{-1} := \inf_{u_h \in U_h} \sup_{v_h \in V_h} \frac{B(u_h, v_h)}{\|u_h\|_U \|v_h\|_V} = \beta_h > \beta > 0, \quad (3.2.9)$$

and we find that  $\|L_h^{-1}\|_{\mathcal{L}(V'_h, U_h)} = \beta_h^{-1}$ . So the discretization error (3.2.8) tends to zero for  $h \rightarrow 0$  if the consistency error tends to zero for  $h \rightarrow 0$  and the stability constant is uniformly bounded. From the discrete inf-sup relation, (3.2.9), the consistency error can be bounded in terms of the product of the continuity constant and the interpolation error,

$$\begin{aligned} \|L_h \pi_h u - f_h\|_{V'} &= \sup_{v_h \in V_h} \frac{B(\pi_h u, v_h) - F(v_h)}{\|v_h\|_V} \\ &= \sup_{v_h \in V_h} \frac{B(\pi_h u - u, v_h)}{\|v_h\|_V} \leq c_B \|u - \pi_h u\|_U. \end{aligned} \quad (3.2.10)$$

Combining this with the triangle inequality applied to (3.2.7) results in the a priori error estimate for a generalized Galerkin approximation, also known as Céa's Lemma on norm convergence.

**Theorem 2 (Convergence).** *Let  $u$  and  $u_h$  be the solutions of well-posed problems given in (3.2.1) and (3.2.5), respectively. Then the following a priori error estimate holds,*

$$\|u - u_h\|_U \leq \left(1 + \frac{c_B}{\beta_h}\right) \inf_{w_h \in U_h} \|u - w_h\|_U. \quad (3.2.11)$$

*Proof.* Combine (3.2.10) with (3.2.8) and substitute this in the triangle inequality obtained from (3.2.7). We find the following a priori error estimate as function of the interpolation error,

$$\|u - u_h\|_U \leq \left(1 + \frac{c_B}{\beta_h}\right) \|u - \pi_h u\|_U. \quad (3.2.12)$$

If we would do the same analysis, except that we substitute  $w_h \in U_h$  instead of  $\pi_h u$  in (3.2.7), and we take the infimum over all  $w_h$  in  $U_h$  we retrieve (3.2.11).  $\square$

Cea's Theorem shows that the error of the Galerkin approximation is proportional to the best approximation error, i.e. the Galerkin approximation is quasi-optimal<sup>4</sup>.

**Commuting diagram** What are the consequences if  $L$  commutes with  $\pi_h$ , i.e.  $\pi_h L = L_h \pi_h$ ?????

In section 1.3.3, the commuting diagram property of a linear operator with a projection operator was introduced. In this section we will highlight the consequences in an abstract setting.

Whereas the interpolation error can usually only be reduced by adding more degrees of freedom to the discrete problem, in terms of  $h$ - or  $p$ -refinement, the discretization error can be reduced by reducing the consistency error, which is obtained by choosing the proper discretization method for  $L_h$ . Ideally we would like to have the following commutation property,

$$\pi_h L = L_h \pi_h, \quad (3.2.13)$$

which is illustrated in the following commuting diagram,

$$\begin{array}{ccc} U & \xrightarrow{L} & V' \\ \pi_h \downarrow & & \pi_h \downarrow \\ U_h & \xrightarrow{L_h} & V'_h \end{array}$$

In this case the consistency error is zero,

$$L_h \pi_h u - f_h = L_h \pi_h u - \pi_h f = \pi_h (Lu - f) = 0,$$

and so the discretization error is zero. In that case the approximation error reduces to the interpolation error.

In practice, we do not work with the strong form (3.1.2), but with the variational statement (3.2.1). The left and right hand sides of (3.2.13) can be written as

$$L_h \pi_h u = \sup_{v_h \in V_h} \frac{B(\pi_h u, v_h)}{\|v_h\|_V}, \quad \pi_h L u = \sup_{v_h \in V_h} \frac{B(u, v_h)}{\|v_h\|_V}.$$

Substitution in (3.2.13) shows that the commuting diagram property results in, for  $u \in U$ ,

$$B(\pi_h u, v_h) = B(u, v_h), \quad \forall v_h \in V_h. \quad (3.2.14)$$

---

<sup>4</sup>Quasi-optimal, because it is a constant multiple of the error in the best possible approximation from the subspace

---

In practice, we do not work with the strong form (3.1.2), but with the variational statement (3.2.1). In order to reduce the consistency error, we would like to have that

$$B(\pi_h u, v_h) = B_h(u, v_h), \quad \forall v_h \in V_h. \quad (3.2.15)$$

In this case the discretization is zero in a weak sense, so

$$(\pi_h u - u_h, w_h)_K = 0, \quad \forall w_h \in U_h, \text{ for all finite elements } K.$$

In these cases where operators commute with the projection onto finite dimensional spaces we obtain that the approximation error reduces to the interpolation error, and so we obtain optimal convergence,

$$\|u - u_h\|_U \approx \|u - \pi_h u\|_U, \quad (3.2.16)$$

where we write  $\approx$  to count for possible numerical integration or quadrature errors. Therefore, the construction of commuting diagrams will play a substantial role throughout the next part.

The analysis on consistency, stability and convergence for linear operators, as is shown above, can be extended to non-linear operators, see [79, 178, 187]. However, this goes beyond the scope of this thesis.

## Part II

# Mimetic Framework for Elliptic Problems



# Chapter 4

## Differential Geometry

This chapter is based on Kreeft et al. [115].

*Let no one ignorant of geometry enter.*

Plato (ca 429-347 BC).

*The basic ideas at the foundations of point and continuum mechanics, electromagnetism, thermodynamics, special and general relativity, and gauge theories are geometrical, and, I believe, should be approached, by both mathematicians and physicists, from this point of view.*

Theodore Frankel, *The Geometry of Physics*.

*To those who do not know mathematics it is difficult to get a real feeling as to the beauty, the deepest beauty, of nature ... If you want to learn about nature, to appreciate nature, it is necessary to understand the language that she speaks in.*

Richard Feynman (1918-1988).

Differential geometry, along with algebraic topology as its discrete counterpart, to be presented in the next chapter, offer significant benefits in the construction of structure-preserving spatial discretizations. These mathematical languages provide a elegant description of geometry and orientation, that form the playground on which physics act. Differential geometry and algebraic topology describe the action of the physical quantities of interest on oriented geometric objects. This is what we know as integration, where the integral provides the oriented geometry and the term that lives under the integral provides the physical quantity, called a differential form.

These mathematical languages provide a clear distinction between purely topological and purely metric relations. Examples of actions that are purely topological are,

---

the boundary operator, which restricts to the boundary of a submanifold, the metric- and coordinate-free action of the exterior derivative that generalizes the gradient, curl and divergence operators from vector calculus and the generalized Stokes theorem that encapsulates their corresponding integration theorems, respectively. The coordinate-free action of the exterior derivative and generalized Stokes theorem give rise to commuting properties with respect to mappings between different manifolds. On the other hand, once we consider inner products and Hodge stars, metric will come into play. Only derived operators like the codifferential that represents the Hilbert adjoint operators  $\text{grad}^*$ ,  $\text{curl}^*$  and  $\text{div}^*$ , have both topological and metric structure. Acknowledging and respecting topological and metric structures are essential for the structure preserving behavior of the mimetic method.

In contrast to conventional vector calculus, which is a topic well known for most readers, differential geometry is a less familiar mathematical language for most readers. Therefore, we include a short introduction in order to make this work as much as possible self-contained and to be able to draw analogies between differential geometry, algebraic topology and the mimetic scheme we will present. Only those concepts from differential geometry which will play a role in the remainder of this thesis are introduced.

In Section 4.1 we start by introducing the concept of manifold, which is the playground in which everything is defined, the geometry. The concept of orientation of geometry is presented in Section 4.2. In Sections 4.3 to 4.8, differential forms, their definition, their transformation under mappings, the operators defined on them and appropriate function spaces are introduced subsequently. An important part of the structure is revealed with the introduction of the Hodge decomposition in Section 4.9. In Part III it will turn out to be an essential ingredient in the functional analysis of physical problems.

The material presented here constitutes the mathematical tools with which the physical quantities and the physical laws will be represented in the continuous world, and what will be mimicked in the numerical framework presented. For a more in depth treatment of differential geometry in physics, we refer to [2, 41, 69, 71, 103, 130, 162, 167].

## 4.1 Manifolds

The concepts which will be introduced all exist associated to sets endowed with enough structure so that one can “do calculus” and which are denoted by manifolds. In  $\mathbb{R}^3$  these are commonly referred to as points, lines, surfaces and volumes. Generalizing to any dimension a manifold can be defined in the following way.

**Definition 1 (Manifold).** [71, 137] *A  $k$ -dimensional manifold is a set  $\mathcal{M}$ , together with a countable collection of subsets  $\mathcal{U}_\alpha \subset \mathcal{M}$ , called coordinate charts, and one-to-one functions  $\varphi_{\mathcal{M},\alpha} : \mathcal{U}_\alpha \rightarrow V_\alpha$  onto connected open subsets  $V_\alpha$  of  $\mathbb{R}^k$ , called local coordinate maps, as in Figure 4.1, which satisfy the following properties:*

- (1) *The coordinate charts cover  $\mathcal{M}$ :*

$$\bigcup_\alpha \mathcal{U}_\alpha = \mathcal{M} .$$

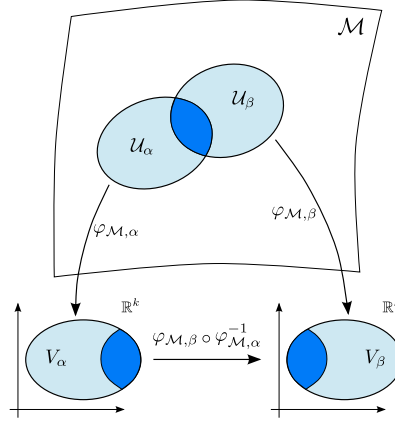


Figure 4.1: Coordinate charts on a manifold.

(2) On the overlap of any pair of coordinate charts  $\mathcal{U}_\alpha \cap \mathcal{U}_\beta$ , the composite map

$$\varphi_{\mathcal{M},\beta} \circ \varphi_{\mathcal{M},\alpha}^{-1} : \varphi_{\mathcal{M},\alpha}(\mathcal{U}_\alpha \cap \mathcal{U}_\beta) \rightarrow \varphi_{\mathcal{M},\beta}(\mathcal{U}_\alpha \cap \mathcal{U}_\beta),$$

is a smooth (infinitely differentiable) function.

(3) If  $\xi \in \mathcal{U}_\alpha$  and  $x \in \mathcal{U}_\beta$  are distinct points in  $\mathcal{M}$ , then there exist open subsets  $W_\alpha$  of  $\varphi_{\mathcal{M},\alpha}(\xi)$  in  $V_\alpha$  and  $W_\beta$  of  $\varphi_{\mathcal{M},\beta}(x)$  in  $V_\beta$  such that

$$\varphi_{\mathcal{M},\alpha}^{-1}(W_\alpha) \cap \varphi_{\mathcal{M},\beta}^{-1}(W_\beta) = \emptyset.$$

Since the image of each point  $p \in (\mathcal{U}_\alpha \cap \mathcal{M})$  by  $\varphi_{\mathcal{M},\alpha}$  is a point in  $\mathbb{R}^k$ , it can be written as a  $k$ -tuple of real numbers:  $\varphi_{\mathcal{M},\alpha}(p) = (\xi^1(p), \dots, \xi^n(p))$ . This  $k$ -tuple is called the local coordinates of  $p$  and  $\mathcal{U}_\alpha \cap \mathcal{M}$  the coordinate neighborhood. The pair  $(\mathcal{U}_\alpha, \varphi_{\mathcal{M},\alpha})$  is called a *local chart* or *local coordinate system*. An *atlas* on a manifold  $\mathcal{M}$  is a collection  $\mathcal{A} = \{(\mathcal{U}_\alpha, \varphi_{\mathcal{M},\alpha})\}$  of charts of  $\mathcal{M}$ , such that  $\bigcup_\alpha \mathcal{U}_\alpha = \mathcal{M}$ ; the collection of open sets  $\{\mathcal{U}_\alpha\}$  constitutes an open covering of the manifold  $\mathcal{M}$ .

**Definition 2 (Maps between manifolds).** Let  $\mathcal{M}$  be a  $k$ -dimensional smooth manifold and  $\mathcal{N}$  an  $l$ -dimensional smooth manifold. The map  $\Phi : \mathcal{M} \rightarrow \mathcal{N}$  maps between manifolds, if for every coordinate chart  $\varphi_{\mathcal{M},\alpha} : \mathcal{U}_\alpha \rightarrow V_\alpha \subset \mathbb{R}^k$  on  $\mathcal{M}$  and every chart  $\varphi_{\mathcal{N},\beta} : \mathcal{U}_\beta \rightarrow V_\beta \subset \mathbb{R}^l$  on  $\mathcal{N}$ , the composite map

$$\varphi_{\mathcal{N},\beta} \circ \Phi \circ \varphi_{\mathcal{M},\alpha}^{-1} : \mathbb{R}^k \rightarrow \mathbb{R}^l,$$

is a smooth map wherever it is defined. See Figure 4.2 for a pictorial representation of the mapping between manifolds.

The map  $\varphi_{\mathcal{N},\beta} \circ \Phi \circ \varphi_{\mathcal{M},\alpha}^{-1}$  is better known as a change of coordinates. Then there are local coordinates  $\xi = (\xi^1, \dots, \xi^l)$  near  $p$  and  $\mathbf{x} = (x^1, \dots, x^k)$  near  $q = \Phi(p) \in \mathcal{N}$  such that these coordinates have the simple form  $x^j = x^j(\xi)$ , for  $j = 1, \dots, l$ .

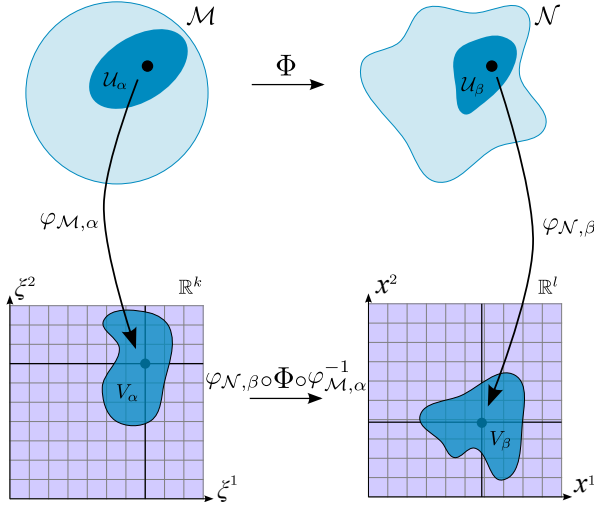


Figure 4.2: Mapping between two manifolds,  $\mathcal{M}$  and  $\mathcal{N}$ .

**Definition 3 (Submanifold).** Let  $\mathcal{M}$  be a smooth manifold. A submanifold of  $\mathcal{M}$  is a subset  $\mathcal{S} \subset \mathcal{M}$ , together with a smooth one-to-one mapping  $\Phi : \tilde{\mathcal{S}} \rightarrow \mathcal{S} \subset \mathcal{M}$  satisfying the maximal rank condition everywhere, where the parameter space  $\tilde{\mathcal{S}}$  is some other manifold and  $\mathcal{S} = \Phi(\tilde{\mathcal{S}})$  is the image of  $\Phi$ . In particular, the dimension of  $\mathcal{S}$  is the same as that of  $\tilde{\mathcal{S}}$ , and does not exceed the dimension of  $\mathcal{M}$ .

An important concept is the boundary of a manifold. This concept plays an essential role in the generalized Stokes theorem, Theorem 3, to be introduced later on.

**Definition 4 (Complement, interior point, exterior point, boundary point, open set and closed set).** [102] Given a subset  $\mathcal{S}$  of a manifold  $\mathcal{M}$ , the complement of  $\mathcal{S}$  in  $\mathcal{M}$  is the set of points  $\mathcal{S}^c := \{p \in \mathcal{M} | p \notin \mathcal{S}\}$ . Let the ball  $B_\epsilon(p) = \{\mathbf{x} \in \mathcal{M} | d(\mathbf{x}, p) < \epsilon\}$ , then

1. A point  $p$  is an interior point of  $\mathcal{S}$  if there exists  $\epsilon > 0$  such that the neighborhood  $B_\epsilon(p)$  around  $p$  has the property that  $B_\epsilon(p) \subset \mathcal{S}$ . One writes  $p \in \text{int}(\mathcal{S})$ .
2. A point  $p$  is an exterior point of  $\mathcal{S}$  if there exists  $\epsilon > 0$  such that the neighborhood  $B_\epsilon(p)$  around  $p$  has the property that  $B_\epsilon(p) \cap \mathcal{S} = \emptyset$ . One writes  $p \in \text{ext}(\mathcal{S})$ .
3. A point  $p$  is a boundary point of  $\mathcal{S}$  if every neighborhood  $B_\epsilon(p)$  around  $p$  with  $\epsilon > 0$  has the property that  $B_\epsilon(p) \cap \mathcal{S} \neq \emptyset$  and  $B_\epsilon(p) \cap \mathcal{S}^c \neq \emptyset$ . One writes  $p \in \partial \mathcal{S}$ .

A set  $\mathcal{S}$  is open if, and only if,  $\mathcal{S} = \text{int}(\mathcal{S})$ . A set  $\mathcal{S}$  is closed if, and only if, its complement  $\mathcal{S}^c$  is open.

In order to introduce the concept of boundary one needs to introduce the closed upper half-space of dimension  $n$ :

$$\mathbb{H}^n = \{(x^1, \dots, x^n) \in \mathbb{R}^n | x^n \geq 0\},$$

with the subspace topology of  $\mathbb{R}^n$ . From Definition 4 it follows that points with  $x^n > 0$  are the interior points of  $\mathbb{H}^n$ , the points with  $x^n < 0$  are the exterior points of  $\mathbb{H}^n$  and the points with  $x^n = 0$  are the boundary points of  $\mathbb{H}^n$ .

**Proposition 1.** [176] Let  $P$  and  $Q$  be subsets of  $\mathbb{H}^n$  and  $\Phi : P \rightarrow Q$  a diffeomorphism. Then  $\Phi$  maps interior points to interior points and boundary points to boundary points.

One can then define an  $n$ -manifold with boundary:

**Definition 5 (n-Manifold with boundary, interior point and boundary point of an n-manifold with boundary).** [176] An  $n$ -manifold with boundary,  $\mathcal{M}$ , is a topological space which is locally  $\mathbb{H}^n$ . A point  $p$  of  $\mathcal{M}$  is an interior point if there is a chart  $\varphi_{\mathcal{M},\alpha}$  in which  $\varphi_{\mathcal{M},\alpha}(p)$  is an interior point of  $\mathbb{H}^n$ . In the same way, a point  $p$  is a boundary point of  $\mathcal{M}$  if  $\varphi_{\mathcal{M},\alpha}(p)$  is a boundary point of  $\mathbb{H}^n$ . The set of boundary points of  $\mathcal{M}$  is denoted by  $\partial\mathcal{M}$ .

**Definition 6 (Boundary operator).** Given an  $n$ -manifold with boundary,  $\mathcal{M}$ , the boundary operator  $\partial$  is a map  $\partial : \mathcal{M} \rightarrow \partial\mathcal{M}$ , where  $\partial\mathcal{M}$  is a boundaryless  $(n-1)$ -manifold.

**Corollary 1 (The boundary of a submanifold).** Since any submanifold  $\mathcal{S} \subset \mathcal{M}$  is in itself a manifold, the boundary of a submanifold is defined as in Definition 6.

**Corollary 2 (Nilpotency of boundary operator).** Given an  $n$ -manifold with boundary,  $\mathcal{M}$ . Its boundary,  $\partial\mathcal{M}$ , is an  $(n-1)$ -dimensional boundaryless manifold. Therefore

$$\partial\partial\mathcal{M} = \emptyset. \quad (4.1.1)$$

**Proposition 2 (Boundary is mapped into a boundary and the boundary is independent of chart).** Given two  $n$ -dimensional manifolds with boundary,  $\mathcal{M}$  and  $\mathcal{N}$ , and a mapping (diffeomorphism) between them,  $\Phi : \mathcal{M} \rightarrow \mathcal{N}$ , then the interior points and boundary points of  $\mathcal{M}$  are mapped onto interior points and boundary points of  $\mathcal{N}$ , respectively. That is:

$$\partial\Phi(\mathcal{M}) = \Phi(\partial\mathcal{M}). \quad (4.1.2)$$

Moreover, interior and boundary points are independent of the choice of chart.

*Proof.* For the first statement, let  $\varphi_{\mathcal{M},\alpha} : \mathcal{U}_\alpha \subset \mathcal{M} \rightarrow \mathbb{R}^k$  and  $\varphi_{\mathcal{N},\beta} : \mathcal{U}_\beta \subset \mathcal{N} \rightarrow \mathbb{R}^k$ , then  $\varphi_{\mathcal{N},\beta} \circ \Phi \circ \varphi_{\mathcal{M},\alpha}^{-1} : \mathbb{R}^k \rightarrow \mathbb{R}^k$  is a diffeomorphism and according to Proposition 1 this maps boundary points onto boundary points and interior points onto interior points.

As for the second statement, one takes  $\mathcal{M} = \mathcal{N}$  and in this case the two charts will be  $\varphi_{\mathcal{M},\alpha}$  and  $\varphi_{\mathcal{M},\beta}$  and the mapping between the two charts (change of coordinates) will be given by  $\varphi_{\mathcal{M},\beta} \circ \Phi \circ \varphi_{\mathcal{M},\alpha}^{-1} = \varphi_{\mathcal{M},\beta} \circ \varphi_{\mathcal{M},\alpha}^{-1}$ , since  $\Phi$  in this case is the identity map, and again  $\varphi_{\mathcal{M},\beta} \circ \varphi_{\mathcal{M},\alpha}^{-1} : \mathbb{R}^k \rightarrow \mathbb{R}^k$  is a diffeomorphism and according to Proposition 1 this maps boundary points onto boundary points and interior points onto interior points.  $\square$

Equations (4.1.1) and (4.1.2) in Corollary 2 and Proposition 2, respectively, are important results, as they will contribute to many of the upcoming results in this chapter and the next one.

The theory of manifolds and the numerical framework presented in this thesis does not restrict to manifolds that are contractible or simply connected. It allows the manifold to have holes, voids, etc. The structure of a manifold is given by the Betti number  $\mathfrak{B}_k$ ,

$$\mathfrak{B}_k = \begin{cases} \# \text{ connected components of } \mathcal{M} & k = 0, \\ \# \text{ holes through } \mathcal{M} & k = 1, \\ \# \text{ voids in } \mathcal{M} & k = 2, \\ 0 & k = 3, \end{cases} \quad \begin{array}{l} (\text{almost always one}), \\ (\text{holes, e.g. airfoil in domain}), \\ (\text{e.g. inside a tennisbal}), \\ (\text{always zero in 3D}). \end{array} \quad (4.1.3)$$

The Betti number of a domain will give the dimension of the space of harmonic forms. Examples of non-contractible domains in  $\mathbb{R}^2$  and  $\mathbb{R}^3$  are given in Figures 4.3 and 4.4.

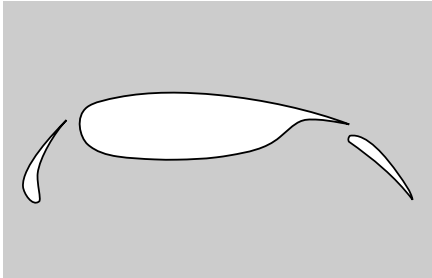


Figure 4.3: This two-dimensional domain with multi-element airfoil configuration has Betti number  $\mathfrak{B} = \{1, 3, 0\}$ .

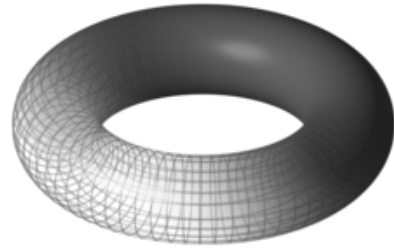


Figure 4.4: Illustration of a torus, a 2D surface embedded in  $\mathbb{R}^3$ , that has Betti number  $\mathfrak{B} = \{1, 2, 1, 0\}$ , since the torus is a hollow tube.

## 4.2 Orientation

In  $n$ -dimensional space it is possible to define  $n + 1$  contractible submanifolds of dimension 0, 1, ...,  $n$ , respectively. For the case  $n = 3$  one can define, points, lines, surfaces and volumes. Moreover, it is also possible to orient these objects. By orientation one means the generalization of concepts such as left and right, front and back, clockwise or counterclockwise, outward and inward, etc. The different kinds of orientation will be presented for all the geometric objects that exist in 3-manifolds (points, lines, surfaces and volumes), as well as generalizations for geometric objects of arbitrary dimension. The distinction between inner orientation (solely related to the geometric object) and outer orientation (related to both the object and the embedding space) will be given. For a more detailed discussion on orientation we recommend [2, 41, 123, 162, 174].

The concept of orientation on manifolds is a generalization of the one for vector spaces and hence, by extension, to  $\mathbb{R}^k$ . One starts with the notion of orientation in vector spaces and the charts  $\varphi$  will induce an orientation on the manifold.

In  $\mathbb{R}^1$  an orientation is one of the two possible directions, see Figure 4.5(a). In  $\mathbb{R}^2$  an orientation is one of the two possible rotations, clockwise or counterclockwise, see Figure 4.5(b). In  $\mathbb{R}^3$  an orientation is one of the two possible screw senses, upward clockwise or upward counterclockwise, see Figure 4.5(c). In these figures we have chosen a positive orientation according to the right hand rule. Consequently, the other is negative.

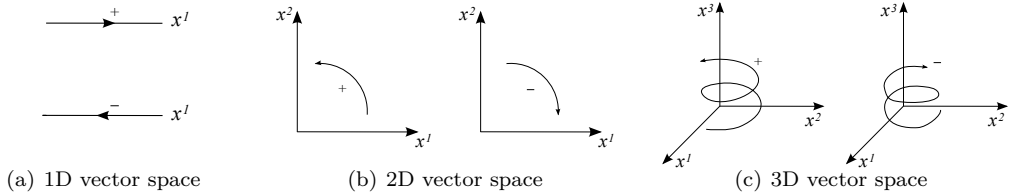


Figure 4.5: Possible orientations of vector spaces.

The question is how to generalize this heuristic definition to arbitrary dimensions. In a vector space of dimension  $k$  one can transform one set of basis vectors,  $\{\vec{v}_1, \vec{v}_2, \dots, \vec{v}_k\}$ , into another one,  $\{\vec{u}_1, \vec{u}_2, \dots, \vec{u}_k\}$ , in the following way:

$$\vec{u}_i = \sum_j S_{ij} \vec{v}_j,$$

where  $S_{ij}$  are the coefficients of the transformation matrix  $S$  with  $\det(S) \neq 0$ .

**Definition 7 (Orientation).** *In a vector space of dimension  $k$ , orientation is an equivalence class of ordered sets of basis vectors whose equivalence relation states that two sets of basis vectors belong to the same equivalence class if the transformation matrix,  $S$ , between them has  $\det(S) > 0$ .*

Since the determinant of a change of basis is either positive or negative, there are only two such classes. Hence, any vector space has only two orientations. If one chooses one of them as positive, then other is negative. It is simple to see that this definition of orientation is equivalent for the three cases presented above and generalizes this concept to any dimension  $k$ .

As seen in Definition 1,  $k$ -manifolds are locally like  $\mathbb{R}^k$ , and therefore, locally like a  $k$ -dimensional vector space. In this way, orientation on a manifold can be defined as:

**Definition 8 (Inner orientation on a manifold).** *A manifold  $\mathcal{M}$  is said to be inner oriented if for any two overlapping charts,  $(U_\alpha, \varphi_{\mathcal{M},\alpha})$  and  $(U_\beta, \varphi_{\mathcal{M},\beta})$ , the Jacobian determinant of the transformation  $\varphi_{\mathcal{M},\beta}^{-1} \circ \varphi_{\mathcal{M},\alpha}$  is positive. The inner orientation being the one of the equivalence classes of the sets of basis vectors of the tangent space at each point,  $T_p \mathcal{M}$ , associated to these charts.*

If one considers the space in which the  $k$ -manifold  $\mathcal{M}$  is embedded to be  $\mathbb{R}^n$ , with dimension  $n \geq k$ , then at each point on the manifold there is a space perpendicular to the tangent space,  $T_p \mathcal{M}$ , denoted by  $T_p^\perp \mathcal{M}$  whose dimension is  $(n - k)$ ; the normal

bundle to the submanifold  $\mathcal{M}$  embedded in  $\mathbb{R}^n$ . Then  $T_p\mathbb{R}^n = T_p\mathcal{M} \oplus T_p^\perp\mathcal{M}$ . This allows one to define an outer orientation of a manifold as:

**Definition 9 (Outer orientation on a manifold).** Consider an oriented  $k$ -manifold  $\mathcal{M}$ , with inner orientation  $\{\vec{u}_1, \vec{u}_2, \dots, \vec{u}_k\}$  at  $T_p\mathcal{M}$ , embedded in an  $n$ -dimensional Euclidean space. An outer orientation of  $\mathcal{M}$  is an orientation for the perpendicular vector space at each point in the manifold,  $T_p^\perp\mathcal{M}$ ,  $\{\vec{u}_{k+1}, \vec{u}_{k+2}, \dots, \vec{u}_n\}$  such that all the oriented basis  $\{\vec{u}_1, \vec{u}_2, \dots, \vec{u}_k, \vec{u}_{k+1}, \dots, \vec{u}_n\}$  are in one of the two equivalence classes of the embedding space  $T_p\mathbb{R}^n$ .

The particular cases of inner orientation of a 0-manifold (point) and outer orientation of a  $n$ -manifold embedded in a  $n$ -dimensional space are treated in a similar way. In both cases, the tangent space (points) and the perpendicular space ( $n$ -manifolds) have dimension zero. Therefore, the points and the  $n$ -manifolds are simply considered as sources or sinks and their orientation can be seen as simply induced by the inner orientation of the lines stemming out of them (points) or by the outer orientation of its faces ( $n$ -manifold), see [123, 174]. The following example illustrates both inner and outer orientations of all  $k$ -dimensional objects, embedded in up to three dimensional space.

**Example 1 (Inner- and outer oriented manifolds).** Figures 4.6(a) and 4.6(b) show  $k$ -manifolds embedded in  $\mathbb{R}^n$ ,  $n = 0, \dots, 3$ , with corresponding inner- and outer-orientation. The inner-orientation on a  $k$ -manifold is the same for all  $n \geq k$ , while for outer-orientation the orientation depends on the embedding space  $\mathbb{R}^n$ .

Observe that for each  $k$  and each  $n$ , the orientation in Figure 4.6(a) is the same as in Figure 4.6(b). It is the manifold that changes.

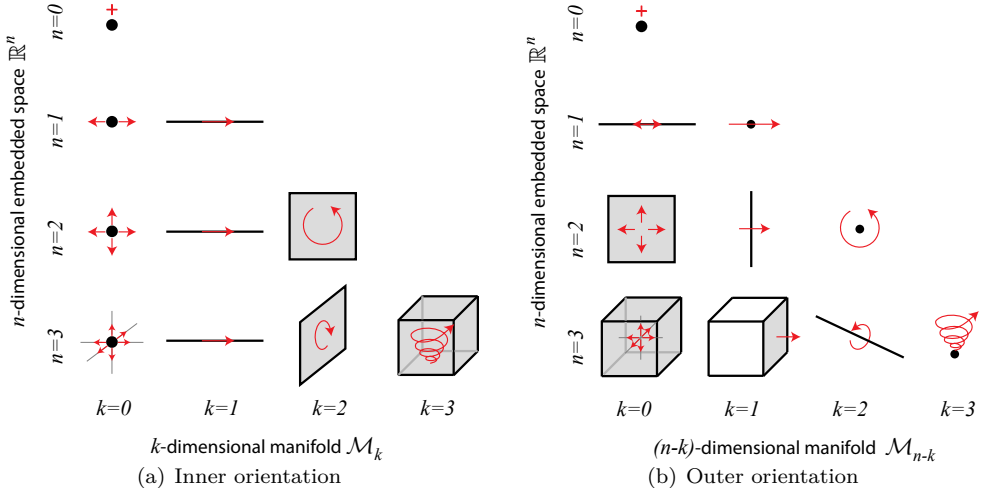


Figure 4.6: Illustrations of the inner and outer orientations of  $k$ -dimensional objects embedded in a  $n$ -dimensional space. The objects in (a) and (b) are each others dual, while they possess the same orientation.

Next, let's concentrate on sequences in three-dimensional space. The top row in Figure 4.7 presents a sequence of outer-oriented geometric objects of increasing dimension in  $\mathbb{R}^3$ , and the bottom row a sequence of inner-oriented geometric objects of decreasing dimension. The objects are arranged in such a way that it reveals the similarities with the double de Rham complex and action of the Hodge star operator. Both are introduced in this chapter later on. Following the ideas pointed out in [175],

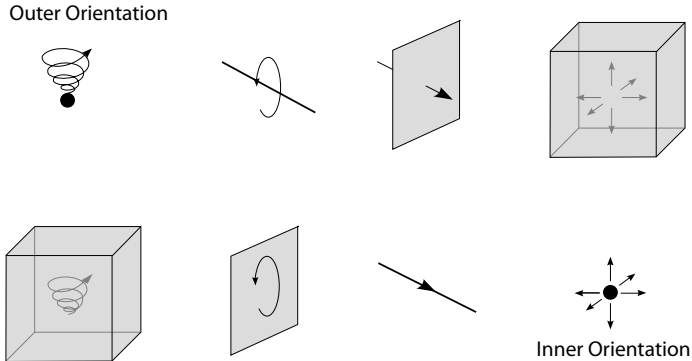


Figure 4.7: Inner and outer orientation of  $k$ -manifolds,  $k = \{0, 1, 2, 3\}$ , in  $\mathbb{R}^3$ .

it is important to stress that orientation plays an essential role in integration, and so in the generalized Stokes theorem, Theorem 3 (p. 55). In this case, the orientation of a  $k$ -manifold and its boundary have to be compatible when integrating, for the theorem to hold. Consequently, the distinction between inner and outer oriented manifolds will play a central role in the discretization to be presented in this thesis. This distinction motivates the use of dual grids.

Finally, this work is restricted to manifolds for which a global consistent orientation can be defined, called *orientable manifolds*. Remark that presenting orientation of a manifold in this way is a generalization of the concepts ‘normal’ and ‘tangential’ in vector calculus.

### 4.3 Differential forms

A Physical system generally preserves integral quantities and these quantities are topological in the sense that they do not depend on a particular coordinate system or the metric employed. The integration of differential forms is independent of any metric notions in space, [71, Ch.3]; no Riemann metric, dot products or  $k$ -dimensional volume elements are required. If we would have used vectors for integration all these metric concepts need to be taken into account. Integrals are of paramount importance in mimetic discretizations, because we cannot represent differential forms and the operations on and between differential forms in a finite dimensional setting. But we *can* represent integrals of differential forms and the integral relations between them exactly.

---

As Burke [41] puts it:

*Were this a mere change in notation, it would make no sense to change things. It is not a mere change in notation, however, but a basic change in the fundamental concepts. The new concepts are better for unarguable reasons: they [differential forms] correctly represent a larger symmetry group, and therefore correctly represent more features of the real world.*

The language of continuum mechanics is calculus on manifolds. Although the majority of engineers and scientists are familiar with vector calculus, exterior calculus or differential geometry offers an interesting alternative. As the name differential geometry already suggests, there exists a strong connection between differential  $k$ -forms and the geometry and orientation of manifolds. Therefore, some say that  $k$ -forms can be seen as integrands that can be integrated over oriented  $k$ -dimensional manifolds, [69]. Others see differential 1-forms as the naturally dual to vector fields on the tangent space of the manifold. A  $k$ -form is then dual to a tangent bundle. Differential  $k$ -forms are in the class of skew symmetric covariant tensors, [71]. In fact, both interpretations will appear to be useful. In Appendix A a thorough derivation is given for  $k$ -forms, based on vectors and covectors. Here we immediately give the definition of differential  $k$ -forms.

**Definition 10 (Differential  $k$ -forms).** [2, 71, 103, 167] Let  $\mathcal{M}$  be an  $n$ -dimensional differentiable oriented manifold. A differential  $k$ -form,  $a^{(k)}$ , is a  $k$ -linear, skew symmetric tensor field over  $\mathcal{M}$  with mapping

$$a^{(k)} : \underbrace{T_p \mathcal{M} \times \cdots \times T_p \mathcal{M}}_k \rightarrow \mathbb{R}, \quad \text{with } k = 0, 1, \dots, n.$$

For any permutation of the indices we have,

$$a^{(k)}(\dots, \vec{v}_r, \dots, \vec{v}_s, \dots) = -a^{(k)}(\dots, \vec{v}_s, \dots, \vec{v}_r, \dots),$$

for any  $\vec{v}_1, \dots, \vec{v}_k \in T_p \mathcal{M}$ , the tangent vector space of the manifold  $\mathcal{M}$ . A 0-form,  $a^{(0)}$ , is defined simply as a standard scalar function on  $\mathcal{M}$ . The space of  $k$ -forms on the manifold  $\mathcal{M}$  is denoted by  $\Lambda^k(\mathcal{M})$ .  $a^{(k)} = 0$  when  $k < 0$  or  $k > n$ .

**Definition 11 (Wedge product).** [2, 167] The wedge (or exterior) product,  $\wedge$ , of two differential forms  $a^{(k)} \in \Lambda^k(\mathcal{M})$  and  $b^{(l)} \in \Lambda^l(\mathcal{M})$  is a mapping  $\wedge : \Lambda^k(\mathcal{M}) \times \Lambda^l(\mathcal{M}) \rightarrow \Lambda^{k+l}(\mathcal{M})$ ,  $k + l \leq n$ , such that:

$$a^{(k)} \wedge b^{(l)} = (-1)^{kl} b^{(l)} \wedge a^{(k)}, \quad (\text{Skew symmetry}) \quad (4.3.1a)$$

$$f a^{(k)} \wedge b^{(l)} = a^{(k)} \wedge f b^{(l)} = f(a^{(k)} \wedge b^{(l)}), \quad (\text{Multiplication by functions}) \quad (4.3.1b)$$

$$(a^{(k)} + b^{(l)}) \wedge c^{(m)} = a^{(k)} \wedge c^{(m)} + b^{(l)} \wedge c^{(m)}, \quad (\text{Distributivity}) \quad (4.3.1c)$$

$$(a^{(k)} \wedge b^{(l)}) \wedge c^{(m)} = a^{(k)} \wedge (b^{(l)} \wedge c^{(m)}), \quad (\text{Associativity}) \quad (4.3.1d)$$

From property (4.3.1a) we have

$$a^{(k)} \wedge a^{(k)} = 0, \quad \forall a^{(k)} \in \Lambda^k(\mathcal{M}), \quad \text{if } k \text{ is odd or } k > \frac{n}{2}. \quad (4.3.2)$$

---

**Proposition 3.** [2] On an  $n$ -dimensional manifold  $\mathcal{M}$  the space of 1-forms  $\Lambda^1(\mathcal{M})$  is a linear vector space of dimension  $n$  that is spanned by  $n$  basis elements. A canonical basis, given a local coordinate system  $\mathbf{x} := (x^1, \dots, x^n)$ , is  $\{\mathrm{d}x^1, \dots, \mathrm{d}x^n\}$ . The space of  $k$ -forms  $\Lambda^k(\mathcal{M})$  is a linear vector space of dimension  $\frac{n!}{(n-k)!k!}$  and has a canonical basis given by:

$$\{\mathrm{d}x^{i_1} \wedge \cdots \wedge \mathrm{d}x^{i_k} \mid 1 \leq i_1 < \cdots < i_k \leq n\}. \quad (4.3.3)$$

From this it follows that we can express the  $k$ -form  $a^{(k)} \in \Lambda^k(\mathcal{M})$  as

$$a^{(k)} = \sum_I f_I(\mathbf{x}) \mathrm{d}x^{i_1} \wedge \cdots \wedge \mathrm{d}x^{i_k}, \quad (4.3.4)$$

where  $I = i_1, \dots, i_k$  with  $1 \leq i_1 < \cdots < i_k \leq n$  and where  $f_I(\mathbf{x})$  is a continuously differentiable scalar function,  $f_i(\mathbf{x}) \in C^\infty(\mathcal{M})$ .

**Example 2.** Examples of 0-forms, 1-forms, 2-forms and 3-forms in  $\mathbb{R}^3$  are given by:

$$\begin{cases} a^{(0)} = a(\mathbf{x}), \\ b^{(1)} = b_1(\mathbf{x}) \mathrm{d}x + b_2(\mathbf{x}) \mathrm{d}y + b_3(\mathbf{x}) \mathrm{d}z, \\ c^{(2)} = c_{1,2}(\mathbf{x}) \mathrm{d}x \wedge \mathrm{d}y + c_{1,3}(\mathbf{x}) \mathrm{d}x \wedge \mathrm{d}z + c_{2,3}(\mathbf{x}) \mathrm{d}y \wedge \mathrm{d}z, \\ w^{(3)} = w(\mathbf{x}) \mathrm{d}x \wedge \mathrm{d}y \wedge \mathrm{d}z. \end{cases} \quad (4.3.5)$$

**Example 3** ( $a^{(1)} \wedge a^{(1)}$  in  $\mathbb{R}^3$ ).  $\mathrm{d}x \wedge \mathrm{d}x = \mathrm{d}y \wedge \mathrm{d}y = \mathrm{d}z \wedge \mathrm{d}z = 0$ .

**Example 4** ( $a^{(2)} \wedge a^{(2)}$  in  $\mathbb{R}^4$ ). In  $\mathbb{R}^4$ , let  $a^{(2)} = \mathrm{d}x \wedge \mathrm{d}y + \mathrm{d}z \wedge \mathrm{d}t$ , then

$$a^{(2)} \wedge a^{(2)} = (\mathrm{d}x \wedge \mathrm{d}y + \mathrm{d}z \wedge \mathrm{d}t) \wedge (\mathrm{d}x \wedge \mathrm{d}y + \mathrm{d}z \wedge \mathrm{d}t) = 2 \mathrm{d}x \wedge \mathrm{d}y \wedge \mathrm{d}z \wedge \mathrm{d}t \neq 0.$$

**Example 5.** The minus sign in (4.3.1a) refers to a change in sense of orientation, e.g. in  $\mathbb{R}^2$ ,

$$\mathrm{d}x \wedge \mathrm{d}y = -\mathrm{d}y \wedge \mathrm{d}x.$$

The minus sign appears because we changed from a counterclockwise oriented coordinate system to a clockwise one, see Figure 4.5(b). So in this case,  $\det(\mathbf{S}) < 0$ . The type of orientation, inner or outer, remains unchanged. A change in the latter will appear in the discussion of the Hodge star operator in Section 4.7.

**Definition 12 (Standard volume form).** [2] In an  $n$ -dimensional manifold  $\mathcal{M}$ , a volume form  $\sigma^{(n)}$  is defined in a local coordinate system  $\mathbf{x} := (x^1, \dots, x^n)$  as:

$$\sigma^{(n)} := \mathrm{d}x^1 \wedge \cdots \wedge \mathrm{d}x^n,$$

where  $\sigma^{(n)}$  is the standard volume form.

## 4.4 Differential forms under mappings

In Section 4.1 the mapping of manifolds was discussed. Next we proceed with how differential forms transform under a mapping between two manifolds and how integration of  $k$ -forms over mapped manifolds is defined. See Figure 4.2 for an example of a mapping for  $n = 2$  and where  $(x^1, x^2) = \Phi(\xi^1, \xi^2)$ .

---

**Definition 13 (Pullback operator).** [2, 71] Consider two  $n$ -dimensional manifolds,  $\mathcal{M}$  and  $\mathcal{N}$  and a mapping between them,  $\Phi : \mathcal{M} \rightarrow \mathcal{N}$ , such that local coordinates  $\xi^i$  in  $\mathcal{M}$  are mapped into local coordinates  $x^i = \Phi^i(\xi^1, \dots, \xi^n)$  in  $\mathcal{N}$ . Then the pullback of a  $k$ -form,  $\Phi^* : \Lambda^k(\mathcal{N}) \rightarrow \Lambda^k(\mathcal{M})$ ,  $k \geq 1$ , is given by:

$$\Phi^*(a^{(k)})(\vec{v}_1, \dots, \vec{v}_k) := a^{(k)}(\Phi_*(\vec{v}_1), \dots, \Phi_*(\vec{v}_k)),$$

where  $\Phi_*(\vec{v})$  is the usual change of basis or pushforward of a vector  $\vec{v}$ , see [2, 71].

**Proposition 4.** [71] The pullback  $\Phi^*$  has the following properties:

$$\Phi^*(a^{(k)} + b^{(k)}) = \Phi^*a^{(k)} + \Phi^*b^{(k)} \quad (\text{Linearity}) \quad (4.4.1a)$$

$$\Phi^*(a^{(k)} \wedge b^{(k)}) = \Phi^*a^{(k)} \wedge \Phi^*b^{(k)} \quad (\text{Algebra homomorphism}) \quad (4.4.1b)$$

$$(\Phi_2 \circ \Phi_1)^* = \Phi_1^* \circ \Phi_2^* \quad (\text{Composition}) \quad (4.4.1c)$$

The pullback of a 0-form,  $a^{(0)} \in \Lambda^0(\mathcal{N})$ , is given simply by the composition of the maps

$$\Phi^*(a^{(0)}) := a^{(0)} \circ \Phi. \quad (4.4.2a)$$

In case  $\mathcal{M}, \mathcal{N} \in \mathbb{R}^3$ , the pullback of a  $k$ -form  $a^{(k)} \in \Lambda^k(\mathcal{N})$  is given in [94] as,

$$\Phi^*a^{(1)} := (D\Phi)^T(a^{(1)} \circ \Phi), \quad (4.4.2b)$$

$$\Phi^*a^{(2)} := \det(D\Phi)(D\Phi)^{-1}(a^{(2)} \circ \Phi), \quad (4.4.2c)$$

$$\Phi^*a^{(3)} := \det(D\Phi)(a^{(3)} \circ \Phi), \quad (4.4.2d)$$

where  $D\Phi$  is the Jacobian matrix of the mapping  $\Phi$ . Such a mappings is also known as Piola transforms.

Differential  $k$ -forms are naturally integrated over  $k$ -dimensional manifolds. Integration of differential forms can now be defined in the following way.

**Definition 14 (Pullback integration formulation).** [167] The integral of a differential  $k$ -form,  $a^{(k)}$ , over a manifold  $\mathcal{M}$  of dimension  $k$  is:

$$\int_{\mathcal{M}} a^{(k)} := \int_S (\varphi^{-1})^*(a^{(k)}), \quad (4.4.3)$$

where  $\varphi^{-1} : S \subset \mathbb{R}^k \rightarrow \mathcal{M}$  is the inverse of the global chart from  $\mathcal{M}$  to  $S \subset \mathbb{R}^k$ . On the right hand side of (4.4.3) one has the usual integral in  $S \subset \mathbb{R}^k$ .

Integration can be considered as duality pairing between a  $k$ -dimensional manifold  $\mathcal{M}$  and a differential  $k$ -form  $a^{(k)}$  in the following way<sup>1</sup>

$$\langle \mathcal{M}, a^{(k)} \rangle := \int_{\mathcal{M}} a^{(k)} \in \mathbb{R}. \quad (4.4.4)$$

Such a duality pairing indicates the connection between  $k$ -forms and oriented  $k$ -dimensional manifolds. This duality pairing is a metric-free operation, see [71]. Duality pairings will be used mainly to indicate how operators that act on  $k$ -forms relate to operators acting on  $k$ -dimensional manifolds.

If integration is interpreted as the duality pairing between differential forms and geometry, then there exists a direct relation between a mapping and the pullback.

---

<sup>1</sup>(., .) denotes metric dependent inner products, while  $\langle \cdot, \cdot \rangle$  denotes the metric-free duality pairing.

---

**Proposition 5.** Given a mapping  $\Phi : \mathcal{M} \rightarrow \mathcal{N}$ , a differential form  $a^{(k)} \in \Lambda^k(\mathcal{N})$  and its associated pullback  $\Phi^*$ , then the following holds:

$$\int_{\Phi(\mathcal{M})} a^{(k)} = \int_{\mathcal{M}} \Phi^*(a^{(k)}) \Leftrightarrow \langle \Phi(\mathcal{M}), a^{(k)} \rangle = \langle \mathcal{M}, \Phi^* a^{(k)} \rangle. \quad (4.4.5)$$

So the pullback is the formal adjoint of the map  $\Phi$  in this duality pairing.

Having defined a mapping, a pullback and their relation by duality pairing, we can define some special cases of these maps which appear to be useful later on.

**Definition 15 (Inclusion map).** [71] Let  $\mathcal{S}$  be a subset of  $\mathcal{M}$ . The function  $\iota : \mathcal{S} \rightarrow \mathcal{M}$  defined by  $\iota(x) = x$  for every  $x \in \mathcal{S}$ , is the inclusion map (or the embedding, or the injection) of  $\mathcal{S}$  into  $\mathcal{M}$ . In other words, the inclusion map of a subset of  $\mathcal{M}$  is the restriction to that subset of the identity map on  $\mathcal{M}$ .

**Definition 16 (Trace operator).** [7] Given two manifolds  $\mathcal{M}$  and  $\mathcal{M}'$  such that  $\mathcal{M}' \subset \mathcal{M}$ , the trace operator,  $\text{tr}_{\mathcal{M}, \mathcal{M}'} : \Lambda^k(\mathcal{M}) \rightarrow \Lambda^k(\mathcal{M}')$ , is the pullback of the inclusion  $\mathcal{M}' \hookrightarrow \mathcal{M}$ . If the manifold  $\mathcal{M}$  is clear from the context, one may write  $\text{tr}_{\mathcal{M}'}$  instead of  $\text{tr}_{\mathcal{M}, \mathcal{M}'}$ . If  $\mathcal{M}'$  is the boundary of  $\mathcal{M}$ ,  $\partial\mathcal{M}$ , one just writes  $\text{tr}$ .

**Example 6.** Consider an inclusion map  $\iota$  and its associated pullback  $\iota^* = \text{tr}$ , such as the one depicted in Figure 4.8 that generates the inclusion of the manifold  $\mathcal{M}'$ , a circle, on the manifold  $\mathcal{M}$ , a disk. In local polar coordinates  $\theta'$  and  $(\theta, r)$  the inclusion map takes the form:

$$(\theta, r) = \iota(\theta') = (\theta', 1).$$

The trace of the 1-form  $a^{(1)} = a_\theta d\theta + a_r dr$  is given by:

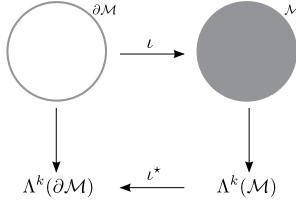


Figure 4.8: Pictorial view of the inclusion map  $\iota$  and its associated pullback  $\iota^*$ .

$$\text{tr } a^{(1)} \stackrel{\text{def.}}{=} {}^{16} \iota^* a^{(1)} \stackrel{(4.4.2b)}{=} (a_\theta \circ \iota)(\theta') d\theta'.$$

## 4.5 Differential forms and orientation

In Section 4.2 inner- and outer-orientation were defined for geometric objects. By the duality pairing in (4.4.4), this means that differential  $k$ -forms are either associated to inner-oriented manifolds or to outer-oriented manifolds. Next we need to discuss orientation of differential forms.

Whereas orientation is something we need for our calculations, physics should – in a sense – be independent of the choice of our orientation. From our earliest physics

---

courses orientation has played a role: the right-hand rule in electromagnetism, the outward unit normal for fluxes, clockwise or counter-clockwise for circulations, etc. Many sign conventions in physics are also due to a preferred orientation. The basic question with orientation is: ‘What happens in the description of physics if we change the orientation?’ Of course, it will only affect the description of physics and not physics itself. A few examples might illustrate the point.

**Example 7.** Consider a curve in  $\mathbb{R}^3$ . If the 1-form integrated along this curve denotes a force, then the line integral denotes the amount of work,  $W$ , done by the force along the curve. Now suppose that we change the direction (orientation) in which we traverse the curve, then the value of this integral is  $-W$  for a conservative force. This is as expected. So changing the orientation in the calculation of work for a conservative force leaves the differential form unchanged and reverses the integral:  $W_{AB} = -W_{BA}$ , if the point  $A$  and  $B$  are the endpoints of the curve on the manifold  $\mathcal{M}$ .

Is this generally true? If we change the orientation of the domain of integration, does the integral quantity always change sign? The answer is no. A simple counter example is the 3-form mass density,  $\rho^{(3)}$ .

**Example 8.** If we integrate  $\rho^{(3)}$  over a positively oriented volume,  $\mathcal{M}_3^+$ , we obtain the mass in that volume

$$M = \int_{\mathcal{M}_3^+} \rho^{(3)} \geq 0 .$$

If we change the orientation of the volume and the differential form  $\rho^{(3)}$  would remain unchanged, the integral would be

$$M = \int_{\mathcal{M}_3^-} \rho^{(3)} = - \int_{\mathcal{M}_3^+} \rho^{(3)} \leq 0 .$$

So a change in orientation would lead to negative mass, which is physically unacceptable. Not because we think of mass as being positive – hypothetically mass can be negative –, but because its sign depends on the orientation. In order to restore our faith in physics, the mass density 3-form should change sign when the orientation is changed. In this case, mass will always be positive, regardless of the sense of orientation.

So we have (at least) two classes of differential forms: those that do not change sign when the orientation is reversed and those that do change sign when the sense orientation is changed.

Therefore, orientation is an indispensable part the description of physics and physics compatible numerical techniques should take orientation into account, both in the computational mesh and in the computation of physics.

**Forms and pseudo-forms** In the examples above, work and mass, we saw that some variables change sign when the orientation is reversed, while others do not change sign. The forms which do not change sign are called *genuine forms* or simply *forms*, while forms which do change sign are called *pseudo-forms*. This is an important

---

distinction between physical variables. We can never directly equate a form to a pseudo form, because of incompatible orientations. Before we can equate a form to a pseudo form, either the form needs to be mapped to a pseudo-form, or the pseudo-form needs to be converted to a form.

The notions form and pseudo-form are taken from differential geometry and can be found in almost any book on the subject, see e.g. Frankel, [71] and Bossavit, [26]. One may find other classifications in literature which mean exactly the same thing: Tonti, [174], describes the two classes as *configuration variables* and *source variables*. In this thesis we referred to *inner-oriented variables* and *outer-oriented variables*. The genuine forms were referred to as inner-oriented variables and the pseudo-forms were called outer-oriented. Bossavit, [26] talks about *axial vectors* or *twisted vectors* and *true vectors*. Whatever the names one uses to refer to the two distinct types of forms, it is important to acknowledge this difference. Not only for the sake of a sound physical description, but also for a proper numerical model.

The operator which converts forms into pseudo-forms and vice versa is the Hodge star operator, to be defined in Section 4.7. Since indicating the associated orientation of a differential  $k$ -form can be important, we make the following distinction between differential form spaces.

**Definition 17 (Differential forms and orientation).** *With  $\tilde{\Lambda}^k(\mathcal{M})$  we indicate the space of differential  $k$ -forms, which have a duality pairing with inner-oriented  $k$ -dimensional manifolds. For  $k$ -forms that have a duality pairing with outer-oriented  $k$ -dimensional manifolds, we use the standard notation  $\Lambda^k(\mathcal{M})$ .*

**Remark 1.** *We use the standard notation for the space of  $k$ -forms associated to outer-oriented, because in Parts III and IV we mainly work with outer-oriented differential forms.*

**Remark 2.** *In fact, the spaces  $\Lambda$  and  $\tilde{\Lambda}$  are the same, i.e. both spaces contain the same elements, only the interpretation of the elements differ. Therefore, where orientation does not play an essential role, like in most of the remainder of this chapter, we simply use  $\Lambda^k(\mathcal{M})$ , but the same relations, definitions and propositions also hold for  $\tilde{\Lambda}^k(\mathcal{M})$ .*

## 4.6 Exterior derivative

The exterior derivative,  $d$ , plays an important role in differential geometry and the numerical framework we present. The exterior derivative is a metric-free operator that generalizes the vector operators grad, curl and div (also rot in 2D), and is defined in the following way:

**Definition 18 (Exterior derivative).** [2, 6, 69] *The exterior derivative on a  $n$ -dimensional manifold  $\mathcal{M}$  is a mapping  $d : \Lambda^k(\mathcal{M}) \rightarrow \Lambda^{k+1}(\mathcal{M})$ ,  $0 \leq k \leq n - 1$ . In in*

a local coordinate system  $(x^1, \dots, x^n)$  this map is given by

$$\begin{aligned} da^{(k)} &\stackrel{(4.3.4)}{=} d \sum_I f_I(\mathbf{x}) dx^{i_1} \wedge \dots \wedge dx^{i_k} \\ &= \sum_I df_I(\mathbf{x}) \wedge dx^{i_1} \wedge \dots \wedge dx^{i_k} \\ &= \sum_I \sum_{j=1}^n \frac{\partial f_I}{\partial x^j} dx^j \wedge dx^{i_1} \wedge \dots \wedge dx^{i_k}, \end{aligned} \quad (4.6.1)$$

where  $I = i_1, \dots, i_k$  with  $1 \leq i_1 < \dots < i_k \leq n$ , where  $f_I(\mathbf{x})$  is a continuously differentiable scalar function,  $f_I(\mathbf{x}) \in C^\infty(\mathcal{M})$  and where  $\frac{\partial}{\partial x^j}$  is the partial derivative to  $x^j$ .

The exterior derivative satisfies Leibniz rule,

$$d(a^{(k)} \wedge b^{(l)}) = da^{(k)} \wedge b^{(l)} + (-1)^k a^{(k)} \wedge db^{(l)}, \quad k + l < n, \quad (4.6.2)$$

and is nilpotent,

$$d^2a^{(k)} := 0, \quad \forall a^{(k)} \in \Lambda^k(\mathcal{M}). \quad (4.6.3)$$

**Example 9.** In a 3-dimensional Euclidean space and in a local coordinate system  $(x^1, x^2, x^3)$  the exterior derivative of a 0-form  $a^{(0)} \in \Lambda^0(\mathcal{M})$ ,

$$da^{(0)} := \frac{\partial a}{\partial x^1} dx^1 + \frac{\partial a}{\partial x^2} dx^2 + \frac{\partial a}{\partial x^3} dx^3,$$

and the exterior derivative of a 1-form,  $b^{(1)} = \sum_{i=1}^3 b_i dx^i$ , is given by:

$$db^{(1)} = \left( \frac{\partial b_2}{\partial x^1} - \frac{\partial b_1}{\partial x^2} \right) dx^1 \wedge dx^2 + \left( \frac{\partial b_3}{\partial x^1} - \frac{\partial b_1}{\partial x^3} \right) dx^1 \wedge dx^3 + \left( \frac{\partial b_3}{\partial x^2} - \frac{\partial b_2}{\partial x^3} \right) dx^2 \wedge dx^3,$$

and the exterior derivative of a 2-form,  $c^{(2)} = c_3 dx^1 \wedge dx^2 + c_2 dx^3 \wedge dx^1 + c_1 dx^2 \wedge dx^3$ , is given by:

$$dc^{(2)} = \left( \frac{\partial c_1}{\partial x^1} + \frac{\partial c_2}{\partial x^2} + \frac{\partial c_3}{\partial x^3} \right) dx^1 \wedge dx^2 \wedge dx^3.$$

Recalling the vector calculus operators, gradient, curl, and divergence, one can see the similarity between these and the above expressions. Indeed there exists a clear relation between the two sets of equations, for more details see [2, 69].

**Example 10 (Conservation of mass).** Consider a space-time manifold  $\mathbb{R}^4$  with coordinates  $\mathbf{x} := (t, x, y, z)$ , and define following 3-form for mass,

$$m^{(3)} = \rho(dx - u dt) \wedge (dy - v dt) \wedge (dz - w dt),$$

where the function  $\rho = \rho(\mathbf{x})$  represents the density and  $\mathbf{u} := (u(\mathbf{x}), v(\mathbf{x}), w(\mathbf{x}))$  the velocity components in the three space directions. Now set  $r^{(3)} = (dx - u dt) \wedge (dy - v dt) \wedge (dz - w dt)$ , then

$$dm^{(3)} = d(\rho r^{(3)}) = d\rho \wedge r^{(3)} + \rho dr^{(3)}.$$

Since,

$$\begin{aligned} d\rho \wedge r^{(3)} &= \left( \frac{\partial \rho}{\partial t} dt + \frac{\partial \rho}{\partial x} dx + \frac{\partial \rho}{\partial y} dy + \frac{\partial \rho}{\partial z} dz \right) \wedge r^{(3)} \\ &= \left( \frac{\partial \rho}{\partial t} + u \frac{\partial \rho}{\partial x} + v \frac{\partial \rho}{\partial y} + w \frac{\partial \rho}{\partial z} \right) dt \wedge dx \wedge dy \wedge dz, \end{aligned}$$

and

$$\begin{aligned} dr^{(3)} &= - \left( \frac{\partial u}{\partial x} dx \wedge dt \right) \wedge dy \wedge dz + dx \wedge \left( \frac{\partial v}{\partial y} dy \wedge dt \right) \wedge dz - dx \wedge dy \wedge \left( \frac{\partial w}{\partial z} dz \wedge dt \right) \\ &= (\operatorname{div} \mathbf{u}) dt \wedge dx \wedge dy \wedge dz, \end{aligned}$$

we recognize that  $dm^{(3)} = 0$  described the conservation of mass in space-time, i.e.,

$$\begin{aligned} dm^{(3)} &= \left( \frac{\partial \rho}{\partial t} + \mathbf{u} \cdot \operatorname{grad} \rho + \rho \operatorname{div} \mathbf{u} \right) dt \wedge dx \wedge dy \wedge dz, \\ &= \left( \frac{\partial \rho}{\partial t} + \operatorname{div}(\rho \mathbf{u}) \right) dt \wedge dx \wedge dy \wedge dz = 0. \end{aligned}$$

By duality pairing, the exterior derivative is the formal adjoint of the boundary operator acting on manifolds, as will be shown in the next Theorem.

**Theorem 3 (Generalized Stokes' Theorem).** [2, 167] Given a  $k$ -form  $a^{(k)}$  on a (sub)-manifold  $\mathcal{M}$  of dimension  $k+1$  that is paracompact with boundary, then

$$\int_{\mathcal{M}} da^{(k)} = \int_{\partial \mathcal{M}} a^{(k)} \quad \Leftrightarrow \quad \langle \mathcal{M}, da^{(k)} \rangle = \langle \partial \mathcal{M}, a^{(k)} \rangle. \quad (4.6.4)$$

The duality pairing between the boundary operator and exterior derivative also illustrates that the exterior derivative is a metric-free and coordinate independent operator. The generalized Stokes' Theorem condenses and generalizes three key theorems of vector calculus: the classical Newton-Leibnitz, Stokes' circulation and Gauss' divergence theorems, for 3-dimensional space, when applied to 0-forms, 1-forms and 2-forms, respectively.

**Remark 3.** Another important property of the generalized Stokes' Theorem is that if  $\mathcal{M}$  and  $\tilde{\mathcal{M}}$  are two manifolds of dimension  $k+1$  with the same boundary, i.e.  $\partial \mathcal{M} \equiv \partial \tilde{\mathcal{M}}$ , we have

$$\langle \mathcal{M}, da^{(k)} \rangle = \langle \partial \mathcal{M}, a^{(k)} \rangle = \langle \partial \tilde{\mathcal{M}}, a^{(k)} \rangle = \langle \tilde{\mathcal{M}}, da^{(k)} \rangle, \quad \forall a^{(k)} \in (\Lambda^k(\mathcal{M}) \cup \Lambda^k(\tilde{\mathcal{M}})). \quad (4.6.5)$$

Another way of expressing this particular independence of the manifold is that we can always add to the manifold  $\mathcal{M}$  a manifold  $\bar{\mathcal{M}}$  with  $\partial \bar{\mathcal{M}} = 0$  without effecting any change in the generalized Stokes' Theorem. For  $k=0$ , this corresponds to the gradient theorem which states that if two points  $A$  and  $B$  are connected by a curve  $\mathcal{C}$ , then

$$\int_{\mathcal{C}} \operatorname{grad} \phi \cdot dl = \phi(B) - \phi(A). \quad (4.6.6)$$

This theorem holds for any curve connecting the points  $A$  and  $B$ , provided that the domain is contractible. There is no preferred curve and therefore is seems reasonable

to identify all curves  $\mathcal{C}$  which satisfy (4.6.6). Such an identification will be formalized in the next section.

The exterior derivative and pullback satisfy the following commuting property:

**Proposition 6.** *Given a mapping  $\Phi : \mathcal{M} \rightarrow \mathcal{N}$  and the associated pullback,  $\Phi^*$ , the exterior derivative commutes with the pullback:<sup>2</sup>*

$$\Phi^* d a^{(k)} = d \Phi^* a^{(k)}, \quad \forall a^{(k)} \in \Lambda^k(\mathcal{M}). \quad (4.6.7)$$

and is illustrated as

$$\begin{array}{ccc} \Lambda^k(\mathcal{M}) & \xrightarrow{d} & \Lambda^k(\mathcal{M}) \\ \Phi^* \downarrow & & \Phi^* \downarrow \\ \Lambda^k(\mathcal{N}) & \xrightarrow{d} & \Lambda^k(\mathcal{N}). \end{array}$$

*Proof.* For all  $(k+1)$ -dimensional sub-manifolds  $\mathcal{S}$  in  $\mathcal{M}$ , we have

$$\langle \mathcal{S}, \Phi^* d a^{(k)} \rangle \stackrel{(4.4.5)}{=} \langle \Phi \mathcal{S}, d a^{(k)} \rangle \stackrel{(4.6.4)}{=} \langle \partial \Phi \mathcal{S}, a^{(k)} \rangle \stackrel{(4.1.2)}{=} \langle \Phi \partial \mathcal{S}, a^{(k)} \rangle = \langle \mathcal{S}, d \Phi^* a^{(k)} \rangle.$$

Since  $\mathcal{S}$  was completely arbitrary and it needs to hold for all  $a^{(k)} \in \Lambda^k(\mathcal{M})$ , we have  $\Phi^* d = d \Phi^*$ . See [69, 176] for alternative proofs.  $\square$

From Definition 18 the  $(n+1)$ -spaces of differential forms satisfy the following sequence, called the *de Rham complex*, denoted by  $(\Lambda, d)$ :

$$\mathbb{R} \hookrightarrow \Lambda^0(\mathcal{M}) \xrightarrow{d} \Lambda^1(\mathcal{M}) \xrightarrow{d} \cdots \xrightarrow{d} \Lambda^n(\mathcal{M}) \xrightarrow{d} 0. \quad (4.6.8)$$

This sequence is *exact* on contractible domains, as will be shown in Section 4.9.

## 4.7 Hodge star operator, inner product and Hilbert spaces

The exterior derivative, wedge product and the operators related to mappings onto different manifolds are topological operators that do not require any metric structure. To perform physical relevant calculations, we assume that  $\mathcal{M} \subset \mathbb{R}^n$  is a smooth Riemannian manifold and that the spaces  $\Lambda^k(\mathcal{M})$  are endowed with an inner product. The inner product between  $k$ -forms can be defined in the following way:

**Definition 19 (Inner product  $k$ -forms).** [2, 103, 130, 167] *The space of  $k$ -forms,  $\Lambda^k(\mathcal{M})$ , can be equipped with a pointwise positive-definite inner product,  $(\cdot, \cdot) : \Lambda^k(\mathcal{M}) \times \Lambda^k(\mathcal{M})$ , such that:*

$$(a_1^{(1)} \wedge \cdots \wedge a_k^{(1)}, b_1^{(1)} \wedge \cdots \wedge b_k^{(1)}) := \det \left\{ \begin{bmatrix} (a_1^{(1)}, b_1^{(1)}) & \cdots & (a_k^{(1)}, b_1^{(1)}) \\ \vdots & \ddots & \vdots \\ (a_1^{(1)}, b_k^{(1)}) & \cdots & (a_k^{(1)}, b_k^{(1)}) \end{bmatrix} \right\},$$

---

<sup>2</sup>Note that on the left hand side of this equation we consider the pullback of a  $(k+1)$ -form, whereas on the right hand side the pullback of a  $k$ -form. We could have written this as  $\Phi_{k+1}^* d_k a^{(k)} = d_k \Phi_k^* a^{(k)}$ . In order to improve readability and knowing that the meaning of these operators is clear from the context we do not explicitly denote this.

---

where  $a_i^{(1)}, b_j^{(1)} \in \Lambda^1(\mathcal{M})$ ,  $i, j = 1, \dots, k$  and  $(a_i^{(1)}, b_j^{(1)})$  is the inner product of 1-forms, induced by the inner product on tangent vectors and by the duality pairing between vectors and 1-forms.

The Hodge star operator is an operator that maps a  $k$ -form associated with an inner-oriented manifold onto a  $(n - k)$ -form associated with an outer-oriented manifold, and vice versa. The associations with oriented manifolds follow from the duality pairing (4.4.4). Moreover, the Hodge star is constructed using the inner product, Definition 19, which makes it a metric operator, and the wedge product, Definition 11, which causes the change in sign of orientation (not the type of orientation). The Hodge star operator is then defined in the following way.

**Definition 20 (Hodge star operator).** [2, 69] The Hodge star operator in an  $n$ -dimensional manifold  $\mathcal{M}$  is an operator,  $\star : \Lambda^k(\mathcal{M}) \rightarrow \Lambda^{n-k}(\mathcal{M})$ , induced by the inner product (metric) and wedge product (orientation),

$$a^{(k)} \wedge \star b^{(k)} := (a^{(k)}, b^{(k)})\sigma^{(n)}, \quad (4.7.1)$$

where  $\sigma^{(n)}$  is the unit volume form, see Definition 12. Application of the Hodge star to the unit 0-form yields  $\star 1 := \sigma^{(n)}$ .

For  $f, g \in C^\infty(\mathcal{M})$  and  $a^{(k)}, b^{(k)} \in \Lambda^k(\mathcal{M})$  the Hodge star operator satisfies, [130]

$$\star(fa^{(k)} + gb^{(k)}) = f\star a^{(k)} + g\star b^{(k)}, \quad (4.7.2a)$$

$$\star\star a^{(k)} = (-1)^{k(n-k)}a^{(k)}, \quad (4.7.2b)$$

$$a^{(k)} \wedge \star b^{(k)} = b^{(k)} \wedge \star a^{(k)} = (a^{(k)}, b^{(k)})\sigma^{(n)}, \quad (4.7.2c)$$

$$(\star a^{(k)}, \star b^{(k)}) = (a^{(k)}, b^{(k)}), \quad (4.7.2d)$$

and on a canonical basis we have

$$\star(dx^{i_1} \wedge \dots \wedge dx^{i_k}) = dx^{i_{k+1}} \wedge \dots \wedge dx^{i_n}. \quad (4.7.3)$$

**Example 11.** In  $\mathbb{R}^2$  we have that,  $\star 1 = dx \wedge dy$ ,  $\star dx = dy$ ,  $\star dy = -dx$  and  $\star(dx \wedge dy) = 1$ .

Both inner- and outer-oriented spaces of differential forms,  $\Lambda^k(\mathcal{M})$  and  $\tilde{\Lambda}^k(\mathcal{M})$ , possess a de Rham sequence (4.6.8). The two are connected by the Hodge star operator, and constitute a double de Rham complex,

$$\begin{array}{ccccccccc} \mathbb{R} & \longrightarrow & \Lambda^0(\mathcal{M}) & \xrightarrow{d} & \Lambda^1(\mathcal{M}) & \xrightarrow{d} & \dots & \xrightarrow{d} & \Lambda^n(\mathcal{M}) & \xrightarrow{d} & 0 \\ & & \star \uparrow & & \star \uparrow & & & & \star \uparrow & & \\ 0 & \xleftarrow{d} & \tilde{\Lambda}^n(\mathcal{M}) & \xleftarrow{d} & \tilde{\Lambda}^{n-1}(\mathcal{M}) & \xleftarrow{d} & \dots & \xleftarrow{d} & \tilde{\Lambda}^0(\mathcal{M}) & \longleftarrow & \mathbb{R}, \end{array} \quad (4.7.4)$$

where the tildes denote spaces associated with inner-oriented manifolds and without tildes with outer-oriented manifolds. Observe the similarity between this diagram and Figure 1.1, which is due to the fact that the exterior derivative is the formal adjoint of the boundary operator through the generalized Stokes Theorem, Theorem 3. Next consider the map  $\Phi : \mathcal{M} \rightarrow \mathcal{N}$ . How does the Hodge star transform under this mapping? Since the Hodge star is metric dependent, in general it does not commute with the pullback.

**Proposition 7 (Transformation of the Hodge star operator).** [30] If  $a^{(k)} \in \Lambda^k(\mathcal{N})$ ,  $\Phi^* a^{(k)} \in \Lambda^k(\mathcal{M})$  and  $\Phi : \mathcal{M} \rightarrow \mathcal{N}$ , then the Hodge star operator in  $\mathcal{M}$ , denoted  $\hat{\star} : \Lambda^k(\mathcal{M}) \rightarrow \Lambda^{n-k}(\mathcal{M})$ , is given by:

$$\hat{\star} \Phi^* = \Phi^* \star \quad \Leftrightarrow \quad \hat{\star} = \Phi^* \star (\Phi^*)^{-1}. \quad (4.7.5)$$

This can be illustrated as

$$\begin{array}{ccc} \Lambda^k(\mathcal{N}) & \xrightarrow{\star} & \Lambda^{n-k}(\mathcal{N}) \\ \downarrow \Phi^* & & \downarrow \Phi^* \\ \Lambda^k(\mathcal{M}) & \xrightarrow{\hat{\star}} & \Lambda^{n-k}(\mathcal{M}), \end{array}$$

where the diagram commutes.

When considering some basic mappings, we see that translation and rotation are exceptions in that in these cases the Hodge star does commute with the pullback, while for stretching and shear indeed the Hodge star and pullback do not commute.

Sobolev spaces and Hilbert spaces play an important role in the analysis of numerical methods. On an oriented Riemannian manifold, we can define Hilbert spaces for differential forms, [163]. Let all  $f_I(\mathbf{x})$  in (4.3.4) be functions in  $L^2(\mathcal{M})$ , then  $a^{(k)}$  in (4.3.4) is a  $k$ -form in the Hilbert space  $L^2 \Lambda^k(\mathcal{M}) \supset \Lambda^k(\mathcal{M})$ , where the corresponding  $L^2$ -inner product is defined as follows:

**Definition 21 ( $L^2$ -inner product).** [2] The space of  $k$ -forms,  $\Lambda^k(\mathcal{M})$  is endowed with an  $L^2$ -inner product,  $(\cdot, \cdot)_{\mathcal{M}} : L^2 \Lambda^k(\mathcal{M}) \times L^2 \Lambda^k(\mathcal{M}) \rightarrow \mathbb{R}$ , given by:

$$(a^{(k)}, b^{(k)})_{\mathcal{M}} := \int_{\mathcal{M}} (a^{(k)}, b^{(k)}) \sigma^{(n)} = \int_{\mathcal{M}} a^{(k)} \wedge \star b^{(k)}. \quad (4.7.6)$$

In case we consider the map  $\Phi : \mathcal{M} \rightarrow \mathcal{N}$ , applying the pullback results in,

$$\int_{\Phi(\mathcal{M})} (a^{(k)}, b^{(k)}) \sigma^{(n)} = \int_{\mathcal{M}} (\Phi^* a^{(k)}, \Phi^* b^{(k)}) \Phi^* \sigma^{(n)}. \quad (4.7.7)$$

In physical problems, the Hodge star is associated to a constitutive relation, [174]. Think of the relation between temperature and internal energy. Then the Hodge star is  $\star_{c_v}$ , which includes the heat capacity  $c_v$  as a weight factor. This weight factor may also be tensorial. The weighted Hodge star induces a weighted  $L^2$ -inner product.

**Definition 22 (Weighted  $L^2$ -inner product).** Let  $\mathbb{K}(\mathbf{x})$  be a location dependent symmetric positive definite tensor, that is, for some  $0 < k_0 \leq k_1 < \infty$ ,

$$k_0 \|\boldsymbol{\xi}\|^2 \leq \boldsymbol{\xi}^T \mathbb{K}(\mathbf{x}) \boldsymbol{\xi} \leq k_1 \|\boldsymbol{\xi}\|^2, \quad \forall \mathbf{x} \in \mathcal{M}, \quad \forall \boldsymbol{\xi} \in \mathbb{R}^n,$$

then we define a weighted  $L^2$ -inner products as,

$$(a^{(k)}, b^{(k)})_{\mathbb{K}, \mathcal{M}} := \int_{\mathcal{M}} a^{(k)} \wedge \star_{\mathbb{K}} b^{(k)}. \quad (4.7.8)$$

The norm corresponding to the space  $L^2\Lambda^k(\mathcal{M})$  is  $\|a^{(k)}\|_{L^2\Lambda^k} = \sqrt{(a^{(k)}, a^{(k)})_{\mathcal{M}}}$  or simply  $\|a^{(k)}\|$ . Higher degree Sobolev spaces,  $H^m\Lambda^k$ , consists of all  $k$ -forms as in (4.3.4) where  $f_I(\mathbf{x}) \in H^m(\mathcal{M})$ , with corresponding norms  $|a^{(k)}|_{H^m\Lambda^k}$  and  $\|a^{(k)}\|_{H^m\Lambda^k}$ . The Hilbert space associated to the exterior derivative  $H\Lambda^k(\mathcal{M})$  is defined as

$$H\Lambda^k(\mathcal{M}) := \{a^{(k)} \in L^2\Lambda^k(\mathcal{M}) \mid da^{(k)} \in L^2\Lambda^{k+1}(\mathcal{M})\}. \quad (4.7.9)$$

and the norm corresponding to  $H\Lambda^k(\mathcal{M})$  is defined as  $\|a^{(k)}\|_{H\Lambda^k}^2 := \|a^{(k)}\|_{L^2\Lambda^k}^2 + \|da^{(k)}\|_{L^2\Lambda^{k+1}}^2$ . The  $H\Lambda^k$ -semi-norm is the  $L^2$ -norm of the exterior derivative,  $|a^{(k)}|_{H\Lambda^k} = \|da^{(k)}\|_{L^2\Lambda^{k+1}}$ . Note that  $H^1\Lambda^k(\mathcal{M}) \subseteq H\Lambda^k(\mathcal{M}) \subseteq L^2\Lambda^k(\mathcal{M})$ , where the left equality holds for  $k = 0$  and the right for  $k = n$ . The  $L^2$ -de Rham complex, also called *Hilbert complex* [38],  $(H\Lambda, d)$ , is the exact sequence of maps and spaces given by

$$\mathbb{R} \hookrightarrow H\Lambda^0(\mathcal{M}) \xrightarrow{d} H\Lambda^1(\mathcal{M}) \xrightarrow{d} \cdots \xrightarrow{d} H\Lambda^n(\mathcal{M}) \xrightarrow{d} 0. \quad (4.7.10)$$

Since the range of the exterior derivative is closed in  $L^2\Lambda^k(\mathcal{M})$ , the  $(H\Lambda, d)$  complex is a closed Hilbert complexes, [8, 9, 37]. In vector calculus the Hilbert complex  $(H\Lambda, d)$  has an equivalent complex in  $\mathcal{M} \subset \mathbb{R}^3$ ,

$$H^1(\mathcal{M}) \xrightarrow{\text{grad}} H(\text{curl}, \mathcal{M}) \xrightarrow{\text{curl}} H(\text{div}, \mathcal{M}) \xrightarrow{\text{div}} L^2(\mathcal{M}), \quad (4.7.11)$$

and for  $\mathcal{M} \subset \mathbb{R}^2$ , either

$$H^1(\mathcal{M}) \xrightarrow{\text{grad}} H(\text{rot}, \mathcal{M}) \xrightarrow{\text{rot}} L^2(\mathcal{M}), \quad \text{or} \quad H(\text{curl}, \mathcal{M}) \xrightarrow{\text{curl}} H(\text{div}, \mathcal{M}) \xrightarrow{\text{div}} L^2(\mathcal{M}). \quad (4.7.12)$$

The two are related by the Hodge star operator, Definition 20, see [138],

$$\begin{array}{ccc} H\Lambda^0(\mathcal{M}) \xrightarrow{d} H\Lambda^1(\mathcal{M}) \xrightarrow{d} L^2\Lambda^2(\mathcal{M}) & \Leftrightarrow & H(\text{curl}, \mathcal{M}) \xrightarrow{\text{curl}} H(\text{div}, \mathcal{M}) \xrightarrow{\text{div}} L^2(\mathcal{M}) \\ \star \uparrow & \star \uparrow & \star \uparrow \quad \star \downarrow & \star \uparrow & \star \downarrow \\ L^2\Lambda^2(\mathcal{M}) \xleftarrow{d} H\Lambda^1(\mathcal{M}) \xleftarrow{d} H\Lambda^0(\mathcal{M}) & & L^2(\mathcal{M}) \xleftarrow{\text{rot}} H(\text{rot}, \mathcal{M}) \xleftarrow{\text{grad}} H^1(\mathcal{M}) \end{array} \quad (4.7.13)$$

A similar double Hilbert complex can be constructed in  $\mathbb{R}^3$ . Again note the similarities with these double Hilbert complexes and that of (4.7.4) and geometric structure depicted in Figures 1.1 and 2.1.

**Remark 4.** *The upper complex in (4.7.13) is associated with outer-oriented  $k$ -forms, i.e.  $k$ -forms that are associated with outer-oriented manifolds, and the lower complex is associated with inner-oriented  $k$ -forms.*

The discussion on Sobolev spaces and Hilbert complexes can be extended to the boundary of the manifold,  $\partial\mathcal{M}$ . For Hilbert spaces with essential boundary conditions we write,

$$H_0\Lambda^k(\Omega) := \{a^{(k)} \in H\Lambda^k(\Omega) \mid \text{tr } a^{(k)} = 0\},$$

with  $\text{tr} : H\Lambda^k(\mathcal{M}) \rightarrow H^{-\frac{1}{2}}\Lambda^k(\partial\mathcal{M})$  and for natural boundary conditions we consider the following trace map,  $\text{tr } \star : H\Lambda^k(\mathcal{M}) \rightarrow H^{-\frac{1}{2}}\Lambda^{n-k}(\partial\mathcal{M})$ . For more details, we refer to Section 3.2 in Kurz and Auchmann, [116], which gives an excellent overview, mainly based on the work of Buffa and coworkers (see references therein).

Finally, as any subcomplex of a Hilbert complex is again a Hilbert complex, [8], the finite dimensional framework we construct in the next three chapters inherits the same cohomology structures as the continuous representation described above. This is called the *subcomplex property*.

## 4.8 Codifferential and Hodge-Laplacian

The formal Hilbert adjoint of the exterior derivative is a metric dependent differential operator defined as follows.

**Definition 23 (The codifferential operator).** [71] *The codifferential operator,  $d^* : H^* \Lambda^k(\mathcal{M}) \rightarrow L^2 \Lambda^{k-1}(\mathcal{M})$ , where*

$$H^* \Lambda^k(\mathcal{M}) := \{a^{(k)} \in L^2 \Lambda^k(\mathcal{M}) \mid d^* a^{(k)} \in L^2 \Lambda^{k-1}(\mathcal{M})\}, \quad (4.8.1)$$

*is an operator that is the formal Hilbert adjoint of the exterior derivative, with respect to the  $L^2$ -inner product (4.7.6): for all  $a^{(k-1)} \in H_0 \Lambda^{k-1}(\mathcal{M})$  and  $b^{(k)} \in H^* \Lambda^k(\mathcal{M})$ ,*

$$(da^{(k-1)}, b^{(k)})_{\mathcal{M}} = (a^{(k-1)}, d^* b^{(k)})_{\mathcal{M}}. \quad (4.8.2)$$

**Proposition 8.** *If  $a^{(k-1)} \in H_0 \Lambda^{k-1}(\mathcal{M})$ ,  $b^{(k)} \in H^* \Lambda^k(\mathcal{M})$ , then*

$$\int_{\mathcal{M}} d(a^{(k-1)} \wedge \star b^{(k)}) = \int_{\partial \mathcal{M}} \text{tr}(a^{(k-1)} \wedge \star b^{(k)}) = 0, \quad (4.8.3)$$

*and so for all  $b^{(k)} \in H^* \Lambda^k(\mathcal{M})$ ,*

$$\star d^* b^{(k)} = (-1)^k d \star b^{(k)} \Leftrightarrow d^* b^{(k)} = (-1)^{n(k+1)+1} \star d \star b^{(k)}. \quad (4.8.4)$$

*Proof.* The proof follows directly from the integrals:

$$(da^{(k-1)}, b^{(k)})_{\mathcal{M}} \stackrel{(4.7.6)}{=} \int_{\mathcal{M}} da^{(k-1)} \wedge \star b^{(k)} \stackrel{(4.6.2)}{=} \int_{\mathcal{M}} d(a^{(k-1)} \wedge \star b^{(k)}) - (-1)^{k-1} \int_{\mathcal{M}} a^{(k-1)} \wedge d \star b^{(k)}.$$

The first term on the right is zero, see (4.8.3), and the second one is simply:

$$-(-1)^{k-1} \int_{\mathcal{M}} a^{(k-1)} \wedge d \star b^{(k)} \stackrel{(4.7.2b)}{=} \int_{\mathcal{M}} a^{(k-1)} \wedge \star [(-1)^{n(k+1)+1} \star d \star] b^{(k)} \stackrel{(4.7.6)}{=} (a^{(k-1)}, d^* b^{(k)})_{\mathcal{M}}.$$

□

**Corollary 3 (Integration by parts).** *For all  $a^{(k-1)} \in H \Lambda^{k-1}(\mathcal{M})$  and  $b^{(k)} \in H^* \Lambda^k(\mathcal{M})$ ,*

$$(a^{(k-1)}, d^* b^{(k)})_{\mathcal{M}} = (da^{(k-1)}, b^{(k)})_{\mathcal{M}} - \int_{\partial \mathcal{M}} \text{tr} a^{(k-1)} \wedge \text{tr} \star b^{(k)}. \quad (4.8.5)$$

**Corollary 4 (Weighted codifferential).** *Let  $\mathbb{K}$  and  $\mathbb{L}$  be two location dependent symmetric positive definite weight tensors. If  $c^{(k-1)} = d_{\mathbb{KL}-1}^* b^{(k)}$ , with  $d_{\mathbb{KL}-1}^* = (-1)^{n(k+1)+1} \star_{\mathbb{K}} d \star_{\mathbb{L}}$ , then the codifferential  $d_{\mathbb{KL}-1}^*$  is the formal adjoint of the exterior derivative with respect to the weighted  $L^2$ -inner products,*

$$(a^{(k-1)}, c^{(k-1)})_{\mathbb{L}, \mathcal{M}} = (a^{(k-1)}, d_{\mathbb{KL}-1}^* b^{(k)})_{\mathbb{L}, \mathcal{M}} = (da^{(k-1)}, b^{(k)})_{\mathbb{K}, \mathcal{M}}. \quad (4.8.6)$$

---

**Proposition 9 (Nilpotency of codifferential).** *The codifferential satisfies*

$$d^* d^* a^{(k)} = 0, \quad \forall a^{(k)} \in H^* \Lambda^k(\mathcal{M}). \quad (4.8.7)$$

*Proof.* It follows directly from (4.8.4), (4.7.2b) and (4.6.3).  $\square$

Due to Proposition 9, there exists an equivalent Hilbert complex for the codifferential  $(H^* \Lambda, d^*)$ , where the  $(n+1)$ -spaces of differential forms satisfy the following sequence:

$$0 \xleftarrow{d^*} H^* \Lambda^0(\mathcal{M}) \xleftarrow{d^*} H^* \Lambda^1(\mathcal{M}) \xleftarrow{d^*} \cdots \xleftarrow{d} H^* \Lambda^n(\mathcal{M}) \hookrightarrow \mathbb{R}. \quad (4.8.8)$$

Alternative to the interpretation given to the two complexes in (4.7.12) in the previous section, we can say that one is isomorphic to the  $(H\Lambda, d)$  complex, while the other is isomorphic to the  $(H^* \Lambda, d)$  complex.

**Definition 24 (Hodge-Laplace operator).** [2, 41] *The Hodge-Laplace operator,  $\Delta : H^2 \Lambda^k(\mathcal{M}) \rightarrow L^2 \Lambda^k(\mathcal{M})$ , is a composition of the exterior derivative and the codifferential operator and is given by*

$$-\Delta a^{(k)} := (d^* d + dd^*) a^{(k)}, \quad \forall a^{(k)} \in H^2 \Lambda^k(\mathcal{M}). \quad (4.8.9)$$

**Proposition 10 (Self-adjointness).** *Under the conditions of (4.8.3) the Hodge-Laplacian satisfies:*

$$(\Delta a^{(k)}, b^{(k)})_{\mathcal{M}} = (a^{(k)}, \Delta b^{(k)})_{\mathcal{M}},$$

i.e.  $\Delta^* = \Delta$ . The Hodge-Laplace operator is self adjoint. Moreover  $(\Delta a^{(k)}, a^{(k)})_{\mathcal{M}} \geq 0$ .

*Proof.* Self-adjointness follows directly from the definition of the Hodge-Laplacian (4.8.9) and (4.8.2). If we choose  $b^{(k)} = a^{(k)}$ . As intermediate step for the proof we find

$$(\Delta a^{(k)}, a^{(k)})_{\mathcal{M}} = (da^{(k)}, da^{(k)})_{\mathcal{M}} + (d^* a^{(k)}, d^* a^{(k)})_{\mathcal{M}} = \|da^{(k)}\|^2 + \|d^* a^{(k)}\|^2 \geq 0.$$

$\square$

## 4.9 Hodge decomposition

In the following definition we will split the space  $L^2 \Lambda^k(\mathcal{M})$ ,  $H\Lambda^k(\mathcal{M})$  and  $H^* \Lambda^k(\mathcal{M})$  into a set of subspaces resulting from the action of the exterior derivative and codifferential. These decompositions are known as *Hodge decompositions* or Helmholtz decompositions as they are called in vector calculus. These give additional structure to the actions of the exterior derivative and codifferential and they show that these mappings are a bijections.

**Definition 25.** A differential form  $a^{(k)}$  is called exact if there exists a differential form  $b^{(k-1)}$  such that  $a^{(k)} = db^{(k-1)}$ . The space of exact  $k$ -forms is the range of the exterior derivative, i.e.

$$\mathcal{B}^k := dH\Lambda^{k-1}(\mathcal{M}) \subset L^2 \Lambda^k(\mathcal{M}).$$

---

A differential form  $a^{(k)}$  is called closed if  $\mathrm{d}a^{(k)} = 0$ . The space of closed  $k$ -forms is the nullspace or kernel of the exterior derivative, i.e.

$$\mathcal{Z}^k := \{\forall a^{(k)} \in H\Lambda^k(\mathcal{M}) \mid \mathrm{d}a^{(k)} = 0\} \subset L^2\Lambda^k(\mathcal{M}).$$

It follows from (4.6.3) that all exact differential forms are closed,  $\mathcal{B}^k \subseteq \mathcal{Z}^k$ . The reverse is only true on contractible manifolds, and is known as Poincaré lemma.

**Lemma 1 (Poincaré Lemma).** [2] On a contractible manifold all closed differential forms are exact, so  $\mathcal{Z}^k = \mathcal{B}^k$ . That is,

For all  $a^{(k)} \in \mathcal{Z}^k$ , there exists  $b^{(k-1)} \in H\Lambda^{k-1}(\mathcal{M})$  such that  $a^{(k)} = \mathrm{d}b^{(k-1)}$ .

The Poincaré Lemma shows the existence of potentials. They appear in both fluid dynamics and electromagnetism. In fluid dynamics we identify the velocity potential  $\phi$  and stream vector  $\vec{\psi}$  (or stream function in 2D) as the potentials corresponding to irrotational and incompressible flow, respectively,

$$\begin{aligned} \text{irrotational flow : } \vec{\omega} &= \mathrm{curl} \vec{u} = 0 & \Rightarrow & \text{there exists } \phi \text{ s.t. } \vec{u} = \mathrm{grad} \phi, \\ \text{incompressible flow : } \mathrm{div} \vec{u} &= 0 & \Rightarrow & \text{there exists } \vec{\psi} \text{ s.t. } \vec{u} = \mathrm{curl} \vec{\psi}. \end{aligned}$$

Similarly, in electromagnetism the Poincaré Lemma guarantees the existence of the electric scalar potential and the magnetic vector potential,

$$\begin{aligned} \text{electric potential } \mathrm{curl} \vec{E} &= 0 & \Rightarrow & \text{there exists } \phi \text{ s.t. } \vec{E} = \mathrm{grad} \phi, \\ \text{magnetic potential } \mathrm{div} \vec{B} &= 0 & \Rightarrow & \text{there exists } \vec{A} \text{ s.t. } \vec{B} = \mathrm{curl} \vec{A}. \end{aligned}$$

In Minkowski space there exists the electromagnetic four-potential, a relativistic four-vector that combines the electric and magnetic potentials.

With the introduction of the range and kernel subspaces, Definition 25, one can decompose the space of  $k$ -forms,  $L^2\Lambda^k(\mathcal{M})$ , as

$$L^2\Lambda^k(\mathcal{M}) = \mathcal{B}^k \oplus \mathcal{B}^{k,\perp}, \quad (4.9.1)$$

where  $\mathcal{B}^{k,\perp}$  is the orthogonal complement of  $\mathcal{B}^k$  in  $L^2\Lambda^k(\mathcal{M})$ . Then any  $k$ -form  $a^{(k)}$  can be written as

$$a^{(k)} = \mathrm{d}b^{(k-1)} + c^{(k)}, \quad a^{(k)} \in L^2\Lambda^k(\mathcal{M}), \quad b^{(k-1)} \in H\Lambda^{k-1}(\mathcal{M}) \quad \text{and} \quad c^{(k)} \in \mathcal{B}^{k,\perp}.$$

Alternatively, we can decompose the space of  $k$ -forms in terms of its nullspace and its orthogonal complement,

$$L^2\Lambda^k(\mathcal{M}) = \mathcal{Z}^k \oplus \mathcal{Z}^{k,\perp}. \quad (4.9.2)$$

So the exterior derivative is a bijection,  $\mathrm{d} : \mathcal{Z}^{k,\perp} \rightarrow \mathcal{B}^{k+1}$ , [71]. Therefore, sequences (4.6.8) and (4.7.10) are *exact* on contractible domains, in which case  $\mathcal{B}^k = \mathcal{Z}^k$ . A useful inequality in stability analysis, that follows from the bijection of the exterior derivative, and that relates the  $H\Lambda^k$ -norm to the  $L^2\Lambda^k$ -norm, is Poincaré inequality.

**Lemma 2 (Poincaré inequality).** [8] Consider a closed Hilbert complex  $(H\Lambda, d)$ , then the exterior derivative is a bounded bijection from  $\mathcal{Z}^{k,\perp}$  to  $\mathcal{B}^{k+1}$ , and hence, by Banach's bounded inverse theorem, there exists a constant  $c_P$  such that

$$\|a^{(k)}\|_{H\Lambda^k} \leq c_P \|\mathrm{d}a^{(k)}\|_{L^2\Lambda^{k+1}}, \quad \forall a^{(k)} \in \mathcal{Z}^{k,\perp}. \quad (4.9.3)$$

**Remark 5.** The Poincaré constant can be interpreted as a measure for the operator norm of the inverse of the exterior derivative, so  $c_P = \|\mathrm{d}^{-1}\|_{\mathcal{L}(\mathcal{B}^{k+1}, \mathcal{Z}^{k,\perp})}$ .

The Poincaré lemma, Lemma 1, that states that every exact form is closed, only holds on contractible manifolds. In general we have that  $\mathcal{B}^k \subseteq \mathcal{Z}^k$ , as depicted in Figure 4.9. One can define the space of *harmonic forms* as those differential forms

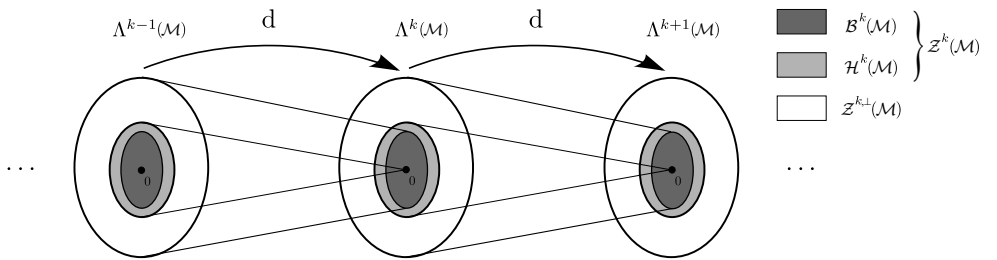


Figure 4.9: Pictorial view of de Rham complex on differential forms. The exterior derivative  $d$  maps the elements of  $H\Lambda^k$  into the kernel of  $d$  of  $L^2\Lambda^{k+1}$ ,  $\mathcal{B}^{k+1} \subset \mathcal{Z}^{k+1}$ .

which are closed, but not exact, i.e., the space of differential forms that are in the nullspace of the exterior derivative and orthogonal to the range of the previous exterior derivative,

$$\mathcal{H}^k := \mathcal{Z}^k \cap \mathcal{B}^{k,\perp} \implies \mathcal{Z}^k = \mathcal{H}^k \cup \mathcal{B}^k. \quad (4.9.4)$$

The dimension of the harmonic form space is equal to the Bettie number of the domain. So if  $\mathfrak{B}_0 = 1$ , then  $\mathcal{H}^0$  is also of dimension one. This is for example the constant level in a scalar Laplace problem with Neumann boundary conditions. Similarly, if  $\mathfrak{B}_1 = 1$ , then also  $\mathcal{H}^1$  is of dimension one. This could be the amount of circulation around an airfoil in potential flow. This harmonic function also requires an additional constraint. In this case, known as the Kutta-Joukowski condition.

From the right expression in (4.9.4) it follows that  $\mathcal{Z}^k = \mathcal{B}^k \oplus \mathcal{H}^k$ . If we combine the decomposition in (4.9.2) with (4.9.4), we obtain the following *Hodge decomposition*,

$$L^2\Lambda^k(\mathcal{M}) = \mathcal{B}^k \oplus \mathcal{H}^k \oplus \mathcal{Z}^{k,\perp}. \quad (4.9.5)$$

Note the resemblance with the decomposition of matrices, as is nicely described in [170].

Similarly we can decompose the spaces  $L^2\Lambda^k(\mathcal{M})$  and  $H^*\Lambda^k(\mathcal{M})$  into subspaces based on the action of the codifferential.

**Definition 26.** A differential form  $a^{(k)}$  is called co-exact if there exists a differential form  $b^{(k+1)}$  such that  $a^{(k)} = d^* b^{(k+1)}$ . The space of co-exact  $k$ -forms is given by

$$\mathcal{B}^{*,k} := d^* H^* \Lambda^{k+1}(\mathcal{M}) \subset L^2 \Lambda^k(\mathcal{M}).$$

A differential form  $a^{(k)}$  is called coclosed if  $d^* a^{(k)} = 0$ . The space of coclosed  $k$ -forms is given by

$$\mathcal{Z}^{*,k} := \{ \forall a^{(k)} \in H^* \Lambda^k(\mathcal{M}) \mid d^* a^{(k)} = 0 \} \subset L^2 \Lambda^k(\mathcal{M}).$$

Proposition 9 implies that  $\mathcal{B}^{*,k-1} \subseteq \mathcal{Z}^{*,k-1}$ . Only when  $\mathcal{B}^{*,k-1} = \mathcal{Z}^{*,k-1}$  the sequence in (4.8.8) is exact. So alternatively, one can decompose the space of  $k$ -forms,

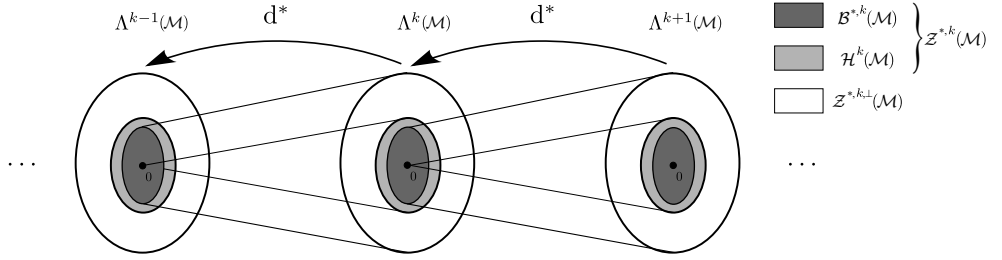


Figure 4.10: Pictorial view of the complex of differential forms acted upon by the codifferential operator. The codifferential  $d^*$  maps the elements of  $H^* \Lambda^k$  into the kernel of  $d^*$  of  $H^* \Lambda^{k-1}$ ,  $\mathcal{B}^{*,k-1} \subset \mathcal{Z}^{*,k-1}$ .

$L^2 \Lambda^k(\mathcal{M})$ , as

$$L^2 \Lambda^k(\mathcal{M}) = \mathcal{B}^{*,k} \oplus \mathcal{B}^{*,k,\perp}, \quad (4.9.6)$$

where  $\mathcal{B}^{*,k,\perp}$  is the orthogonal complement of  $\mathcal{B}^{*,k}$  in  $L^2 \Lambda^k(\mathcal{M})$ . And one can write any  $k$ -form  $a^{(k)}$  as:

$$a^{(k)} = d^* b^{(k+1)} + c^{(k)}, \quad a^{(k)} \in L^2 \Lambda^k(\mathcal{M}), \quad b^{(k+1)} \in H^* \Lambda^{k+1}(\mathcal{M}) \quad \text{and} \quad c^{(k)} \in \mathcal{B}^{*,k,\perp}.$$

The range and nullspace of the codifferential can be related to the orthogonal complements of the range and nullspace of the exterior derivative.

**Proposition 11.** If  $\text{tr } a^{(k)} = 0$  or  $\partial\mathcal{M} = \emptyset$ , then

$$\mathcal{Z}^{*,k} = \mathcal{B}^{k,\perp} \quad \text{and} \quad \mathcal{B}^{*,k} = \mathcal{Z}^{k,\perp}. \quad (4.9.7)$$

*Proof.* Take  $a^{(k)} \in \mathcal{Z}^{*,k}$ , then according to Proposition 9 we have

$$0 = \left( d^* a^{(k)}, b^{(k-1)} \right)_{\mathcal{M}} = \left( a^{(k)}, db^{(k-1)} \right)_{\mathcal{M}}, \quad \forall b^{(k-1)} \in H^* \Lambda^{k-1}(\mathcal{M}).$$

Since  $db^{(k-1)} \in \mathcal{B}^{k-1}$ , we have  $a^{(k)} \perp \mathcal{B}^{k-1}$ , i.e.  $a^{(k)} \in \mathcal{B}^{k,\perp}$ . Therefore,  $\mathcal{Z}^{*,k} \subset \mathcal{B}^{k,\perp}$ . Conversely, if  $a^{(k)} \in \mathcal{B}^{k,\perp}$ , then  $(d^* a^{(k)}, b^{(k-1)})_{\mathcal{M}} = 0$  for all  $b^{(k-1)}$  which implies that  $d^* a^{(k)} = 0$ , therefore  $\mathcal{B}^{k,\perp} \subset \mathcal{Z}^{*,k}$ . So we have  $\mathcal{B}^{k,\perp} = \mathcal{Z}^{*,k}$ . Next, for all  $a^{(k)} \in \mathcal{Z}^{*,k}$  and all  $b^{(k)} \in \mathcal{B}^{*,k}$ , i.e. there exists a  $c^{(k+1)}$  such that  $b^{(k)} = d^* c^{(k+1)}$ . Then

$$0 = \left( da^{(k)}, c^{(k+1)} \right)_{\mathcal{M}} = \left( a^{(k)}, d^* c^{(k+1)} \right)_{\mathcal{M}} = \left( a^{(k)}, b^{(k)} \right)_{\mathcal{M}}.$$

This implies that  $\mathcal{Z}^{k,\perp} = \mathcal{B}^{*,k}$ . □

Using Proposition 11 in (4.9.4) yields

$$\mathcal{H}^k = \mathcal{Z}^k \cap \mathcal{Z}^{*,k},$$

or

$$\mathcal{H}^k = \{ \forall a \in H\Lambda^k(\mathcal{M}) \mid da = 0, d^*a = 0 \}. \quad (4.9.8)$$

Harmonic forms are therefore both closed and coclosed. Using Proposition 11 and (4.9.5) allows us to write the Hodge decomposition as

$$L^2\Lambda^k(\mathcal{M}) = \mathcal{B}^k \oplus \mathcal{H}^k \oplus \mathcal{B}^{*,k}. \quad (4.9.9)$$

**Remark 6.** Note that the Hodge decomposition (4.9.5) is true, whether  $\mathcal{M}$  has a boundary or not, whereas (4.9.9) is only true if  $\partial\mathcal{M} = \emptyset$ . The Hodge decompositions in the form of (4.9.5) and (4.9.9) will play an important role in the remainder of this thesis. *Wat als  $\mathcal{B}_0^{*,k}$ ??*

**Corollary 5 (Hodge decomposition).** [2] Let  $\mathcal{M}$  be a compact boundaryless oriented Riemannian manifold. Every  $e^{(k)} \in L^2\Lambda^k(\mathcal{M})$  can be written in terms of  $a^{(k-1)} \in H\Lambda^{k-1}(\mathcal{M})$ ,  $b^{(k+1)} \in H^*\Lambda^{k+1}(\mathcal{M})$  and  $c^{(k)} \in \mathcal{H}^k$  such that

$$e^{(k)} = da^{(k-1)} + d^*b^{(k+1)} + c^{(k)}. \quad (4.9.10)$$

**Remark 7.** Let  $\mathcal{M}$  be a compact boundaryless oriented Riemannian manifold and  $c^{(k)} \in \mathcal{H}^k$ . Then it follows that  $c^{(k)}$  is the harmonic solution of the Hodge-Laplace operator,

$$(d^*c^{(k)} = 0 \text{ and } dc^{(k)} = 0) \iff \Delta c^{(k)} = 0. \quad (4.9.11)$$

**Remark 8.** Although  $da^{(k-1)}$ ,  $d^*b^{(k+1)}$  and  $e^{(k)}$  are unique, the differential forms  $a^{(k-1)}$  and  $b^{(k+1)}$  are generally not unique, because we can replace  $a^{(k-1)}$  by  $a^{(k-1)} + dp^{(k-2)}$  for any  $p^{(k-2)}$  and  $b^{(k+1)}$  by  $b^{(k+1)} + d^*q^{(k+2)}$  and this will also satisfy the Hodge decomposition.

**Remark 9.** The  $k$ -th de Rham cohomology group of  $\mathcal{M}$ ,  $H^k$ , is defined as:

$$H^k := \frac{\mathcal{Z}^k}{\mathcal{B}^k}.$$

It is possible to prove that the space of harmonic  $k$ -forms,  $\mathcal{H}^k$ , is isomorphic to the cohomology group  $H^k$ , see [2]. Moreover, the de Rham theorem, see [165], states that for a finite dimensional compact manifold this group is isomorphic to the homology group defined in algebraic topology, the isomorphism being given by integration. This connection between differential geometry and algebraic topology plays an essential role in the development of the numerical scheme presented here, since it enables the representation of differential geometric structures as finite dimensional algebraic topological structures suitable for use in the discretization process, as will be shown in the following chapters.

For a manifold with boundary, the Hodge decomposition theory takes a somewhat different form. A  $k$ -form that has a duality pairing with an inner-oriented

$k$ -dimensional manifold  $\tilde{a}^{(k)} \in \tilde{\Lambda}^k(\mathcal{M})$  is called parallel or tangent to a submanifold  $\mathcal{S} \subset \mathcal{M}$  (usually  $\mathcal{S} = \partial\mathcal{M}$ ) if  $\text{tr}_{\mathcal{M}, \mathcal{S}}(\star \tilde{a}^{(k)}) = 0$  and is called perpendicular or normal to a submanifold  $\mathcal{S}$  if  $\text{tr}_{\mathcal{M}, \mathcal{S}} \tilde{a}^{(k)} = 0$ . In this way the following spaces can be introduced

$$\tilde{\Lambda}_t^k(\mathcal{M}) = \{\tilde{a}^{(k)} \in \tilde{\Lambda}^k(\mathcal{M}) \mid \text{tr}_{\mathcal{M}, \mathcal{S}}(\star \tilde{a}^{(k)}) = 0\}, \quad (4.9.12)$$

$$\tilde{\Lambda}_n^k(\mathcal{M}) = \{\tilde{a}^{(k)} \in \tilde{\Lambda}^k(\mathcal{M}) \mid \text{tr}_{\mathcal{M}, \mathcal{S}} \tilde{a}^{(k)} = 0\}. \quad (4.9.13)$$

In the same way we define spaces with parallel and perpendicular boundary conditions for a  $k$ -form that has a duality pairing with an outer-oriented  $k$ -dimensional manifold  $a^{(k)} \in \Lambda^k(\mathcal{M})$ ,

$$\Lambda_t^k(\mathcal{M}) = \{a^{(k)} \in \Lambda^k(\mathcal{M}) \mid \text{tr}_{\mathcal{M}, \mathcal{S}} a^{(k)} = 0\}, \quad (4.9.14)$$

$$\Lambda_n^k(\mathcal{M}) = \{a^{(k)} \in \Lambda^k(\mathcal{M}) \mid \text{tr}_{\mathcal{M}, \mathcal{S}}(\star a^{(k)}) = 0\}. \quad (4.9.15)$$

Observe that writing the space of harmonic forms as  $\text{d}a^{(k)} = 0$  and  $\text{d}^*a^{(k)} = 0$  for all  $\tilde{a}^{(k)}$  is a stronger condition than  $\Delta a^{(k)} = 0$  for all  $a^{(k)}$  when  $\mathcal{M}$  has a boundary.

**Proposition 12 (Hodge decomposition theorem for manifolds with boundary).** [2] Let  $\mathcal{M}$  be a compact oriented manifold with boundary. The following decompositions hold

$$\tilde{\Lambda}^k(\mathcal{M}) = \text{d}\tilde{\Lambda}_t^{k-1}(\mathcal{M}) \oplus \tilde{\mathcal{H}}^k(\mathcal{M}) \oplus \text{d}^*\tilde{\Lambda}_n^{k+1}(\mathcal{M}), \quad (4.9.16)$$

$$\Lambda^k(\mathcal{M}) = \text{d}\Lambda_n^{k-1}(\mathcal{M}) \oplus \mathcal{H}^k(\mathcal{M}) \oplus \text{d}^*\Lambda_t^{k+1}(\mathcal{M}). \quad (4.9.17)$$

**Example 12.** For a manifold with boundary the Hodge decomposition is unique once boundary conditions are given. Different boundary conditions result in different Hodge decompositions. Consider the following decomposition,

$$\tilde{u}^{(1)} = \tilde{u}_\phi^{(1)} + \tilde{u}_\psi^{(1)} = \text{d}\tilde{\phi}^{(0)} + \text{d}^*\tilde{\psi}^{(2)}.$$

Figure 4.11 shows two Hodge-decompositions on a square domain. For the top row  $\text{tr } \tilde{u}_\phi^{(1)} = 0$  is prescribed and for the bottom row  $\text{tr } \tilde{u}_\phi^{(1)} = \text{tr } \tilde{u}^{(1)}$  is prescribed. Since the domain is contractible there exists no harmonic solution.

Zie literatuur Schwarz en Hirani + Caltech!!!

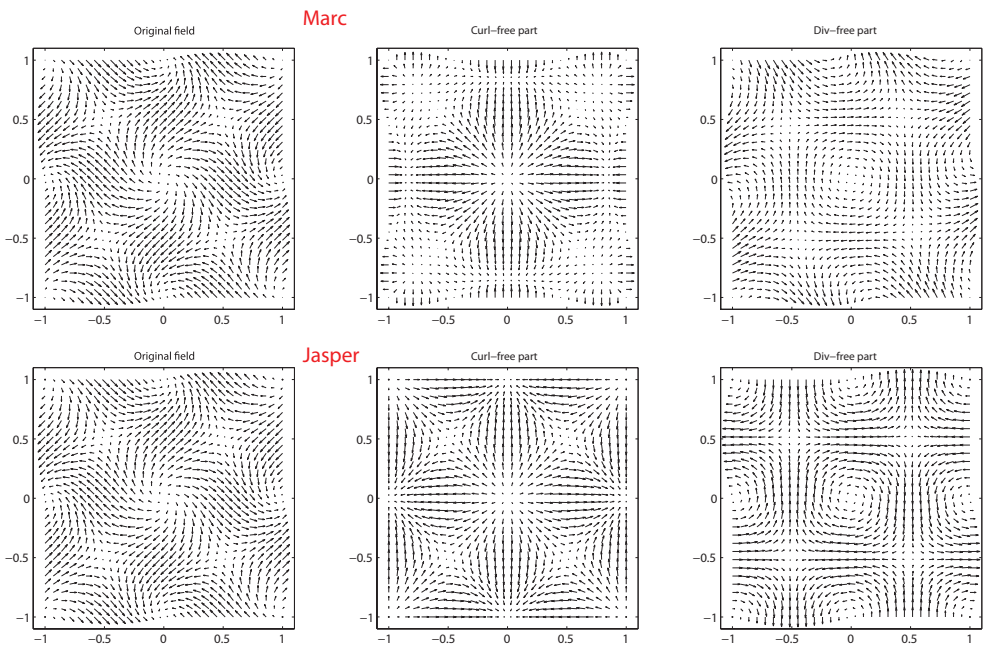


Figure 4.11: Two different Hodge-decompositions of the same vector field, but with different boundary conditions.



# Chapter 5

## Algebraic Topology

This chapter is based on Kreeft et al. [115].

*But it is evident that all analogies of this kind depend on principles of a more fundamental nature; and that, if we had a true mathematical classification of quantities, we should be able at once to detect the analogy between any system of quantities presented to us and other systems of quantities in known sciences, so that we should lose no time in availing ourselves of the mathematical labours of those who had already solved problems essentially the same. [...] At the same time, I think that the progress of science, both in the way of discovery, and in the way of diffusion, would be greatly aided if more attention were paid in a direct way to the classification of quantities.*

Maxwell, *Remarks on the Mathematical Classification of Physical Quantities*, 1871

*In the minds of some people, algebraic topology is a subject which is “esoteric, specialized, and disjoint from the overall mathematical thought.” It is the author’s fervent hope that the emphasis on the geometric motivation for the various concepts, together with the examples of the applications of the subject will help to dispel this point of view.*

William S. Massey, 1988

An important step in the our numerical framework is the discretization of a manifold (physical space) in which the physical laws are embedded. By this we mean the partitioning of a manifold in a collection of non-overlapping subspaces (cells) such that their union is a covering of the manifold under study. This partitioning into a set of distinct subspaces yields a representation of a manifold in terms of a finite number of nodes (0-cells), edges (1-cells), surfaces (2-cells), volumes (3-cells) and their  $k$ -dimensional analogues ( $k$ -cells). A collection of  $k$ -cells of such a partition is called a  $k$ -chain.

---

Several types of geometrical objects ( $k$ -cells) can be used for the subdivision. In this work we will focus on quadrilaterals, hexahedrals and their generalizations to higher dimensions, ( $k$ -cubes).

In this chapter we intend to formally introduce the representation of these collections of  $k$ -cells and to associate them with a suitable algebraic structure that enables a correct discrete representation of the original manifold. The branch of mathematics that provides such a formal discrete representation of a compact manifold is *algebraic topology*.

Having defined a discrete representation of the manifold in terms of  $k$ -chains, we can assign values to the various space elements by defining the dual space of the chains space; the so-called  *$k$ -cochains*. Duality pairing between chains and cochains allows us to introduce operations on cochains as formal adjoint of operations on chains. In this way, the introduction of operations on  $k$ -cochains mimics the operations on  $k$ -forms discussed in the previous chapter.

The main reason this introduction on algebraic topology is given here, is that we will explicitly employ the close relationship between differential geometry in a continuous setting and algebraic topology in the discrete setting in the following chapters. This relationship is also employed by many others, for instance, [18, 58, 99, 123, 174]. For a more thorough treatment of algebraic topology the reader is referred to [84, 119, 120, 132, 165].

In this thesis we assume that the dimension of all manifolds is finite and  $\dim(\mathcal{M}) = n$ .

## 5.1 Finite dimensional topology

### 5.1.1 Cell complex and boundary operator

**Definition 27 ( $k$ -cell).** [84, 132] A  $k$ -cell,  $\tau_{(k)}$ , of a manifold  $\mathcal{M}$  of dimension  $n \geq k$  is a set of points of  $\mathcal{M}$  that is homeomorphic to a closed  $k$ -ball  $B_k = \{\mathbf{x} \in \mathbb{R}^k : \|\mathbf{x}\| \leq 1\}$ .

The boundary of a  $k$ -cell  $\tau_{(k)}$ ,  $\partial\tau_{(k)}$ , is the subset of  $\mathcal{M}$  associated by the above mentioned homeomorphism to the boundary  $\partial B_k = \{\mathbf{x} \in \mathbb{R}^k : \|\mathbf{x}\| = 1\}$  of  $B_k$ .

The two most popular classes to describe the topology of a manifold are in terms of *simplices*, see for instance [132, 165, 185], and in terms of *cubes*, see [119, 120, 167, 174, 175]. From a topological point of view both descriptions are equivalent, see [57]. Despite this equivalence of simplicial complexes and cubical complexes, the reconstruction maps to be discussed in Chapter 6 differ significantly. For mimetic methods based on simplices see [6, 8, 55, 95, 152, 153], whereas for mimetic methods based on cubes see [4, 51, 24, 101, 98, 158].

First we list the terminology to set a homology theory in terms of  $k$ -cubes as given by [120].

**Definition 28 ( $k$ -cube).** [120] Consider a unit  $k$ -cube given by  $I^k = I \times I \times \cdots \times I$  ( $k$  factors,  $k \geq 0$ ), where  $I = [-1, 1]$  is a one-dimensional closed interval. By definition  $I^0$  is a space consisting of a single point. A  $k$ -cube in an  $n$ -dimensional manifold  $\mathcal{M}$  is a continuous map  $\tau_{(k)} : I^k \rightarrow \mathcal{M}$ ,  $0 \leq k \leq n$ .

**Remark 10.** With a  $k$ -cube we refer to a non-degenerate singular  $k$ -cube as defined in [120]. A (non-degenerate singular)  $k$ -cube is a  $k$ -cell as defined by Definition ??.

**Remark 11.** All  $k$ -cells are oriented. The orientation of a  $k$ -cell is implied by the orientation of the unit  $k$ -cube  $I^k$ , which is implied by the orientation of  $\mathbb{R}^k$  (see e.g. Figure 4.5), that is defined positive in positive coordinate axis direction. Then the determinant of the Jacobian of the maps  $\tau_{(k)}$  from  $I^k$  to  $\mathcal{M}$  determines the (inner) orientation of the  $k$ -cube according to Definition 7. The outer orientation then follows from Definition 9.

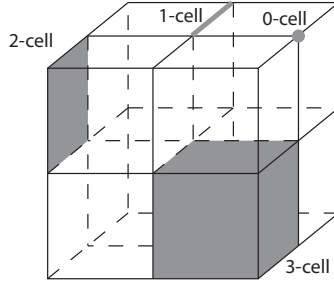


Figure 5.1: Example of a 0-cell, a 1-cell, a 2-cell and a 3-cell in  $\mathbb{R}^3$ .

Figure 5.1 depicts some examples of  $k$ -cubes in  $\mathbb{R}^3$ . The  $k$ -cubes are geometric objects which resemble the geometric objects shown in Figure 4.7.

The concept of orientation shown in Figures 1.1 and 2.1 also gives rise to the boundary operator acting on  $k$ -cells. It relates a  $k$ -cell to a set of surrounding  $(k-1)$ -cells. Before we formally define the boundary of  $k$ -cubes, we first define faces of a  $k$ -cube.

**Definition 29 (The faces of a  $k$ -cube).** [120, 167] For  $0 < k \leq n$  let  $\tau_{(k)}$  be a  $k$ -cube in  $\mathcal{M}$ . For  $i = 1, 2, \dots, k$ , we define the  $(k-1)$ -cubes  $F_i^- \tau_{(k-1)}$ ,  $F_i^+ \tau_{(k-1)} : I^{k-1} \rightarrow \mathcal{M}$ , by the formulae (face maps):

$$F_i^- \tau_{(k-1)}(x_1, x_2, \dots, x_{k-1}) = \tau_{(k)}(x_1, \dots, x_{i-1}, -1, x_i, \dots, x_{k-1}),$$

$$F_i^+ \tau_{(k-1)}(x_1, x_2, \dots, x_{k-1}) = \tau_{(k)}(x_1, \dots, x_{i-1}, +1, x_i, \dots, x_{k-1}).$$

Figure 5.2 depicts some examples of faces of  $k$ -cells with outer orientation in  $\mathbb{R}^3$ , where the faces of the  $k$ -cells are shown in black. **is dit wel een goed voorbeeld??**

**Remark 12.** Note that the face maps,  $F_i^- \tau_{(k-1)}$  and  $F_i^+ \tau_{(k-1)}$  defined in Definition 29 are inclusion maps as defined in Definition 15.

**Definition 30 (The boundary of a  $k$ -cube).** [120] The boundary  $\partial$  of a  $k$ -cube  $\tau_{(k)}$ ,  $k > 0$  is given by

$$\partial \tau_{(k)} := \sum_{i=1}^k (-1)^i [F_i^- \tau_{(k-1)} - F_i^+ \tau_{(k-1)}]. \quad (5.1.1)$$

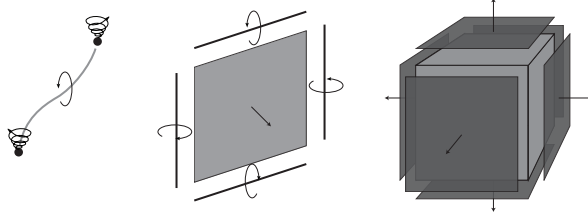


Figure 5.2: Examples of faces of a  $k$ -cell in  $\mathbb{R}^3$  with outer orientation.

**example?** This definition describes the boundary of the submanifold  $\tau_{(k)}$ , see Corollary 1 (p. 43). The collection of  $k$ -cells or  $k$ -cubes is called a cell complex.

**Definition 31 (Cell complex).** [84] A cell complex,  $D$ , in a compact manifold  $\mathcal{M}$  is a finite collection of cells with default orientation such that:

1. the set of  $n$ -cells in  $D$  covers the manifold  $\mathcal{M}$ ,
2. every face of a  $k$ -cell in  $D$  is contained in  $D$ ,
3. the intersection of any two  $k$ -cells,  $\tau_{(k)}$  and  $\sigma_{(k)}$  in  $D$  either share a common  $l$ -cell,  $l = 0, \dots, k - 1$ , is empty, or  $\tau_{(k)} = \sigma_{(k)}$ .

We call a cell complex an *oriented cell complex*, once we add to each  $k$ -cell a default orientation according to the definition of  $k$ -cubes, Definition 28. An *oriented cell-complex*  $D$  that covers the manifold  $\mathcal{M}$ , describes the topology of the computational mesh, that consists of  $k$ -cells  $\tau_{(k)}$ ,  $k = 0, \dots, n$ . In this framework we will focus on: nodes (0-cells), edges (1-cells), surfaces (2-cells), volumes (3-cells) and  $k$ -dimensional generalizations ( $k$ -cells), considered as  $k$ -cubes. Figure 5.3 depicts an example of a cell complex in a compact manifold  $\mathcal{M} \subset \mathbb{R}^3$ . Remark that the elements in a cell complex do not necessarily need to be straight orthogonal as might be suggested by Figure 5.3, but these might be curved as well. This depends on the map  $\tau_{(k)}$ .

### 5.1.2 $k$ -Chains

The above presented definitions constitute a formalization of the concept of discretization of space. The ordered collection of all  $k$ -cells in an oriented cell complex  $D$  generate a basis for the space of  $k$ -chains,  $C_k(D)$ .

**Definition 32 ( $k$ -chain).** [84, 120] Given an oriented cell complex  $D$ , the space of  $k$ -chains of  $D$ ,  $C_k(D)$ , is the free Abelian group written additively, generated by a basis consisting of all the oriented  $k$ -cells of  $D$ . A  $k$ -chain  $\mathbf{c}_{(k)}$  in  $D$  is an element of  $C_k(D)$ .

A  $k$ -chain,  $\mathbf{c}_{(k)} \in C_k(D)$ , is a collection or formal sum of  $k$ -cells,  $\tau_{(k),i} \in D$ :

$$\forall \mathbf{c}_{(k)} \in C_k(D) \Rightarrow \mathbf{c}_{(k)} = \sum_i c_i \tau_{(k),i}, \quad c_i \in \{-1, 0, 1\}, \quad \tau_{(k),i} \in D. \quad (5.1.2)$$

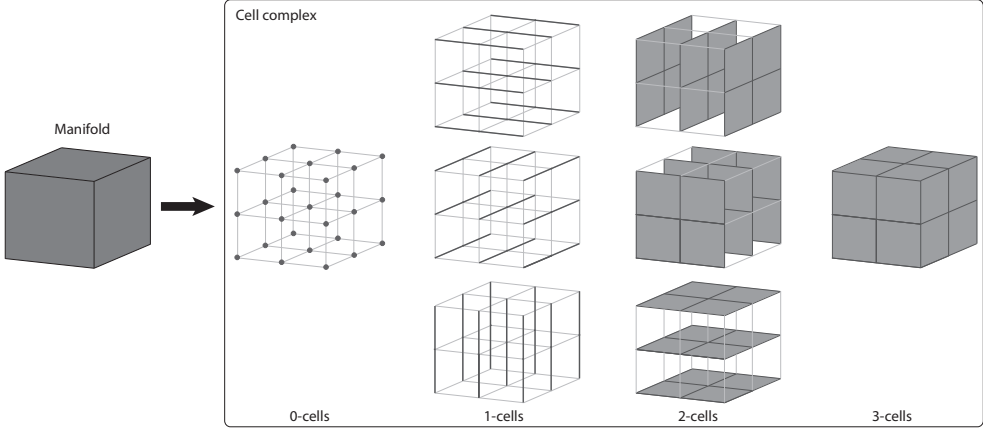


Figure 5.3: Example of a cell complex. Left: a three dimensional compact manifold. Right: the  $k$ -cells that constitute the cell complex.

The  $k$ -cells,  $\tau_{(k),i}$ , form a basis for the  $k$ -chains. Formally, given a set of  $k$ -cells, it is possible to generate any  $k$ -chain by specifying the coefficients in the chain. Although this is possible for arbitrary fields, we will, in the description of geometry, restrict ourselves mainly to chains with coefficients in  $\mathbb{Z}/3 = \{-1, 0, 1\}$ . The meaning of these coefficients is : 1 if the cell in the chain has the same orientation as its default orientation in the cell complex, -1 if the cell in the chain has the opposite orientation and 0 if the cell is not part of the chain. The orientation of the cell is imposed by the orientation of  $\mathbb{R}^k$  and the map  $\tau_k$  as pointed out in Remark 11. For an example of  $k$ -chains, see Figure 5.4.

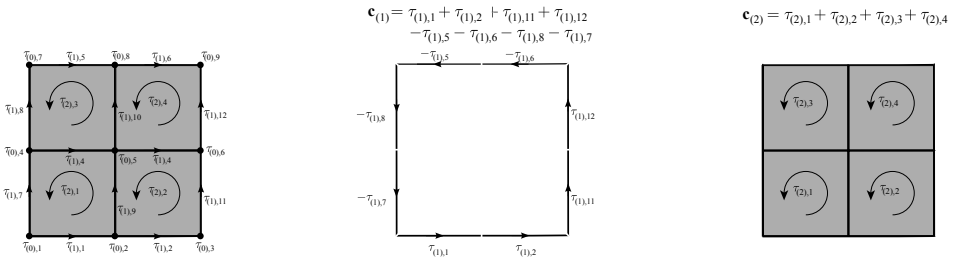


Figure 5.4: Example of a cell complex, a 1-chain and a 2-chain.

**Definition 33 (Coefficient vector for chains).** *The space of  $k$ -chains,  $C_k(D)$ , can be represented by a row vector containing only the coefficients of the chain. That is, there is an isomorphism  $\psi$  from a  $k$ -chain to a row vector:*

$$\psi : C_k(D) \mapsto \mathbb{R}^p, \quad p = \text{rank}(C_k(D)), \quad (5.1.3)$$

defined by

$$\psi(\mathbf{c}_{(k)}) = \psi\left(\sum_i^p c_i \tau_{(k),i}\right) = [c_1 \cdots c_p]^T, \quad (5.1.4)$$

where the rank of  $C_k(D)$  is the number of  $k$ -cells in the cell complex  $D$ . The  $k$ -chain,  $\mathbf{c}_{(k)}$ , is printed in boldface, whereas the vector  $\mathbf{c}_{(k)}$  of coefficients is printed in sans serif.

We can now extend the boundary operator applied to a  $k$ -cell, Definition 30, to the boundary of a  $k$ -chain.

**Definition 34 (Boundary of a  $k$ -chain).** [84, 132] The boundary operator,  $\partial : C_k(D) \rightarrow C_{k-1}(D)$ , is an homomorphism, defined by

$$\partial \mathbf{c}_{(k)} = \partial \sum_i c_i \tau_{(k),i} := \sum_i c_i \partial \tau_{(k),i}, \quad (5.1.5)$$

where the action of the boundary operator on the  $k$ -cubes is given in Definition 30.

The boundary of a  $k$ -cell  $\tau_{(k)}$  will then be a  $(k-1)$ -chain formed by the faces of  $\tau_{(k)}$ . The coefficients of this  $(k-1)$ -chain associated to each of the faces is given by the corresponding orientations:

$$\partial \tau_{(k),i} = \sum_j e_{i,j} \tau_{(k-1),j},$$

with

$$\begin{cases} e_{i,j} = 1, & \text{if the orientation of } \tau_{(k-1),j} \text{ equals the default orientation,} \\ e_{i,j} = -1, & \text{if the orientation of } \tau_{(k-1),j} \text{ is opposite to the default orientation,} \\ e_{i,j} = 0, & \text{if } \tau_{(k-1),j} \text{ is not a face of } \tau_{(k),i}. \end{cases}$$

And the boundary of a 0-cell is empty. Then the boundary operator applied to a  $k$ -chain  $\mathbf{c}_{(k)}$  gives,

$$\partial \mathbf{c}_{(k)} = \partial \left( \sum_i c_i \tau_{(k),i} \right) = \sum_i c_i \partial \tau_{(k),i} = \sum_{ij} c_i e_{i,j} \tau_{(k-1),j}. \quad (5.1.6)$$

In case all  $k$ -cells in the chain  $\mathbf{c}_{(k)}$  have positive orientation w.r.t. the default orientation, so  $c_i = 1$ , then

$$\partial \mathbf{c}_{(k)} = \sum_i \sum_j e_{i,j} \tau_{(k-1),j}.$$

**Example 13.** The boundary of the 2-cell  $\tau_{(2),1}$  in Figure 5.4 constitutes the following 1-chain:

$$\partial \tau_{(2),1} = \tau_{(1),1} + \tau_{(1),9} - \tau_{(1),4} - \tau_{(1),7}.$$

One clearly sees that, in this case, we have:  $e_{1,1} = 1$ ,  $e_{1,9} = 1$ ,  $e_{1,4} = -1$ ,  $e_{1,7} = -1$  and  $e_{1,j} = 0$  for  $j \notin \{1, 4, 7, 9\}$ .

Recalling that the space of  $k$ -chains is a linear vector space it follows that the boundary operator can be represented as a matrix acting on the column vector of the  $k$ -chain.

---

**Definition 35 (Incidence matrix for chains).** The coefficients  $e_{i,j}$  constitute a  $\text{rank}(C_k) \times \text{rank}(C_{k-1})$  incidence matrix  $E_{(k,k-1)}$  that represents the boundary operator, with  $(E_{(k,k-1)})_{i,j} = e_{i,j}$ .

**Proposition 13 (Boundary operator and incidence matrix).** Let  $\psi(\mathbf{c}_{(k)}) = \mathbf{c}_{(k)}$  be a row vector with the coefficients of the  $k$ -chain,  $\partial$  the boundary operator acting on  $k$ -chains and  $E_{(k,k-1)}$  the incidence matrix acting on a row vector of coefficients of a  $k$ -chain, then

$$\psi(\partial\mathbf{c}_{(k)}) = \psi(\mathbf{c}_{(k)})E_{(k,k-1)}. \quad (5.1.7)$$

*Proof.* This result follows directly from (5.1.6) and Definitions 33 and 35.  $\square$

An essential result that follows from the definition of the boundary operator is that applying the boundary operator twice results in a zero chain.

**Proposition 14 (The boundary of the boundary is empty).** The boundary operator satisfies:

$$\partial\partial\mathbf{c}_{(k)} = \mathbf{0}_{(k-2)}, \quad \forall \mathbf{c}_{(k)} \in C_k(D). \quad (5.1.8)$$

*Proof.* The proof follows from repeated application of Definition 30 to  $k$ -cells which extends by Definition 34 to  $k$ -chains. See also [120, 167] for this derivation.  $\square$

This is the discrete version of Corollary 2, which by the generalized Stokes' Theorem is directly related to the nilpotency of the exterior derivative. An example of Proposition 14 is illustrated in Figure 5.5.

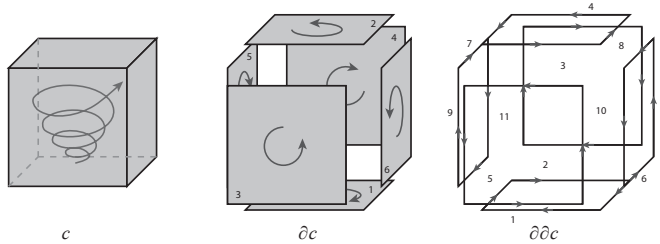


Figure 5.5: The boundary of the boundary of a 3-cell is zero because all edges have opposite orientation.

**Corollary 6.** From Propositions 13 and 14 we find that

$$\mathbf{c}_{(k+1)} E_{(k+1,k)} E_{(k,k-1)} = \mathbf{0}, \quad \forall \mathbf{c}_{(k+1)}. \quad (5.1.9)$$

**Example 14.** The property  $\partial\partial = 0$  is reflected in the incidence matrices, since they are matrix representations of the topological boundary operators. Therefore  $E_{(k,k-1)} E_{(k-1,k-2)} = 0$ , where for Figure 5.5 we have

$$E_{(3,2)} = \begin{bmatrix} -1 & 1 & -1 & 1 & -1 & 1 \end{bmatrix},$$

$$E_{(2,1)} = \begin{bmatrix} -1 & 1 & 0 & 0 & 1 & -1 & 0 & 0 & 0 & 0 & 0 & 0 \\ 0 & 0 & 1 & -1 & 0 & 0 & -1 & 1 & 0 & 0 & 0 & 0 \\ 1 & 0 & -1 & 0 & 0 & 0 & 0 & 0 & -1 & 1 & 0 & 0 \\ 0 & -1 & 0 & 1 & 0 & 0 & 0 & 0 & 0 & 0 & 1 & -1 \\ 0 & 0 & 0 & 0 & -1 & 0 & 1 & 0 & 1 & 0 & -1 & 0 \\ 0 & 0 & 0 & 0 & 0 & 1 & 0 & -1 & 0 & -1 & 0 & 1 \end{bmatrix},$$

and therefore  $E_{(3,2)}E_{(2,1)} = 0$ .

**Example 15.** Apply the boundary operator to the 2-chain in Figure 5.4:  $\mathbf{c}_{(2)} = \tau_{(2),1} + \tau_{(2),2} + \tau_{(2),3} + \tau_{(2),4}$ .

$$\begin{aligned} \partial\mathbf{c}_{(2)} &= \partial(\tau_{(2),1} + \tau_{(2),2} + \tau_{(2),3} + \tau_{(2),4}) \\ &= \tau_{(1),1} + \tau_{(1),2} + \tau_{(1),11} + \tau_{(1),12} - \tau_{(1),6} - \tau_{(1),5} - \tau_{(1),8} - \tau_{(1),7}. \end{aligned}$$

This is the 1-chain depicted in the middle in Figure 5.4. Applying the boundary operator again we get:

$$\partial\partial\mathbf{c}_{(2)} = \partial(\tau_{(1),1} + \tau_{(1),2} + \tau_{(1),11} + \tau_{(1),12} - \tau_{(1),6} - \tau_{(1),5} - \tau_{(1),8} - \tau_{(1),7}) = 0.$$

This result could also be obtained by the use of incidence matrices, since they are a matrix representation of the topological boundary operator:  $\mathbf{c}_{(2)}E_{(2,1)}E_{(1,0)} = 0$ . Consider the cell complex in Figure 5.4. The incidence matrices  $E_{(2,1)}$  and  $E_{(1,0)}$  are

$$E_{(2,1)} = \begin{bmatrix} 1 & 0 & -1 & 0 & 0 & 0 & -1 & 0 & 1 & 0 & 0 & 0 \\ 0 & 1 & 0 & -1 & 0 & 0 & 0 & -1 & 0 & 1 & 0 & 0 \\ 0 & 0 & 1 & 0 & -1 & 0 & 0 & 0 & -1 & 0 & 1 & 0 \\ 0 & 0 & 0 & 1 & 0 & -1 & 0 & 0 & 0 & -1 & 0 & 1 \end{bmatrix},$$

$$E_{(1,0)} = \begin{bmatrix} -1 & 1 & 0 & 0 & 0 & 0 & 0 & 0 & 0 & 0 & 0 & 0 \\ 0 & -1 & 1 & 0 & 0 & 0 & 0 & 0 & 0 & 0 & 0 & 0 \\ 0 & 0 & 0 & -1 & 1 & 0 & 0 & 0 & 0 & 0 & 0 & 0 \\ 0 & 0 & 0 & 0 & -1 & 1 & 0 & 0 & 0 & 0 & 0 & 0 \\ 0 & 0 & 0 & 0 & 0 & 0 & -1 & 1 & 0 & 0 & 0 & 0 \\ 0 & 0 & 0 & 0 & 0 & 0 & 0 & 0 & -1 & 1 & 0 & 0 \\ -1 & 0 & 0 & 1 & 0 & 0 & 0 & 0 & 0 & 0 & 0 & 0 \\ 0 & 0 & 0 & -1 & 0 & 0 & 0 & 1 & 0 & 0 & 0 & 0 \\ 0 & -1 & 0 & 0 & 1 & 0 & 0 & 0 & 0 & 0 & 0 & 0 \\ 0 & 0 & 0 & 0 & -1 & 0 & 0 & 0 & 1 & 0 & 0 & 0 \\ 0 & 0 & 0 & 0 & 0 & -1 & 0 & 0 & 0 & 0 & 1 & 0 \end{bmatrix},$$

which produces  $E_{(2,1)}E_{(1,0)} = \mathbf{0}$ , as expected.

### 5.1.3 Topological Hodge decomposition

**Definition 36 (Cycles and boundaries).** [175] A  $k$ -chain  $\mathbf{c}_{(k)}$  for which  $\partial\mathbf{c}_{(k)} = \mathbf{0}_{(k-1)}$  is called a cycle. A  $k$ -chain  $\mathbf{c}_{(k)}$  which is the boundary of a  $(k+1)$ -chain  $\mathbf{b}_{(k+1)}$ , i.e.  $\mathbf{c}_{(k)} = \partial\mathbf{b}_{(k+1)}$  is called a boundary. The space of  $k$ -cycles in a cell complex  $D$  is the nullspace of the boundary operator  $\partial$  in  $C_k(D)$ , which is denoted by  $Z_k(D) := \{\mathbf{c}_{(k)} \in C_k(D) \mid \partial\mathbf{c}_{(k)} = \mathbf{0}\}$ , and the space of  $k$ -boundaries is the range of  $\partial$  in  $C_k(D)$  and is denoted by  $B_k(D) = \partial C_{k+1}(D)$ .

Proposition 14 implies that every boundary is a cycle,  $B_k(D) \subset Z_k(D)$ , but the converse is generally not true. Therefore, consider the factor space  $H_k(D)$  consisting of those cycles which are not boundaries

$$H_k(D) = \frac{Z_k(D)}{B_k(D)}. \quad (5.1.10)$$

$H_k(D)$  is an equivalence class and any two cycles  $\mathbf{c}_{(k)}$  and  $\mathbf{d}_{(k)}$  that are associated with the same element whenever the difference  $\mathbf{c}_{(k)} - \mathbf{d}_{(k)}$  is a boundary.  $H_k(D)$  is

called the *homology group* and two elements which differ by a boundary are called *homologous*, [174]. In many applications,  $\dim(H_k(D))$  is finite and this dimension is called the  $k$ -th *Betti number*, see (4.1.3). Two spaces can only be topologically the same, if the their respective Betti numbers are the same. The harmonic  $k$ -chain that belongs to the space  $H_k$  is defined as

$$\mathbf{h}_{(k)} = \{\partial \mathbf{h}_{(k)} = 0 \mid \#\mathbf{a}_{(k+1)} \in C_{k+1}, \text{ such that } \mathbf{h}_{(k)} = \partial \mathbf{a}_{(k+1)}\}. \quad (5.1.11)$$

**Proposition 15 (Chain space decomposition).** *The topological Hodge decomposition of the space of  $k$ -chains or chain space decomposition is given by<sup>1</sup>*

$$C_k = B_k \oplus H_k \oplus Z_k^\perp, \quad (5.1.12)$$

where  $Z_k^\perp = C_k \setminus Z_k$  is the algebraic complement of  $Z_k$  in  $C_k$ .

**Remark 13.** Note that  $H_k$  can only be obtained from global considerations. Therefore, the decomposition  $C_k = B_k \oplus H_k \oplus Z_k^\perp$  can only be obtained globally.

From the topological Hodge decomposition, we observe that the boundary operator is a bijection that maps  $\partial : Z_k^\perp \rightarrow B_{k-1}$ .

The boundary operator induces a differential graded algebra of degree -1,  $(C_k(D), \partial)$ , called the *chain complex*.

**Definition 37 (Chain complex).** [84] A chain complex is a family  $(C_k(D), \partial)$  of  $k$ -chains and boundary operators  $\partial$ , that constitutes a sequence

$$\cdots \xleftarrow{\partial} C_{k-1}(D) \xleftarrow{\partial} C_k(D) \xleftarrow{\partial} C_{k+1}(D) \xleftarrow{\partial} \cdots. \quad (5.1.13)$$

This sequence is the algebraic equivalent of Figure 1.1. Because  $\partial$  is a bijection, this sequence is exact on contractible domains, i.e., when  $H^k(D) = \emptyset$  for all  $k$  and so  $B_k(D) = Z_k(D)$ .

**Example 16.** Consider the cell complex depicted in Figure 5.6 which contains a ‘hole’ in the middle. Its Betti number is  $\mathfrak{B} = \{1, 1, 0\}$ . In Figure 5.6 all 0-cells have positive orientation by default, i.e., all  $c_i = +1$  in (5.1.2). The orientation of the 1- and 2-cells are indicated in the figure. The incidence matrices that relate the 1-cells to the 0-cells and the 2-cells to the 1-cells, are given by

$$\mathsf{E}_{(2,1)} = \begin{bmatrix} 1 & 0 & -1 & 1 & 0 & -1 & 0 & 0 & 0 & 0 & 0 \\ 0 & -1 & 1 & 0 & 0 & 0 & 1 & 0 & 0 & 1 & 0 \\ 0 & 0 & 0 & -1 & 1 & 0 & 0 & -1 & 0 & 0 & -1 \\ 0 & 0 & 0 & 0 & 0 & 0 & 0 & 1 & -1 & 1 & -1 \end{bmatrix},$$

$$\mathsf{E}_{(1,0)} = \begin{bmatrix} -1 & 1 & 0 & 0 & 0 & 0 & 0 & 0 \\ -1 & 0 & 0 & 0 & 0 & 0 & 1 & 0 \\ -1 & 0 & 1 & 0 & 0 & 0 & 0 & 0 \\ 0 & -1 & 0 & 1 & 0 & 0 & 0 & 0 \\ 0 & -1 & 0 & 0 & 0 & 0 & 0 & 1 \\ 0 & 0 & -1 & 1 & 0 & 0 & 0 & 0 \\ 0 & 0 & -1 & 0 & 1 & 0 & 0 & 0 \\ 0 & 0 & 0 & -1 & 0 & 1 & 0 & 0 \\ 0 & 0 & 0 & 0 & -1 & 1 & 0 & 0 \\ 0 & 0 & 0 & 0 & 0 & -1 & 0 & 1 \\ 0 & 0 & 0 & 0 & 0 & 0 & -1 & 1 \end{bmatrix}.$$

<sup>1</sup> Although ‘perpendicular’ in a topological space is not well defined, we  $Z_k^\perp$  to indicate the algebraic complement of  $Z_k$  in  $C_k$ , and to emphasize the similarities with the subspaces  $\mathcal{Z}^k$  and  $\mathcal{Z}^{k,\perp}$  of differential  $k$ -forms.

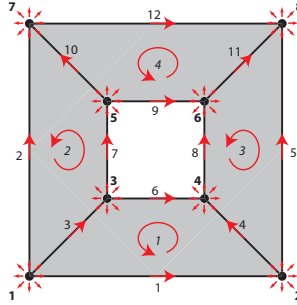


Figure 5.6: A non contractible cell complex.

The matrix  $E_{(1,0)}$  describes the connectivity between the 8 nodes and the 12 edge segments. The range of the matrix is spanned by its 12 column vectors. Not all these column vectors are linearly independent. The rank of this matrix is 7, hence the range of this matrix has dimension 7. Since the dimension of the null space of matrix  $E_{(2,1)}$  is 8, there is one element in the null space of  $E_{(2,1)}$  that is not in the range of  $E_{(1,0)}$ . This confirms that on a non-contractible domain, not every cycle is a boundary. The dimension of the homology group is in this example equal to  $8-7=1$ . This corresponds to the number of ‘holes’ in the domain (formally known as the Betti number  $\mathfrak{B}_1$ ). The harmonic chain corresponding to Figure 5.6 is given by

$$\mathbf{h}_{(1)} = [1, -1, 0, 0, 1, 1, -1, 1, -1, 0, 0, -1].$$

### 5.1.4 Chain map

In the previous section, we discussed how differential forms and operators acting on these differential forms behave under a mapping  $\Phi$ . Similar constructions are also feasible in algebraic topology. These maps are called *chain maps* and *cochain maps*.

**Definition 38 (Chain maps).** [119] Let  $\Phi : \mathcal{M} \rightarrow \mathcal{N}$  be a homeomorphism between manifolds  $\mathcal{M}$  and  $\mathcal{N}$ , then this map induces a homomorphism between  $k$ -cubes in  $\mathcal{M}$  and  $k$ -cubes in  $\mathcal{N}$  given by

$$\begin{array}{ccc} I^k & \xrightarrow{\Phi_{\sharp}(\tau_{(k)})} & C_k(D_{\mathcal{N}}) \\ \downarrow \tau_{(k)} & \nearrow \& \\ C_k(D_{\mathcal{M}}) & & \end{array}$$

where  $\Phi_{\sharp}(\tau_{(k)}) = \Phi \circ \tau_{(k)}$  for any  $k$ -cube  $\tau_{(k)} : I^k \rightarrow \mathcal{M}$ , for  $k = 0, 1, 2, \dots, n$ .  $\Phi_{\sharp}$  is extended to chains to be the homomorphism  $\Phi_{\sharp} : C_k(D_{\mathcal{M}}) \rightarrow C_k(D_{\mathcal{N}})$ , the induced chain homomorphism, by putting

$$\Phi_{\sharp}(\mathbf{c}_{(k)}) = \Phi_{\sharp} \left( \sum_i c_i \tau_{(k),i} \right) = \sum_i c_i \Phi_{\sharp}(\tau_{(k),i}).$$

It can be shown, [119], that  $\Phi_\sharp$  maps  $k$ -cubes in  $\mathcal{M}$  into  $k$ -cubes in  $\mathcal{N}$  and that the diagram

$$\begin{array}{ccc} C_{k-1}(D_{\mathcal{N}}) & \xleftarrow{\partial} & C_k(D_{\mathcal{N}}) \\ \Phi_\sharp \uparrow & & \Phi_\sharp \uparrow \\ C_{k-1}(D_{\mathcal{M}}) & \xleftarrow{\partial} & C_k(D_{\mathcal{M}}). \end{array}$$

commutes. This follows directly from the fact that the face maps, Definition 29, commute with the chain map:  $\Phi_\sharp(F_i^-\tau^k) = F_i^-(\Phi_\sharp\tau^k)$  and  $\Phi_\sharp(F_i^+\tau^k) = F_i^+(\Phi_\sharp\tau^k)$ . Therefore, we have that

$$\partial \circ \Phi_\sharp = \Phi_\sharp \circ \partial, \quad (5.1.14)$$

the chain map  $\Phi_\sharp$  commutes with the boundary operator. The image of the boundary is the boundary of the image. This is the discrete equivalent of Proposition 2 (p. 43).

Since the boundary operator,  $\partial$ , commutes with the chain map,  $\Phi_\sharp$ ,  $\Phi_\sharp$  maps the cycles  $Z_k(D_{\mathcal{M}})$  into  $Z_k(D_{\mathcal{N}})$  and the boundaries  $B_k(D_{\mathcal{M}})$  into  $B_k(D_{\mathcal{N}})$ , for all  $k = 0, \dots, n$ . Therefore, a chain map does not alter the topology. In particular, the incidence matrices for the cell complex  $D_{\mathcal{M}}$  and  $D_{\mathcal{N}}$  are identical.

## 5.2 Degrees of freedom

### 5.2.1 Cochains and coboundary operator

**Definition 39 (Cochains).** [84] The space of  $k$ -cochains,  $C^k(D)$ , is the space dual to the space of  $k$ -chains,  $C_k(D)$ , defined as the set of all the linear maps (linear functionals),  $\mathbf{c}^{(k)} : C_k(D) \rightarrow \mathbb{R}$ , and we write

$$\langle \mathbf{c}_{(k)}, \mathbf{c}^{(k)} \rangle := \mathbf{c}^{(k)}(\mathbf{c}_{(k)}) , \quad (5.2.1)$$

to represent the duality pairing.

**Remark 14.** Note the resemblance between (5.2.1) and (4.4.4). This similarity is one of the fundamental properties of the mimetic framework discussed in this thesis.

**Remark 15.** Strictly speaking  $k$ -cochains are homomorphisms from  $C_k(D)$  into  $\mathbb{R}$ :  $C^k(D) := \text{Hom}(C_k(D); \mathbb{R})$ . Since the cochain spaces are the dual spaces of the chain spaces, we might as well write  $C^k := C_k^*$ .

**Proposition 16 (Canonical basis  $k$ -cochains).** Given a basis of  $C_k(D)$ ,  $\{\tau_{(k),j}\}$  with  $j = 1, \dots, p$  with  $p = \text{rank}(C_k(D))$ , then there exists a dual basis of  $C^k(D)$ ,  $\{\tau^{(k),i}\}$ , with  $i = 1, \dots, p$ , with  $p = \text{rank}(C_k(D))$ , such that:

$$\tau^{(k),i}(\tau_{(k),j}) = \langle \tau_{(k),j}, \tau^{(k),i} \rangle = \delta_j^i . \quad (5.2.2)$$

All linear functionals can be represented as a linear combination of the basis elements:

$$\forall \mathbf{c}^{(k)} \in C^k(D) \Rightarrow \mathbf{c}^{(k)} = \sum_i c^i \tau^{(k),i} . \quad (5.2.3)$$

The proof of this proposition can be found in any book on algebraic topology, for instance, [132]. The individual coefficients of the cochain are obtained by duality pairing with a single  $k$ -cell,

$$\langle \tau_{(k),j}, \mathbf{c}^{(k)} \rangle = c^j. \quad (5.2.4)$$

**Proposition 17 (Duality pairing in terms of coefficients).** *Duality pairing of  $k$ -cochains with  $k$ -chains, (5.2.1), in terms of the coefficients, is given by*

$$\langle \mathbf{c}_{(k)}, \mathbf{c}^{(k)} \rangle = \sum_i c_i c^i. \quad (5.2.5)$$

*Proof.*

$$\langle \mathbf{c}_{(k)}, \mathbf{c}^{(k)} \rangle = \sum_i \sum_j c_j c^i \langle \tau_{(k),j}, \tau^{(k),i} \rangle \stackrel{(5.2.2)}{=} \sum_i \sum_j c_j c^i \delta_j^i = \sum_i c_i c^i.$$

□

The cochains are the discrete analogue of differential forms. With the duality relation between chains and cochains, we can define the formal adjoint of the boundary operator which constitutes a sequence on the spaces of  $k$ -cochains in the cell complex. This formal adjoint is called the coboundary operator.

**Definition 40 (Coboundary operator).** [84] *The coboundary operator,  $\delta : C^k(D) \rightarrow C^{k+1}(D)$ , is defined as the formal adjoint of the boundary operator:*

$$\langle \mathbf{c}_{(k+1)}, \delta \mathbf{c}^{(k)} \rangle := \langle \partial \mathbf{c}_{(k+1)}, \mathbf{c}^{(k)} \rangle, \quad \forall \mathbf{c}^{(k)} \in C^k(D) \text{ and } \forall \mathbf{c}_{(k+1)} \in C_{k+1}(D). \quad (5.2.6)$$

**Proposition 18.** *The coboundary operator is nilpotent,*

$$\delta \delta \mathbf{c}^{(k)} = 0, \quad \forall \mathbf{c}^{(k)} \in C^k(D). \quad (5.2.7)$$

*Proof.* The proof follows directly from Proposition 14:  $\forall \mathbf{c}^{(k)} \in C^k(D)$  and  $\forall \mathbf{c}_{(k+2)} \in C_{k+2}(D)$

$$\langle \mathbf{c}_{(k+2)}, \delta \delta \mathbf{c}^{(k)} \rangle \stackrel{(5.2.6)}{=} \langle \partial \partial \mathbf{c}_{(k+2)}, \mathbf{c}^{(k)} \rangle \stackrel{(5.1.8)}{=} 0 \implies \delta \delta \mathbf{c}^{(k)} = 0.$$

□

Proposition 18 is illustrated in Figure 5.7. The coboundary operator is directly related to the boundary operator on chains by duality pairing. Since the latter is exactly the same operator as the boundary operator on manifolds, the coboundary operator is the discrete version of the exterior derivative by the generalized Stokes' Theorem. The same holds for the nilpotency property. As a consequence there also exists a cochain complex.

**Definition 41 (Cochain complex).** [84] *A cochain complex is a family  $(C^k(D), \delta)$  of  $k$ -cochains and coboundary operators, that constitutes a sequence*

$$\cdots \xrightarrow{\delta} C^{k-1}(D) \xrightarrow{\delta} C^k(D) \xrightarrow{\delta} C^{k+1}(D) \xrightarrow{\delta} \cdots. \quad (5.2.8)$$

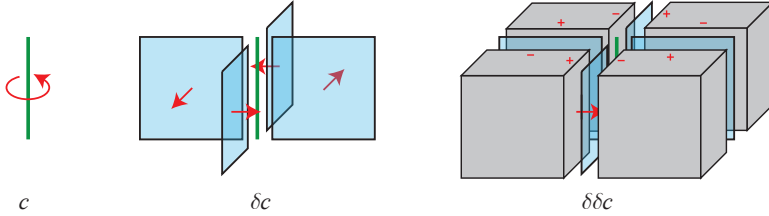


Figure 5.7: The action of twice the coboundary operator  $\delta$  on a 1-cell has a zero net result on its surrounding 3-cells, because they all have both a positive and a negative contribution from its neighboring 2-cells (reproduced from [18]).

Analogous to Definition 33, we have

**Definition 42 (Coefficient vector for cochains).** *The space of  $k$ -cochains,  $C^k(D)$ , can be represented by a column vector containing only the coefficients of the  $k$ -cochain. That is, there is an isomorphism  $\bar{\psi}$  from a  $k$ -cochain to a column vector:*

$$\bar{\psi} : C^k(D) \mapsto \mathbb{R}^p, \quad p = \text{rank}(C^k(D)), \quad (5.2.9)$$

defined by

$$\bar{\psi}(\mathbf{c}^{(k)}) = \bar{\psi}\left(\sum_i c^i \tau^{(k),i}\right) = [c^1 \dots c^p]^T. \quad (5.2.10)$$

The  $k$ -cochain,  $\mathbf{c}^{(k)}$ , is printed in boldface, whereas the vector  $\mathbf{c}^{(k)}$  of coefficients is printed in regular face.

**Proposition 19 (Incidence matrix for coboundary operator).** *Let  $\psi(\mathbf{c}_{(k)})$  and  $\bar{\psi}(\mathbf{c}^{(k)})$  be a row and a column vector, respectively, as defined in Definitions 33 and 42, and let  $\mathbf{c}_{(k)} = \partial\mathbf{b}_{(k+1)}$ . Then*

$$\bar{\psi}(\delta\mathbf{c}^{(k)}) = \mathbf{E}^{(k+1,k)} \bar{\psi}(\mathbf{c}^{(k)}), \quad (5.2.11)$$

where

$$\mathbf{E}^{(k+1,k)} = \mathbf{E}_{(k,k+1)}^T. \quad (5.2.12)$$

*Proof.* For all  $\mathbf{c}^{(k)} \in C^k(D)$  and for all  $\mathbf{b}_{(k+1)} \in C_{k+1}(D)$  we have

$$\begin{aligned} [\psi(\mathbf{b}^{(k+1)})] [\bar{\psi}(\delta\mathbf{c}^{(k)})] &\stackrel{\text{Prop. 17}}{=} \langle \mathbf{b}_{(k+1)}, \delta\mathbf{c}^{(k)} \rangle \stackrel{(5.2.6)}{=} \langle \partial\mathbf{b}_{(k+1)}, \mathbf{c}^{(k)} \rangle \stackrel{\text{Prop. 17}}{=} \\ &[\psi(\mathbf{b}_{(k+1)}) \mathbf{E}_{(k+1,k)}] [\bar{\psi}(\mathbf{c}^{(k)})] = [\psi(\mathbf{b}_{(k+1)})] [\mathbf{E}^{(k+1,k)} \bar{\psi}(\mathbf{c}^{(k)})]. \end{aligned}$$

□

The incidence matrices representing the coboundary operator only depend on the mesh topology. These matrices will explicitly appear in the final matrix systems, see (8.1.28) and (9.4.5) in Part III of this thesis.

---

**Proposition 20.** Let  $E^{(k+1,k)}$  be the incidence matrices for the coboundary operator, then

$$E^{(k+1,k)} E^{(k,k-1)} = 0 . \quad (5.2.13)$$

*Proof.*

$$E^{(k+1,k)} E^{(k,k-1)} \stackrel{\text{Prop. 19}}{=} E_{(k+1,k)} E_{(k,k-1)} \stackrel{\text{Prop. 6}}{=} 0 .$$

□

## 5.2.2 Cohain space decomposition

Recalling the duality pairing of differential forms and manifolds (4.4.4) and the duality pairing of chains and cochains (5.2.1) one clearly notices the algebraic similarity between the continuous and the discrete worlds. Expression (5.2.6) is nothing but a discrete Stokes' theorem. Also for the space of cochains we can set up a cohomology structure.

**Definition 43 (Cocycles, coboundaries and cohomologous cochains).** [174] The cochains  $c^{(k)}$  for which  $\delta c^{(k)} = 0^{(k+1)}$  are called cocycles. The set of all  $k$ -cocycles is the nullspace of  $\delta$  in  $C^k(D)$  with respect to the coboundary operator  $\delta$ , denoted by  $Z^k(D)$ . A  $k$ -cochain that can be written as the coboundary of a  $(k-1)$ -cochain,  $c^{(k)} = \delta d^{(k-1)}$ , is called a  $k$ -coboundary. The space of all  $k$ -coboundaries is the space in the range of  $\delta$ , which is denoted by  $B^k(D)$ .

**Corollary 7 (Cochain space decomposition).** From Proposition 18 it follows that  $B^k(D) \subseteq Z^k(D)$ . We therefore consider the cohomology group

$$H^k(D) = \frac{Z^k(D)}{B^k(D)} , \quad (5.2.14)$$

of all  $k$ -cocycles which are not  $k$ -coboundaries. The space  $H^k(D)$  is the topological equivalent of the space of harmonic forms  $\mathcal{H}^k(\mathcal{M})$  defined in Section ???. The space of  $k$ -cochains can be decomposed as<sup>2</sup>

$$C^k = B^k \oplus H^k \oplus Z^{k,\perp} ,$$

where  $Z^{k,\perp}$  is the algebraic complement of  $Z^k$  in  $C^k(D)$ . Compare this decomposition with the Hodge decomposition given in (4.9.5).

**Remark 16.** Note that  $\mathfrak{B}_k = \dim(\mathcal{H}^k) = \dim(H^k) = \dim(H_k)$ .

**Proposition 21 (Cochain well-posedness).** Consider the following cochain relation,  $\delta a^{(k)} = f^{(k+1)}$  with  $f^{(k+1)} \in B^{k+1}$ . Then there exists a unique solution for  $a^{(k)} \in Z^{k,\perp}$ . This implies that  $\delta$  is a bijection that maps  $Z^{k,\perp} \rightarrow B^{k+1}$ .

---

<sup>2</sup>Again, although ‘perpendicular’ in a topological space is not well defined, we write  $Z^{k,\perp}$  to indicate the algebraic complement of  $Z^k$  in  $C^k$ , and to emphasize the similarities with the subspaces  $\mathcal{Z}^k$  and  $\mathcal{Z}^{k,\perp}$  of differential  $k$ -forms.

---

*Proof.* There exists a solution  $\mathbf{a}^{(k)}$ , because  $\mathbf{f}^{(k+1)} \in B^{k+1}$ . Now, suppose there exists two solutions,  $\mathbf{a}_1^{(k)}$  and  $\mathbf{a}_2^{(k)}$  in  $Z^{k,\perp}$ , such that  $\delta\mathbf{a}_1^{(k)} = \mathbf{f}^{(k+1)}$  and  $\delta\mathbf{a}_2^{(k)} = \mathbf{f}^{(k+1)}$ . Then  $\delta(\mathbf{a}_1^{(k)} - \mathbf{a}_2^{(k)}) = \mathbf{0}^{(k+1)}$ . Since  $\mathbf{a}_1^{(k)} - \mathbf{a}_2^{(k)} \in Z^k \cap Z^{k,\perp} = \{0\}$ , the solution for  $\delta\mathbf{a}^{(k)} = \mathbf{f}^{(k+1)}$  is unique for  $\mathbf{a}^{(k)} \in Z^{k,\perp}$ .  $\square$

Since  $\delta$  is a bijection from  $Z^{k,\perp}$  to  $B^{k+1}$ , the sequence (5.2.8) is exact on contractible domains, where  $H^k = \emptyset$  and  $Z^k = B^k$ . Note the similarities between the maps of the coboundary operator, the boundary operator on  $k$ -chains and that of the exterior derivative.

**Example 17 (Example 16 continued).** *The dimension of the cohomology is equal to the dimension of the homology due to the duality pairing. The harmonic cochain corresponding to Figure 5.6 is given by*

$$\mathbf{h}^{(1)} = \alpha [1, -1, 0, 0, 1, 1, -1, 1, -1, 0, 0, -1]^T, \quad \alpha \in \mathbb{R}.$$

*This harmonic cochain models a circulation around the hole in Figure 5.6, with strength  $\alpha$ .*

**Remark 17.** *Observe that the harmonic cochain is global. Only global considerations lead to the determination of the harmonic cochains, which is the main reason these solutions cannot be represented by local methods, such as standard finite difference, finite volume or finite element methods. In these cases a cut is made in the computational domain to make it simply connected or contractible again.*

### 5.2.3 Cochain map

**Definition 44 (Cochain map).** *Let  $\Phi_\sharp : C_k(D_{\mathcal{M}}) \rightarrow C_k(D_{\mathcal{N}})$ ,  $k = 0, 1, \dots, n$ , then for every  $k$ -cochain  $\mathbf{c}_n^{(k)} \in C^k(D_{\mathcal{N}})$ , there exists a  $k$ -cochain  $\mathbf{c}_m^{(k)} = \Phi^\sharp \mathbf{c}_n^{(k)} \in C^k(D_{\mathcal{M}})$ , with  $\Phi^\sharp : C^k(D_{\mathcal{N}}) \rightarrow C^k(D_{\mathcal{M}})$  the cochain map, such that*

$$\langle \Phi_\sharp \mathbf{c}_{(k)}, \mathbf{c}_n^{(k)} \rangle = \langle \mathbf{c}_{(k)}, \mathbf{c}_m^{(k)} \rangle := \langle \mathbf{c}_{(k)}, \Phi^\sharp \mathbf{c}_n^{(k)} \rangle, \quad \forall \mathbf{c}_{(k)} \in C_k(D_{\mathcal{M}}). \quad (5.2.15)$$

**Remark 18.** *The cochain map  $\Phi^\sharp$  satisfies  $\langle \Phi_\sharp \mathbf{c}_{(k)}, \mathbf{c}_m^{(k)} \rangle = \langle \mathbf{c}_{(k)}, \Phi^\sharp \mathbf{c}_n^{(k)} \rangle$ . Compare this relation with the duality between a space map  $\Phi$  and its pullback  $\Phi^*$  as discussed in Proposition 5.*

**Proposition 22.** *The cochain map  $\Phi^\sharp$  commutes with the coboundary operator  $\delta$ ,*

$$\delta \circ \Phi^\sharp = \Phi^\sharp \circ \delta, \quad (5.2.16)$$

$$\begin{array}{ccc} C^{k-1}(D_{\mathcal{N}}) & \xrightarrow{\delta} & C^k(D_{\mathcal{N}}) \\ \Phi^\sharp \downarrow & & \Phi^\sharp \downarrow \\ C^{k-1}(D_{\mathcal{M}}) & \xrightarrow{\delta} & C^k(D_{\mathcal{M}}). \end{array}$$

*Proof.*

$$\begin{aligned} \langle \mathbf{c}_{(k)}, \delta \Phi^\sharp \mathbf{c}^{(k)} \rangle &\stackrel{\text{Def. 40}}{=} \langle \Phi^\sharp \partial \mathbf{c}_{(k)}, \mathbf{c}^{(k)} \rangle \stackrel{\text{Def. 44}}{=} \langle \Phi_\sharp \partial \mathbf{c}_{(k)}, \mathbf{c}^{(k)} \rangle \stackrel{(5.1, 14)}{=} \langle \partial \Phi_\sharp \mathbf{c}_{(k)}, \mathbf{c}^{(k)} \rangle \\ &\stackrel{\text{Def. 40}}{=} \langle \Phi_\sharp \mathbf{c}_{(k)}, \delta \mathbf{c}^{(k)} \rangle \stackrel{\text{Def. 44}}{=} \langle \mathbf{c}_{(k)}, \Phi^\sharp \delta \mathbf{c}^{(k)} \rangle, \quad \forall \mathbf{c}^{(k)} \in C^k(D_N), \forall \mathbf{c}_{(k)} \in C_k(D_M). \end{aligned}$$

□

**Remark 19.** The commutative property  $\delta \circ \Phi^\sharp = \Phi^\sharp \circ \delta$  is the discrete analogue of  $d \circ \Phi^* = \Phi^* \circ d$ , see Proposition 6.

Since the cochain map  $\Phi^\sharp$  commutes with the coboundary operator,  $\Phi^\sharp$  maps cocycles onto cocycles and  $k$ -coboundaries onto  $k$ -coboundaries, for all  $k = 0, \dots, n$ . This property ensures that the cochain decomposition retains its structure when we deform the cell complex with a chain map.

### 5.3 Dual complexes

With every cell complex  $D$  one can associate a compatible dual cell complex,  $\tilde{D}$ , [174]. Before we can define a dual cell complex, the adjoint of the faces should be defined.

**Definition 45 (Faces and cofaces).** [174] The faces of a  $k$ -cell are those  $(k-1)$ -cells that form the boundary of the  $k$ -cell, see Definition 29 and Figure 5.8(a). The cofaces of a  $k$ -cell are those  $(k+1)$ -cells which have the  $k$ -cell as common face.

**Example 18.** Consider two neighboring rooms in a hotel. The two neighboring rooms have the wall in between them as common face. Therefore, the cofaces of the wall between the rooms are the two rooms. See also Figure 5.8.

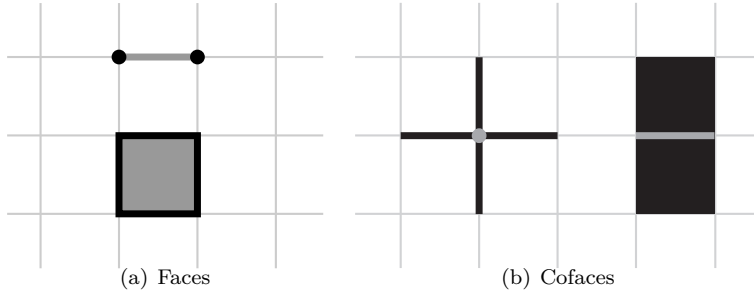


Figure 5.8: Faces and cofaces in  $\mathbb{R}^2$ . The  $k$ -cells indicated in gray are the original  $k$ -cells. Their faces (a) and cofaces (b), respectively, are shown in black.

**Definition 46 (Dual cell).** With every  $k$ -cell,  $\tau_{(k)}$ , in  $D$  there corresponds a  $(n-k)$ -cell,  $\tilde{\tau}_{(n-k)}$ , in the dual complex  $\tilde{D}$ , such that the dual cells of the boundary of a  $k$ -cell are the cofaces of the dual cell  $\tilde{\tau}_{(n-k)}$ .

---

**Definition 47 (Dual cell complex).** A dual cell complex,  $\tilde{D}$ , is the smallest cell complex according to Definition 31, that contains all dual cells  $\tilde{\tau}_{(n-k)}$  as defined in Definition 46.

We denote the map, which associates a cell  $\tau_{(k)}$  with its dual  $\tilde{\tau}_{(n-k)}$ , by  $*$ , i.e.  $*\tau_{(k)} = \tilde{\tau}_{(n-k)}$ . Operator  $*$  is the geometric Hodge star, [75, 83]. If we denote the coface operator by  $\partial^*$  then Definition 46 states that the following diagram commutes.

$$\begin{array}{ccc} \tau_{(p)} & \xrightarrow{\partial} & \partial\tau_{(p)} \\ \downarrow * & & \downarrow * \\ \tilde{\tau}_{(n-p)} & \xrightarrow{\partial^*} & \partial^*\tilde{\tau}_{(n-p)} \end{array}$$

Therefore we have  $*\partial = \partial^**$ . An example of these relations is shown in Figure 5.9.

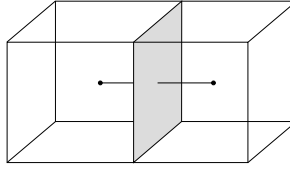


Figure 5.9: Pictorial view of Definition 46: The dual of an edge in  $D \subset \mathbb{R}^3$  is gray shaded surface in  $\tilde{D}$ . The cofaces of this gray surface are the two adjoining volumes in  $\tilde{D}$ . The boundary of the edge are the two endnodes in  $D$ . The dual of the two endnodes are again the volumes in  $\tilde{D}$  surrounding these points.

We make a distinction in cell complexes with and without boundary.

**Definition 48 (Dual cell complex without boundary).** If the collection of all dual cells of  $D$ , denoted by  $*D$ , constitutes a cell complex according to Definition 31, then the dual cell complex  $\tilde{D} \equiv *D$  and both the cell complex  $D$  and its dual  $\tilde{D}$  are cell complexes without boundary.

**Corollary 8.** For a cell complex without boundary the cell complex  $\tilde{D}$  is dual to the cell complex  $D$  and the cell complex  $D$  is dual to the cell complex  $\tilde{D}$  modulo orientation. As a consequence  $*^{-1}$  exists and is  $*^{-1} = \pm *$ . This allows us to express the coface operator in terms of the dual operator  $*$  and the boundary operator  $\partial$  by

$$*\partial = \partial^* * \quad \Rightarrow \quad \partial^* = *\partial *^{-1} = \pm * \partial * . \quad (5.3.1)$$

**Remark 20.** The dual grid in Figure 5.10 is only a cell complex in case the top side is connected to the bottom side and the left side to the right side. This holds for domains with periodic boundary conditions.

**Remark 21.** Note that, in Figure 5.10, the primal cell complex,  $D$ , is chosen outer oriented. Then by duality, the dual cell complex,  $\tilde{D}$ , is inner oriented. In fact, the orientation itself does not change, only the corresponding cell changes. This was shown before in Figure 4.7.

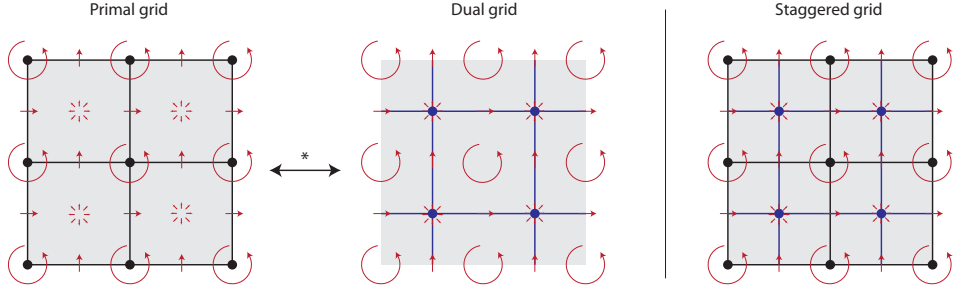


Figure 5.10: Example of a primal grid and dual grid is shown (not necessarily a cell complex), with for every cell  $\tau_{(k)}$  the associated dual cell  $\tilde{\tau}_{(n-k)}$  and corresponding orientation. On the right the staggered grid, an overlap of both grids, is shown.

**Remark 22.** If we equip the cell complex,  $D$ , with an outer orientation, the the dual complex,  $\tilde{D}$ , models geometric objects with inner orientation. Alternatively, inner orientation could be represented on the cell complex  $D$ , in which case the outer representation is modeled on the dual cell complex  $\tilde{D}$ . In this respect, dual cell complexes are able to model the inner- and outer-orientation as discussed in Section 4.1.

## 5.4 The boundary of cell complexes

A collection of  $k$ -cells forms a cell complex if the boundary of these  $k$ -cells are also in the cell complex. Therefore, cell complexes consist of an interior  $D_i$  and a boundary part  $D_b$ , where  $D = D_i \cup D_b$ . The boundary part contains cells up to degree  $(n - 1)$ . Since  $\tilde{D}$  is dual to  $D$ , we have that  $\tilde{D}_i \cup \tilde{D}_b$  is dual to  $D_i \cup D_b$ . More precisely,  $\tilde{D}_i = *D_i$  and  $\tilde{D}_b = *D_b$ . The individual parts do not need to be cell complexes themselves. In case  $D_i$  is a cell complex on a manifold with boundary, then  $\tilde{D}_i$  is not a cell complex, because not all faces of the  $k$ -cells in  $\tilde{D}_i$ ,  $k = 1, \dots, n$ , are also in  $\tilde{D}_i$ . Examples can be found in [165] and Examples 19 and 20 below.

**Definition 49. (The boundary of cell complexes)** Let  $D$  be a cell complex. If  $*D$  is not a cell complex, let  $\tilde{D}$  be the smallest cell complex which contains all the  $k$ -cells of  $*D$ . All the  $k$ -cells in  $\tilde{D} \setminus *D$  form a  $(n - 1)$ -dimensional cell complex,  $\tilde{D}_b := \partial \tilde{D}$  called the boundary of  $\tilde{D}$ . The dual cells of  $\partial \tilde{D}$  with respect to the  $(n - 1)$ -dimensional embedding space,  $D_b := \partial D = *(\partial \tilde{D})$  form a  $(n - 1)$ -dimensional subcomplex  $D_b$ , called the boundary of  $D$ . A dual cell in  $\tilde{D}_b$  is given by  $\tilde{\tau}_{(n-1-k)} = *\tau_{(k)}$ . The boundary and its dual are a cell complexes. This follows from Definition 48 given that the boundary of the boundary is empty.

**Example 19 (1D primal- and dual- cell complex).** Let the interior part of the primal cell complex,  $D_i$ , be given by three 0-cells, connected by two 1-cells, see Figure 5.11. Then its dual,  $\tilde{D}_i$ , consists of two 0-cells and three 1-cells. The outer two 1-cells are open ended, and therefore  $\tilde{D}_i$  is not a cell complex. To make it a cell complex,  $\tilde{D}_i$  must be closed by adding the boundary cells,  $\tilde{D}_b$ . The boundary part  $\tilde{D}_b$  consists of two 0-cells. The dual of  $\tilde{D}_b$  are the boundary cells of the primal cell

complex. In this one-dimensional example,  $D_b$  also consists of two 0-cells. Note that for the primal cell complex, the boundary cells in  $D_b$  coincide with the cells in  $D_i$ . Although the boundary nodes in  $D_b$  were already contained in  $D_i$ , the addition of orientation requires us to treat the boundary nodes as distinct nodes from  $D_i$ . This is because outer orientation of a node in a 1D embedding space differs from outer orientation of a node in a 0D embedding space, see Figure 4.6(b). So  $D_i$  and  $D_b$  together form the primal cell complex  $D$ , and  $\tilde{D}_i$  and  $\tilde{D}_b$  together form the dual cell complex  $\tilde{D}$ .

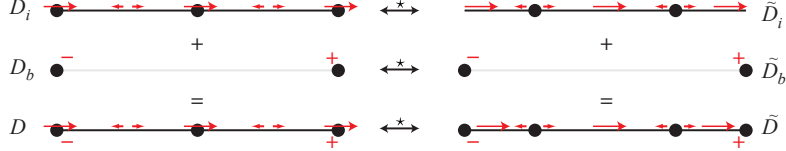


Figure 5.11: Primal and dual cell complexes, split into their interior and boundary part. The corresponding orientation to all  $k$ -cells are indicated. Note that the end-nodes in  $D$  have two types of orientation.

**Example 20 (2D primal- and dual cell complex).** Now consider in two dimensions the interior part of the primal cell complex,  $D_i$ , as given in Figure 5.12. The corresponding dual is the interior part  $\tilde{D}_i$ , of the dual cell complex  $\tilde{D}$ . Then  $\tilde{D}$  becomes a cell complex by adding the boundary cells  $\tilde{D}_b$ . Note that there do not exist 0-cells at the corners. The dual of  $\tilde{D}_b$  are the boundary cells  $D_b$ . They again coincide with the cells in  $D_i$ . Although  $D_b$  is already contained in  $D_i$  as nodes and edges, the role of the nodes and edges is completely different. This is indicated by the orientations in Figure 5.12. The outer orientation along the boundary – a 1D cell complex – differs from the outer orientation of these same geometric objects considered as elements from  $D_i$  embedded in 2D.

**Remark 23.** The boundaries  $D_b$  and  $\tilde{D}_b$  are boundaryless cell complexes.

The construction of the boundary of a cell complex and its dual given above, indicates that the boundary of a cell complex is disjoint from the cell complex itself. In order to formally 'glue' the boundary to its cell complex, we introduce the chain inclusions  $\iota_\sharp : C_k(\partial D) \rightarrow C_k(D)$  and  $\tilde{\iota}_\sharp : C_k(\partial \tilde{D}) \rightarrow C_k(\tilde{D})$ , such that, for  $k = 0, \dots, n-1$ ,

$$\iota_\sharp(\tau_{(k)} \in C_k(\partial D)) = \tau_{(k)} \in C_k(D) , \quad \text{and} \quad \tilde{\iota}_\sharp(\tilde{\tau}_{(k)} \in C_k(\partial \tilde{D})) = \tilde{\tau}_{(k)} \in C_k(\tilde{D}) . \quad (5.4.1)$$

Chain inclusions  $\iota_\sharp$  and  $\tilde{\iota}_\sharp$  are the discrete analogues of the continuous inclusion map defined in Definition 15. Using duality pairing between chains and cochains, we can define the associated cochain maps  $\iota^\sharp : C^k(D) \rightarrow C^k(\partial D)$  and  $\tilde{\iota}^\sharp : C^k(\tilde{D}) \rightarrow C^k(\partial \tilde{D})$  of the inclusion maps.

**Definition 50 (Discrete trace operator).** For all  $c^{(k)} \in C^k(D)$ , there must exist  $b^{(k)} \in C^k(\partial D)$ , such that

$$\langle c_{(k)}, b^{(k)} \rangle = \langle \iota_\sharp(c_{(k)}), c^{(k)} \rangle , \quad \forall c_{(k)} \in C_k(\partial D) . \quad (5.4.2)$$

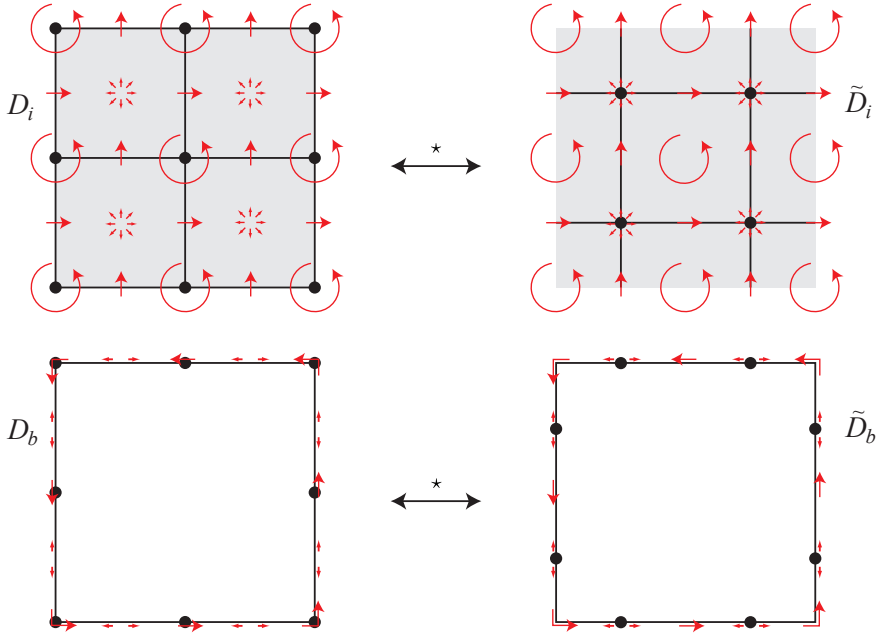


Figure 5.12: Interior and boundary parts of the primal and dual cell complexes,  $D = D_i \cup D_b$  and  $\tilde{D} = \tilde{D}_i \cup \tilde{D}_b$ , respectively. Orientation of all cells are included.

The map  $i^\sharp$  is then defined by

$$i^\sharp(c^{(k)}) = b^{(k)}. \quad (5.4.3)$$

The cochain map  $\tilde{i}^\sharp$  is defined similarly. The cochain maps  $i^\sharp$  and  $\tilde{i}^\sharp$  are the discrete analogues of the pullback of the inclusion map given in Definition 16. We therefore will write  $\text{tr}$  and  $\tilde{\text{tr}}$  instead of  $i^\sharp$  and  $\tilde{i}^\sharp$ .

**Remark 24.** Note that the inclusion chain maps can be defined more generally: Let  $K$  be a sub cell complex in  $D$ , then we can define the map  $i_\sharp : C_k(K) \rightarrow C_k(D)$  and its associated dual operation on cochains. Although useful in some applications, in this thesis we restrict ourselves to  $K = \partial D$ .

If we associate the primal complex  $D$  with a cell complex endowed with outer orientation and the dual complex  $\tilde{D}$  with a cell complex endowed with inner orientation, we have

**Definition 51. (Tangent k-cochains)** A  $k$ -cochain  $\mathbf{c}^{(k)} \in C^k(D)$  is called parallel or tangent to the cell complex  $D$ , if  $\text{tr}(\mathbf{c}^{(k)}) = \mathbf{0}^{(k)}$  on  $D_b$ , that is, if all the outer-oriented  $k$ -cells on the boundary are zero. We will denote the set of all tangent  $k$ -cochains on a given cell complex  $D$  by  $C_t^k(D)$ .

**Definition 52. (Normal k-cochains)** A  $k$ -cochain  $\tilde{\mathbf{c}}^{(k)} \in C^k(\tilde{D})$  is called perpendicular or normal to the cell complex  $\tilde{D}$ , if  $\text{tr}(\tilde{\mathbf{c}}^{(k)}) = \tilde{\mathbf{0}}^{(k)}$  on  $\tilde{D}_b$ , that is, if all the inner-oriented  $k$ -cells on the boundary are zero. We will denote the set of all normal  $k$ -cochains on the cell complex  $\tilde{D}$  by  $C_n^k(\tilde{D})$ .

---

If the dual cells are labeled with the same number as the associated primal cells, and if the orientations of primal and dual cells are in agreement with the orientation of the embedding space, then the incidence matrix  $\tilde{E}_{(k,k-1)}$  on the dual complex is related to the incidence matrices on the primal complex by

$$\tilde{E}_{(k,k-1)} = E_{(n-k+1,n-k)}^T, \quad k = 1, \dots, n. \quad (5.4.4)$$

**Remark 25.** This seemingly uninteresting relation has quite some consequences for numerical operators to be developed. The incidence matrices encode the boundary operator,  $\partial$ , but by Stokes equation, also the coboundary operator,  $\delta$ . The coboundary operator is the discrete analogue of the exterior derivative. Take for instance  $k = 1$  in (5.4.4), then  $\tilde{E}^{(1,0)} = \tilde{E}_{(1,0)}$  is the discrete analogue of the exterior derivative acting on 0-forms. We identified this operator with the gradient operator.

The coboundary operator acting on  $(n-1)$ -cochains discretely represents the exterior derivative acting on  $(n-1)$ -forms, i.e. the divergence operator. Therefore,

$$E^{(n,n-1)} = (\tilde{E}^{(1,0)})^T. \quad (5.4.5)$$

states that the discrete divergence operator (on the primal complex) is the transpose of the discrete gradient (on the dual complex). In vector calculus it says  $\text{div} = -\text{grad}^*$ . The minus sign is a consequence of the fact that orientation is not taken into account consistently in vector calculus. Furthermore, vector calculus does not reveal that these two operators act on spaces with a different type of orientation (inner and outer). The notion of inner- and outer-oriented complexes will lead to staggered grids.

**Remark 26.** Consider in 2D the discrete gradient operator, applied to the dual cell complex. Then the incidence matrix  $\tilde{E}^{(1,0)}$  relates the 0- and 1-cells as shown in Figure 5.13. Note that the discrete gradient does not give rise to 1-cells between the 0-cells on the boundary, so between the points indicated by ■. The 1-cells in the boundary complex  $\tilde{D}_b$  in Figure 5.12 only appear when considering the discrete curl operator. In that case the 0-cells on the boundary are not considered.

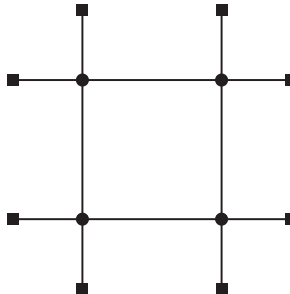


Figure 5.13: Part of a cell complex showing all 0- and 1-cells that are involved in the discrete gradient on the dual cell complex in 2D. It consists of four internal 0-cells (●), eight boundary 0-cells (■) and twelve line segments.



# Chapter 6

## Mimetic Operators

This chapter is based on Kreeft et al. [115].

$$\begin{array}{ccccccc}
 & C^0(D) & \xrightarrow{\delta} & C^1(D) & \xrightarrow{\delta} & C^2(D) & \xrightarrow{\delta} C^3(D) \\
 \Lambda^0(\mathcal{M}) & \xrightarrow{\mathcal{I}^0} & \uparrow \mathcal{R}^0 & \xrightarrow{\delta} & \xrightarrow{\mathcal{I}^1} & \uparrow \mathcal{R}^1 & \xrightarrow{\delta} \xrightarrow{\mathcal{I}^2} \uparrow \mathcal{R}^2 & \xrightarrow{\delta} \xrightarrow{\mathcal{I}^3} \uparrow \mathcal{R}^3 \\
 & \downarrow d & & \downarrow d & & \downarrow d & & \downarrow d \\
 & \tilde{C}^3(D) & \leftarrow \tilde{\mathcal{I}}^3 & \tilde{C}^2(D) & \leftarrow \tilde{\mathcal{I}}^2 & \tilde{C}^1(D) & \leftarrow \tilde{\mathcal{I}}^1 & \tilde{C}^0(D) \\
 \Lambda^3(\mathcal{M}) & \xrightarrow{\star_h} & \Lambda^1(\mathcal{M}) & \xrightarrow{\star_h} & \Lambda^2(\mathcal{M}) & \xrightarrow{\star_h} & \Lambda^0(\mathcal{M}) & \xrightarrow{\star_h} \\
 & \uparrow \mathcal{R}^3 & & \uparrow \mathcal{R}^2 & & \uparrow \mathcal{R}^1 & & \uparrow \mathcal{R}^0 \\
 & \tilde{\Lambda}^3(\mathcal{M}) & \xleftarrow{d} & \tilde{\Lambda}^2(\mathcal{M}) & \xleftarrow{d} & \tilde{\Lambda}^1(\mathcal{M}) & \xleftarrow{d} & \tilde{\Lambda}^0(\mathcal{M})
 \end{array}$$

Let  $\Lambda_h^k(\Omega; C_k)$  be a finite dimensional subspace of the differential form space  $\Lambda^k(\Omega)$  with corresponding  $k$ -chain space  $C_k$ . The general philosophy in this section is to develop projections and coprojections, denoted by  $\pi$  and  $\pi^*$ , respectively, onto a finite dimensional space of differential forms,  $\Lambda_h^k(\Omega; C_k) \subset \Lambda^k(\Omega)$ , such that an operation  $T$  at the finite dimensional space  $\Lambda_h^k(\Omega; C_k)$ , behaves in the same way as at the continuous level,  $\Lambda^k(\Omega)$ . By ‘behaves in the same way’ we mean that either  $\pi \circ T = T \circ \pi$  or  $\pi^* \circ T = T \circ \pi^*$ , i.e. when one of the following diagrams commute

$$\begin{array}{ccc}
 \Lambda^k(\Omega) & \xrightarrow{T} & \Lambda^l(\Omega) \\
 \pi \downarrow & & \pi \downarrow \\
 \Lambda_h^k(\Omega; C_k) & \xrightarrow{T} & \Lambda_h^l(\Omega; C_l)
 \end{array}
 \quad
 \begin{array}{ccc}
 \Lambda^k(\Omega) & \xrightarrow{T} & \Lambda^l(\Omega) \\
 \pi^* \downarrow & & \pi^* \downarrow \\
 \Lambda_h^k(\Omega; C_k) & \xrightarrow{T} & \Lambda_h^l(\Omega; C_l).
 \end{array}$$

In the previous sections, we denoted a manifold with either  $\mathcal{M}$  or  $\mathcal{N}$ . In computational science and engineering it is customary to denote the manifold – or computational

---

domain – by  $\Omega$ . Therefore, from now on we will refer to the manifold as  $\Omega$ . Furthermore, we only use Hilbert spaces  $L^2\Lambda^k(\Omega)$  and  $H\Lambda^k(\Omega)$  when needed, in all other cases we simply write  $\Lambda^k(\Omega)$ .

This chapter starts with the construction of a mimetic projection operator, that constitutes of a reduction and reconstruction operator. These terms were mentioned before in Section 1.3.1, but will be formally defined in Section 6.1. In Section 6.2 we discuss the action of the operators defined in Chapter 4 on the finite dimensional subspace, and new operators will be defined where needed. Section 6.4 treats the discrete Hodge decomposition, its relation with the cochain space decomposition and the comparison with the continuous Hodge decomposition. This chapter is closed with a discussion and some concluding remarks.

## 6.1 Reduction, reconstruction and projection operator

The discretization of the (flow) variables involves a bounded projection operator,  $\pi_h$ , from the complete space  $\Lambda^k(\Omega)$  to a conforming subspace  $\Lambda_h^k(\Omega; C_k) \subset \Lambda^k(\Omega)$ . In this subspace differential forms are expressed in terms of  $k$ -cochains defined on  $k$ -chains, and corresponding  $k$ -cochain interpolation forms (often called basis functions or basis forms). The subspaces treated here are polynomial spaces, as is commonly used in finite element methods. The projection operation actually consists of two steps, a *reduction operator*,  $\mathcal{R}$ , from  $\Lambda^k(\Omega)$  to  $C^k(D)$ , that integrates the  $k$ -forms on  $k$ -chains to get  $k$ -cochains, and a *reconstruction operator*,  $\mathcal{I}$ , from  $C^k(D)$  to  $\Lambda_h^k(\Omega; C_k)$ , to reconstruct  $k$ -forms from  $k$ -cochains using the appropriate basis-functions. These mimetic operators were already introduced before in the work of Hyman and Scovel [99] and in Bochev and Hyman [18]. A composition of the two gives the projection operator  $\pi_h = \mathcal{I} \circ \mathcal{R}$  and is illustrated below.

$$\begin{array}{ccc} \Lambda^k(\Omega) & \xrightarrow{\pi_h} & \Lambda_h^k(\Omega; C_k) \\ \mathcal{R} \downarrow & \nearrow \mathcal{I} & \\ C^k(D) & & \end{array}$$

We already saw the similarities between differential geometry and algebraic topology. We now impose constraints on the maps  $\mathcal{R}$  and  $\mathcal{I}$  to ensure that these structures are preserved while mapping from one to the other. By imposing structure-preserving constraints on these operations, these three operators together set up the mimetic framework. The coprojections cannot be written directly in terms of reduction and reconstruction. However coprojections are expressed in terms of Hodge star operators and projections. The latter are written in terms of reduction and reconstruction. In this section we focus on the discretization of the differential forms, involving the reduction, reconstruction and projection operators.

---

**Definition 53 (Reduction).** *The reduction operator  $\mathcal{R} : \Lambda^k(\Omega) \rightarrow C^k(D)$  is a homomorphism that maps differential forms to cochains. This linear map is also called the De Rham map and is defined by integration as*

$$\langle \tau_{(k)}, \mathcal{R}a^{(k)} \rangle := \int_{\tau_{(k)}} a^{(k)}, \quad \forall \tau_{(k)} \in C_k(D). \quad (6.1.1)$$

*Then for all  $\mathbf{c}_{(k)} \in C_k(D)$ , the reduction of the  $k$ -form,  $a^{(k)} \in \Lambda^k(\Omega)$ , to the  $k$ -cochain,  $\mathbf{a}^{(k)} \in C^k(D)$ , is given by*

$$\mathbf{a}^{(k)}(\mathbf{c}_{(k)}) := \langle \mathbf{c}_{(k)}, \mathcal{R}a^{(k)} \rangle \stackrel{\text{Def. 32}}{=} \sum_i c_i \langle \tau_{(k),i}, \mathcal{R}a^{(k)} \rangle \stackrel{(6.1.1)}{=} \sum_i c_i \int_{\tau_{(k),i}} a^{(k)} = \int_{\mathbf{c}_{(k)}} a^{(k)}. \quad (6.1.2)$$

The reduction map  $\mathcal{R}$  provides the *integral quantities* that were mentioned in the Introduction. It is the integration of a  $k$ -form over all  $k$ -cells in a  $k$ -chain that results in a  $k$ -cochain. Note that since  $\tau_{(k),i}$  is compact and  $C^k(D)$  is a finite dimensional free Abelian group, the reduction operator  $\mathcal{R}$  is well-defined with  $f_I(\mathbf{x}) \in L_{\text{loc}}(\Omega)$  in (4.3.4). A special case of reduction is integration of an  $n$ -form over  $\Omega$ .

**Definition 54.** *Let  $a^{(n)} \in \Lambda^n(\Omega)$ , then the integral over the domain  $\Omega$  is given by*

$$\int_{\Omega} a^{(n)} := \langle \boldsymbol{\sigma}_{(n)}, \mathcal{R}a^{(n)} \rangle,$$

*where the chain  $\boldsymbol{\sigma}_{(n)} = \sum_i \tau_{(n),i}$  (so all  $c_i = +1$ ) covers the entire computational domain  $\Omega$ .*

We can list the following properties of the reduction map. First of all, the reduction operator is a non-injective and surjective map.

**Definition 55.** *Consider two  $k$ -forms  $a_1^{(k)}, a_2^{(k)} \in \Lambda^k(\Omega)$  and  $a_1^{(k)} \neq a_2^{(k)}$ , they are in the same equivalence class if*

$$\mathcal{R}a_1^{(k)} = \mathcal{R}a_2^{(k)} \Leftrightarrow \mathcal{R}(a_1^{(k)} - a_2^{(k)}) = 0. \quad (6.1.3)$$

Secondly, the reduction map commutes with respect to differentiation.

**Lemma 3.** *The reduction map has a commuting property with respect to continuous and discrete differentiation,*

$$\mathcal{R}\mathbf{d} = \delta\mathcal{R} \quad \text{on } \Lambda^k(\Omega). \quad (6.1.4)$$

*This commutation can be illustrated as*

$$\begin{array}{ccc} \Lambda^k & \xrightarrow{\mathbf{d}} & \Lambda^{k+1} \\ \downarrow \mathcal{R} & & \downarrow \mathcal{R} \\ C^k & \xrightarrow{\delta} & C^{k+1} \end{array}$$

*Proof.* This property can be proven using Stokes' Theorem (4.6.4) and the duality property (5.2.6),

$$\langle \mathbf{c}_{(k)}, \mathcal{R}da^{(k)} \rangle \stackrel{(6.1.1)}{=} \int_{\mathbf{c}_{(k)}} da^{(k)} \stackrel{(4.6.4)}{=} \int_{\partial \mathbf{c}_{(k)}} a^{(k)} \stackrel{(6.1.1)}{=} \langle \partial \mathbf{c}_{(k)}, \mathcal{R}a^{(k)} \rangle \stackrel{(5.2.6)}{=} \langle \mathbf{c}_{(k)}, \delta \mathcal{R}a^{(k)} \rangle. \quad (6.1.5)$$

□

Thirdly, the reduction map commutes with the pullback,  $\Phi^*$ , and the cochain map,  $\Phi^\sharp$ .

**Lemma 4.** *Let  $\Phi : \Omega_M \rightarrow \Omega_N$  be a continuous map between two manifolds, let  $\Phi_\sharp : C_k(D_M) \rightarrow C_k(D_N)$  be the associated chain map of  $k$ -chains between two cell complexes and let  $D_M$  be a covering of the manifold  $\Omega_M$  and  $D_N$  the covering of  $\Omega_N$ , according to Definition 31. Then the reduction map commutes with the continuous and discrete pullback,*

$$\mathcal{R}\Phi^* = \Phi^\sharp \mathcal{R} \quad \text{on } \Lambda^k(\Omega_N). \quad (6.1.6)$$

This commutation is illustrated by

$$\begin{array}{ccc} \Lambda^k(\Omega_N) & \xrightarrow{\Phi^*} & \Lambda^k(\Omega_M) \\ \downarrow \mathcal{R} & & \downarrow \mathcal{R} \\ C^k(D_N) & \xrightarrow{\Phi^\sharp} & C^k(D_M) \end{array}$$

where  $\Phi^*$  and  $\Phi^\sharp$  are defined in Definitions 14 and 44, respectively.

*Proof.* For all  $\mathbf{c}_{(k)} \in C_k(D_M)$  and for all  $a^{(k)} \in \Lambda^k(\Omega_N)$  we have

$$\langle \mathbf{c}_{(k)}, \mathcal{R}\Phi^*a^{(k)} \rangle \stackrel{(6.1.1)}{=} \int_{\mathbf{c}_{(k)}} \Phi^*a^{(k)} \stackrel{(4.4.5)}{=} \int_{\Phi_\sharp \mathbf{c}_{(k)}} a^{(k)} \stackrel{(6.1.1)}{=} \langle \Phi_\sharp \mathbf{c}_{(k)}, \mathcal{R}a^{(k)} \rangle \stackrel{\text{Def. 44}}{=} \langle \mathbf{c}_{(k)}, \Phi^\sharp \mathcal{R}a^{(k)} \rangle.$$

□

The operator acting in opposite direction of the reduction operator is the *reconstruction operator*. The reconstruction operator  $\mathcal{I} : C^k(D) \rightarrow \Lambda_h^k(\Omega; C_k)$ , also called the *Whitney map*, is an isomorphism that maps cochains back to differential forms. The reconstructed  $k$ -forms, also called *finite dimensional  $k$ -forms*, belong to the space  $\Lambda_h^k(\Omega; C_k)$ , which is a proper subset of the complete  $k$ -form space  $\Lambda^k(\Omega)$ . While the reduction step is clearly defined in Definition 53, in the choice of interpolation forms there exists some freedom. Nevertheless, any method of reconstruction must satisfy a list of requirements.

**Definition 56 (Reconstruction).** *The reconstruction operator  $\mathcal{I} : C^k(D) \rightarrow \Lambda_h^k(\Omega; C_k)$  must satisfy the following properties:*

- Reconstruction  $\mathcal{I}$  must be the right inverse of  $\mathcal{R}$ , so it returns identity (consistency property),

$$\mathcal{R}\mathcal{I} = Id \quad \text{on } C^k(D). \quad (6.1.7)$$

- Like  $\mathcal{R}$ , also the reconstruction operator  $\mathcal{I}$  has to possess a commuting property with respect to differentiation. A properly chosen reconstruction operator  $\mathcal{I}$  must satisfy a commuting property with respect to the exterior derivative and coboundary operator,

$$d\mathcal{I} = \mathcal{I}\delta \quad \text{on } C^k(D). \quad (6.1.8)$$

This commutation can be illustrated as

$$\begin{array}{ccc} \Lambda_h^k & \xrightarrow{d} & \Lambda_h^{k+1} \\ \uparrow \mathcal{I} & & \uparrow \mathcal{I} \\ C^k & \xrightarrow{\delta} & C^{k+1} \end{array}$$

- The reconstruction should commute with continuous and discrete pullback, i.e.

$$\mathcal{I}\Phi^\sharp = \Phi^*\mathcal{I} \quad \text{on } C^k(D_N). \quad (6.1.9)$$

This commutation relation can be represented by

$$\begin{array}{ccc} \Lambda_h^k(\Omega_N; C_k) & \xrightarrow{\Phi^*} & \Lambda_h^k(\Omega_M; C_k) \\ \uparrow \mathcal{I} & & \uparrow \mathcal{I} \\ C^k(D_N) & \xrightarrow{\Phi^\sharp} & C^k(D_M) \end{array}$$

- Let  $\tilde{D}_i = *D_i$  be as defined in Definition 49. For all  $\tilde{\mathbf{c}}^{(n-k)} \in C^{n-k}(\tilde{D}_i)$  there should exist a  $\mathbf{c}^{(k)} \in C^k(D_i)$ , such that

$$\tilde{\mathcal{I}}\tilde{\mathbf{c}}^{(n-k)} = \mathcal{I}\mathbf{c}^{(k)}, \quad (6.1.10)$$

where  $\tilde{\mathcal{I}}$  reconstructs cochains on  $\tilde{D}_i$  and  $\mathcal{I}$  reconstructs cochains on the cell complex  $D_i$ . The same must hold in the opposite direction.

These conditions should also hold for the boundary part of the primal and dual cell complexes, i.e. for  $D_b$  and  $\tilde{D}_b$ . Let  $\tilde{D}_b = *D_b$  be as defined Definition 49. For all  $\tilde{\mathbf{c}}^{(n-1-k)} \in C^{n-1-k}(\tilde{D}_b)$ , there should exist a  $\mathbf{c}^{(k)} \in C^k(D_b)$ , such that

$$\tilde{\mathcal{I}}\tilde{\mathbf{c}}^{(n-1-k)} = \mathcal{I}\mathbf{c}^{(k)},$$

where  $\tilde{\mathcal{I}}$  reconstructs cochains on  $\tilde{D}_b$  and  $\mathcal{I}$  reconstructs cochains on  $D_b$ . Again the same must hold in opposite direction.

**Remark 27.** Moreover, we want  $\mathcal{I}$  to be an approximate left inverse of  $\mathcal{R}$ , so the result is close to identity (approximation property),

$$\mathcal{I}\mathcal{R} = Id + \mathcal{O}(h^p) \quad \text{in } \Lambda^k(\Omega),$$

where  $\mathcal{O}(h^p)$  indicates a truncation error in terms of a measure of the grid size,  $h$ , and a polynomial order  $p$ . This means that the finite dimensional representation converges on grid refinement or by increasing polynomial order,

$$\lim_{h^p \rightarrow 0} \|a^{(k)} - \mathcal{I}\mathcal{R}a^{(k)}\|_{H\Lambda^k} \rightarrow 0, \quad \forall a^{(k)} \in H\Lambda^k(\Omega). \quad (6.1.11)$$

The composition in the last remark gives rise to the definition of a new operator,  $\pi_h$ , which is a projection operator.

**Definition 57.** Define the operator  $\pi_h : \Lambda^k(\Omega) \rightarrow \Lambda_h^k(\Omega; C_k)$  as the composition  $\mathcal{I} \circ \mathcal{R}$ . It allows for an approximate continuous representation of a  $k$ -form  $a^{(k)}$ ,

$$a_h^{(k)} = \pi_h a^{(k)} = \mathcal{I} \mathcal{R} a^{(k)}, \quad \pi_h a^{(k)} \in \Lambda_h^k(\Omega; C_k) \subset \Lambda^k(\Omega). \quad (6.1.12)$$

where  $\mathcal{I} \mathcal{R} a^{(k)}$  is expressed as a combination of  $k$ -cochains and interpolating  $k$ -forms.

**Proposition 23 (Projection).** The operator  $\pi_h : \Lambda^k(\Omega) \rightarrow \Lambda_h^k(\Omega; C_k)$  is a projection operator.

*Proof.* For  $\pi_h$  to be a projection, it must be a homomorphism, which is true since both the reduction and the reconstruction operators are homomorphisms, therefore for all  $a^{(k)}, b^{(k)} \in \Lambda^k(\Omega)$  it holds

$$\pi_h(a^{(k)} + b^{(k)}) = \pi_h a^{(k)} + \pi_h b^{(k)}, \quad (6.1.13)$$

and the projection operator must be idempotent. Let  $a_h^{(k)} \in \Lambda_h^k(\Omega; C_k)$ , then  $\pi_h a_h^{(k)} = a_h^{(k)}$ , and so  $\pi_h \equiv Id$  on  $\Lambda_h^k(\Omega; C_k)$ . For all  $a_h^{(k)} \in \Lambda_h^k(\Omega; C_k)$ , there exists  $a^{(k)} \in \Lambda^k(\Omega)$  such that  $a_h^{(k)} = \pi_h a^{(k)} = \mathcal{I} \mathcal{R} a^{(k)}$ , so

$$\mathcal{I} \mathcal{R} a_h^{(k)} = \mathcal{I} \mathcal{R} (\mathcal{I} \mathcal{R} a^{(k)}) \stackrel{(6.1.7)}{=} \mathcal{I} \mathcal{R} a^{(k)} = a_h^{(k)}. \quad (6.1.14)$$

□

Since  $\pi_h a^{(k)} = \mathcal{I} \mathcal{R} a^{(k)}$  is a linear combination of  $k$ -cochains and interpolation  $k$ -forms, the expansion coefficients in the mimetic spectral element formulation to be discussed in Chapter 7 are the cochains which in turn are the integral quantities mentioned in the Introduction.

**Proposition 24.** Using the projection operator, the differential form space  $\Lambda^k(\Omega)$  can be decomposed into a projected space and its complement, so  $\Lambda^k = \Lambda_h^k \oplus \Lambda_h^{k,c}$ , and so any  $k$ -form can be uniquely decomposed as

$$a^{(k)} = a_h^{(k)} + a_h^{(k),c} = \pi_h a^{(k)} + (Id - \pi_h) a^{(k)}, \quad \forall a^{(k)} \in \Lambda^k(\Omega). \quad (6.1.15)$$

Note that  $(Id - \pi_h)$  is also a projection, but now onto the unresolved part. As a consequence of the direct sum decomposition and Proposition 23,  $\pi_h \circ (Id - \pi_h) = (Id - \pi_h) \circ \pi_h = 0$ .

The projection is not an orthogonal projection. This will be demonstrated in Example 25 in the next section. As a consequence the projection,  $\pi_h$ , is not self-adjoint,

$$(\pi_h a^{(k)}, b^{(k)}) \neq (a^{(k)}, \pi_h b^{(k)}), \quad \forall a^{(k)}, b^{(k)} \in \Lambda^k(\Omega). \quad (6.1.16)$$

Both  $a^{(k)} \in \Lambda^k(\Omega)$  and its projected part  $\pi_h a^{(k)} \in \Lambda_h^k(\Omega; C_k)$  are in the same equivalence class, as defined in Definition 55, so

$$\mathcal{R} \pi_h a^{(k)} = \mathcal{R} a^{(k)} \quad \text{and} \quad \mathcal{R} (Id - \pi_h) a^{(k)} = 0, \quad (6.1.17)$$

and for the special case of integration of a volume form over the whole domain, this integral preserving property of the projection gives

$$\int_{\Omega} \pi_h a^{(n)} = \int_{\Omega} a^{(n)}.$$

As for the reduction operator, also the projection operator is non-injective and surjective. Then because of Definitions 55 and 57, there also exists an equivalence class for the projection operator. The projection of  $a^{(k)}$  is not unique, but depends among others on the underlying cell complex, as is illustrated in the following example.

**Example 21.** Consider a uniform and a Gauss-Lobatto grid, then  $\pi_h^{\text{uni}} a^{(k)}, \pi_h^{\text{gl}} a^{(k)} \in \Lambda_h^k([-1, 1])$ , but  $\pi_h^{\text{uni}} a^{(k)} \neq \pi_h^{\text{gl}} a^{(k)}$ , see Figure 6.1 for an example of a 0-form and a 1-form. The difference between the two projections reduces with grid refinement, since

$$\begin{aligned} |\pi_h^{\text{uni}} a^{(k)} - \pi_h^{\text{gl}} a^{(k)}| &= |(I - \pi_h^{\text{gl}})a^{(k)} - (I - \pi_h^{\text{uni}})a^{(k)}| \\ &\leq |(I - \pi_h^{\text{gl}})a^{(k)}| + |(I - \pi_h^{\text{uni}})a^{(k)}| \stackrel{\text{Rem. } 27}{=} \mathcal{O}(h^p). \end{aligned}$$

Moreover note that, according to Proposition 23, it can be observed that  $\pi_h^{\text{uni}} \pi_h^{\text{gl}} a^{(k)} = \pi_h^{\text{gl}} a^{(k)}$ ,  $\pi_h^{\text{gl}} \pi_h^{\text{uni}} a^{(k)} = \pi_h^{\text{uni}} a^{(k)}$  and so  $\pi_h^{\text{uni}} \pi_h^{\text{gl}} a^{(k)} \neq \pi_h^{\text{gl}} \pi_h^{\text{uni}} a^{(k)}$ .

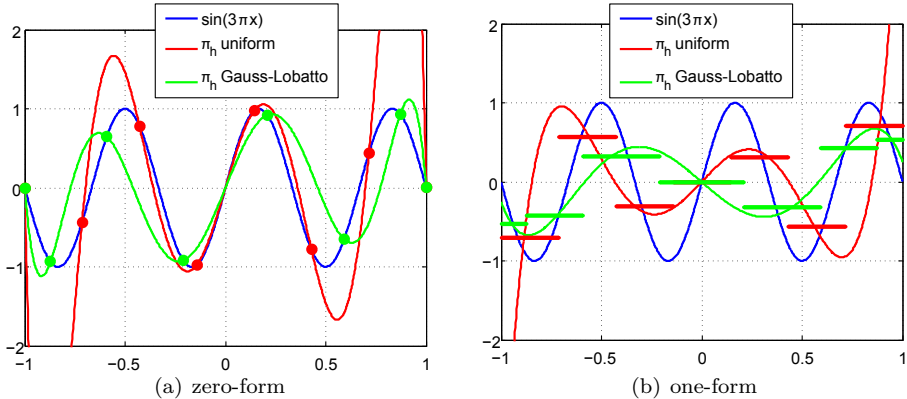


Figure 6.1: These figures illustrate the non-uniqueness of the projection operator for zero-forms (a) and one-forms (b). In (a) the dots indicate the 0-cochains, in (b) the line segments are the 1-cochains. The resolutions are intentionally kept low to show the differences.

In Section 5 staggered cell complexes were introduced. The two complexes are dual with respect to each other as defined in Definition 47 and illustrated in Figures 5.11 and 5.12. This allows us to define two projection operators, one projecting onto the subspace  $\Lambda^k(\Omega; C_k)$  and one projecting onto the subspace  $\Lambda^k(\Omega; \tilde{C}_k)$ , where  $C_k = C_k(D)$  and  $\tilde{C}_k = C_k(\tilde{D})$ .

**Definition 58 (Canonical projections).** Given the outer-oriented cell complex  $D$  and its dual inner-oriented cell complex  $\tilde{D}$ , we define two projections:

- 
- $\pi_h = \mathcal{IR}$ , where the reduction,  $\mathcal{R}$ , and the reconstruction,  $\mathcal{I}$ , are performed on the interior part of the primal cell complex, i.e.  $D_i$ . The corresponding subspace  $\Lambda_h^k(\Omega; C_k)$  is the space of finite dimensional  $k$ -forms, with  $k$ -cochains associated with the outer-oriented cells in  $D_i$ , such that

$$\Lambda_h^k(\Omega; C_k) := \pi_h \Lambda^k(\Omega) = \mathcal{IR} \Lambda^k(\Omega).$$

- $\tilde{\pi}_h = \tilde{\mathcal{I}}\tilde{\mathcal{R}}$ , where the reduction,  $\tilde{\mathcal{R}}$ , and the reconstruction,  $\tilde{\mathcal{I}}$ , are performed on the interior part of the dual cell complex, i.e.  $\tilde{D}_i$ . The space  $\Lambda_h^k(\Omega; \tilde{C}_k)$  is the space of finite dimensional  $k$ -forms, with  $k$ -cochains associated with the inner-oriented cells in  $\tilde{D}_i$ , such that

$$\Lambda_h^k(\Omega; \tilde{C}_k) := \tilde{\pi}_h \Lambda^k(\Omega) = \tilde{\mathcal{I}}\tilde{\mathcal{R}} \Lambda^k(\Omega).$$

To every projection we can define a corresponding coprojection.

**Definition 59 (Canonical coprojections).** Given projection  $\pi_h$  using the outer-oriented cell complex  $D_i$  and projection  $\tilde{\pi}_h$  using the inner-oriented cells in  $\tilde{D}_i$ , we define two coprojections:

- $\pi_h^*$  is defined as

$$\pi_h^* := (-1)^{k(n-k)} \star \tilde{\pi}_h \star. \quad (6.1.18)$$

This coprojection is defined in terms of a projection of  $(n-k)$ -forms,  $\star a^{(k)}$ , on the inner-oriented  $(n-k)$ -chains in  $\tilde{D}_i$  and then represented in terms of the  $k$ -form basis functions on the outer-oriented cell complex  $D_i$ . The corresponding subspace is  $\pi_h^* \Lambda^k(\Omega)$ .

- $\tilde{\pi}_h^*$  is defined as

$$\tilde{\pi}_h^* := (-1)^{k(n-k)} \star \pi_h \star. \quad (6.1.19)$$

This coprojection is defined in terms of a projection of  $(n-k)$ -forms,  $\star a^{(k)}$ , on the outer-oriented  $(n-k)$ -chains in  $D_i$  and then represented in terms of the  $k$ -form basis functions on the interior part of the inner-oriented dual cell complex, i.e.  $\tilde{D}_i$ . The corresponding subspace is  $\tilde{\pi}_h^* \Lambda^k(\Omega)$ .

**Remark 28.** A coprojection is also a projection according to Proposition 23.

**Remark 29.** Although projections and coprojections in Definitions 58 and 59 were defined with the interior parts of cell complexes  $D$  and  $\tilde{D}$ . The same projections and coprojections can be defined for the boundary parts of the cell complexes  $D$  and  $\tilde{D}$ , i.e.  $D_b$  and  $\tilde{D}_b$ .

The projection and coprojection operators possess commutation relations with the operators defined in the previous chapter, as will be shown in the next section. The projected differential forms differ, because the forms are reduced on different chains as illustrated in Example 21, Figure 6.1. See also Figure 7.9 in the next section.

---

**Proposition 25 (Equivalence spaces  $\pi_h \Lambda^k$  and  $\pi_h^* \Lambda^k$ ).** Define the spaces

$$\pi_h \Lambda^k := \left\{ a_h^{(k)} \mid \exists a^{(k)} \in \Lambda^k(\Omega) \text{ s.t. } a_h^{(k)} = \pi_h a^{(k)} \right\},$$

and

$$\pi_h^* \Lambda^k := \left\{ a_h^{(k)} \mid \exists a^{(k)} \in \Lambda^k(\Omega) \text{ s.t. } a_h^{(k)} = \pi_h^* a^{(k)} \right\},$$

then  $\Lambda_h^k = \pi_h \Lambda^k \equiv \pi_h^* \Lambda^k$ , but in general  $\pi_h a^{(k)} \neq \pi_h^* a^{(k)}$ .

*Proof.* The reduction of  $\star a^{(k)}$  on  $(n-k)$ -chains in  $C_k(\tilde{D}_i)$  yields a  $(n-k)$ -cochain in  $C^k(\tilde{D}_i)$  and according to (6.1.10) in Definition 56, there exists a  $k$ -cochain on the cell complex  $D$  such that  $\tilde{\mathcal{I}}\tilde{\mathbf{c}}^{(n-k)} = \mathcal{I}\mathbf{c}^{(k)}$ , therefore  $\pi_h^* \Lambda^k \subset \pi_h \Lambda^k$ . By a similar argument one can show that  $\pi_h \Lambda^k \subset \pi_h^* \Lambda^k$ , so we have  $\pi_h \Lambda^k \equiv \pi_h^* \Lambda^k$ . That  $\pi_h a^{(k)} \neq \pi_h^* a^{(k)}$  will be shown in Figure 7.9 in Section 7.  $\square$

**Proposition 26 (Equivalence on subspaces).** If  $a_h^{(k)} \in \Lambda_h^k(\Omega; C_k)$  then  $\pi_h^* a_h^{(k)} = \pi_h a_h^{(k)}$  and if  $a_h^{(k)} \in \Lambda_h^k(\Omega; \tilde{C}_k)$  then  $\tilde{\pi}_h^* a_h^{(k)} = \tilde{\pi}_h a_h^{(k)}$ .

*Proof.*

$$\text{If } a_h^{(k)} \in \Lambda_h^k \xrightarrow{\text{Prop. 25}} \begin{cases} a_h^{(k)} = \pi_h a_h^{(k)} & \text{because } \pi_h = Id \text{ on } \Lambda_h^k = \pi_h \Lambda^k \\ a_h^{(k)} = \pi_h^* a_h^{(k)} & \text{because } \pi_h^* = Id \text{ on } \Lambda_h^k = \pi_h^* \Lambda^k \end{cases}$$

Therefore  $a_h^{(k)} = \pi_h a_h^{(k)} = \pi_h^* a_h^{(k)}$ . The proof on the dual complex is the same.  $\square$

**Remark 30.** Although  $\pi_h^* a^{(k)} = \pi_h a^{(k)}$  holds in the finite dimensional subspace  $\Lambda_h^k(\Omega; C_k)$ , it does not hold on the entire space  $\Lambda^k(\Omega)$ . The difference between these two projections could give rise to natural and derived operators, [18]. However, from our point of view projections  $\pi_h$  and coprojections  $\pi_h^*$  are essentially different operators.

**Definition 60.** Whenever we refer to the projection  $\pi$  it can be any of the projections from Definition 58.

Although  $\pi_h = Id$  on  $\Lambda_h^k$ , (Proposition 23), it will be shown that it can be a very useful operation when changing the expression of a finite dimensional  $k$ -form. A finite dimensional  $k$ -form  $a_h^{(k)}$  is usually expressed in terms of a  $k$ -cochain  $\mathbf{a}^{(k)} \in C^k(D)$  and interpolating  $k$ -forms. If this is not the case, for example if the  $k$ -form  $a_h^{(k)}$  is expressed in terms of an  $l$ -cochain corresponding to a chain in  $\hat{C}_l := C_l(\hat{D})$ , where  $\hat{D}$  is either the primal cell complex  $D$  or the dual cell complex  $\tilde{D}$ , then a projection is used to express the finite dimensional  $k$ -form in terms of its corresponding  $k$ -cochains. For this special case we introduce a separate projection operator,  $\pi_M$ .

**Definition 61.** Define a special, bijective projection  $\pi_M : \Lambda_h^k(\Omega; \hat{C}_l) \rightarrow \Lambda_h^k(\Omega; C_k)$ , such that

$$\pi_M = Id \quad \text{on } \Lambda_h^k(\Omega; \hat{C}_l). \tag{6.1.20}$$

---

So  $\pi_M a_h = a_h$ , but its expression changes in terms of cochains, from an  $l$ -cochain in  $C^l(\hat{D})$  to a  $k$ -cochain in  $C^k(D)$ , and its expression changes with respect to the basis functions. In terms of reduction and reconstruction this is

$$a_h = \hat{\mathcal{I}}\hat{\mathcal{R}}a = \mathcal{IR}(\hat{\mathcal{I}}\hat{\mathcal{R}}a) = \pi_M a_h. \quad (6.1.21)$$

This seemingly redundant projection  $\pi_M$  will reappear almost everywhere, but we will not explicitly mention this in the next section. It will be more instructive to show its action with concrete reconstruction operators in Section 7.

## 6.2 Discrete operators

In this section we discuss operations of the operators discussed in Section 4, restricted to the set of finite dimensional subspaces  $\Lambda_h^k(\Omega; C_k)$ , i.e.  $d, \star, d^*, \Phi^*, \wedge_h$  and  $(\cdot, \cdot)_h$ .

### 6.2.1 The wedge product

The first operator to be considered in the subspaces  $\Lambda_h^k(\Omega; C_k) \subset \Lambda^k(\Omega)$ ,  $0 \leq k \leq n$ , is the wedge product. A product of a  $k$ - and  $l$ -form from subspaces  $\Lambda_h^k$  and  $\Lambda_h^l$  gives a  $(k+l)$ -form that is not in the subspace  $\Lambda_h^{k+l}$ . It therefore requires again a projection step.

**Definition 62.** A discrete wedge product is defined such that  $\wedge_h : \Lambda_h^k(\Omega; C_k) \times \Lambda_h^l(\Omega; C_l) \rightarrow \Lambda_h^{k+l}(\Omega; C_{k+l})$ , given by

$$a_h^{(k)} \wedge_h b_h^{(l)} := \pi(a_h^{(k)} \wedge b_h^{(l)}), \quad (6.2.1)$$

where  $\pi$  is either  $\pi_h$  or  $\tilde{\pi}_h$ , as defined in Definition 60.

As a consequence the discrete wedge product,  $\wedge_h$ , approximates the wedge product,  $\wedge$ , because

$$a_h^{(k)} \wedge b_h^{(l)} - a_h^{(k)} \wedge_h b_h^{(l)} = (Id - \pi)(a_h^{(k)} \wedge b_h^{(l)}) \stackrel{(27)}{=} \mathcal{O}(h^p).$$

Let us verify whether the discrete wedge product satisfies the same properties as the original wedge product. Let  $a_h^{(k)}, c_h^{(k)} \in \Lambda_h^k$ ,  $b_h^{(l)} \in \Lambda_h^l$ , with  $2k + l \leq n$ . Using the linearity of the projection it is straightforward to show that

$$(a_h^{(k)} + c_h^{(k)}) \wedge_h b_h^{(l)} = a_h^{(k)} \wedge_h b_h^{(l)} + c_h^{(k)} \wedge_h b_h^{(l)}.$$

Also the skew-symmetry follows from the linearity of the projection,

$$a_h^{(k)} \wedge_h b_h^{(l)} = \pi(a_h^{(k)} \wedge b_h^{(l)}) = (-1)^{kl} \pi(b_h^{(l)} \wedge a_h^{(k)}) = (-1)^{kl} b_h^{(l)} \wedge_h a_h^{(k)}.$$

The third property of the wedge product is associativity (4.3.1d). As stated already in [55], the associativity property is in general not satisfied. Now let  $a \in \Lambda_h^k$ ,  $b \in$

---

$\Lambda_h^l$ ,  $c \in \Lambda_h^m$ , with  $k + l + m \leq n$ , then<sup>1</sup>

$$\begin{aligned} & (a \wedge_h b) \wedge_h c - a \wedge_h (b \wedge_h c) \\ &= \pi(\pi(a \wedge b) \wedge c) - \pi(a \wedge \pi(b \wedge c)) \\ &= \pi[(a \wedge b) \wedge c - (I - \pi)(a \wedge b) \wedge c - a \wedge (b \wedge c) + a \wedge (I - \pi)(b \wedge c)] \\ &= \pi \left[ a \wedge \underbrace{(I - \pi)(b \wedge c)}_{\mathcal{O}(h^p)} - \underbrace{(I - \pi)(a \wedge b) \wedge c}_{\mathcal{O}(h^p)} \right] = \mathcal{O}(h^p). \end{aligned}$$

When considering bilinear products, the wedge product and discrete wedge product are in the same equivalence class,

$$\mathcal{R}(a_h^{(k)} \wedge_h b_h^{(l)}) = \mathcal{R}(a_h^{(k)} \wedge b_h^{(l)}). \quad (6.2.2)$$

In case  $k + l = n$ , we get

$$\int_{\Omega} a_h^{(k)} \wedge_h b_h^{(l)} = \int_{\Omega} a_h^{(k)} \wedge b_h^{(l)}.$$

### 6.2.2 The pullback

In mimetic discretization we do not restrict ourselves to affine mappings only, as is required in many other compatible finite elements, like Nédélec and Raviart-Thomas elements and their generalizations [6, 133, 154], but also allow non-affine maps such as curvilinear transfinite or isoparametric mappings of quadrilaterals or hexahedrals, [80], where the mapping  $\Phi$  and its inverse are assumed to be piecewise sufficiently smooth, i.e.

1.  $\Phi$  is a  $C^{p+1}$ -diffeomorphism,
2.  $|\Phi|_{W_{\infty}^l} \leq Ch^l$ ,  $l \leq p + 1$ ,
3.  $|\Phi^{-1}|_{W_{\infty}^l} \leq Ch^{-l}$ ,  $l \leq p + 1$ ,

where  $W_{\infty}^l$  is the Sobolev max-norm. This allows for better approximations in complex domains with curved boundaries, without the need for excessive refinement, while maintaining design interpolation and convergence rates, [46]. This is possible since the projection operator  $\pi_h$  commutes with the pullback  $\Phi^*$ .

**Lemma 5.** *Let  $\pi$  be either  $\pi_h$  or  $\tilde{\pi}_h$  as in Definition 60. For all  $a^{(k)} \in \Lambda^k(\Omega_N)$  and for  $\Phi : \Omega_M \rightarrow \Omega_N$ , there exists a commuting property between the projection operator  $\pi$  and the pullback  $\Phi^*$ , such that*

$$\Phi^* \pi = \pi \Phi^* \quad \text{on } \Lambda^k(\Omega_N). \quad (6.2.3)$$

This commutation can be illustrated as

$$\begin{array}{ccc} \Lambda^k(\Omega_N) & \xrightarrow{\Phi^*} & \Lambda^k(\Omega_M) \\ \downarrow \pi & & \downarrow \pi \\ \Lambda_h^k(\Omega_N; C_k(D_N)) & \xrightarrow{\Phi^*} & \Lambda_h^k(\Omega_M; C_k(D_M)) \end{array}$$

---

<sup>1</sup>Both sub- and superscripts are intentionally suppressed for readability.

where  $\Lambda_h^k(\Omega_{\mathcal{N}}; C_k(D_{\mathcal{N}})) = \Lambda_h^k(\Phi(\Omega_{\mathcal{M}}); \Phi_{\sharp}C_k(D_{\mathcal{M}}))$ .

*Proof.* The proof is based on the commuting properties of the discrete pullback,  $\Phi^{\sharp}$ :

$$\mathcal{IR}\Phi^{\star}a^{(k)} \stackrel{(6.1.6)}{=} \mathcal{I}\Phi^{\sharp}\mathcal{R}a^{(k)} \stackrel{(6.1.9)}{=} \Phi^{\star}\mathcal{IR}a^{(k)}.$$

An alternative proof can be given, based on (4.4.5) and (6.1.17). Integrate over a  $k$ -cell  $\tau_{(k)}$ , then

$$\begin{aligned} \langle \tau_{(k)}, \Phi^{\star}\pi a^{(k)} \rangle &\stackrel{(4.4.5)}{=} \langle \Phi(\tau_{(k)}), \pi a^{(k)} \rangle \stackrel{(6.1.17)}{=} \langle \Phi(\tau_{(k)}), a^{(k)} \rangle \\ &\stackrel{(4.4.5)}{=} \langle \tau_{(k)}, \Phi^{\star}a^{(k)} \rangle \stackrel{(6.1.17)}{=} \langle \tau_{(k)}, \pi\Phi^{\star}a^{(k)} \rangle. \end{aligned}$$

□

This commutation does not hold for the coprojections. Since the pullback operator  $\Phi^{\star}$  commutes with the projection operator, the discrete algebra homomorphism is satisfied

$$\Phi^{\star}(a_h^{(k)} \wedge_h b_h^{(l)}) = \Phi^{\star}\pi(a_h^{(k)} \wedge b_h^{(l)}) = \pi\Phi^{\star}(a_h^{(k)} \wedge b_h^{(l)}) = \pi(\Phi^{\star}a_h^{(k)} \wedge \Phi^{\star}b_h^{(l)}) = \Phi^{\star}a_h^{(k)} \wedge_h \Phi^{\star}b_h^{(l)}.$$

### 6.2.3 The exterior derivative

Now consider the exterior derivative. With (6.1.4) and (6.1.8) a commuting property of the projection with respect to the exterior derivative can be shown.

**Lemma 6 (Commuting property).** *The projections  $\pi_h = \mathcal{IR}$  and  $\tilde{\pi}_h = \tilde{\mathcal{I}}\tilde{\mathcal{R}}$  commute with the exterior derivative,<sup>2</sup>*

$$d\pi_h = \pi_h d \quad \text{and} \quad d\tilde{\pi}_h = \tilde{\pi}_h d \quad \text{on } \Lambda^k(\Omega). \quad (6.2.4)$$

This can be illustrated as

$$\begin{array}{ccc} \Lambda^k & \xrightarrow{d} & \Lambda^{k+1} \\ \downarrow \pi_h & & \downarrow \pi_h \\ \Lambda_h^k & \xrightarrow{d} & \Lambda_h^{k+1} \end{array} \quad \begin{array}{ccc} \Lambda^k & \xrightarrow{d} & \Lambda^{k+1} \\ \downarrow \tilde{\pi}_h & & \downarrow \tilde{\pi}_h \\ \tilde{\Lambda}_h^k & \xrightarrow{d} & \tilde{\Lambda}_h^{k+1}. \end{array}$$

*Proof.* Express the projection in terms of the reduction and reconstruction operator, then for all  $a^{(k)} \in \Lambda^k(\Omega)$ ,

$$d\pi_h a^{(k)} \stackrel{\text{Def. 57}}{=} d\mathcal{IR}a^{(k)} \stackrel{(6.1.8)}{=} \mathcal{I}\delta\mathcal{R}a^{(k)} \stackrel{(6.1.4)}{=} \mathcal{IR}da^{(k)} \stackrel{\text{Def. 57}}{=} \pi_h da^{(k)}.$$

The proof for  $\tilde{\pi}_h = \tilde{\mathcal{I}}\tilde{\mathcal{R}}$  is the same. □

<sup>2</sup>Note that the two projections  $\pi_h$  in (6.2.4) are not the same as can be seen from the commuting diagram. One projection maps  $\Lambda^k$  onto  $\Lambda_h^k$  while the other one maps  $\Lambda^{k+1}$  onto  $\Lambda_h^{k+1}$ . This distinction is generally clear from the context.

Note that it is the intermediate step  $\mathcal{I}\delta\mathcal{R}a^{(k)}$  in the proof of Lemma 6 that is used in practice for the discretization, see Examples 27-29 in Section 7.3 and Examples 35 and 36 in Section 9.4.1. Since we have a matrix representation of the coboundary operator in terms of incidence matrices, we actually see the incidence matrices appear explicitly in the spectral element formulation, see (8.1.28) and (9.4.5).

The discrete wedge product in combination with the exterior derivative gives the Leibniz rule (4.6.2),

$$\begin{aligned} d(a_h^{(k)} \wedge_h b_h^{(l)}) &= d\pi(a_h^{(k)} \wedge b_h^{(l)}) = \pi d(a_h^{(k)} \wedge b_h^{(l)}) \\ &= \pi \left( da_h^{(k)} \wedge b_h^{(l)} + (-1)^k a_h^{(k)} \wedge db_h^{(l)} \right) \\ &= da_h^{(k)} \wedge_h b_h^{(l)} + (-1)^k a_h^{(k)} \wedge_h db_h^{(l)}. \end{aligned} \quad (6.2.5)$$

Combining the commutation relations (6.2.4) and (6.2.3) gives  $\pi\Phi^*d = \Phi^*\pi d = \Phi^*d\pi = d\Phi^*\pi = d\pi\Phi^* = \pi d\Phi^*$ .

### 6.2.4 The discrete inner product

The next operator to be defined is the inner product restricted to the finite dimensional subspace  $\Lambda_h^k$ .

**Definition 63 (Discrete inner product).** Define a discrete inner product  $(\cdot, \cdot)_h : \Lambda_h^k \times \Lambda_h^k \rightarrow \Lambda_h^n$  as

$$(a_h^{(k)}, b_h^{(k)})_h := \pi \left[ (a_h^{(k)}, b_h^{(k)}) \sigma^{(n)} \right], \quad (6.2.6)$$

with either  $\pi = \pi_h$  or  $\pi = \tilde{\pi}_h$ . This discrete inner product is bilinear, symmetric, positive definite.

**Corollary 9 (Discrete  $L^2$ -inner product).** The corresponding  $L^2$ -inner product  $(\cdot, \cdot)_{\Omega, h} : \Lambda_h^k \times \Lambda_h^k \rightarrow \mathbb{R}$  is essentially the same as (4.7.6), because of (6.1.17) and that  $\Lambda_h^k \subset L^2 \Lambda^k$ . Let  $a_h^{(k)}, b_h^{(k)} \in \Lambda_h^k$ , then

$$\begin{aligned} (a_h^{(k)}, b_h^{(k)})_{\Omega, h} &:= \int_{\Omega} (a_h^{(k)}, b_h^{(k)})_h \stackrel{(6.2.6)}{=} \int_{\Omega} \pi \left[ (a_h^{(k)}, b_h^{(k)}) \sigma^{(n)} \right] \\ &\stackrel{(6.1.17)}{=} \int_{\Omega} (a_h^{(k)}, b_h^{(k)}) \sigma^{(n)} = (a_h^{(k)}, b_h^{(k)})_{\Omega}. \end{aligned} \quad (6.2.7)$$

The Hodge star was defined in Definition 20 as a combination of the inner product and the wedge product. Although we defined a discrete wedge product and discrete inner product, the Hodge star remains unchanged because it is an isomorphism,

$$(a_h^{(k)}, b_h^{(k)})_h = a_h^{(k)} \wedge_h \star b_h^{(k)}. \quad (6.2.8)$$

In weak formulations, integrals over  $\Omega$  are considered. In that case (6.2.8) reduces, according to (6.2.2) and (6.2.7), to

$$(a_h^{(k)}, b_h^{(k)})_{\Omega} = \int_{\Omega} a_h^{(k)} \wedge \star b_h^{(k)}. \quad (6.2.9)$$

This result shows that in a weak formulation, the original inner product, wedge product and Hodge star operator can be used.

### 6.2.5 The Hodge star operator

As was mentioned before, since the Hodge star operator is an isomorphism it does not require a discrete counterpart. The Hodge star operator possesses a commuting diagram property with the projection and coprojection operators.

**Proposition 27.** *We have for all  $a^{(k)} \in \Lambda^k(\Omega)$  the following commutation relations,*

$$\pi_h^\star \star = \star \tilde{\pi}_h \quad \text{and} \quad \star \pi_h^\star = \tilde{\pi}_h \star. \quad (6.2.10)$$

*Proof.* From Definition 58 we have

$$\pi_h^\star = (-1)^{k(n-k)} \star \tilde{\pi}_h \star \iff \pi_h^\star \star = \star \tilde{\pi}_h \quad \text{and} \quad \star \pi_h^\star = \tilde{\pi}_h \star.$$

So the Hodge- $\star$  operator at the continuous level commutes with the Hodge star in the finite dimensional setting with respect to the projections  $\tilde{\pi}_h$  and  $\pi_h^\star$ .

$$\begin{array}{ccc} \Lambda^k & \xrightarrow{\star} & \Lambda^{n-k} \\ \downarrow \tilde{\pi}_h & & \downarrow \pi_h^\star \\ \tilde{\Lambda}_h^k & \xrightarrow{\star} & \Lambda_h^{n-k} \end{array} \qquad \begin{array}{ccc} \Lambda^k & \xrightarrow{\star} & \Lambda^{n-k} \\ \downarrow \pi_h^\star & & \downarrow \tilde{\pi}_h \\ \Lambda_h^k & \xrightarrow{\star} & \tilde{\Lambda}_h^{n-k} \end{array}$$

□

Similar commutation relations can be set up on the dual cell complex and this gives: for all  $a^{(k)} \in \Lambda^k(\Omega)$ ,

$$\tilde{\pi}_h^\star \star = \star \pi_h \quad \text{and} \quad \star \tilde{\pi}_h^\star = \pi_h \star, \quad (6.2.11)$$

with the associated commutating diagrams.

**Corollary 10.** *Proposition 27 combined with Proposition 26 gives that for  $a^{(k)} \in \Lambda_h^k$*

$$\tilde{\pi}_h \star \stackrel{\text{Prop. 27}}{=} \star \pi_h^\star \stackrel{\text{Prop. 26}}{=} \star \pi_h.$$

In Definition 20 the Hodge star was defined as a mapping from  $k$ -forms to  $(n-k)$ -forms. As a consequence, not only the dimension of the chain over which they are integrated changes, but also the orientation changes from inner to outer orientation or vice versa. This corresponds to the vertical relations in Figure 4.7. On finite dimensional subspaces, the Hodge star operator is a mapping from  $\Lambda_h^k(\Omega; C_k)$  to  $\Lambda_h^{n-k}(\Omega; \tilde{C}_{n-k})$ , as defined in Definition 58.

With the Hodge star and exterior derivative, the finite dimensional double De Rham complex can be set up similar to (4.7.4) as

$$\begin{array}{ccccccccc} \mathbb{R} & \longrightarrow & \Lambda_h^0(\Omega; C_0) & \xrightarrow{d} & \Lambda_h^1(\Omega; C_1) & \xrightarrow{d} & \dots & \xrightarrow{d} & \Lambda_h^n(\Omega; C_n) & \xrightarrow{d} & 0 \\ & & \star \uparrow & & \star \uparrow & & & & \star \uparrow & & \\ 0 & \xleftarrow{d} & \Lambda_h^n(\Omega; \tilde{C}_n) & \xleftarrow{d} & \Lambda_h^{n-1}(\Omega; \tilde{C}_{n-1}) & \xleftarrow{d} & \dots & \xleftarrow{d} & \Lambda_h^0(\Omega; \tilde{C}_0) & \longleftarrow & \mathbb{R}. \end{array}$$

### 6.2.6 The codifferential

With Definition 58 a commuting property of the coprojection with respect to the codifferential can be shown.

**Proposition 28.** *For all  $a^{(k)} \in \Lambda^k(\Omega)$  we have*

$$\pi_h^* d^* = d^* \pi_h^* \quad \text{and} \quad \tilde{\pi}_h^* d^* = d^* \tilde{\pi}_h^*.$$

*Proof.*

$$\begin{aligned} \pi_h^* d^* &\stackrel{\text{Def. 59, Prop. 8}}{=} (-1)^{k(n-k)} \star \tilde{\pi}_h \star (-1)^{n(k+1)+1} \star d \star \stackrel{(4.7.2b)}{=} (-1)^{n+k+1} \star \tilde{\pi}_h d \star \\ &\stackrel{\text{Lem. 6}}{=} (-1)^{n+k+1} \star d \tilde{\pi}_h \star \stackrel{(4.7.2b)}{=} (-1)^{n(k+1)+1} \star d \star (-1)^{k(n-k)} \star \tilde{\pi}_h \star \stackrel{\text{Def. 59, Prop. 8}}{=} d^* \pi_h^*. \end{aligned}$$

The proof for  $\tilde{\pi}_h^*$  is the same.  $\square$

This means that the codifferential is exact with respect to the coprojection, i.e. the following diagram commutes

$$\begin{array}{ccc} \Lambda^{k+1} & \xrightarrow{d^*} & \Lambda^k \\ \downarrow \pi_h^* & & \downarrow \pi_h^* \\ \Lambda_h^{k+1} & \xrightarrow{d^*} & \Lambda_h^k \end{array} \quad \begin{array}{ccc} \Lambda^{k+1} & \xrightarrow{d^*} & \Lambda^k \\ \downarrow \tilde{\pi}_h^* & & \downarrow \tilde{\pi}_h^* \\ \Lambda_h^{k+1} & \xrightarrow{d^*} & \Lambda_h^k \end{array}$$

**Corollary 11.** *Combining Proposition 28 and Proposition 26 shows that for  $a_h^{(k)} \in \Lambda_h^k$  we have*

$$\pi_h d^* \stackrel{\text{Prop. 26}}{=} \pi_h^* d^* \stackrel{\text{Prop. 28}}{=} d^* \pi_h^* \stackrel{\text{Prop. 26}}{=} d^* \pi_h.$$

The projection does *not* commute with codifferential operator on the whole of  $\Lambda^k$ . This is the main reason why we rewrite the codifferentials into exterior derivatives and boundary integrals, by means of integration by parts in the mixed formulations used in Part III of this thesis.

## 6.3 $L^2$ -bounded projection operator

Essential ingredients in proving numerical stability are a bounded projection that commutes with the exterior derivative, a discrete Hodge decomposition and a discrete Poincaré inequality. The projection operator  $\pi_h$  only projects smooth differential forms onto finite dimensional space, but not differential forms that have only  $L^2\Lambda^k$  or  $H\Lambda^k$  regularity. Christiansen [45] and Arnold et al. [6] introduced a smoothing operator  $\mathfrak{R}_h^\varepsilon : L^2\Lambda^k(\Omega) \rightarrow \Lambda^k(\Omega)$  that commutes with the exterior derivative,  $d\mathfrak{R}_h^\varepsilon = \mathfrak{R}_h^\varepsilon d$ . Then  $\pi_h \mathfrak{R}_h^\varepsilon : L^2\Lambda^k(\Omega) \rightarrow \Lambda_h^k(\Omega; C_k)$ . The smoothing operator  $\mathfrak{R}_h^\varepsilon$  constitutes of a convolution product between an extension function and a mollifier function. Premultiplication with  $(\pi_h \mathfrak{R}_h^\varepsilon)^{-1}$ , which is an identity map  $\Lambda_h^k \rightarrow \Lambda_h^k$ , makes it a projection. This gives the  $L^2\Lambda^k$ -regular projection,  $\pi_h^\varepsilon$ ,

$$\pi_h^\varepsilon = (\pi_h \mathfrak{R}_h^\varepsilon)^{-1} \pi_h \mathfrak{R}_h^\varepsilon. \quad (6.3.1)$$

---

**Corollary 12 (Commutation property).** *Since the smoothing operator and mimetic projection both commute with the exterior derivative, it follows that the  $L^2\Lambda^k$ -regular projection commutes with the exterior derivative on  $H\Lambda^k(\Omega)$ ,*

$$d\pi_h^\varepsilon = \pi_h^\varepsilon d. \quad (6.3.2)$$

This can be illustrated as

$$\begin{array}{ccc} H\Lambda^k & \xrightarrow{d} & L^2\Lambda^{k+1} \\ \downarrow \pi_h^\varepsilon & & \downarrow \pi_h^\varepsilon \\ \Lambda_h^k & \xrightarrow{d} & \Lambda_h^{k+1}. \end{array}$$

For a projection operator  $\pi_h$  to be a useful operator, we require it to be a bounded projection operator.

**Definition 64 (Bounded projection).** *Let  $\pi_h := \mathcal{IR} : \Lambda^k(\Omega) \rightarrow \Lambda_h^k(\Omega; C_k)$  denotes the projection operator, and let  $:L^2\Lambda^k(\Omega) \rightarrow \Lambda^k(\Omega)$  be a smoothing operator, then the  $L^2\Lambda^k$ -regular projection,  $\pi_h^\varepsilon : L^2\Lambda^k(\Omega) \rightarrow \Lambda_h^k(\Omega; C_k)$ , is a bounded operator if for  $C_1 < \infty$  and for all  $a \in H\Lambda^k(\Omega)$  we have*

$$\|\pi_h^\varepsilon\|_{\mathcal{L}(H\Lambda^k, \Lambda_h^k)} := \sup_{a^{(k)} \in H\Lambda^k} \frac{\|\pi_h^\varepsilon a^{(k)}\|_{H\Lambda^k}}{\|a^{(k)}\|_{H\Lambda^k}} \leq C_1. \quad (6.3.3)$$

**Corollary 13.** *Alternatively, one can write for the bounded projection operator*

$$\|\pi_h^\varepsilon a^{(k)}\|_{H\Lambda^k} \leq C_1 \|a^{(k)}\|_{H\Lambda^k}. \quad (6.3.4)$$

From the triangle inequality applied to  $\|a^{(k)}\|_{\Lambda^k}$  it follows that there exists  $C_2 = C_1 + 1 < \infty$ , such that

$$\|(Id - \pi_h^\varepsilon)a^{(k)}\|_{H\Lambda^k} \leq C_2 \|a^{(k)}\|_{H\Lambda^k}. \quad (6.3.5)$$

In Section ?? boundedness is proven for mimetic spectral elements. More details on smoothed projections can be found in [6, 45].

## 6.4 Discrete Hodge decomposition

The continuous Hodge decomposition and the cochain space decompositon, are related to each other by means of the reduction and reconstruction operators. Moreover, it defines the subspaces that constitute the discrete Hodge decomposition. From the definition of the reduction operator  $\mathcal{R}$ , the Hodge decomposition for  $k$ -forms and the cochain space decomposition, it follows that

$$\mathcal{B}^k \xrightarrow{\mathcal{R}} B^k, \quad \mathcal{H}^k \xrightarrow{\mathcal{R}} H^k, \quad \mathcal{Z}^{k,\perp} \xrightarrow{\mathcal{R}} Z^{k,\perp}. \quad (6.4.1)$$

In opposite direction, the reconstruction operator  $\mathcal{I}$  maps each subspace of the cochain space decomposition into their corresponding finite dimensional subspace,

$$B^k \xrightarrow{\mathcal{I}} \mathcal{B}_h^k, \quad H^k \xrightarrow{\mathcal{I}} \mathcal{H}_h^k, \quad Z^{k,\perp} \xrightarrow{\mathcal{I}} \mathcal{Z}_h^{k,\perp}. \quad (6.4.2)$$

From this it follows that  $\mathcal{B}_h^k = \pi_h^\varepsilon \mathcal{B}^k$ ,  $\mathcal{B}_h^k = \pi_h^\varepsilon \mathcal{Z}^k$ ,  $\mathcal{H}_h^k = \pi_h^\varepsilon \mathcal{H}^k$  and  $\mathcal{Z}_h^{k,\perp} = \pi_h^\varepsilon \mathcal{Z}^{k,\perp}$ . As a consequence we obtain discrete well-posedness.

---

**Theorem 4 (Discrete well-posedness).** For  $f^{(k+1)} \in \mathcal{B}^{k+1}$  and  $a^{(k)} \in \mathcal{Z}^{k,\perp}$ , the equation  $da^{(k)} = f^{(k+1)}$  is well-posed in the sense that there exists a solution and the solution is unique. Then the discrete equation  $da_h^{(k)} = f_h^{(k+1)}$  is also well-posed in case the projection  $\pi$  is either  $\pi_h$  or  $\tilde{\pi}_h$ .

*Proof.* For  $f^{(k+1)} \in \mathcal{B}^k$  and  $a^{(k)} \in \mathcal{Z}^{k,\perp}$  there exists a unique solution by the Hodge decomposition (4.9.5). The discrete equation follows by projection,

$$0 = \pi(da^{(k)} - f^{(k+1)}) = d\pi a^{(k)} - \pi f^{(k+1)} = da_h^{(k)} - f_h^{(k+1)}.$$

Moreover we can write

$$\pi da^{(k)} - \pi f^{(k+1)} = \mathcal{I}(\delta \mathcal{R} a^{(k)} - \mathcal{R} f^{(k+1)}) = \mathcal{I}(\delta \mathbf{a}^{(k)} - \mathbf{f}^{(k+1)}).$$

By (6.4.1),  $\mathcal{R} a^{(k)} = \mathbf{a}^{(k)} \in Z^{k,\perp}$  and  $\mathcal{R} f^{(k+1)} = \mathbf{f}^{(k+1)} \in B^{k+1}$ . Because  $\mathcal{I}$  is bijective, the discrete problem is also well-posed, since the cochain relation  $\delta \mathbf{a}^{(k)} = \mathbf{f}^{(k+1)}$  is well-posed, see Proposition 21 (p. 82). Furthermore, it follows that  $a_h^{(k)}$  has a unique solution, because  $\mathbf{a}^{(k)}$  is a unique cochain of the problem  $\delta \mathbf{a}^{(k)} = \mathbf{f}^{(k+1)}$ .  $\square$

Of most interest is that we obtain a pointwise divergence-free solution of the velocity field as expressed by the incompressibility constraint in fluid dynamics problems. This is illustrated in the following example (see also Chapter 9 and [113]).

**Example 22 (Pointwise divergence-free).** Consider the relation  $du^{(n-1)} = g^{(n)}$ , with  $u^{(n-1)} \in H\Lambda^{n-1}(\Omega)$  and  $g \in \mathcal{B}^n(\Omega)$ . In vector notation the  $d$  represents the div operator. Now let  $du_h^{(n-1)} = g_h^{(n)}$  be the discretization of our continuous problem, with  $u_h \in \Lambda_h^{n-1}(\Omega)$  and  $g_h \in \mathcal{B}_h^n(\Omega)$ . Then by using (6.2.4) we get

$$du_h^{(n-1)} - g_h^{(n)} = d\pi_h u^{(n-1)} - \pi_h g^{(n)} = \pi_h(du^{(n-1)} - g^{(n)}) = 0.$$

It follows that our discretization is exact. In case  $g^{(n)} = 0$ , we have a pointwise divergence-free solution of  $u_h^{(n-1)}$ .

Let  $\Lambda_h^k \subset H\Lambda^k$  be the space of finite dimensional differential forms, and let  $(\Lambda_h, d)$  be a finite-dimensional subcomplex with  $d\Lambda_h^k \subset \Lambda_h^{k+1}$ . Since the exterior derivative commutes with the projection operator, Lemma 6 (p. 102), it follows that  $\mathcal{B}_h^k \subset \mathcal{B}^k$ ,  $\mathcal{Z}_h^k \subset \mathcal{Z}^k$  and that  $\mathcal{B}_h^k \subseteq \mathcal{Z}_h^k$ . We can make the following decomposition of the space of discrete differential forms,

$$\Lambda_h^k = \mathcal{B}_h^k \oplus \mathcal{B}_h^{k,\perp}.$$

The space of discrete harmonic forms is defined as  $\mathcal{H}_h^k = \mathcal{Z}_h^k \cap \mathcal{B}_h^{k,\perp}$ . This gives the following decomposition,  $\mathcal{B}_h^{k,\perp} = \mathcal{H}_h^k \oplus \mathcal{Z}_h^{k,\perp}$ . Although  $\mathcal{B}_h^{k,\perp} \subset \mathcal{B}^{k,\perp}$ , in general,  $\mathcal{H}_h^k \not\subset \mathcal{H}^k$  and  $\mathcal{Z}_h^{k,\perp} \not\subset \mathcal{Z}^{k,\perp}$ . Both harmonic spaces  $\mathcal{H}^k$  and  $\mathcal{H}_h^k$  are finite dimensional spaces and their dimension depends only on the topology of the domain  $\Omega$ . Because the dimension only depends on the topology (its Bettie number), we have  $\mathfrak{B}_k = \dim \mathcal{H}_h^k = \dim \mathcal{H}^k$ . Take for instance  $\mathfrak{B}^k = 1$ , then  $\mathcal{H}_h^k$  is a polynomial function, while  $\mathcal{H}^k$  could be any harmonic function. Therefore  $\mathcal{H}_h^k \not\subset \mathcal{H}^k$ . The gap between  $\mathcal{H}_h^k$  and  $\mathcal{H}^k$  vanishes then as  $h \rightarrow 0$ . See Theorem 3.5 in [8] for the definition and details about

the gap between the two harmonic form spaces. Similarly,  $\mathcal{Z}_h^{k,\perp}$  approaches  $\mathcal{Z}^{k,\perp}$  as  $h \rightarrow 0$ . Substitution of the decompositions gives the discrete Hodge decomposition,

$$\Lambda_h^k = \mathcal{B}_h^k \oplus \mathcal{H}_h^k \oplus \mathcal{Z}_h^{k,\perp}. \quad (6.4.3)$$

Lemma 6 (p. 102), in combination with the discrete Hodge decomposition has some nice consequences concerning consistency and stability of the numerical method.

**Corollary 14 (Compatible discretization).** *Lemma 6 makes the discretization method compatible, such that we have,  $\mathcal{B}_h^k \subset \mathcal{B}^k$ ,  $\mathcal{Z}_h^k \subset \mathcal{Z}^k$ ,  $\pi_h^\varepsilon \mathcal{Z}^{k,\perp} = \mathcal{Z}_h^{k,\perp}$  and, on contractible domains,  $\mathcal{Z}_h^{k,\perp} \subset \mathcal{Z}^{k,\perp}$ . Consequently if  $d : \mathcal{Z}^{k,\perp} \rightarrow \mathcal{B}^{k+1}$  is a bijection, so is  $d : \mathcal{Z}_h^{k,\perp} \rightarrow \mathcal{B}_h^{k+1}$ .*

Because the complexes  $(H\Lambda, d)$  and  $(\Lambda_h, d)$  are each others supercomplex and subcomplex, respectively, the discrete Poincaré inequality is directly related to the Poincaré inequality in Lemma 2 (p. 63), and the bounded projection defined in Definitions 57 (p. 96) and 64 (p. 106).

**Lemma 7 (Discrete Poincaré inequality).** [8] *Let  $(H\Lambda, d)$  and subcomplex  $(\Lambda_h, d)$  be closed Hilbert complexes, and  $\pi_h^\varepsilon$  a bounded projection. Then*

$$\|a_h\|_{H\Lambda^k} \leq c_{Ph} \|da_h\|_{L^2\Lambda^k}, \quad a_h \in \mathcal{Z}_h^{k,\perp}. \quad (6.4.4)$$

*Proof.* For contractible domains: Given  $a_h \in \mathcal{Z}_h^{k,\perp}$ . From the Hodge decomposition and the bounded projection it follows that  $\mathcal{B}_h^k \subset \mathcal{B}^k$  and  $\mathcal{Z}_h^k \subset \mathcal{Z}^k$  and from the commutation relation (6.2.4) it follows that  $\mathcal{Z}_h^{k,\perp} \subset \mathcal{Z}^{k,\perp}$  on contractible domains. Since we consider a proper subspace, Lemma 2 is still valid, with  $1 \leq c_{Ph} \leq c_P$ .

For non-contractible domains: Given  $a_h \in \mathcal{Z}_h^{k,\perp}$ , define  $z \in \mathcal{Z}^{k,\perp} \subset H\Lambda^k$  by  $dz = da_h$ . It holds that  $\mathcal{B}_h^{k+1} \subset \mathcal{B}^{k+1}$ , but on non-contractible domains,  $\mathcal{Z}_h^{k,\perp} \not\subset \mathcal{Z}^{k,\perp}$ . By the Poincaré inequality,  $\|z\|_{H\Lambda^k} \leq c_P \|da_h\|_{L^2\Lambda^{k+1}}$ , so it is enough to show that  $\|a_h\|_{H\Lambda^k} \leq \|\pi_h^\varepsilon z\|_{H\Lambda^k}$ . Now,  $a_h - \pi_h^\varepsilon z \in \Lambda_h^k$  and  $d(a_h - \pi_h^\varepsilon z) = da_h - \pi_h^\varepsilon dz = da_h - \pi_h^\varepsilon da_h = 0$  by Lemma 6, so  $a_h - \pi_h^\varepsilon z \in \mathcal{Z}_h^k$ . Therefore

$$\|a_h\|_{H\Lambda^k}^2 = (a_h, \pi_h^\varepsilon z)_{H\Lambda^k} + (a_h, a_h - \pi_h^\varepsilon z)_{H\Lambda^k} = (a_h, \pi_h^\varepsilon z)_{H\Lambda^k} \leq \|a_h\|_{H\Lambda^k} \|\pi_h^\varepsilon z\|_{H\Lambda^k}.$$

The result follows from the boundedness of the projection operator norm, Definition 64, with  $c_{Ph} \leq c_p \|\pi_h^\varepsilon\|$ .  $\square$

The commuting property (6.2.4) prevents the approximate solution from having spurious oscillations, in case of elliptic problems, without the need for artificial stabilization, as in [96, 97]. In other words it automatically satisfies the Ladyshenskaya-Babuška-Brezzi (LBB) stability condition or inf-sup condition, [14, 37].

**Corollary 15 (Inf-sup condition).** *Let  $a_h^{(k)} \in \mathcal{Z}_h^{k,\perp}$  and  $b_h^{(k+1)} \in \mathcal{B}_h^{k+1}$  and consider the bilinear form  $(da_h^{(k)}, b_h^{(k+1)})_\Omega$ . Then by Lemma 6 the discrete inf-sup condition is automatically satisfied, i.e. there exists a positive constant  $c$  such that*

$$\inf_{b_h^{(k+1)} \in \mathcal{B}_h^{k+1}} \sup_{a_h^{(k)} \in \mathcal{Z}_h^{k,\perp}} \frac{(da_h^{(k)}, b_h^{(k+1)})_\Omega}{\|a_h^{(k)}\|_{H\Lambda^k} \|b_h^{(k+1)}\|_{H\Lambda^{k+1}}} \geq c.$$

*Proof.* Given  $b_h^{(k+1)} \in \mathcal{B}_h^{k+1}$ , there exists a unique  $a_{b,h}^{(k)} \in \mathcal{Z}_h^{k,\perp}$  such that  $\mathrm{d}a_{b,h}^{(k)} = b_h^{(k+1)}$  and  $\|a_{b,h}^{(k)}\|_{H\Lambda^k} \leq c_{Ph}\|b_h^{(k+1)}\|_{H\Lambda^{k+1}}$  by Lemma 7. Therefore,

$$\sup_{a_h^{(k)} \in \mathcal{Z}_h^{k,\perp}} \frac{(\mathrm{d}a_h^{(k)}, b_h^{(k+1)})_\Omega}{\|a_h^{(k)}\|_{H\Lambda^k}} \geq \frac{(\mathrm{d}a_{b,h}^{(k)}, b_h^{(k+1)})_\Omega}{\|a_{b,h}^{(k)}\|_{H\Lambda^k}} = \frac{\|b_h^{(k+1)}\|_{H\Lambda^{k+1}}^2}{\|a_{b,h}^{(k)}\|_{H\Lambda^k}} \geq \frac{1}{c_{Ph}} \|b_h^{(k+1)}\|_{H\Lambda^{k+1}}.$$

□

So as a direct consequence of Lemma 6 we satisfy the LBB stability criterion, see [37, 79, 111].

Since  $\mathcal{Z}^{k,\perp} = \mathcal{B}^{*,k}$  for boundaryless domains (Proposition 11 (p. 64)), we can express the discrete Hodge decomposition alternatively as

$$\Lambda_h^k = \mathcal{B}_h^k \oplus \mathcal{H}_h^k \oplus \mathcal{B}_h^{*,k}. \quad (6.4.5)$$

**Example 23.** Consider the Hodge decomposition, Corollary 5 (p. 65), of a  $k$ -form,  $a^{(k)} \in \Lambda^k$ , in terms of  $b^{(k-1)} \in \Lambda^{k-1}$ ,  $h^{(k)} \in \mathcal{H}^k$  and  $c^{(k+1)} \in \Lambda^{k+1}$ ,

$$a^{(k)} = \mathrm{d}b^{(k-1)} + h^{(k)} + \mathrm{d}^*c^{(k+1)}.$$

Then apply the projection operator,  $\pi_h$ ,

$$\pi_h a^{(k)} = \mathrm{d}\pi_h b^{(k-1)} + \pi_h(h^{(k)} + \mathrm{d}^*c^{(k+1)}) = \underbrace{\mathrm{d}b_h^{(k-1)}}_{\in \mathcal{B}_h^k} + \underbrace{(h_h^{(k)} + \mathrm{d}^*e_h^{(k+1)})}_{\in \mathcal{B}_h^{k,\perp}},$$

where  $h_h^{(k)} \in \mathcal{H}_h^k \not\subset \mathcal{H}^k$  and  $e_h^{(k+1)} \in \Lambda_h^{k+1}$ , but  $e_h^{(k+1)} \neq \pi_h c^{(k+1)}$ . If we apply the coprojection operator,  $\pi_h^*$ , to  $a^{(k)}$ , we obtain

$$\pi_h^* a^{(k)} = \pi_h^* \mathrm{d}b^{(k-1)} + \pi_h^* h^{(k)} + \mathrm{d}^*\pi_h^* c^{(k+1)} = \underbrace{\mathrm{d}r_h^{(k-1)}}_{\in \mathcal{B}_h^{*,k,\perp}} + \underbrace{h_{h^*}^{(k)}}_{\in \mathcal{B}_h^{*,k}} + \underbrace{\mathrm{d}^*c_h^{(k+1)}}_{\in \mathcal{B}_h^{*,k}},$$

where  $h_{h^*}^{(k)} \in \mathcal{H}_{h^*}^k \not\subset \mathcal{H}^k$  and  $r_h^{(k-1)} \in \Lambda_h^{k-1}$ , but  $r_h^{(k-1)} \neq \pi_h^* b^{(k-1)}$ .

Finally, Example 23 showed the decomposition of the finite dimensional  $k$ -form  $a_h^{(k)} \in \Lambda_h^k$  and  $h_h^{(k)} \in \mathcal{H}_h^k$  its harmonic part by the discrete Hodge decomposition. In order to find the harmonic form  $h_h^{(k)}$ , we first determine the harmonic chains,  $\mathbf{h}_{(k)}$  in the cell complex, as described in Example 16 (p. 77), and the harmonic cochains,  $\mathbf{h}^{(k)}$ , as described in Example 17 (p. 83). Both the harmonic chains and cochains can be obtained by purely topological considerations and the calculations are performed through the incidence matrices. For  $\mathfrak{B}_k = \dim(\mathcal{H}_h^k) = 1$ , we set  $h_h^{(k)} = \mathcal{I}(\alpha \mathbf{h}^{(k)})$ , where  $\alpha$  is obtained from the definition of reduction,

$$\langle \mathbf{h}_{(k)}, \mathcal{R}a^{(k)} \rangle = \langle \mathbf{h}_{(k)}, \alpha \mathbf{h}^{(k)} \rangle \implies \alpha = \frac{\langle \mathbf{h}_{(k)}, \mathcal{R}a^{(k)} \rangle}{\langle \mathbf{h}_{(k)}, \mathbf{h}^{(k)} \rangle}. \quad (6.4.6)$$

---

When  $\mathfrak{B}_k > 1$ , we repeat this process for all harmonic chain-cochain pairs and set

$$h_h^{(k)} = \sum_{j=1}^{\mathfrak{B}_k} \alpha_j \mathcal{I} \mathbf{h}_i^{(k)} . \quad (6.4.7)$$

Note that, by construction,  $d h_h^{(k)} \equiv 0$ .

## 6.5 Discussion

Although the reduction operator  $\mathcal{R}$  and the reconstruction operator  $\mathcal{I}$  are also introduced in [18, 99], we have chosen to work in  $\Lambda_h^k = \mathcal{I}\mathcal{R}\Lambda^k$  instead of  $C^k = \mathcal{R}\Lambda^k$ . The reason is that inner product and Hodge star operators are metric concepts which cannot be modeled in topology. Furthermore, these metric concepts are independent of the reduction operator, but depend explicitly on the reconstruction operator  $\mathcal{I}$ .

# Chapter 7

## Mimetic Spectral Elements

This chapter is based on Kreeft et al. [115].

$$Rapetti : \quad \|u - u_h\|_{1,\Omega} \leq C(s)h^{\min(N+1,s)}N^{1-s}\|u\|_{s,\Omega}.$$

Now that a mimetic framework is formulated using differential geometry, algebraic topology and the relations between those - the mimetic operators - we derive reconstruction functions,  $\mathcal{I}$ , that satisfy the properties of the mimetic operators. In combination with the reduction operator,  $\mathcal{R}$ , it defines the mimetic projection operators,  $\pi_h$ . The finite dimensional  $k$ -forms used in this thesis are polynomials, based on the ideas of finite and spectral element methods, [42]. Spectral element methods have many desirable features such as arbitrary polynomial representation, favourable conditioning, element wise local support, and optimal stability and approximation properties. However, the definition of the reconstruction operator requires a new set of spectral element interpolation functions. The *mimetic spectral elements* were derived independently by [73, 157], and are more extensively discussed in this thesis and the related paper, [115].

This chapter starts with the introduction of a domain decomposition of the computational domain into a set of ‘large’ elements. With each element we define a corresponding sub cell complex. In Section 7.2 the mimetic spectral element basis functions are derived, which, together with the reduction step, constitutes the projection operators on the primal and dual grids. Subsequently, properties like boundedness and interpolation errors are derived. In Section 7.3 examples of the action of discrete operators are shown for the mimetic spectral element method. That mimetic spectral elements are not the only type of basis functions suitable for this mimetic framework is shown in Section 7.4. This chapter is closed in Section 7.5 with a discussion and some concluding remarks.

Fischer SEM: Relative error  $h$  vs  $p$  refinement  $u_t + u_x = 0 \Rightarrow$  fraction of accurately resolved modes is increased *only* through increased order  $\Rightarrow p$ -refinement. HOE??

---

Fischer SEM: Long distance  $\rightarrow$  Longtime simulations require methods with low dispersion error. High-order methods can efficiently deliver small dispersion errors, Kreiss & Oliger 72, Gottlieb 2007.

## 7.1 Domain partitioning

Instead of solving in the infinite-dimensional space  $\Lambda^k(\Omega)$  we restrict our search to a proper subspace  $\Lambda_h^k(\Omega; C_k) \subset \Lambda^k(\Omega)$ . Although there already exists several methods for the subspace  $\Lambda_h^k(\Omega; C_k)$ , (see for example [6, 40, 93, 133, 134, 153, 154]), here we focus on a spectral element based method for curvilinear quadrilaterals or hexahedrals.

In spectral element methods the mesh  $\mathcal{Q}$  is a covering of the computational domain  $\Omega$  and is decomposed into  $M$ , in this case curvilinear quadrilateral or hexahedral subdomains  $Q_m$ ,

$$\mathcal{Q} = \bigcup_{m=1}^M Q_m, \quad \overset{\circ}{Q}_m \cap \overset{\circ}{Q}_l = \emptyset, \quad m \neq l, \quad (7.1.1)$$

where in each sub-domain a Gauss-Lobatto grid is constructed, see Figure 7.1. The collection of Gauss-Lobatto grids in all elements  $Q_m \in \mathcal{Q}$  constitutes the cell complex  $D$ . For each spectral element there exists a sub cell complex,  $D_m$ , i.e. the sub cell complex in the spectral element  $Q_m$ . Note that  $D_m \cap D_l$ ,  $m \neq l$ , is not an empty set in case they are neighboring elements, but contains all  $k$ -cells,  $k = 0, 1, \dots, n - 1$ , of the common boundary, see Definition 31 (p. 72).

Each sub-domain  $Q_m \in \mathcal{Q}$  is obtained from the map  $\Phi_m : \widehat{Q} \rightarrow Q_m$ , where the reference domain  $\widehat{Q}$  is a unit  $n$ -cube  $\widehat{Q} := [-1, 1]^n$ , with  $n = \dim(\Omega)$ . All differential forms defined on  $Q_m$  are pulled back onto this reference element using the following pullback operation<sup>1</sup>,  $\Phi_m^* : \Lambda_h^k(Q_m; C_k) \rightarrow \Lambda^k(\widehat{Q}; C_k)$ . In three dimensions the reference element is given by

$$\widehat{Q} := \{(\xi, \eta, \zeta) \mid -1 \leq \xi, \eta, \zeta \leq 1\}. \quad (7.1.2)$$

The solution within each sub-domain is expanded with respect to a polynomial basis, corresponding to the chains in that element.

**Remark 31.** *The map  $\Phi_m = \varphi_m^{-1}$  is essentially the inverse of a chart from the computational domain  $\Omega$  to the unit cube in  $\mathbb{R}^n$ . The map from the cells formed by the Gauss-Lobatto grid in  $[-1, 1]^n$  to the cells in  $\mathcal{Q}$  are the singular  $n$ -cubes.*

## 7.2 Reconstruction, mimetic basis functions and projections

In the previous section two reconstruction operators were introduced,  $\mathcal{I}$  acting on the primal cell complex  $D$  and  $\tilde{\mathcal{I}}$  acting on the dual cell complex  $\tilde{D}$ . Together with the two reduction operators  $\mathcal{R}$  and  $\tilde{\mathcal{R}}$ , they define two projection and two coprojection operators.

---

<sup>1</sup>formally, the chain-space is also mapped, using the chain map  $\Phi_\sharp$ . Then  $\Phi_m^* : \Lambda_h^k(\Phi_m(\widehat{Q}); \Phi_\sharp C_k) \rightarrow \Lambda_h^k(\widehat{Q}; C_k)$ . However, we ignore the mapping on the topology space.

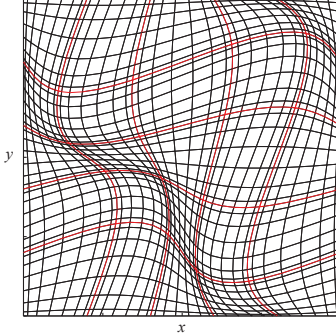


Figure 7.1: A  $5 \times 5$  curvilinear multi-element Gauss-Lobatto grid.

In this section we derive mimetic spectral interpolatory basis functions as reconstruction, that are cardinal basis functions of arbitrary polynomial order, and that are capable of reconstructing  $k$ -cochains according to Definition 56 (p. 94). Because we consider only tensor product based mimetic spectral elements for the reconstruction, it is sufficient to do the derivation and analysis in one dimension only, and use tensor products afterwards to construct  $n$ -dimensional basis functions. A similar approach was taken in [40]. Because the projection operator and the pullback operator commute (6.2.3), the interpolation functions are discussed for the reference element only. Since the mappings  $\Phi_m$  and their inverse are assumed to be sufficiently smooth, see Section 6.2.2, the rates of convergence for interpolation estimates on the physical elements are equal to that of the reference element. Only the constants  $C$  that will appear below will depend on the mappings  $\Phi_m$ , but will be independent of the meshsize and polynomial order.

### 7.2.1 Projection $\pi_h$ using $D$

In spectral element methods the  $k$ -forms on  $Q_m$  are approximated by piecewise polynomial expansions. The domain is given by  $\Omega = \mathcal{Q} = Q_1 = \widehat{Q} := \{\xi \mid -1 \leq \xi \leq 1\}$ . We start with the projection operator  $\pi_h$ , which is formed by the reconstruction of the reduction of a  $k$ -form on the interior cell complex  $D_i$ , see Section 5.4. On  $\widehat{Q}$  a cell complex  $D$  is defined according to Definition 31, that consists of  $N + 1$  nodes (0-cells),  $\tau_{(0),i} = \xi_i$ , where  $-1 \leq \xi_0 < \dots < \xi_N \leq 1$ , and  $N$  line segments (1-cells),  $\tau_{(1),i} = [\xi_{i-1}, \xi_i]$ , of which the nodes constitute the boundary, see Figure 5.11. Consider a 0-form  $a^{(0)} = a(\xi) \in \Lambda^0(\widehat{Q})$ . Corresponding to this set of nodes (0-chain) there exists a projection,  $\pi_h$ , using  $N^{\text{th}}$  order *Lagrange polynomials*,  $l_i(\xi)$ , to approximate a 0-form, as

$$\pi_h a^{(0)}(\xi) = \sum_{i=0}^N a_i l_i(\xi), \quad (7.2.1)$$

where  $a_i = \bar{\psi}_i(\mathbf{a}^{(0)}) = \bar{\psi}_i(\mathcal{R}(a^{(0)})) = a(\xi_i)$ , and where  $\bar{\psi}$  is the isomorphism which associates a  $k$ -cochain to its coefficients in the expansion in terms of canonical basis  $k$ -cochains, see Definition 42. The  $i^{\text{th}}$  coefficient is referred to as  $\bar{\psi}_i$ . Lagrange polyno-

mials have the property that they interpolate nodal values and are therefore suitable to reconstruct the cochain  $\mathbf{a}^{(0)} = \mathcal{R}a^{(0)}$  containing the set  $a_i = a(\xi_i)$  for  $i = 0, \dots, N$ . So these polynomials can be used to reconstruct a 0-form from a 0-cochain. Lagrange polynomials are in fact 0-forms themselves,  $l_i^{(0)}(\xi) \in \Lambda_h^0(\widehat{Q}; C_0)$ . They are constructed such that its value is one in the corresponding point and zero in all other grid points,

$$\mathcal{R}l_i^{(0)}(\xi) = l_i^{(0)}(\xi_p) = \begin{cases} 1 & \text{if } i = p \\ 0 & \text{if } i \neq p \end{cases}. \quad (7.2.2)$$

This is a special case of (6.1.7), where in this case  $\mathcal{I} = l_i^{(0)}(\xi)$ . It is straightforward

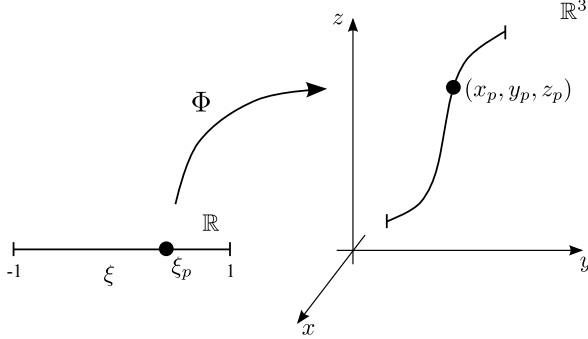


Figure 7.2: The map from  $\xi \in [-1, 1]$  into a 1-dimensional sub-manifold in  $\mathbb{R}^2$ .

to show that Lagrange polynomials are invariant under a coordinate transformation. If  $\bar{l}_i(\mathbf{x})$  is a Lagrange polynomial defined on a curvilinear 1-manifold embedded in a three-dimensional domain, with  $\mathbf{x} := (x, y, z)$ , then on that manifold there exist 0-cells  $\tau_{(0),p}(\mathbf{x})$ , associated to each Gauss-Lobatto node  $p$ ,  $\mathbf{x}_p$ , of the mesh of that manifold. In this case the mapping is given by  $\mathbf{x} = \Phi(\xi)$  and the mapping of node  $p$  by  $\mathbf{x}_p = \Phi(\xi_p)$ , see Figure 7.2. As a consequence  $\Phi^* \bar{l}_i(\mathbf{x}) = l_i(\xi)$ , and so:

$$\bar{l}_i(\mathbf{x})|_{\mathbf{x}=\mathbf{x}_p} = \bar{l}_i(\Phi(\xi))|_{\xi=\xi_p} = (\Phi^* \bar{l}_i)(\xi)|_{\xi=\xi_p} = l_i(\xi)|_{\xi=\xi_p} = \delta_{i,p}.$$

Other useful properties of Lagrange polynomials are

$$\sum_{i=0}^N l_i(\xi) = 1, \quad \sum_{i=0}^N d l_i(\xi) = 0. \quad (7.2.3)$$

Gerritsma [73] and Robidoux [157] independently derived the same projection for 1-forms, consisting of 1-cochains and 1-form polynomials, that is called the *edge polynomial*,  $e_i^{(1)}(\xi) \in \Lambda_h^1(\widehat{Q}; C_1)$ .

**Lemma 8.** *Following Definitions 53 (p. 92) and 56 (p. 94), apply the exterior derivative  $d$  to  $\pi_h a^{(0)}$ , it gives the 1-form  $\pi_h b^{(1)} = \mathcal{I} \delta \mathcal{R}a^{(0)} = d \pi_h a^{(0)}$  given by*

$$\pi_h b^{(1)}(\xi) = \sum_{i=1}^N b_i e_i^{(1)}(\xi), \quad (7.2.4)$$

with 1-cochain  $\mathbf{b}^{(1)}$ . Let  $\tau_{(1),i} = [\xi_{i-1}, \xi_i]$ , the coefficients of the 1-cochain  $\mathbf{b}^{(1)}$  are given by

$$\begin{aligned} b_i &= \bar{\psi}_i(\mathbf{b}^{(1)}) = \bar{\psi}_i(\mathcal{R}b^{(1)}) \\ &= \int_{\tau_{(1),i}} b^{(1)}(\xi) = \int_{\tau_{(1),i}} da^{(0)}(\xi) \stackrel{\text{Th. 3}}{=} \int_{\partial\tau_{(1),i}} a^{(0)}(\xi) \\ &= a^{(0)}(\xi_i) - a^{(0)}(\xi_{i-1}) = a_i - a_{i-1}, \end{aligned} \quad (7.2.5)$$

and with the edge polynomial defined as

$$e_i^{(1)}(\xi) = - \sum_{k=0}^{i-1} dl_k^{(0)}(\xi) = \sum_{k=i}^N dl_k^{(0)}(\xi) = \frac{1}{2} \sum_{k=i}^N dl_k^{(0)}(\xi) - \frac{1}{2} \sum_{k=0}^{i-1} dl_k^{(0)}(\xi). \quad (7.2.6)$$

*Proof.* First take the exterior derivative of (7.2.1):

$$d\pi_h a^{(0)}(\xi) = \sum_{i=0}^N a_i dl_i^{(0)}(\xi).$$

Now the 1-form  $d\pi_h a^{(0)}$  is expanded in terms of the 0-cochain  $\mathbf{a}^{(0)}$ . Then a change of basis is applied to rewrite this expansion in terms of the 1-cochain  $\delta\mathbf{a}^{(0)}$  using the projection  $\pi_M$ , see Definition 61 (p. 99). The trick is to subtract  $a_k \sum_{i=0}^N dl_i^{(0)}(\xi)$ , being equal to zero, and rewrite it such that we retrieve the coboundary operator and an edge polynomial,

$$\begin{aligned} \pi_h b^{(1)}(\xi) &= \pi_h da^{(0)}(\xi) = \pi_M d\pi_h a^{(0)}(\xi) \stackrel{(7.2.3)}{=} \sum_{i=0}^N (a_i - a_k) dl_i^{(0)}(\xi) \\ &= \sum_{i=0}^N \left[ - \sum_{j=i+1}^k (a_j - a_{j-1}) + \sum_{j=k+1}^i (a_j - a_{j-1}) \right] dl_i^{(0)}(\xi) \\ &\stackrel{(7.2.5)}{=} - \sum_{i=0}^{k-1} dl_i^{(0)}(\xi) \sum_{j=i+1}^k b_j + \sum_{i=k+1}^N dl_i^{(0)}(\xi) \sum_{j=k+1}^i b_j \\ &= - \sum_{j=1}^k b_j \left( \sum_{i=0}^{j-1} dl_i^{(0)}(\xi) \right) + \sum_{j=k+1}^N b_j \left( \sum_{i=j}^N dl_i^{(0)}(\xi) \right) \\ &\stackrel{(7.2.3)}{=} \sum_{j=1}^N b_j \left( - \sum_{i=0}^{j-1} dl_i^{(0)}(\xi) \right) \stackrel{(7.2.6)}{=} \sum_{j=1}^N b_j e_j^{(1)}(\xi). \end{aligned}$$

□

The cochain corresponding to line segment (1-cell)  $\tau_{(1),i}$  is given by  $b_i = a_i - a_{i-1}$  and so  $\mathbf{b}^{(1)} = \delta\mathbf{a}^{(0)}$  is the discrete derivative operator in 1D. This operation is purely topological, no metric is involved. It satisfies (6.1.8), since  $d\mathcal{I}\mathbf{a}^{(0)} = \mathcal{I}\delta\mathbf{a}^{(0)}$ . Note that according to (4.6.3), we have  $de_i(\xi) = \sum d\circ dl_i^{(0)}(\xi) = 0$ . The polynomial 1-form

can be decomposed into a polynomial and the canonical basis for differential forms (see Proposition 3),

$$e_i^{(1)}(\xi) = \varepsilon_i(\xi) d\xi, \quad \text{with} \quad \varepsilon_i(\xi) = - \sum_{k=0}^{i-1} \frac{dl_k}{d\xi}.$$

Similar to (7.2.2), the edge functions are constructed such that when integrating  $e_i^{(1)}(\xi)$  over a line segment it gives one for the corresponding element and zero for any other line segment.

**Corollary 16.** *Following the derivation of the edge function,  $e_i^{(1)}(\xi) \in \Lambda^1([-1, 1])$ , in Lemma 8, we proof that the edge functions satisfy (6.1.7), i.e.,*

$$\mathcal{R}e_i^{(1)}(\xi) = \int_{\xi_{p-1}}^{\xi_p} e_i^{(1)}(\xi) = \begin{cases} 1 & \text{if } i = p \\ 0 & \text{if } i \neq p \end{cases}. \quad (7.2.7)$$

*Proof.* Substitute generalized Stokes theorem, Theorem 3 (p. 55),

$$\begin{aligned} \int_{\xi_{p-1}}^{\xi_p} e_i^{(1)}(\xi) &= - \sum_{k=0}^{i-1} \int_{\xi_{p-1}}^{\xi_p} dl_k^{(0)}(\xi) \\ &= - \sum_{k=0}^{i-1} (l_k^{(0)}(\xi_p) - l_k^{(0)}(\xi_{p-1})). \end{aligned}$$

By substitution of (7.2.2), this is zero for  $i \neq p$  and one for  $i = p$ .  $\square$

The last property to verify is invariance under transformations. If  $\bar{e}_i(\mathbf{x})$ , with  $\mathbf{x} := (x, y, z)$ , is an edge function defined on a curvilinear 1-manifold embedded in a three dimensional domain, then on that manifold there exist 1-cells  $\tau_{(1),\epsilon}(\mathbf{x})$ , associated to each edge,  $\epsilon$ , connecting two Gauss-Lobatto nodes in the mesh of that manifold. Again the mapping is given by  $\mathbf{x} = \Phi(\xi)$ , as illustrated in Figure 7.2, and the mapping of an edge  $\epsilon$  is given by  $\tau_{(1),\epsilon}(\mathbf{x}) = \Phi(\tau_{(1)}^\epsilon(\xi))$ . As a consequence  $\Phi^* \bar{e}_i(\mathbf{x}) = e_i(\xi)$  and so:

$$\int_{\tau_{(1)}^\epsilon(\mathbf{x})} \bar{e}_i(\mathbf{x}) = \int_{\Phi(\tau_{(1)}^\epsilon(\xi))} (\Phi^{-1})^*(e_i(\xi)) = \int_{(\Phi^{-1} \circ \Phi)(\tau_{(1)}^\epsilon(\xi))} e_i(\xi) = \int_{\tau_{(1)}^\epsilon(\xi)} e_i(\xi) = \delta_{i,\epsilon}.$$

This is what could be expected, since the generalized Stokes Theorem (4.6.4) is purely topological and does not depend on the particular coordinate system or polynomial representation.

Let  $N = 4$  be the number of line segments in a spectral element. Then Lagrange basis interpolating  $N + 1 = 5$  0-cells with fourth-order polynomials, corresponding to a Gauss-Lobatto grid, is shown in Figure 7.3. The edge basis interpolating  $N = 4$  line segments with third-order polynomials, corresponding to a Gauss-Lobatto grid, is shown in Figure 7.4. *The fourth-order Lagrange and third-order edge polynomials, corresponding to a Gauss-Lobatto grid with  $N = 4$ , are shown in Figures 7.3 and 7.4.*

Now that the mimetic basis functions are defined it can be proven by example that the projection,  $\pi_h$ , is in general not a Galerkin projection.

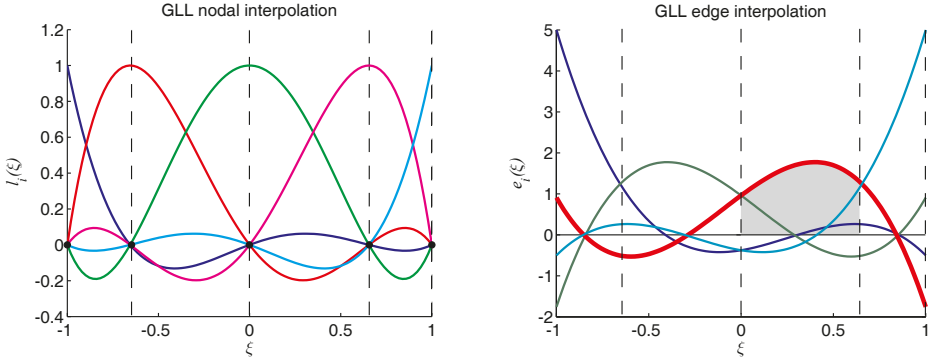


Figure 7.3: Lagrange polynomials on Gauss-Lobatto-Legendre grid.

Figure 7.4: Edge polynomials on Gauss-Lobatto-Legendre grid. Surface of grey area equals one.

**Example 25.** Let  $\Pi_h$  be a Galerkin projection, and  $\Pi_h a^{(1)}$  be expanded using edge basis functions as  $\Pi_h a^{(1)} = \sum_{i=1}^N \bar{a}_i e_i(\xi)$ , then the coefficients  $\bar{a}_i$  are determined by

$$(\Pi_h a^{(1)}, e_i(\xi)) = (a^{(1)}, e_i(\xi)).$$

In general,  $[\bar{a}_1 \dots \bar{a}_N]^T \neq \mathcal{R}a^{(1)}$ , and therefore  $[\bar{a}_1 \dots \bar{a}_N]^T$  is not a cochain, and  $\Pi_h$  is not a cochain projection. As an example, let  $a^{(1)} = x^3 dx$  for  $x \in [-1, 1]$ , then for  $N = 2$ ,  $[\bar{a}_1 \bar{a}_2]^T = [-\frac{3}{10} \frac{3}{10}]^T \neq \mathcal{R}a^{(1)} = [-\frac{1}{4} \frac{1}{4}]^T$ .

The following example shows the commutation property between projection and exterior derivative.

**Example 26.** In Figure 7.5 (p. 118), a graphical representation of the commuting diagram for the projection and the exterior derivative is given. This figure illustrates Lemma 6.

## 7.2.2 Bounded projections

As mentioned in Definition 64 (p. 106), boundedness of the projection is a requirement, and is therefore shown for the projections introduced above.

The mimetic framework uses Lagrange,  $l_i(\xi) \in \Lambda_h^0(\widehat{Q}; C_0) \subset H\Lambda^0(\widehat{Q})$ , and edge functions,  $e_i(\xi) \in \Lambda_h^1(\widehat{Q}; C_1) \subset L^2\Lambda^1(\widehat{Q})$ , for the reconstruction,  $\mathcal{I}$ , where the latter is constructed using the former; i.e., from the finite dimensional 0-form  $\pi_h a^{(0)} = \sum_{i=0}^N a_i l_i(\xi) \in \Lambda_h^0(Q; C_0)$ , we define  $\pi_h b^{(1)} \in \Lambda_h^1(\widehat{Q}; C_1)$ , such that

$$\pi_h b^{(1)} = \pi_h da^{(0)} = \sum_{i=1}^N b_i e_i(\xi).$$

Due to the way the edge functions are constructed, there exists a commuting diagram

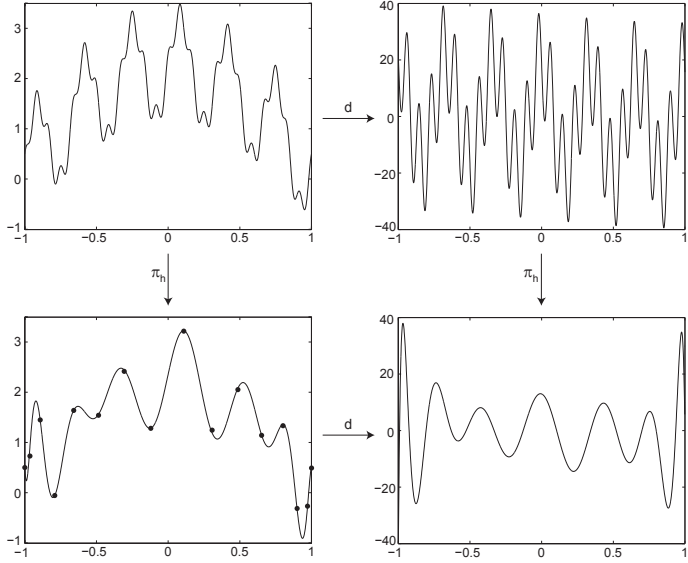


Figure 7.5: **UPDATE NEEDED!!! Zie Rene en Deepesh!!!** An oscillatory 0-form (Top left) is projected onto a polynomial 0-form (Bottom left) using Lagrange functions. The exterior derivative of the oscillatory 0-form (Top right) is projected onto polynomials using edge functions (Bottom right). This diagram commutes.

property between projection and exterior derivative,

$$\begin{array}{ccccccc} \mathbb{R} & \longrightarrow & H\Lambda^0(\widehat{Q}) & \xrightarrow{d} & L^2\Lambda^1(\widehat{Q}) & \longrightarrow & 0 \\ & & \downarrow \pi_h & & \downarrow \pi_h & & \\ \mathbb{R} & \longrightarrow & \Lambda_h^0(\widehat{Q}; C_0) & \xrightarrow{d} & \Lambda_h^1(\widehat{Q}; C_1) & \longrightarrow & 0, \end{array}$$

which gives, for  $a^{(0)} \in H\Lambda^0(\widehat{Q})$ , the 1-form

$$d\pi_h a^{(0)} = \pi_h da^{(0)}, \quad \text{in } \Lambda_h^1(\widehat{Q}; C_1).$$

Lagrange interpolation by itself does not guarantee a convergent approximation, [62, 67], but it requires a suitably chosen set of points,  $-1 \leq \xi_0 < \xi_1 < \dots < \xi_N \leq 1$ . Here, (extended)-Gauss and Gauss-Lobatto distributions are proposed, because of their superior convergence behaviour, [42]. For  $a^{(k)} \in H^m\Lambda^0(\widehat{Q})$  the a priori error estimate in the  $H\Lambda^0$ -norm is given by [42],

$$\|a^{(0)} - \pi_h a^{(0)}\|_{H\Lambda^0} \leq C \frac{h^{l-1}}{p^{m-1}} |a^{(0)}|_{H^m\Lambda^0}, \quad l = \min(p+1, m), \quad (7.2.8)$$

where  $p = N$  indicates the polynomial order and  $m$  the degree of regularity of the 0-form. Equation (7.2.8) also implies that the projection of 0-forms is bounded in the  $H\Lambda^0(\widehat{Q})$ , as is shown in the following proposition.

---

**Proposition 29.** For  $a^{(0)} \in H\Lambda^0(\widehat{Q})$  and the projection  $\pi_h : H\Lambda^0 \rightarrow \Lambda_h^0$ , there exists the following two stability estimates in  $H\Lambda^0$ -norm and  $H\Lambda^0$ -semi-norm:

$$\|\pi_h a^{(0)}\|_{H\Lambda^0} \leq C \|a^{(0)}\|_{H\Lambda^0}, \quad \text{and} \quad |\pi_h a^{(0)}|_{H\Lambda^0} \leq C |a^{(0)}|_{H\Lambda^0}. \quad (7.2.9)$$

*Proof.* The  $H\Lambda^0$ -norm of  $\pi_h a^{(0)}$  can be bounded from above using triangle inequality,

$$\|\pi_h a^{(0)}\|_{H\Lambda^0} \leq \|a^{(0)}\|_{H\Lambda^0} + \|a^{(0)} - \pi_h a^{(0)}\|_{H\Lambda^0}.$$

For  $a^{(0)} \in H\Lambda^0$ , we use Poincaré inequality, Lemma 2 (p. 63), to bound the first term,

$$\|a^{(0)}\|_{H\Lambda^0} \leq c_P \|da^{(0)}\|_{L^2\Lambda^0} = c_P |a^{(0)}|_{H\Lambda^0}.$$

Substituting this inequality and the interpolation estimate (7.2.8) into the triangle inequality gives the following result,

$$\|\pi_h a^{(0)}\|_{H\Lambda^0} \leq C |a^{(0)}|_{H\Lambda^0}.$$

Then the inequalities in (7.2.9) follow directly

$$|\pi_h a^{(0)}|_{H\Lambda^0} \leq \|\pi_h a^{(0)}\|_{H\Lambda^0} \leq C |a^{(0)}|_{H\Lambda^0} \leq C \|a^{(0)}\|_{H\Lambda^0}.$$

□

Now that we have a bounded projection of 0-forms in one dimension, we can also proof boundedness of the projection for 1-forms.

**Proposition 30.** Let  $a^{(0)} \in H\Lambda^0(\widehat{Q})$  and  $b^{(1)} = da^{(0)} \in L^2\Lambda^1(\widehat{Q})$ , then the projection  $\pi_h : L^2\Lambda^1(\widehat{Q}) \rightarrow \Lambda_h^1(\widehat{Q}; C_1)$  given by Lemma 8 (p. 114) is bounded,

$$\|\pi_h b^{(1)}\|_{L^2\Lambda^1} \leq C \|b^{(1)}\|_{L^2\Lambda^1}. \quad (7.2.10)$$

*Proof.* Because  $L^2\Lambda^1 = \mathcal{B}^1$  if  $\dim(\Omega) = 1$ , we can write  $b^{(1)} = da^{(0)}$ . Then the proof follows from Proposition 29 and the commutation between projection and exterior derivative, Lemma 6 (p. 102),

$$\begin{aligned} \|\pi_h b^{(1)}\|_{L^2\Lambda^1} &= |\pi_h da^{(0)}|_{L^2\Lambda^1} = |d\pi_h a^{(0)}|_{L^2\Lambda^1} = |\pi_h a^{(0)}|_{H\Lambda^0} \\ &\leq C |a^{(0)}|_{H\Lambda^0} = C |da^{(0)}|_{L^2\Lambda^1} = C \|b^{(1)}\|_{L^2\Lambda^1}. \end{aligned}$$

□

Propositions 29 and 30 show that the projection  $\pi_h$  is a *bounded projection*, based on Lagrange functions and edge functions. Just like for 0-forms using Lagrange interpolation, we can also give an estimate for the interpolation error of 1-forms, interpolated using edge functions.

**Proposition 31.** Let  $a^{(0)} \in H\Lambda^0(\widehat{Q})$  and  $b^{(1)} = da^{(0)} \in L^2\Lambda^1(\widehat{Q})$ , the interpolation error  $b^{(1)} - \pi_h b^{(1)} \in L^2\Lambda^1$  is given by

$$\|b^{(1)} - \pi_h b^{(1)}\|_{L^2\Lambda^1} \leq C \frac{h^{l-1}}{p^{m-1}} |b^{(1)}|_{H^{m-1}\Lambda^1}, \quad (7.2.11)$$

with  $l = \min(N+1, m)$  and  $p = N-1$ .

*Proof.*

$$\|b^{(1)} - \pi_h b^{(1)}\|_{L^2 \Lambda^1} = \|\mathrm{d}(a^{(0)} - \pi_h a^{(0)})\|_{L^2 \Lambda^1} = |a^{(0)} - \pi_h a^{(0)}|_{H \Lambda^0}$$

and

$$|a^{(0)} - \pi_h a^{(0)}|_{H \Lambda^0} \leq \|a^{(0)} - \pi_h a^{(0)}\|_{H \Lambda^0}.$$

Then (7.2.11) follows from (7.2.8), with the semi-norm rewritten as

$$|a^{(0)}|_{H^m \Lambda^0} = |\mathrm{d}a^{(0)}|_{H^{m-1} \Lambda^1} = |b^{(1)}|_{H^{m-1} \Lambda^1}.$$

□

### 7.2.3 Tensor product interpolation functions

Now that we have developed interpolation basis functions in one dimension, it can be extended to the multidimensional framework by means of tensor products. This allows for the interpolation of integral quantities defined on  $k$ -dimensional cubes. Consider a reference domain in  $\mathbb{R}^3$ ,  $\hat{Q} = [-1, 1]^3$ . Then the interpolation basis functions for point, line, surface and volume elements are given by,

- point :  $P_{i,j,k}^{(0)}(\xi, \eta, \zeta) = l_i(\xi) \otimes l_j(\eta) \otimes l_k(\zeta)$ ,
- edge :  $E_{i,j,k}^{(1)}(\xi, \eta, \zeta) = \{e_i(\xi) \otimes l_j(\eta) \otimes l_k(\zeta), l_i(\xi) \otimes e_j(\eta) \otimes l_k(\zeta), l_i(\xi) \otimes l_j(\eta) \otimes e_k(\zeta)\}$ ,
- surface :  $S_{i,j,k}^{(2)}(\xi, \eta, \zeta) = \{e_i(\xi) \otimes e_j(\eta) \otimes l_k(\zeta), e_i(\xi) \otimes l_j(\eta) \otimes e_k(\zeta), l_i(\xi) \otimes e_j(\eta) \otimes e_k(\zeta)\}$ ,
- volume :  $V_{i,j,k}^{(3)}(\xi, \eta, \zeta) = e_i(\xi) \otimes e_j(\eta) \otimes e_k(\zeta)$ .

The corresponding polynomial spaces are,

$$\begin{aligned} P_{i,j,k}^{(0)} &\in \mathcal{P}_{N,N,N}, \\ E_{i,j,k}^{(1)} &\in \mathcal{P}_{N-1,N,N} \times \mathcal{P}_{N,N-1,N} \times \mathcal{P}_{N,N,N-1}, \\ S_{i,j,k}^{(2)} &\in \mathcal{P}_{N-1,N-1,N} \times \mathcal{P}_{N-1,N,N-1} \times \mathcal{P}_{N,N-1,N-1}, \\ V_{i,j,k}^{(3)} &\in \mathcal{P}_{N-1,N-1,N-1}. \end{aligned}$$

Note that  $V_{i,j,k}^{(3)}$  is indeed a 3-form, since  $e_i e_j e_k = \varepsilon_i \varepsilon_j \varepsilon_k \mathrm{d}\xi \mathrm{d}\eta \mathrm{d}\zeta$ . So the approximation spaces are spanned by combinations of Lagrange and edge basis functions,

$$\begin{aligned} \Lambda_h^0(\mathcal{Q}; C_0) &:= \text{span} \left\{ P_{i,j,k}^{(0)} \right\}_{i=0, j=0, k=0}^{N,N,N}, \\ \Lambda_h^1(\mathcal{Q}; C_1) &:= \text{span} \left\{ (E_{i,j,k}^{(1)})_1 \right\}_{i=1, j=0, k=0}^{N,N,N} \times \text{span} \left\{ (E_{i,j,k}^{(1)})_2 \right\}_{i=0, j=1, k=0}^{N,N,N} \times \text{span} \left\{ (E_{i,j,k}^{(1)})_3 \right\}_{i=0, j=0, k=1}^{N,N,N}, \\ \Lambda_h^2(\mathcal{Q}; C_2) &:= \text{span} \left\{ (S_{i,j,k}^{(2)})_1 \right\}_{i=1, j=1, k=0}^{N,N,N} \times \text{span} \left\{ (S_{i,j,k}^{(2)})_2 \right\}_{i=1, j=0, k=1}^{N,N,N} \times \text{span} \left\{ (S_{i,j,k}^{(2)})_3 \right\}_{i=0, j=1, k=1}^{N,N,N}, \\ \Lambda_h^3(\mathcal{Q}; C_3) &:= \text{span} \left\{ V_{i,j,k}^{(3)} \right\}_{i=1, j=1, k=1}^{N,N,N}. \end{aligned}$$

So, finally we can present the full commuting diagram in  $\mathbb{R}^3$ ,

$$\begin{array}{ccccccc} H\Lambda^0(\Omega) & \xrightarrow{d} & H\Lambda^1(\Omega) & \xrightarrow{d} & H\Lambda^2(\Omega) & \xrightarrow{d} & L^2\Lambda^3(\Omega) \\ \pi_h \downarrow & & \pi_h \downarrow & & \pi_h \downarrow & & \pi_h \downarrow \\ \Lambda_h^0(Q; C_0) & \xrightarrow{d} & \Lambda_h^1(Q; C_1) & \xrightarrow{d} & \Lambda_h^2(Q; C_2) & \xrightarrow{d} & \Lambda_h^3(Q; C_3) \end{array}$$

**Corollary 17.** *Although Propositions 29, 30 and 31 were derived for the 0- and 1-forms on the one-dimensional reference domain  $\widehat{Q}$ . Due to the assumptions in Section 6.2.2 on the map  $\Phi : \widehat{Q} \rightarrow Q$ , and the commuting property between the pullback and exterior derivative, Proposition 6, these propositions also hold on any curvilinear quadrilateral or hexahedral domain  $\Omega$ , obtained from a transfinite mapping  $\Phi_m : \widehat{Q} \rightarrow Q_m$ . Since it holds for all  $m$  it holds for the complete mesh  $Q$ , where only the constants  $C$  depend on the mappings  $\Phi_m$ .*

### 7.2.4 Projection $\tilde{\pi}_h$ using $\tilde{D}$

Given a cell complex  $D_i$ , a corresponding dual grid  $\tilde{D}_i$  was defined in Section 5.3 (p. 84). For simplicity, consider again a one-dimensional manifold,  $\Omega = Q = Q_1 = \widehat{Q}$ , on which the two cell complexes are defined (see Figure 7.6 and also Figure 5.11 (p. 87)). Let the Gauss-Lobatto grid be the primal cell complex,  $D_i$ , consisting of  $N + 1$  points and  $N$  line segments. The dual of  $D_i$ , being  $\tilde{D}_i$ , consists of  $N$  points and  $N + 1$  line segments, according to Definition 47 (p. 85). Having a Gauss-Lobatto

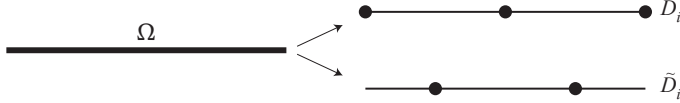


Figure 7.6: blablabla

primal cell complex, the points for the dual part could be the Gauss points,  $-1 < \xi_1 < \dots < \xi_N < 1$ , [30, 42]. We indicate the Gauss-Lagrange interpolant corresponding to  $\tilde{D}_i$  by  $\tilde{l}_i^g(\xi) \in \tilde{\Lambda}_h^0(\widehat{Q}; C_0(\tilde{D}_i))$ . The projection of a 0-form,  $\tilde{a}^{(0)} \in \tilde{\Lambda}^0(\widehat{Q})$ , using the 0-cells in  $\tilde{D}_i$ , is a polynomial of degree  $N - 1$ , and is given by

$$\tilde{\pi}_h \tilde{a}^{(0)}(\xi) = \sum_{i=1}^N \tilde{a}_i \tilde{l}_i^g(\xi). \quad (7.2.12)$$

The dual complex  $\tilde{D}$  is the union of  $\tilde{D}_i$  and  $\tilde{D}_b$ . Then  $\tilde{D}_b$  is given by the two additional boundary points  $\xi_0 = -1$  and  $\xi_{N+1} = 1$ . The 0-cells of the dual cell complex  $\tilde{D}$  are interpolated using *extended-Gauss-Lagrange* polynomials,  $\tilde{l}_i^{\text{eg}}(\xi) \in \tilde{\Lambda}_h^0(\widehat{Q}; C_0(\tilde{D}))$ . The projection of a 0-form,  $\tilde{a}^{(0)} \in \tilde{\Lambda}^0(\widehat{Q})$ , using the 0-cells in cell complex  $\tilde{D}$ , is a polynomial of degree  $N + 1$ , and is given by

$$\tilde{\pi}_h \tilde{a}^{(0)}(\xi) = \sum_{i=0}^{N+1} \tilde{a}_i \tilde{l}_i^{\text{eg}}(\xi). \quad (7.2.13)$$

The *extended-Gauss edge* functions,  $\tilde{e}_i^{\text{eg}} \in \tilde{\Lambda}_h^1(\tilde{Q}; C_1(\tilde{D}))$ , are derived similarly to the Gauss-Lobatto edge functions in Lemma 8 (p. 114). The projection of a one-form  $\tilde{b}^{(1)} \in \tilde{\Lambda}^1(\tilde{Q})$ , using the 1-cells in  $\tilde{D}$ , is a polynomial of degree  $N$ , and is given by

$$\tilde{\pi}_h \tilde{b}^{(1)}(\xi) = \sum_{i=1}^{N+1} \tilde{b}_i \tilde{e}_i^{\text{eg}}(\xi), \quad \text{with} \quad \tilde{e}_i^{\text{eg}}(\xi) = - \sum_{k=0}^{i-1} d\tilde{l}_i^{\text{eg}}(\xi). \quad (7.2.14)$$

The extended-Gauss polynomials in the context of mimetic discretization were first preliminarily discussed in [30, 76].

**Remark 32.** *The boundary cells in  $\tilde{D}_b$  can be seen as connectivity cells. Either they connect the computational domain to the outside world in terms of boundary conditions, or they connect adjacent spectral elements within the computational domain, thus providing  $C^0$ -continuity for 0-forms.*

**Remark 33.** *Although the boundary cells are part of the solution and thus should be solved for, the integral over the domain  $[-1, 1]$  of the boundary polynomials is zero, i.e.*

$$\int_{-1}^1 \tilde{l}_0^{\text{eg}}(\xi) d\xi = \int_{-1}^1 \tilde{l}_{N+1}^{\text{eg}}(\xi) d\xi \equiv 0.$$

*Therefore they do not contribute to the domain integrals over  $\tilde{Q} = [-1, 1]$ . There is a strong analogy with integration by parts. Let  $q_h^{(0)} \in \Lambda_h^0(\tilde{Q}; C_0)$  be represented using the primal cell complex and  $\tilde{a}_h^{(0)} \in \tilde{\Lambda}_h^0(\tilde{Q}; \tilde{C}_0)$  be expressed using the dual cell complex. Then integration by parts gives*

$$\int_{-1}^1 dq_h^{(0)} \wedge \tilde{a}_h^{(0)} = - \int_{-1}^1 q_h^{(0)} \wedge d\tilde{a}_h^{(0)} + \left[ q_h^{(0)} \wedge \tilde{a}_h^{(0)} \right]_{\xi=-1}^{\xi=1}, \quad \forall q_h^{(0)} \in \Lambda_h^0(\tilde{Q}; C_0).$$

*This shows that the derivative on the primal cell complex  $D$  is related to the derivative on the interior part of the dual complex,  $\tilde{D}_i$ , supplemented with boundary part,  $\tilde{D}_b$ .*

Figure 7.7 shows the extended-Gauss Lagrange basis functions on the dual grid, while Figure 7.8 shows the extended-Gauss edge basis functions on the dual grid. Together with the basis functions depicted in Figures 7.3 and 7.4, these four sets of basis functions make up the entire set of reconstruction operators discussed in Chapter 6.

### 7.2.5 The coprojections $\pi_h^*$ and $\tilde{\pi}_h^*$

Now that the reconstruction polynomials on the primal and the dual complex have been introduced, the coprojections can be directly expressed in terms of these polynomials. For  $\pi_h^*$ , we take the Hodge star of a  $k$ -form  $a^{(k)}$  at the continuous level, which yields a  $(n-k)$ -form. This  $(n-k)$ -form is projected by  $\tilde{\pi}_h$  with respect to the dual grid. Then the Hodge star operator is applied to the projected differential form and multiplied by  $(-1)^{k(n-k)}$ . This result is then expanded in terms of the  $k$ -form basis functions on the primal grid. This is possible thanks to property (6.1.10).

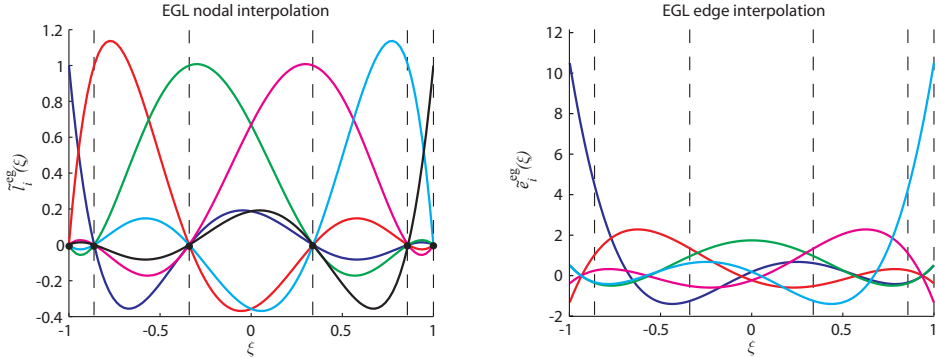


Figure 7.7: Lagrange polynomials on extended Gauss-Legendre grid.

Figure 7.8: Edge polynomials on extended Gauss-Legendre grid.

A similar route is followed by the coprojection  $\tilde{\pi}_h^*$ , where in this case the projection is with respect to the primal grid and the final result is expanded in terms of the  $k$ -form basis functions on the dual complex. In Figure 7.9, the four projection operators are applied to a 0-form,  $a^{(0)} = \sin(3\pi x + 0.08)$ , and the resulting projected 0-forms are plotted. Note that if one approximation looks better than the other in Figure 7.9, this is accidentally and depends on the chosen sine function and the low polynomial order.

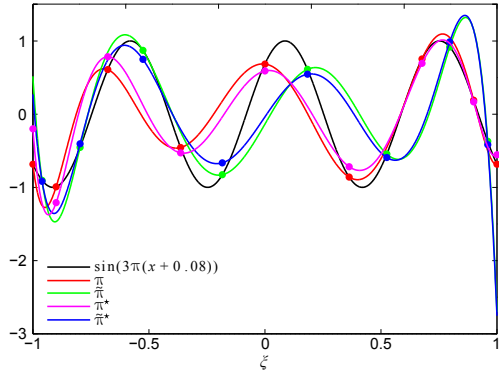


Figure 7.9: Comparison between the four projections,  $\pi$ ,  $\tilde{\pi}$ ,  $\pi^*$  and  $\tilde{\pi}^*$ , for a one-dimensional mesh of order  $N = 8$ .

### 7.3 Applications of discrete operators

In this section some examples will be shown where use is made of the mimetic spectral interpolatory basis functions and the action of the operators  $d$ ,  $*$  and  $d^*$  described in Section 6.2. We start with the analogy between the exterior derivative and the

coboundary operator in 3D, as illustrated in the diagram below. [this is the discrete analogue of figure 2.1](#)

$$\begin{array}{ccccccc}
 \Lambda_h^0(\Omega; C_0) & \xrightarrow[\text{grad}]{\quad d \quad} & \Lambda_h^1(\Omega; C_1) & \xrightarrow[\text{curl}]{\quad d \quad} & \Lambda_h^2(\Omega; C_2) & \xrightarrow[\text{div}]{\quad d \quad} & \Lambda_h^3(\Omega; C_3) \\
 \mathcal{R} \uparrow \mathcal{I} & & \mathcal{R} \uparrow \mathcal{I} & & \mathcal{R} \uparrow \mathcal{I} & & \mathcal{R} \uparrow \mathcal{I} \\
 C^0(D) & \xrightarrow{\delta} & C^1(D) & \xrightarrow{\delta} & C^2(D) & \xrightarrow{\delta} & C^3(D)
 \end{array}$$

We recognize the continuous and discrete gradient, curl and divergence operator from vector calculus. Again for clarity, we restrict ourselves to  $\Omega = \mathcal{Q} = \widehat{Q}$ , see (7.1.2). A similar De Rham complex can be set up for the dual complex using the nodal and edge functions given in the previous section.

**Example 27 (Gradient).** Consider a velocity  $u_h^{(1)} = dp_h^{(0)}$ , where  $p_h^{(0)}$  is a potential expanded in standard coordinates  $\xi := (\xi, \eta, \zeta)$  as

$$p_h^{(0)} = \sum_{i=0}^N \sum_{j=0}^N \sum_{k=0}^N p_{i,j,k} l_i(\xi) l_j(\eta) l_k(\zeta). \quad (7.3.1)$$

Apply the exterior derivative in the same way as in Lemma 8, it gives

$$\begin{aligned}
 u_h^{(1)} = & \sum_{i=1}^N \sum_{j=0}^N \sum_{k=0}^N u_{i,j,k}^\xi e_i(\xi) l_j(\eta) l_k(\zeta) \\
 & + \sum_{i=0}^N \sum_{j=1}^N \sum_{k=0}^N u_{i,j,k}^\eta e_i(\xi) l_i(\eta) l_k(\zeta) \\
 & + \sum_{i=0}^N \sum_{j=0}^N \sum_{k=1}^N u_{i,j,k}^\zeta e_i(\xi) l_j(\eta) e_k(\zeta),
 \end{aligned} \quad (7.3.2)$$

where

$$u_{i,j,k}^\xi = p_{i,j,k} - p_{i-1,j,k}, \quad u_{i,j,k}^\eta = p_{i,j,k} - p_{i,j-1,k} \text{ and } u_{i,j,k}^\zeta = p_{i,j,k} - p_{i,j,k-1}, \quad (7.3.3)$$

can compactly be written as  $\mathbf{u}^{(1)} = \delta \mathbf{p}^{(0)}$ , or in matrix notation as  $\bar{\psi}(\mathbf{u}^{(1)}) = \mathbf{E}^{(1,0)} \bar{\psi}(\mathbf{p}^{(0)})$ . This relation is exact and invariant under transformations. Note that in terms of function spaces the vector proxies of  $p_h^{(0)}$  are in  $H^1$  and that of  $u_h^{(1)}$  are in  $H(\text{curl})$ .

**Example 28 (Curl).** Let  $u_h^{(1)}$  be a velocity defined as in (7.3.2), then vorticity is given by  $w_h^{(2)} = du_h^{(1)}$ . Apply the exterior derivative as in Lemma 8 and consider the

wedge product property (4.3.2), it gives

$$\begin{aligned} w_h^{(2)} &= \sum_{i=0}^N \sum_{j=1}^N \sum_{k=1}^N w_{i,j,k}^\xi l_i(\xi) e_j(\eta) e_k(\zeta) \\ &\quad + \sum_{i=1}^N \sum_{j=0}^N \sum_{k=1}^N w_{i,j,k}^\eta e_i(\xi) l_j(\eta) e_k(\zeta) \\ &\quad + \sum_{i=1}^N \sum_{j=1}^N \sum_{k=0}^N w_{i,j,k}^\zeta e_i(\xi) e_j(\eta) l_k(\zeta), \end{aligned} \tag{7.3.4}$$

where

$$\begin{aligned} w_{i,j,k}^\xi &= u_{i,j,k}^\xi - u_{i,j-1,k}^\xi - u_{i,j,k}^\eta + u_{i,j,k-1}^\eta, \\ w_{i,j,k}^\eta &= u_{i,j,k}^\xi - u_{i-1,j,k}^\xi - u_{i,j,k}^\xi + u_{i,j,k-1}^\xi, \\ w_{i,j,k}^\zeta &= u_{i,j,k}^\eta - u_{i-1,j,k}^\eta - u_{i,j,k}^\xi + u_{i,j-1,k}^\xi, \end{aligned} \tag{7.3.5}$$

can compactly be written as  $\mathbf{w}^{(2)} = \delta\mathbf{u}^{(1)}$ , or in matrix notation as  $\bar{\psi}(\mathbf{w}^{(2)}) = \mathbf{E}^{(2,1)}\bar{\psi}(\mathbf{u}^{(1)})$ . This relation is exact and invariant under transformations. Note that in terms of function spaces the vector proxies of  $w_h^{(2)}$  are in  $H(\text{div})$ . If  $u_h^{(1)}$  is the gradient of  $p_h^{(0)}$ , then  $w_{i,j,k}^\xi = w_{i,j,k}^\eta = w_{i,j,k}^\zeta = 0$  and so  $w_h^{(2)} = 0$ . This is in accordance with (5.2.7) and (4.6.3).

**Example 29 (Divergence).** Let the 2-form  $q_h^{(2)}$  be a velocity flux defined as

$$\begin{aligned} q_h^{(2)} &= \sum_{i=0}^N \sum_{j=1}^N \sum_{k=1}^N q_{i,j,k}^\xi l_i(\xi) e_j(\eta) e_k(\zeta) \\ &\quad + \sum_{i=1}^N \sum_{j=0}^N \sum_{k=1}^N q_{i,j,k}^\eta e_i(\xi) l_j(\eta) e_k(\zeta) \\ &\quad + \sum_{i=1}^N \sum_{j=1}^N \sum_{k=0}^N q_{i,j,k}^\zeta e_i(\xi) e_j(\eta) l_k(\zeta), \end{aligned} \tag{7.3.6}$$

then conservation of mass is given by  $dq_h^{(2)} = m_h^{(3)}$ , where  $m_h^{(3)}$  is a mass source function. Apply the exterior derivative as in Lemma 8 and consider the wedge product property (4.3.2), it gives

$$m_h^{(3)} = \sum_{i=1}^N \sum_{j=1}^N \sum_{k=1}^N v_{i,j,k} e_i(\xi) e_j(\eta) e_k(\zeta), \tag{7.3.7}$$

where

$$m_{i,j,k} = q_{i,j,k}^\xi - q_{i-1,j,k}^\xi + q_{i,j,k}^\eta - q_{i,j-1,k}^\eta + q_{i,j,k}^\zeta - q_{i,j,k-1}^\zeta, \tag{7.3.8}$$

can compactly be written as  $\mathbf{m}^{(3)} = \delta\mathbf{q}^{(2)}$ , or in matrix notation as  $\bar{\psi}(\mathbf{m}^{(3)}) = \mathbf{E}^{(3,2)}\bar{\psi}(\mathbf{q}^{(2)})$ . This relation is exact and invariant under transformations. It shows

---

that  $\mathrm{d}q_h^{(2)} = \mathrm{d}\pi_h q^{(2)} = \mathrm{d}\mathcal{IR}q^{(2)} = \mathcal{I}\delta\mathcal{R}q^{(2)} = \mathcal{I}\mathcal{R}\mathrm{d}q^{(2)} = \pi_h \mathrm{d}q^{(2)} = \pi_h m^{(3)} = m_h^{(3)}$ . In case  $q_h^{(2)} = w_h^{(2)} = \mathrm{d}u_h^{(1)}$ , then it can be shown that  $m_h^{(3)} = 0$ . In case  $m_h^{(3)} = 0$  equations (7.3.7)-(7.3.8) show that the velocity flux  $q_h^{(2)}$  is strongly divergence-free. Note that in terms of function spaces the vector proxy of  $m_h^{(3)}$  is in  $L^2$ .

**Remark 34.** Given a mesh  $\mathcal{Q}$  as defined in (7.1.1), with  $M > 1$ . The expansion of 0-forms  $a_h^{(0)} \in \Lambda_h^0(Q_m; C_0)$  has  $C^0$  continuity over the sub domain boundaries,  $\partial\Omega_m$ . For  $a_h^{(1)} \in \Lambda_h^1(Q_m; C_1)$ , the tangential component is  $C^0$  continuous and for  $a_h^{(2)} \in \Lambda_h^2(Q_m; C_2)$  the normal component has  $C^0$  continuity over the sub domain boundaries. The expansion of volume-forms,  $a_h^{(3)} \in \Lambda_h^3(Q_m; C_3)$  are discontinuous over the sub domain boundaries.

**Example 30 (Trace).** Without loss of generality, consider one-dimensional domain  $\widehat{Q} = \{\xi \mid -1 \leq \xi \leq 1\}$ . We can apply the trace on a 0-form  $a_h^{(0)} \in \Lambda_h^0(\widehat{Q}; C_0)$  and a one-form  $b_h^{(1)} \in \Lambda_h^1(\widehat{Q}; C_1)$ , then we find:

$$\begin{aligned}\mathrm{tr}_{\partial\Omega_L} a_h^{(0)} &= \mathrm{tr}_{\partial\Omega_L} \left( \sum_{i=0}^N a_i l_i(\xi) \right) = -a_0, \\ \mathrm{tr}_{\partial\Omega_R} a_h^{(0)} &= \mathrm{tr}_{\partial\Omega_R} \left( \sum_{i=0}^N a_i l_i(\xi) \right) = +a_N,\end{aligned}$$

and

$$\begin{aligned}\mathrm{tr}_{\partial\Omega_L} b_h^{(1)} &= \mathrm{tr}_{\partial\Omega_L} \left( \sum_{i=1}^N b_i e_i(\xi) \right) = - \sum_{i=1}^N b_i e_i(-1), \\ \mathrm{tr}_{\partial\Omega_R} b_h^{(1)} &= \mathrm{tr}_{\partial\Omega_R} \left( \sum_{i=1}^N b_i e_i(\xi) \right) = + \sum_{i=1}^N b_i e_i(+1).\end{aligned}$$

The plus and minus signs in front indicate the corresponding orientation, see left in Figure 5.11. So if we evaluate the trace on the left boundary point, where the orientation is negative, we obtain the positive value  $a_0$  for the 0-form and  $+\sum_{i=1}^N b_i e_i(-1)$  for the 1-form. Because we consider tensor products to consider higher-dimensional  $k$ -forms, the trace on  $k$ -forms in higher dimensional domains can be constructed straightforward using the above relations.

**Example 31 (Hodge star).** Consider a 1D domain  $\widehat{Q} = \{\xi \mid -1 \leq \xi \leq 1\}$ . Let  $a_h^{(0)}(\xi) = \star u_h^{(1)}(\xi)$ . This example shows how to perform the Hodge star. The action of the Hodge star is followed by a projection  $\tilde{\pi}_M : \Lambda^0(\widehat{Q}; C_1) \rightarrow \Lambda^0(\widehat{Q}; \tilde{C}_0)$  to write the outcome in the preferred basis. Let  $u_h^{(1)}(\xi)$  be expanded in terms of 1-cochains and edge basis functions,

$$u_h^{(1)}(\xi) = \sum_{i=1}^N u_i e_i(\xi), \quad \text{with } u_h^{(1)} \in \Lambda_h^1(\widehat{Q}; C_1).$$

Then apply the Hodge star to get  $a_h^{(0)}(\xi) \in \Lambda_h^0(\widehat{Q}; C_1)$ , as follows

$$a_h^{(0)} = \star u_h^{(1)} = \sum_{i=1}^N u_i (\star e_i(\xi)) = \sum_{i=1}^N u_i \varepsilon_i(\xi) (\star d\xi) = \sum_{i=1}^N u_i \varepsilon_i(\xi).$$

Rewrite the basis using the action of  $\tilde{\pi}_M$

$$a_h^{(0)} = \tilde{\pi}_M a_h^{(0)} = \sum_{j=1}^N \left[ \sum_{i=1}^N u_i \varepsilon_i(\tilde{\xi}_j^g) \right] \tilde{l}_j^g(\xi) = \sum_{j=1}^N a_j \tilde{l}_j^g(\xi).$$

In this case, what is usually called the Hodge star matrix [18, 92], is given by  $(H^{(0,1)})_{j,i} = \varepsilon_i(\tilde{\xi}_j^g)$ . The action of this Hodge star is illustrated in Figure 7.10. Note that the function does not change, but only the expression in terms of coefficients and basis-functions, and the type of form, i.e. 1-form  $\rightarrow$  0-form,

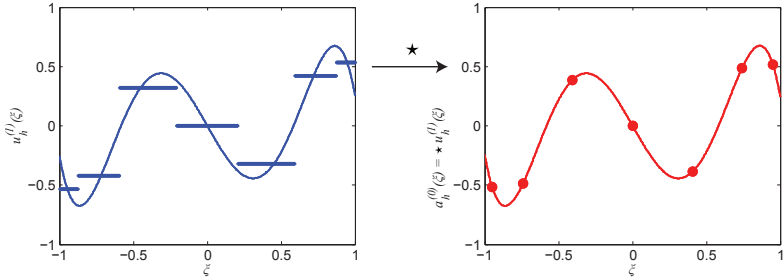


Figure 7.10: Example of the action of the Hodge star operator, followed by the projection  $\tilde{\pi}_M$ , i.e.  $\tilde{\pi}_M \circ \star$ . Left the function and corresponding cochain for  $u_h^{(1)} \in \Lambda^1(\widehat{Q}; C_1)$ . Right the function and corresponding cochain for  $a_h^{(0)} \in \Lambda^0(\widehat{Q}; \tilde{C}_0)$ .

**Example 32 (Codifferential).** Again consider a one-dimensional domain  $\widehat{Q} = \{\xi \mid -1 \leq \xi \leq 1\}$ . We apply the codifferential on  $u_h^{(1)} \in \Lambda_h^1(\widehat{Q}; C_1)$  according to (4.8.4):

$$\begin{aligned} d^* u_h^{(1)} &= \pi_M d^* u_h^{(1)} = -\pi_M \star d \star \left( \sum_{i=1}^N u_i \varepsilon_i(\xi) d\xi \right) \\ &= -\pi_M \left( \sum_{i=1}^N u_i \frac{d\varepsilon_i(\xi)}{d\xi} \right) = \sum_{j=0}^N \left[ \sum_{i=1}^N u_i \left( - \sum_{k=0}^{i-1} \frac{d^2 l_k}{d\xi^2} \Big|_{\xi=\xi_j} \right) \right] l_j(\xi). \end{aligned}$$

The codifferential matrix  $D^*$  is given by

$$(D^*)_{i,j} = - \sum_{k=0}^{i-1} \frac{d^2 l_k}{d\xi^2} \Big|_{\xi=\xi_j}. \quad (7.3.9)$$

The coefficients in this codifferential matrix are independent of the location of the dual grid, as would be expected. Even when the codifferential matrix is constructed

using two Hodge matrices and an incidence matrix, identically the same codifferential matrix is found. The same is true when retrieving the codifferential matrix from the formal adjoint formulation (4.8.2) when the 1-form  $u_h^{(1)}$  is zero at the boundary. The proof is left as an excercise for the reader.

**Example 33 (Hodge decomposition).** In this example we show the result of the discrete Hodge decomposition applied to a velocity field,  $v_h^{(1)}$ , obtained from a potential flow problem on an annulus. The Hodge decomposition of the velocity field is given in terms of the gradient of the potential,  $\phi_h^{(0)}$ , and a harmonic function,  $h_h^{(1)}$ ,

$$v_h^{(1)} = d\phi_h^{(0)} + h_h^{(1)}.$$

For the annulus, consider the domain  $(r, \theta) \in [1, R] \times [0, 2\pi]$  and the cell complex  $D$  which covers this domain as shown in Figure 7.11. The topology of the cell complex is equal to the topology of the cell complex shown in Figure 5.6.

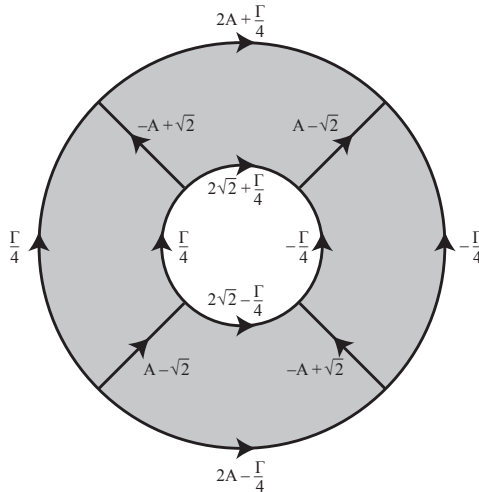


Figure 7.11: The cell complex which covers the  $(r, \theta) \in [1, R] \times [0, 2\pi]$  and the 1-cochain values associated with each 1-cell, where  $A = R\sqrt{2}(1 + \frac{1}{R^2})$ .

The velocity 1-form on the annulus is given by

$$v^{(1)} = \underbrace{r \cos \theta \left(1 - \frac{1}{r^2}\right) dr - \sin \theta \left(1 + \frac{1}{r^2}\right) d\theta}_{=d\phi^{(0)}} - \underbrace{\frac{\Gamma}{2\pi r} d\theta}_{=h^{(1)}}. \quad (7.3.10)$$

Application of the reduction map,  $\mathcal{R}$ , gives the 1-cochain values associated with each 1-chain in the cell complex. These values are given in Figure 7.11. If we apply the coboundary to this 1-cochain we get the zero 2-chain. Because the topology is the same as in Figure 5.6, the harmonic 1-chain is still given by

$$\mathbf{h}_{(1)} = [1, -1, 0, 0, 1, 1, -1, 1, -1, 0, 0, -1],$$

and therefore

$$\langle \mathbf{h}_{(1)}, \mathcal{R}v^{(1)} \rangle = 2\Gamma, \quad \langle \mathbf{h}_{(1)}, \alpha \mathbf{h}^{(1)} \rangle = 8\alpha, \quad \Rightarrow \quad \alpha = \frac{\Gamma}{4}.$$

The harmonic cochain  $\mathbf{h}^{(1)}$  was determined in Example 17 (p. 83). The values of the 1-cochain  $\delta\phi^{(0)} + \frac{\Gamma}{4}\mathbf{h}^{(1)}$  are given in Figure 7.11. The projection of the velocity field becomes,

$$\pi_h v^{(1)} = \mathcal{I} \left( \delta\phi^{(0)} + \frac{\Gamma}{4} \mathbf{h}^{(1)} \right).$$

Figure 7.12 shows the reconstruction of the velocity field components and the total velocity field, for different vortical strengths and different polynomial order.

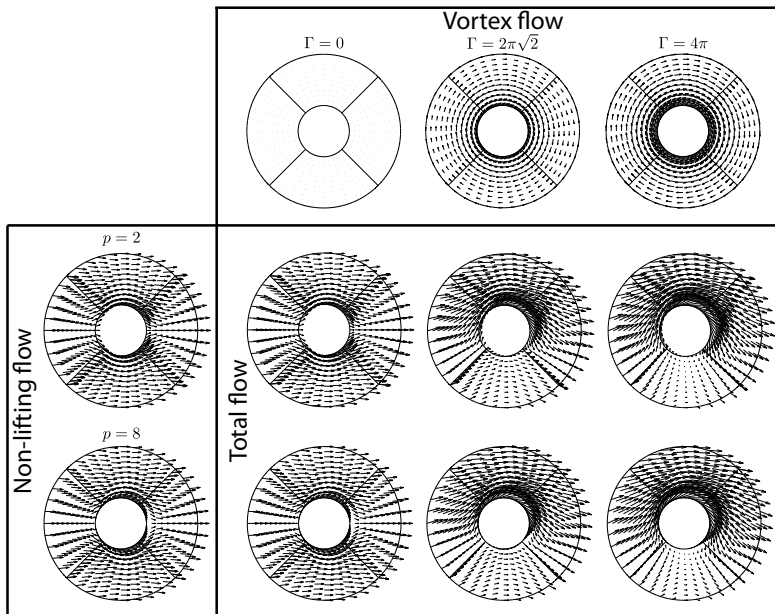


Figure 7.12: Decomposition of velocity field. It shows the curl-free components (left), the harmonic components (top) and the total velocity field, for different vortical strengths and different polynomial orders.

## 7.4 Mimetic B-splines

Although this thesis focusses on the use of mimetic spectral elements, the mimetic framework is not restricted to mimetic spectral elements only. Closely related to the interpolation basis functions are the mimetic B-splines. B-splines are well-known polynomial functions that have a well-established reputation in both ‘computer aided design’ (CAD) as well as computational science and analysis. Nowadays especially the combination, called isogeometric analysis (IGA) [49], enjoys increasing popularity

---

in the scientific community of computational fluid and solid mechanics and computational electromagnetism.

Recently the ideas of B-splines and IGA were extended with ideas that are in line with the current work, that is, compatible B-splines as were developed by Buffa et. al. [39, 40], and mimetic B-splines as proposed in [10]. Both methods have much in common with each other as well as with the mimetic method presented above. Emphasis on the similarities and differences will be given while explaining the methods.

With IGA a computational domain is split into several patches. Each patch is subdivided into smaller subdomains<sup>2</sup>. B-spline basis functions are local within each patch, but are spread over a number of subdomains. In comparison, in finite/spectral element methods (F/SSEM) computational domains are subdivided into elements, where basis functions only span the corresponding element, but are also global within that element. In the mimetic F/SSEM each element again consists of sub-elements. Therefore elements in F/SSEM can be seen as intermediate constructions between IGA patches and sub-domains.

Like mimetic spectral elements, the mimetic and compatible B-splines are based on tensor products and so definition and analysis in one dimension is sufficient to construct  $n$ -dimensional basis functions. Consider two positive integers  $P$  and  $M$ , representing the polynomial degree and the size of the span of B-spline basis functions. The end points of the subdomains in IGA are called knots. Let us introduce an ordered non-uniform open knot vector on an one dimension reference patch, that is, the unit interval  $I = [0, 1]$ ,

$$\Xi := \{0 = \xi_0, \xi_1, \dots, \xi_{M+P} = 1\}, \text{ where } \xi_0 \leq \xi_1 \leq \dots \leq \xi_{M+P}. \quad (7.4.1)$$

The knot vector can be split into a knot vector  $\zeta = \{\zeta_0, \dots, \zeta_N\}$  with  $N + 1$  unique entries connecting the  $N$  sub-intervals  $[\zeta_i, \zeta_{i+1}]$  within a patch, and a repetition vector,  $\mathbf{r} = \{r_0, \dots, r_N\}$ , with  $\sum_{i=0}^N r_i = M + P + 1$ ,  $r_i \leq P + 1$  and  $r_0 = r_N = P + 1$  and  $M = N + P + \sum_{i=1}^{N-1} (r_i - 1)$ .

Let us denote by  $B_i^P(\xi)$  the B-spline of degree  $P$  on a maximal support interval  $[\xi_i, \xi_{i+P+1}]$ . Then  $B_i^P(\xi)$  is defined recursively by the Cox-de Boor formula, [52], given by:

$$B_i^0(\xi) = \begin{cases} 1 & \text{if } \xi_i \leq \xi < \xi_{i+1} \\ 0 & \text{otherwise,} \end{cases} \quad (7.4.2a)$$

and for  $P \geq 1$ ,

$$B_i^P(\xi) = \frac{\xi - \xi_i}{\xi_{i+p} - \xi_i} B_i^{P-1}(\xi) + \frac{\xi_{i+P+1} - \xi}{\xi_{i+P+1} - \xi_{i+1}} B_{i+1}^{P-1}(\xi). \quad (7.4.2b)$$

By convention we set  $\frac{0}{0}$  equal to 0. Similar to the Lagrange interpolation basis, the standard B-spline basis forms a partition of unity. The B-splines are  $C^{P-r_j}$  continuous at the knots and are  $C^0$ -continuous between adjacent patches. As a consequence of this regularity there exists a global dependence in spite of the local support, as will be shown later on. The last property we like to mention here is that the basis functions

---

<sup>2</sup>Sometimes called elements, but renamed here to avoid confusion.

---

are non-negative. This non-negativity is often related to a monotone reconstruction, but this depends on the kind of projection used. A finite dimensional representation of a 0-form  $f^{(0)}(\xi)$  in terms coefficients  $b_i$  and B-splines basis functions  $B_i^P(\xi)$  is given by

$$f_h^{(0)}(\xi) = \sum_{i=0}^{M-1} b_i B_i^P(\xi). \quad (7.4.3)$$

The coefficients  $b_i$  are the values of the control points. Control points are located in the control mesh. The control mesh is a linear grid. The actual function lies in the convex hull of the control mesh. So the B-spline basis is not an interpolation basis. The location of the control points  $\boldsymbol{\eta} = \{\eta_0, \dots, \eta_{M-1}\}$ ,  $\eta_{j-1} < \eta_j < \eta_{j+1}$ , are given by the Greville abscissa [52],

$$\eta_j = \frac{1}{P} \sum_{i=j+1}^{j+P} \xi_i, \quad \text{for } j = 0, \dots, M-1. \quad (7.4.4)$$

The values of the coefficients  $b_i$  depend on the kind of projection used to obtain  $f_h^{(0)}$  in (7.4.3). We distinguish between three types of projection related to B-splines:

1.  $L^2$ -projection,  $P_{L^2}$ ;
2. mimetic projection,  $\pi_h$ ;
3. projection by means of dual basis functionals.

$L^2$ -projections are assumed to be familiar to the reader. Projection by means of dual basis functionals can be found in [40, 90, 161]. Mimetic projection follows the procedure explained in the previous chapter, it consists of a reduction and a reconstruction step,  $\pi_h := \mathcal{IR}$ . The reduction step for a 0-form,  $\mathcal{R}f^{(0)}$ , means evaluating the function in a given set of points, i.e., a 0-cochain consisting of a set of 0-cells,  $\boldsymbol{\eta}$ ,

$$f^{(0)}(\eta_j) = \sum_{i=0}^{M-1} b_i B_i^P(\eta_j). \quad (7.4.5)$$

Introduce the row vectors of reduced data  $\mathbf{f} = \{f_0, \dots, f_{M-1}\}$ , where  $f_j = f^{(0)}(\eta_j)$  and of unknown control points  $\mathbf{b} = \{b_0, \dots, b_{M-1}\}$ , and a matrix  $\mathbf{B}$  with  $\{\mathbf{B}\}_{i,j} = B_i^P(\eta_j)$ , then  $\mathbf{f} = \mathbf{b}\mathbf{B}$ . Then the values in the control points are given by

$$\mathbf{b} = \mathbf{f}\mathbf{B}^{-1} \Leftrightarrow b_i = \sum_{j=0}^{M-1} f_j \{\mathbf{B}^{-1}\}_{j,i}. \quad (7.4.6)$$

Here it is assumed that matrix  $\mathbf{B}$  is non-singular. Conditions for this non-singularity are given in [10, 52]. Equation (7.4.6) is in fact a change of basis from coefficients representing integral values to control point values. The mimetic projection of a 0-form then follows from reconstruction by means of B-splines corresponding to the

control points found in (7.4.6). The change of basis is substituted to show the relation between the mimetic spectral method and the mimetic B-spline method,

$$\begin{aligned}
\pi_h f^{(0)}(\xi) &= \mathcal{IR}f^{(0)}(\xi) = \sum_{i=0}^{M-1} b_i B_i^P(\xi) \\
&= \sum_{i=0}^{M-1} \left[ \sum_{j=0}^{M-1} f_j \{\mathbf{B}^{-1}\}_{j,i} \right] B_i^P(\xi) \\
&= \sum_{j=0}^{M-1} f_j \left[ \sum_{i=0}^{M-1} \{\mathbf{B}^{-1}\}_{j,i} B_i^P(\xi) \right] \\
&= \sum_{j=0}^{M-1} f_j L_j(\xi).
\end{aligned} \tag{7.4.7}$$

The basis function  $L_j(\xi)$  are Lagrange polynomials derived from a B-spline basis. These Lagrange polynomials have support over the full patch. Quadratic B-spline basis functions on a patch of five sub-intervals are shown in Figure 7.13. The control mesh consists of  $4+2+0=6$  control points. The Lagrange basis functions derived from the change of basis in (7.4.7) are shown in Figure 7.14.

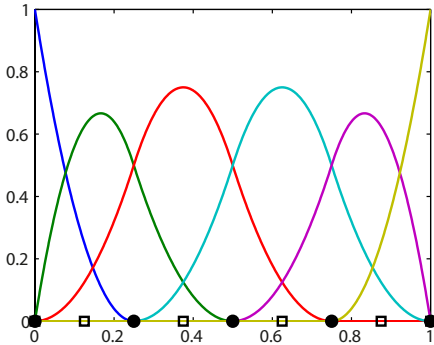


Figure 7.13: Quadratic B-spline basis functions, (7.4.2b).

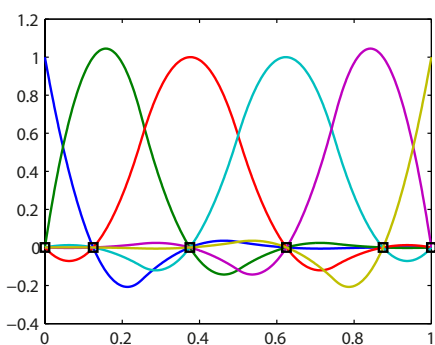


Figure 7.14: Lagrange basis function derived from quadratic B-splines, (7.4.7).

Similar to the edge functions of Lemma 8 (p. 114), which form an interpolation basis for 1-forms, there exists a 1-form ‘edge’ B-spline basis  $D_i^P(\xi)$  that corresponds to 1-control points,  $d_i$ . Since in one dimension every 1-form can be written as the exterior derivative of a 0-form, i.e.  $g^{(1)} = d f^{(0)}$ , we obtain,

$$d \underbrace{\sum_{i=0}^{M-1} b_i B_i^P(\xi)}_{\mathcal{d}\mathcal{IR}f^{(0)}} = \underbrace{\sum_{i=1}^{M-1} (b_i - b_{i-1}) D_i^{P-1}(\xi)}_{\mathcal{I}\delta\mathcal{R}f^{(0)}} = \underbrace{\sum_{i=1}^{M-1} d_i D_i^{P-1}(\xi)}_{\mathcal{I}\mathcal{R}g^{(1)}}, \tag{7.4.8}$$

where

$$d_i = \sum_{j=1}^{M-1} g_j \{D\}_{i,j}, \quad (7.4.9)$$

with non-singular matrix  $D$  given by the coefficients  $\{D\}_{i,j} = \int_{\eta_{j-1}}^{\eta_j} D_i^{P-1}(\xi)$  and  $g_j = \int_{\eta_{j-1}}^{\eta_j} g^{(1)}$  the reduction of the 1-form  $g^{(1)}$ . Following the same steps as in Lemma 8 we find the following expression for the 1-form ‘edge’ B-spline basis functions,

$$D_i^P(\xi) = P \frac{B_i^{P-1}(\xi)}{\xi_{i+P} - \xi_i}, \quad (7.4.10)$$

which can be constructed using the recursive relation in (7.4.2b). This ‘edge’ B-spline basis function is better known as the Curry-Schoenberg B-spline, [52]. It has the property that integrating over its own support  $[\zeta_{i-1}, \zeta_{i+P}]$  gives one,

$$\int_{\zeta_{i-1}}^{\zeta_{i+P}} D_i^P(\xi) = 1.$$

This property is not identical, but in line with the consistency property given in (6.1.7). Similar to (7.4.7) we can perform a change of basis to show the relation between ‘edge’ B-splines and edge interpolation functions,

$$\begin{aligned} \pi_h g^{(1)} &= \mathcal{IR} g^{(1)} = \sum_{i=1}^N d_i D_i^P(\xi) \\ &= \sum_{j=1}^N g_j \left[ \sum_{i=1}^N \{D^{-1}\}_{i,j} D_i^P(\xi) \right] \\ &= \sum_{j=1}^N g_j E_j(\xi), \end{aligned} \quad (7.4.11)$$

where basis function  $E_j(\xi)$  is an edge interpolation function derived from a 1-form ‘edge’ B-spline basis. Linear ‘edge’ B-spline basis functions on the same patch as in the previous figures are shown in Figure 7.15. The edge interpolation basis functions derived from the change of basis in (7.4.7) are shown in Figure 7.16. Notice that for the interval between two control points we have  $\int_{\eta_{i-1}}^{\eta_i} E_j(\xi) = \delta_{i,j}$  and that at the knots the basis functions have reduced continuity.

Also for mimetic B-splines there exists a dual grid and so a finite dimensional representation of the dual complex. Remember that  $\zeta = \{0 = \zeta_0, \dots, \zeta_N = 1\}$  is the unique knot vector of the primal grid, then we define a dual knot vector  $\tilde{\zeta} = \{0 = \tilde{\zeta}_0, \tilde{\zeta}_{1/2}, \dots, \tilde{\zeta}_{i+1/2}, \dots, \tilde{\zeta}_{N+1/2}, \tilde{\zeta}_{N+1} = 1\}$ , where  $\tilde{\zeta}_{i+1/2} = \frac{1}{2}(\zeta_i + \zeta_{i+1})$ . The dual grid consists of the midpoints of the primal grid supplemented with the two boundary knots. So the dual grid has in total one knot more than the primal grid. On this dual grid a B-spline basis for both 0-forms and one-forms can be constructed similar to the primal grid as was shown above.

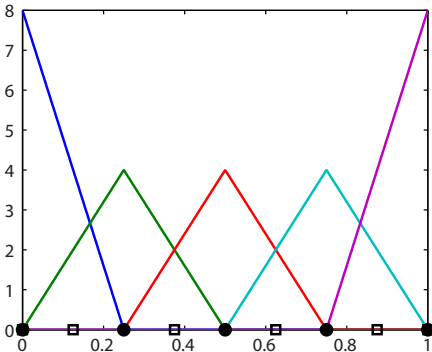


Figure 7.15: Linear ‘edge’ B-spline basis functions.

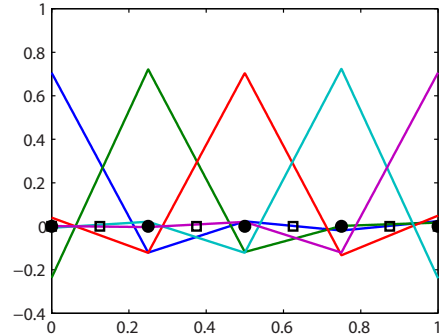


Figure 7.16: Edge basis function derived from linear ‘edge’ B-splines.

Having basis function on both grids for both 0- and 1-forms, and having a direct relation between a B-spline basis and an interpolation basis, all tools and steps that hold for the mimetic spectral element method also hold for the mimetic B-spline method.

**Remark 35.** *In principe kan je voor elke 1D basis met partition of unity een ‘nodale’ en een ‘edge’ functie construeren. Met behulp van tensor products kan je dus voor elke  $k$ -cube een interpolatie functie ontwikkelen. (Lagrange, B-spline, NURBS, etc.)*

Laagste orde Whitney forms, zie PhD thesis Heumann. AFW functie??

## 7.5 Discussion

Deze moet nog volledig worden herschreven

Closely related to the presented mimetic basis functions are (higher-order) Whitney forms, [28, 93, 185]. They share that there exists points, edges, faces and volumes ( $0, 1, 2, 3$ -cells) both on the element boundary as well as in the element interior. These  $k$ -cells have physical relevance [153]. The main difference exists in the way they are constructed.

On the other hand in mixed finite elements, Raviart-Thomas [154] ( $H(\text{div})$  conforming) and Nédélec [133] ( $H(\text{curl})$  conforming) elements are frequently used basis functions. Main difference with our mimetic basis functions is that these basis functions are moment based polynomials, where each  $k$ -cell may have a higher-order moment degree, but the number of  $k$ -cells remains unchanged when increasing the polynomial order. A consequence is that Raviart-Thomas and Nédélec elements allow only affine mappings, whereas the present mimetic basis functions allow for curvilinear elements. Where the mimetic basis functions are constructed especially for quadrilateral and hexahedral elements, the Whitney and mixed finite element basis functions also work on triangles and tetrahedrals. In case of the lowest order quadrilaterals or hexahedrals, all three types of basis functions are the same.

---

As shown in Section 5, we need two cell-complexes to represent inner- and outer oriented variables. The use of such overlapping grids is well-known in staggered finite volume methods. A spectral staggered grid approach was presented by Kopriva and Koli  as, [110], and Kopriva, [108, 109].



## **Part III**

# **Application of Mimetic Discretization**



# Chapter 8

## Hodge-Laplace problems

*Be careful of the naive view that a physical law is a mathematical relation between previously defined quantities. The situation is, rather, that a certain mathematical structure represents a given physical structure.*

Burke, Applied differential geometry, 1985.

This chapter treats the discretization of problems based on the Hodge-Laplace operator, Definition 24 (p. 61). The Hodge-Laplace operator resembles the scalar and vector Laplace operator from vector calculus. These type of problems, often of academic nature, are well-known to both mathematicians and engineers and therefore serve as excellent toy problem to display the proposed discretization technique based on the abstract framework for elliptic problems as was presented in the previous part.

This chapter is organized as follows. In the first section, we start with the most basic of them all, the scalar Poisson problem. This problem already displays most of the tools of the mimetic framework. Two different approaches will be discussed, a staggered grid approach and a single grid approach. The focus here is mainly on the application of the mimetic framework and to discuss some of the implementation issues. Next the model problem is extended to problems with non-constant tensorial constitutive relations and to non-contractible domains, i.e. domains with holes. Section 8.2 extends these ideas and treats the general Hodge-Laplacian. It introduces and motivates the use of a mixed formulation and discusses stability and convergence of the discrete system. Operator convergence in a strong sence is shown in Section 8.3 using eigenvalue problems of the Hodge-Laplacian, with special attention to the resonant cavity eigenvalue problem that appears in electromagnetism.

This chapter contains a wide variety of numerical test cases to illustrate the performance the discretization method. These test cases show, among others, convergence of the discrete source problems and discrete eigenvalue problems. Most of them are considered to be difficult, and many of the popular methods fail for one or more of these test cases, see [5, 21, 22, 48].

---

## 8.1 Scalar Hodge-Laplace problems

We start with the most basic of all Laplace problems, the scalar Poisson problem. This problem already displays most of the tools described in the previous part. Two different approaches will be discussed. The first makes use of the staggered grid structure as described in Section 5.3 on dual complexes and as illustrated in Figure 5.10. *Staggered grid approaches* are more common in finite volume methods. Classical is the work on incompressible flow problems by Harlow and Welch [82]. This idea was extended to unstructured simplicial meshes by Subramanian and Perot [172]. Similar to the current method, the discrete unknowns are located on all  $k$ -cells, that is, pressures in volumes, velocity fluxes in surfaces, vorticity on lines, temperature in points, etc.. The methods differ in that the referenced methods consider averaged quantities as their unknowns, whereas we consider integral quantities as our discrete unknowns. While the first already contains approximation, the latter is exact. This allows for purely topological relations between the unknowns. As a result it gives more flexibility for example in the use of curvilinear meshes, as will be illustrated below.

Recently the Discrete Exterior Calculus (DEC) method, [55, 95], was developed that uses a staggered approach on simplices using Delaunay and Voronoi grids. DEC is based on a one-to-one translation of each of the continuous operator in Chapter 4 into a discrete operator. It deviates from our approach in the sense that we translated each continuous operator acting on an infinitely dimensional space into operators acting on finite dimensional spaces, see Chapter 6. By translating all operators into discrete operators, the DEC method restricts themselves to lowest order approximations only.

Alternatively to a staggered grid approach we also present the *single grid approach*. Single grid approaches are found in most finite element methods and in collocated finite volume methods. In single grid approaches all variables defined on the dual grid are mapped onto the primal grid using their corresponding constitutive Hodge star relations. This approach will also be used in remainder of this thesis.

In both methods the topological relations are represented by the exterior derivative and the coboundary operator as its discrete counterpart. In the staggered approach metric relations are given by the constitutive Hodge star operator. The single grid approach uses the (weighted) inner product as metric operator. The two metric operators are directly related as was shown in (4.7.1).

In the second part of this section, the standard scalar Poisson problem is extended to non-constant tensorial constitutive relations and to domains with holes. The first extension has physical relevance since in practice viscosity and permeability coefficients are tensors as function of among others temperature or location, such as in Darcy flows. For the second, think for example of a potential flow around an airfoil, and other applications on more complex domains containing holes, tunnels or voids.

### 8.1.1 Staggered grid approach

This section considers the scalar or 0-form Poisson problem as a sample problem to show the steps of the staggered grid approach. This approach is motivated by the formal structures of PDEs as was first described by Tonti [174] and illustrated in the so-called *Tonti diagrams*. Here the PDEs are unraveled in physical laws, like kinematic equations and balance laws, and constitutive relations. Physical laws are exact and

of topological nature. Constitutive relations are man made relations that are based on approximations. They are metric dependent. A nice low-level introduction can be found in [171].

### The scalar Poisson problem

Consider the scalar Poisson equation, used among others to model the fields of potential flow or electric potentials and heat problems. The scalar Poisson equation is given by  $-\operatorname{div}(\operatorname{grad} \alpha) = f$  in a domain  $\Omega \subset \mathbb{R}^n$ , supplemented with a prescribed linear combination of  $\alpha$  (Dirichlet) and  $\vec{q} \cdot \vec{n}$  (Neumann) on boundary  $\partial\Omega$ . Instead of a single second-order PDE, we choose to consider the following system of first derivatives, with the kinematic and balance laws given by

$$\vec{u} = -\operatorname{grad} \alpha, \quad \operatorname{div} \vec{q} = f. \quad (8.1.1a)$$

The corresponding constitution relation is

$$\vec{q} = \vec{u}. \quad (8.1.1b)$$

The corresponding Tonti diagram is illustrated below,

$$\begin{array}{ccc} \vec{q} & \xrightarrow{\operatorname{div}} & f \\ \uparrow & & \\ \vec{u} & \xleftarrow[-\operatorname{grad}]{} & \alpha \end{array}$$

An equivalent representation in terms of differential forms is given by

$$\tilde{u}^{(1)} = d\tilde{\alpha}^{(0)}, \quad dq^{(n-1)} = f^{(n)}. \quad (8.1.2a)$$

with as constitutive relation,

$$q^{(n-1)} = \star \tilde{u}^{(1)}. \quad (8.1.2b)$$

Then the corresponding Tonti diagram becomes,

$$\begin{array}{ccc} q^{(n-1)} & \xrightarrow{d} & f^{(n)} \\ \star \uparrow & & \\ \tilde{u}^{(1)} & \xleftarrow[d]{} & \tilde{\alpha}^{(0)} \end{array}$$

The potential is a 0-form,  $\tilde{\alpha}^{(0)} \in \tilde{\Lambda}^0(\Omega)$ , the velocity a 1-form  $\tilde{u}^{(1)} \in \tilde{\Lambda}^1(\Omega)$ , the flux an  $(n-1)$ -form  $q^{(n-1)} \in \Lambda^{n-1}(\Omega)$  and body force  $f^{(n)} \in \Lambda^n(\Omega)$ . The first two are situated on the lower complex of (4.7.4), i.e. are associated to inner-oriented manifolds by duality pairing, and the latter two are situated on the upper complex of (4.7.4), associated to outer-oriented manifolds. Then the scalar Poisson problem becomes

$$d \star d\tilde{\alpha}^{(0)} = f^{(n)}, \quad (8.1.3)$$

supplemented with a linear combination of Dirichlet,  $\operatorname{tr} \tilde{\alpha}^{(0)}$ , and Neumann,  $\operatorname{tr} \star q^{(n-1)}$ , boundary conditions prescribed on the boundary  $\partial\Omega$ .

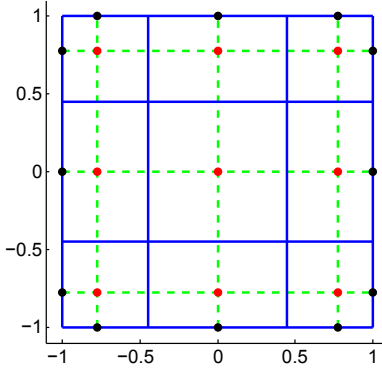


Figure 8.1: Primal (GL) mesh is given in blue, dual (EG) mesh in green, red (interior) and black (boundary) dots are the unknowns potentials.

### Discretization on staggered grid

Let us consider two cell complexes, the outer-oriented cell-complex  $D$  being the primal grid and the inner-oriented cell-complex  $\tilde{D}$  representing the dual grid, as explained in Chapter 5. The cochains of the fluxes and body forces are outer oriented-cochains and thus are defined on the primal mesh, and the potential and velocity cochains are inner-oriented cochains and are therefore defined on the dual mesh. Associated with the two cell complexes we have two reduction maps,  $\mathcal{R}$  and  $\tilde{\mathcal{R}}$  and two reconstruction maps  $\mathcal{I}$  and  $\tilde{\mathcal{I}}$ , and so, two projection operators,  $\pi_h$  and  $\tilde{\pi}_h$ .

We use mimetic spectral element cochain interpolation for the reconstruction. The primal mesh within each spectral element consists of a *Gauss-Lobatto* mesh (GL) and the *Extended Gauss* mesh (EG) will be used for the dual mesh. Figure 8.1 shows a two-dimensional ( $n = 2$ ) reference element with the two meshes, for  $N = 3$ , where  $N$  indicates the number of cells in horizontal and vertical direction on the primal mesh.

The finite dimensional representation of the Poisson problem is obtained by applying the projection operator of Definition 57, that maps  $k$ -forms into the finite dimensional space  $\Lambda_h^k(\Omega; C_k)$ . Applying the mimetic projections to the equations (8.1.2a) and using the commutation relation (6.1.8) gives,

$$\tilde{\mathcal{I}}\tilde{\mathcal{R}}\tilde{u}^{(1)} = \tilde{\mathcal{I}}\delta\tilde{\mathcal{R}}\tilde{a}^{(0)}, \quad \mathcal{I}\delta\mathcal{R}q^{(n-1)} = \mathcal{I}\mathcal{R}f^{(n)}. \quad (8.1.4)$$

Because the reconstruction operators are the same on both sides of the equality sign, i.e.  $\tilde{\mathcal{I}}(\tilde{\mathcal{R}}\tilde{u}^{(1)} - \delta\tilde{\mathcal{R}}\tilde{a}^{(0)}) = 0$  and  $\mathcal{I}(\delta\mathcal{R}q^{(n-1)} - \mathcal{R}f^{(n)}) = 0$ , the relations are solved on cochain level, where the coboundary operators will be represented by incidence matrices as given in Proposition 19 (p. 81).

**Divergence relation on primal grid** Let's consider for the moment a two-dimensional physical domain that is equal to the two-dimensional reference element,  $\Omega \equiv \hat{Q} = [-1, 1]^2$ , with coordinates  $\xi := (\xi, \eta)$ , and thus  $\Phi = Id$  and  $\Phi^* = Id$ .

Consider the right equation of (8.1.2a), the divergence relation. Let the body force  $f^{(n)}$ , on a two-dimensional reference domain, written as  $\hat{f}^{(2)}$ , be expressed as

$$\pi_h \hat{f}^{(2)} = \mathcal{IR} \hat{f}^{(2)}(\xi) = \sum_{i=1}^N \sum_{j=1}^N f_{i,j} e_i(\xi) e_j(\eta), \quad (8.1.5)$$

where  $f_{i,j}$  are 2-cochains and  $s_{i,j}(\xi) = e_i(\xi) e_j(\eta) = \varepsilon_i(\xi) \varepsilon_j(\eta) d\xi \wedge d\eta$  the surface (2D volume) interpolation basis functions. The flux density  $\hat{q}^{(n-1)}$  is expressed as

$$\hat{q}^{(1)} = -q^\eta(\xi) d\xi + q^\xi(\xi) d\eta, \quad (8.1.6)$$

where  $q^\xi(\xi)$  and  $q^\eta(\xi)$  are the normal flux density components in  $\xi$ - and  $\eta$ -direction, respectively. The finite dimensional expression of the flux on the two-dimensional reference domain is associated with the primal grid and is given by

$$\pi_h \hat{q}^{(1)} = \mathcal{IR} \hat{q}^{(1)} = - \sum_{i=1}^N \sum_{j=0}^N q_{i,j}^\eta e_i(\xi) l_j(\eta) + \sum_{i=0}^N \sum_{j=1}^N q_{i,j}^\xi l_i(\xi) e_j(\eta), \quad (8.1.7)$$

where the unknowns  $q_{i,j}^\xi$  and  $q_{i,j}^\eta$  are fluxes on the primal grid. These fluxes are the normal components of the flux densities integrated over their corresponding edges. Apply the exterior derivative to (8.1.7) gives the 2-form

$$\begin{aligned} d\pi_h \hat{q}^{(1)}(\xi, \eta) &= - \sum_{i=1}^N \sum_{j=0}^N q_{i,j}^\eta e_i(\xi) dl_j(\eta) + \sum_{i=0}^N \sum_{j=1}^N q_{i,j}^\xi dl_i(\xi) e_j(\eta) \\ &\stackrel{(7.2.6)}{=} \sum_{i=1}^N \sum_{j=1}^N \left( q_{i,j}^\xi - q_{i-1,j}^\xi + q_{i,j}^\eta - q_{i,j-1}^\eta \right) e_i(\xi) e_j(\eta) \\ &\stackrel{(6.1.8)}{=} \mathcal{I} \delta \mathcal{R} \hat{q}^{(1)} \stackrel{(6.1.4)}{=} \pi_h d\hat{q}^{(1)}, \end{aligned} \quad (8.1.8)$$

So (6.1.8) is indeed satisfied and with (6.1.4) it reduces to the approximation of  $d\hat{q}^{(1)}$ . Then from the divergence relation (8.1.2a) we obtain

$$\sum_{i=1}^N \sum_{j=1}^N \left( q_{i,j}^\xi - q_{i-1,j}^\xi + q_{i,j}^\eta - q_{i,j-1}^\eta - f_{i,j} \right) e_i(\xi) e_j(\eta) = 0. \quad (8.1.9)$$

This shows that the values of the cochain  $\mathbf{q}^{(1)}$  only depends on  $\mathbf{f}^{(2)}$  and is independent of the interpolation functions, i.e.  $\mathcal{R} dq^{(1)} = \delta \mathcal{R} q^{(1)} = \mathcal{R} f^{(2)}$ , so

$$q_{i,j}^\xi - q_{i-1,j}^\xi + q_{i,j}^\eta - q_{i,j-1}^\eta = f_{i,j}, \quad \text{for } i, j = 1, \dots, N. \quad (8.1.10)$$

The discrete divergence equation becomes  $E^{(2,1)} \mathbf{q}^{(1)} = \mathbf{f}^{(2)}$ . The result is a finite-volume-like formulation for the divergence equation. This relation is exact and metric-free, [73].

---

**Gradient on dual grid** Next consider the left relation of (8.1.2a). The 0-form  $\hat{\alpha}^{(0)}$  is expressed on the dual grid, as

$$\tilde{\pi}_h \hat{\alpha}^{(0)} = \tilde{\mathcal{I}} \tilde{\mathcal{R}} \hat{\alpha}^{(0)} = \sum_{i=1}^N \sum_{j=1}^N \alpha_{i,j} \tilde{l}_i^g(\xi) \tilde{l}_j^g(\eta), \quad (8.1.11)$$

where  $\alpha_{i,j}$  are the interior potential unknowns. For the dual grid, the mimetic spectral element basis functions are constructed using the Lagrange polynomials through the Gauss points,  $\tilde{l}_i^g(\xi)$ , and those through the extended Gauss points  $\tilde{l}_i^{\text{eg}}(\xi)$ , and the Gauss and extended Gauss edge polynomials,  $\tilde{e}_i^g(\xi)$  and  $\tilde{e}_i^{\text{eg}}(\xi)$ , respectively. Similar to (8.1.8) we can apply the exterior derivative. This gives,

$$\begin{aligned} d\tilde{\pi}_h \hat{\alpha}^{(0)} = \tilde{\mathcal{I}} \delta \tilde{\mathcal{R}} \hat{\alpha}^{(0)} &= \sum_{i=2}^N \sum_{j=1}^N (\alpha_{i,j} - \alpha_{i-1,j}) \tilde{e}_i^g(\xi) \tilde{l}_j^g(\eta) \\ &\quad + \sum_{i=1}^N \sum_{j=2}^N (\alpha_{i,j} - \alpha_{i,j-1}) \tilde{l}_i^g(\xi) \tilde{e}_j^g(\eta). \end{aligned}$$

Again the second commuting diagram property (6.1.8) is satisfied. Once we add the boundary complex, consisting of the potentials on 0-cells, we find an expression for the velocity,

$$\begin{aligned} \tilde{\pi}_h \hat{u}^{(1)} &= \sum_{i=1}^{N+1} \sum_{j=1}^N (\alpha_{i,j} - \alpha_{i-1,j}) \tilde{e}_i^{\text{eg}}(\xi) \tilde{l}_j^g(\eta) \\ &\quad + \sum_{i=1}^N \sum_{j=1}^{N+1} (\alpha_{i,j} - \alpha_{i,j-1}) \tilde{l}_i^g(\xi) \tilde{e}_j^{\text{eg}}(\eta) \end{aligned} \quad (8.1.12)$$

In matrix notation the discrete gradient becomes  $\tilde{\mathbf{u}}^{(1)} = \tilde{\mathbf{E}}^{(1,0)} \tilde{\mathbf{a}}^{(0)}$ , where  $\tilde{\mathbf{a}}^{(0)}$  is the potential 0-cochain including boundary unknowns,  $\tilde{\mathbf{u}}^{(1)}$  is the velocity 1-cochain, and where  $\tilde{\mathbf{E}}^{(1,0)}$  is the incidence matrix of (8.1.12). Again this equation is exact and metric-free.

**Discrete Hodge star operator** In the discussion of the discrete structures in Chapter 5 there was no section on a discrete counterpart of the Hodge star operator,  $\mathsf{H} : C^k(\tilde{D}) \rightarrow C^{n-k}(D)$ . In fact there is no uniform definition of the discrete Hodge star operator. In Tarhasaari [173] and in Bochev and Hyman [18], definitions for a *natural* and *derived* discrete Hodge star operator are given. An interesting discussion on the construction of a discrete Hodge star is found in [92], where a similar distinction is made.

Because the Hodge star operator can only be performed in continuous space, in the natural definition, the  $k$ -cochains are first interpolated to  $k$ -forms and, after applying the Hodge star, reduced back to  $(n-k)$ -cochains,

$$\mathsf{H} = \mathcal{R} \star \tilde{\mathcal{I}}. \quad (8.1.13)$$

---

Alternatively, for any  $\tilde{a}_h^{(k)} \in \Lambda^k(\Omega; \tilde{C}_k)$  and for all  $b_h^{(n-k)} \in \Lambda_h^{n-k}(\Omega; C_{n-k})$ , a discrete Hodge star can be derived in a weak sense using (4.7.6) as

$$\int_{\Omega} \tilde{a}_h^{(k)} \wedge b_h^{(n-k)} = (\star \tilde{a}_h^{(k)}, b_h^{(n-k)})_{\Omega} = (\mathcal{I}\mathcal{H}\tilde{\alpha}^{(k)}, b_h^{(n-k)})_{\Omega}. \quad (8.1.14)$$

In Chapter 6 it is shown that both definitions are identical for the finite dimensional space  $\Lambda_h^k(\Omega; \tilde{C}_k)$ . The idea of the latter is adopted to make a connection between  $q_h^{(n-1)}$  defined on the primal grid and  $\tilde{u}_h^{(1)}$  defined on the dual grid,

$$(q_h^{(n-1)}, p_h^{(n-1)})_{\Omega} = (\star \tilde{u}_h^{(1)}, p_h^{(n-1)})_{\Omega} = \int_{\Omega} \tilde{u}_h^{(1)} \wedge p_h^{(n-1)}, \quad \forall p_h^{(n-1)} \in \Lambda_h^{n-1}. \quad (8.1.15)$$

Equation (8.1.15) makes use of the definition of the Hodge star in terms of the  $L^2$  inner product and the wedge product. A matrix representation of the Hodge star operator can be extracted from (8.1.15). From that we can formulate a matrix system for the Poisson problem,

$$(\tilde{\mathbf{E}}^{(1,0)})^T \mathbf{H} \tilde{\mathbf{E}}^{(1,0)} \tilde{\boldsymbol{\alpha}}^{(0)} = \mathbf{f}^{(2)}, \quad (8.1.16)$$

where we used (5.4.4), which states that  $\mathbf{E}^{(2,1)} = (\tilde{\mathbf{E}}^{(1,0)})^T$ . Note that to obtain  $\mathbf{H}$  we already inverted an inner product matrix resulting from the left hand term expression in (8.1.15). Although all eigenvalues of the resulting left hand side matrix in (8.1.16) are real, the discrete Hodge star matrix is not necessarily symmetric.

Alternatively, one could cast the problem into a saddle point system which solves for  $\tilde{\alpha}_h^{(0)}$  and  $q_h^{(n-1)}$  in the following system,

$$q_h^{(n-1)} = \star d\tilde{\alpha}_h^{(0)}, \quad dq_h^{(n-1)} = f_h^{(n)}. \quad (8.1.17)$$

To obtain a saddle point system, we slightly modify the previous approach by splitting the righthand term in (8.1.15) into an interior part and boundary part of domain  $\Omega$  using Leibniz rule (4.6.2), for all  $p_h^{(n-1)} \in \Lambda_h^{n-1}(\Omega; C_{n-1})$ ,

$$\begin{aligned} (p_h^{(n-1)}, q_h^{(n-1)})_{\Omega} &= (p_h^{(n-1)}, \star d\tilde{\alpha}_h^{(0)})_{\Omega} \\ &\stackrel{(4.6.2)}{=} \int_{\partial\Omega} \text{tr } p_h^{(n-1)} \wedge \text{tr } \tilde{\alpha}_h^{(0)} - \int_{\Omega} dp_h^{(n-1)} \wedge \tilde{\alpha}_h^{(0)}, \end{aligned} \quad (8.1.18)$$

A similar split in interior and boundary part we have seen for the dual grid in Chapter 5. Equation (8.1.18) is closely related to the *support operator method* proposed in the context of the mimetic finite difference method by Hyman et al., [100]. This relation also ensures a symmetric matrix system, while (8.1.15) does not. In (8.1.18) we make use of Gauss-Lobatto quadrature for the left hand term and Gauss quadrature

for the right hand side. This gives the following expression,

$$\begin{aligned} \sum_{p=0}^N \sum_{l=1}^N q_{p,l}^\xi \sum_{j=1}^N q_{p,j}^\xi \left\{ w_p^{\text{gl}} \sum_{q=0}^N w_q^{\text{gl}} \varepsilon_j(\eta_q) \varepsilon_l(\eta_q) \right\} + \sum_{k=1}^N \sum_{q=0}^N q_{k,q}^\eta \sum_{i=1}^N q_{i,q}^\eta \left\{ w_q^{\text{gl}} \sum_{p=0}^N w_p^{\text{gl}} \varepsilon_i(\xi_p) \varepsilon_k(\xi_p) \right\} = \\ \sum_{q=1}^N \sum_{l=1}^N \left( q_{N,l}^\xi \alpha_{N+1,q} - q_{0,l}^\xi \alpha_{0,q}^\xi \right) w_q^{\text{g}} \varepsilon_l(\tilde{\eta}_q) + \sum_{k=1}^N \sum_{p=1}^N \left( q_{k,N}^\eta \alpha_{p,N+1} - q_{k,0}^\eta \alpha_{p,0} \right) w_p^{\text{g}} \varepsilon_k(\tilde{\xi}_p) \\ - \sum_{k=1}^N \sum_{l=1}^N \left( q_{k,l}^\xi - q_{k-1,l}^\xi + q_{k,l}^\eta - q_{k,l-1}^\eta \right) \sum_{p=1}^N \sum_{q=1}^N \alpha_{p,q} w_p^{\text{g}} w_q^{\text{g}} \varepsilon_k(\tilde{\xi}_p) \varepsilon_l(\tilde{\eta}_q). \end{aligned}$$

The resulting matrix system becomes either,

$$\begin{bmatrix} \mathbf{M}^{(1)} & \mathbf{E}^{(2,1)\top} \mathbf{W}^{(2,0)} \\ \mathbf{E}^{(2,1)} & 0 \end{bmatrix} \begin{bmatrix} \mathbf{q}^{(1)} \\ \tilde{\boldsymbol{\alpha}}^{(0)} \end{bmatrix} = \begin{bmatrix} \mathbf{B}^{(1,0)} \tilde{\boldsymbol{\alpha}}^{(0)} \\ \mathbf{f}^{(2)} \end{bmatrix} \quad (8.1.19)$$

or when pre-multiplying the second line with the wedge product matrix between two- and zero-forms,  $\mathbf{W}^{(2,0)}$ , we obtain a symmetric system matrix,

$$\begin{bmatrix} \mathbf{M}^{(1)} & \mathbf{E}^{(2,1)\top} \mathbf{W}^{(2,0)} \\ \mathbf{W}^{(2,0)\top} \mathbf{E}^{(2,1)} & 0 \end{bmatrix} \begin{bmatrix} \mathbf{q}^{(1)} \\ \tilde{\boldsymbol{\alpha}}^{(0)} \end{bmatrix} = \begin{bmatrix} \mathbf{B}^{(1,0)} \tilde{\boldsymbol{\alpha}}^{(0)} \\ \mathbf{W}^{(2,0)\top} \mathbf{f}^{(2)} \end{bmatrix} \quad (8.1.20)$$

In the systems above,  $\mathbf{M}^{(1)}$  is the inner-product matrix for one-forms,  $\mathbf{E}^{(2,1)}$  the incidence matrix representing the topological divergence operator, and  $\mathbf{B}^{(1,0)}$  the boundary integral.

The staggered grid discretization presented above can be extended with curvilinear mappings.

**Transfinite mapping onto curvilinear domains** Consider two manifolds, the physical domain  $\Omega = Q$ , discretized with a single spectral element, with basis  $\mathbf{x} := (x_1, \dots, x_n)$  and a reference element  $\hat{Q}$  with basis  $\boldsymbol{\xi} := (\xi_1, \dots, \xi_m)$ . Then the mapping  $\Phi$  gives us the basis in physical space as function of the reference basis, so

$$x_i = x_i(\boldsymbol{\xi}), \quad i = 1, \dots, n. \quad (8.1.21)$$

As is common in many numerical methods, the  $k$ -forms are pulled back onto a reference element using the pullback operator,  $\Phi^*$ , so if

$$\omega^{(k)} = \omega^{(k)}(x_1, \dots, x_n), \quad \text{then} \quad \Phi^* \omega^{(k)} = (\Phi^* \omega^{(k)})(\xi_1, \dots, \xi_m). \quad (8.1.22)$$

Now recall that the  $k$ -forms in our Poisson problem,  $\tilde{\alpha}^{(0)}$ ,  $u^{(1)}$ ,  $q^{(n-1)}$  and  $f^{(n)}$ , are functions of coordinates  $(x_1, \dots, x_n)$ . Introduce  $\hat{\tilde{\alpha}}^{(0)} = \Phi^* \tilde{\alpha}^{(0)}$ ,  $\hat{u}^{(1)} = \Phi^* u^{(1)}$ ,  $\hat{q}^{(n-1)} = \Phi^* q^{(n-1)}$  and  $\hat{f}^{(n)} = \Phi^* f^{(n)}$  on  $\hat{Q}$ , then system (8.1.2a)-(8.1.2b) becomes

$$\hat{u}^{(1)} = d\hat{\tilde{\alpha}}^{(0)}, \quad \hat{q}^{(n-1)} = (\Phi^* \star (\Phi^*)^{-1}) \hat{u}^{(1)}, \quad d\hat{q}^{(n-1)} = \hat{f}^{(n)} \quad (8.1.23)$$

The only operator that changes is the Hodge star operator, as we saw already in (4.7.5). Once we have solved (8.1.23) for  $\hat{\tilde{\alpha}}^{(0)}$  and  $\hat{q}^{(n-1)}$ , we retrieve the solution in physical space by pre-multiplication by  $(\Phi^*)^{-1}$ ,

$$\tilde{\alpha}^{(0)} = (\Phi^*)^{-1} \hat{\tilde{\alpha}}^{(0)}, \quad q^{(n-1)} = (\Phi^*)^{-1} \hat{q}^{(n-1)}. \quad (8.1.24)$$

---

On a curvilinear  $n$ -dimensional domain  $\Omega = \Phi(\hat{Q})$  the support operator relation becomes, for all  $p_h^{(n-1)} \in \Lambda_h^{n-1}(\Omega; C_{n-1})$ ,

$$\begin{aligned}
(p^{(n-1)}, \star d\tilde{\alpha}^{(0)})_{\Phi(\hat{Q})} &= ((\Phi^*)^{-1}\hat{p}^{(n-1)}, \star d(\Phi^*)^{-1}\hat{\alpha}^{(0)})_{\Phi(\hat{Q})} \\
&= ((\Phi^*)^{-1}\hat{p}^{(n-1)}, (\Phi^*)^{-1}\hat{\star}d\hat{\alpha}^{(0)})_{\Phi(\hat{Q})} \\
&= (-1)^{n-1} \int_{\Phi(\hat{Q})} (\Phi^*)^{-1}(\hat{p}^{(n-1)} \wedge d\hat{\alpha}^{(0)}) \\
&= \int_{\partial\hat{Q}} \text{tr } \hat{p}^{(n-1)} \wedge \text{tr } \hat{\alpha}^{(0)} - \int_{\hat{Q}} d\hat{p}^{(n-1)} \wedge \hat{\alpha}^{(0)}. \tag{8.1.25}
\end{aligned}$$

The last line shows that a wedge product of differential forms is coordinate independent. The coordinate mapping is only present in the  $L^2$  inner product in the first line. More on the staggered grid mimetic spectral element method can be found in [30, 114].

### 8.1.2 Single grid approach

Alternative to the staggered grid approach is the single grid approach. This is the common approach used in finite element and collocated finite volume methods. This approach no longer tries to discretize the Hodge star operator, but makes use of inner products as metric operator. All variables associated to inner-oriented manifolds<sup>1</sup>, are mapped to variables associated to outer-oriented manifolds, using the Hodge star, which is an isomorphism. If we substitute  $\tilde{\alpha}^{(0)} = \star\alpha^{(n)}$  with  $\alpha^{(n)} \in \Lambda^n(\Omega)$ , the Poisson problem becomes

$$-d \star d \alpha^{(n)} = f^{(n)} \quad \Leftrightarrow \quad dd^* \alpha^{(n)} = f^{(n)}, \tag{8.1.26}$$

where we made use of (4.8.4) for the codifferential operator. Then the flux is given by  $q^{(n-1)} = d^* \alpha^{(n)}$ .

**Remark 36.** Note that the Hodge star is always related to a constitutive relation. Take for example the heat problem discussed in Section 2.4. The heat problem could be written in terms of temperature,

$$-\text{div}(\mathbb{K}\text{grad } T) = f, \quad \Leftrightarrow \quad -d \star_{\mathbb{K}} d \tilde{T}^{(0)} = f^{(n)}.$$

This could be solved using the staggered grid approach. Alternatively, we could express the heat equation in terms of internal energy. The two are related through the heat capacity coefficient,  $e^{(n)} = \star_{c_v} \tilde{T}^{(0)}$ . Then the heat problem becomes,

$$-\text{div}(\mathbb{K}\text{grad}(\frac{1}{c_v}e)) = f, \quad \Leftrightarrow \quad -d \star_{\mathbb{K}} d \star_{c_v^{-1}} e^{(n)}.$$

This heat problem could well be solved using a single grid approach. The Poisson problem with non-constant coefficients is treated in Section 8.1.4 on Darcy flow problems.

---

<sup>1</sup>indicated with the usual  $\tilde{\cdot}$

The most common way to treat the codifferential is to use integration by parts (4.8.5), which relates the codifferential operator to the exterior derivative and a contribution from the boundary, i.e.

$$\begin{aligned} (\tau^{(n-1)}, q^{(n-1)})_{\Omega} &= (\tau^{(n-1)}, d^* \alpha^{(n)})_{\partial\Omega} \\ &\stackrel{(4.8.5)}{=} (d\tau^{(n-1)}, \alpha^{(n)})_{\Omega} - \int_{\partial\Omega} \operatorname{tr} \tau^{(n-1)} \wedge \operatorname{tr} \star \alpha^{(n)}. \end{aligned} \quad (8.1.27)$$

Again the divergence relation can be performed directly, and so one gets a saddle point system to solve for  $q^{(n-1)}$  and  $\alpha^{(n)}$ . Since the divergence relation is already satisfied in a strong sense, rewriting it in a weak formulation,  $(v^{(n)}, dq^{(n-1)})_{\Omega} = (v^{(n)}, f^{(n)})_{\Omega}$  for all  $v^{(n)} \in \Lambda^n(\Omega)$ , has no affect on the solution, but results in a symmetric saddle point system,

$$\begin{bmatrix} M^{(n-1)} & E^{(n,n-1)T} M^{(n)} \\ M^{(n)} E^{(n,n-1)} & 0 \end{bmatrix} \begin{bmatrix} q^{(n-1)} \\ \alpha^{(n)} \end{bmatrix} = \begin{bmatrix} \mathbf{0}^{(n-1)} \\ M^{(n)} \mathbf{f}^{(n)} \end{bmatrix}. \quad (8.1.28)$$

### 8.1.3 Numerical results scalar Poisson problem

The staggered grid and single grid approach applied to a scalar Poisson problem are tested on a square two-dimensional domain  $\Omega \in [-1, 1]^2$  with solution

$$\alpha^{(0)} = \sin(2\pi x) \sin(2\pi y). \quad (8.1.29)$$

In this test case we only deform the interior of the domain using the following mapping,  $(x, y) = \Phi(\xi, \eta)$ , with

$$x(\xi, \eta) = \xi + c \sin(\pi\xi) \sin(\pi\eta) \quad (8.1.30a)$$

$$y(\xi, \eta) = \eta + c \sin(\pi\xi) \sin(\pi\eta). \quad (8.1.30b)$$

The problem is completed by imposing Dirichlet boundary conditions on the lower and left boundary of  $\partial\Omega$  and Neumann boundary conditions on the upper and right boundary of  $\partial\Omega$ .

For the two methods  $h$ - and  $p$ -convergence results are obtained on meshes of increasing curvature and skewness. In the mapping of the domain  $c$  refers to the amount of deformation applied to the domain. Grids for  $c = 0.0, 0.15, 0.30$  are shown in Figure 8.2. Figure 8.3 and Figure 8.4 show the  $h$ -convergence results in  $L^2$ -norm of the potential  $\alpha^{(0)}$  for the staggered grid and single grid approach, respectively. The  $h$ -convergence in  $L^2$ -norm of the flux  $q^{(1)}$  is identical for both approaches and is given in Figure 8.5. Besides the numerical errors  $\|\tilde{\alpha}^{(0)} - \tilde{\alpha}_h^{(0)}\|_{L^2\Lambda^0}$  and  $\|q^{(1)} - q_h^{(1)}\|_{L^2\Lambda^1}$ , also the interpolation errors  $\|\tilde{\alpha}^{(0)} - \pi_h \tilde{\alpha}^{(0)}\|_{L^2\Lambda^0}$  and  $\|q^{(1)} - \pi_h q^{(1)}\|_{L^2\Lambda^1}$  are plotted. In almost all cases these lie on top of the numerical errors, indicating that the discretization errors  $\|\pi_h \tilde{\alpha}^{(0)} - \tilde{\alpha}_h^{(0)}\|_{L^2\Lambda^0}$  and  $\|\pi_h q^{(1)} - q_h^{(1)}\|_{L^2\Lambda^1}$  are of magnitudes smaller than the theoretical interpolation errors. For all grid configurations the convergence rates are optimal in the sense that they match the interpolation convergence rates. Moreover, the convergence results show that the skewness of the grid only slightly influence the numerical errors. The errors of the potential for the staggered grid approach are

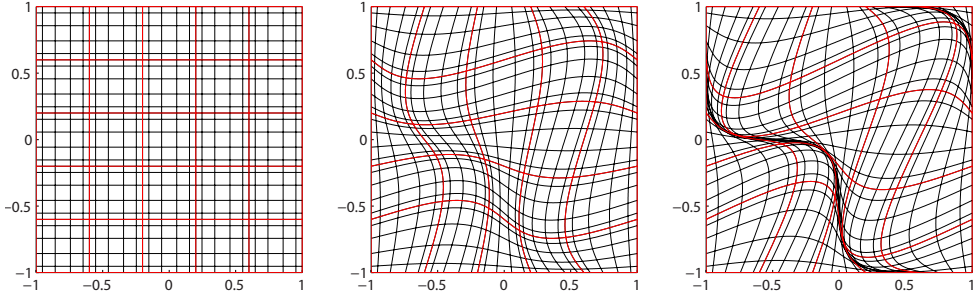


Figure 8.2: Deformed meshes for  $N = 5$  and for  $c = \{0.0, 0.15, 0.3\}$ .

somewhat better than those of the single grid approach. This is because the staggered grid approach uses more unknowns for the potential as the single grid approach due to their unknowns on the inter-element boundaries,

$$\begin{aligned} \text{staggered : } & M_x \cdot M_y \cdot (N^2 + 2N) + (M_x + M_y) \cdot N, \\ \text{single : } & M_x \cdot M_y \cdot N^2, \end{aligned}$$

where  $M_x, M_y$  are the number of element in  $x$ - and  $y$ -direction, and  $M_x \cdot M_y$  the total number of elements used.

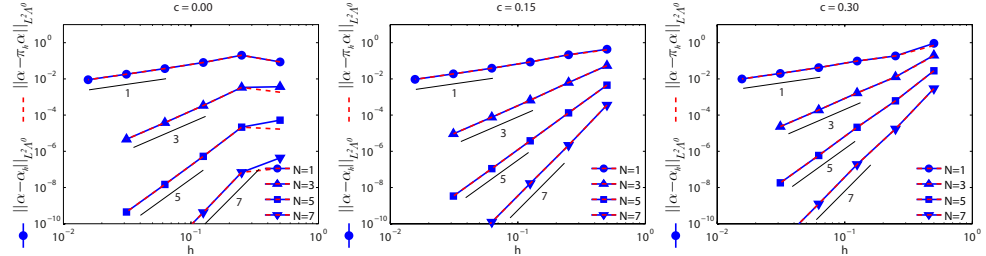


Figure 8.3:  $h$ -convergence potential for staggered grid approach, for  $N = 1, 3, 5, 7$ .

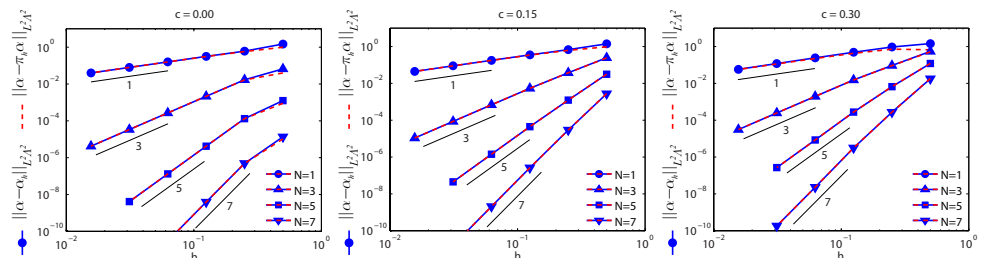


Figure 8.4:  $h$ -convergence potential for single grid approach, for  $N = 1, 3, 5, 7$ .

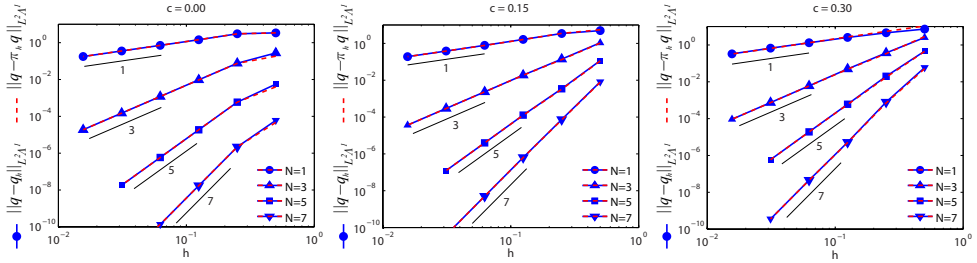


Figure 8.5:  $h$ -convergence flux for both staggered and single grid approaches, for  $N = 1, 3, 5, 7$ .

In Figures 8.6, 8.7 and 8.8 the  $p$ -convergence results are plotted for the potential using staggered grid and single grid approach and the flux for both methods, respectively. For  $p$ -convergence we notice that we obtain exponential convergence for all grid configurations, both square and curvilinear. Again the interpolation errors lie on top of the numerical error indicating that the discretization errors are significantly lower than the interpolation errors.

Note that  $c = 0.3$  is the upper limit of still obtaining a one-to-one mapping. In [30, 74] we also considered self overlapping meshes, which showed reasonable convergence behaviour as well.

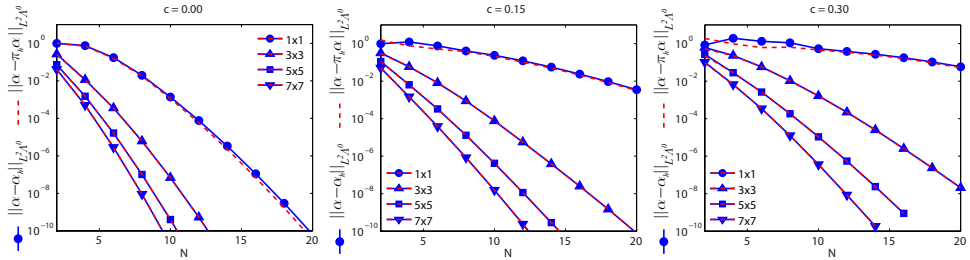


Figure 8.6:  $p$ -convergence potential for staggered grid approach, for  $M_x = M_y = 1, 3, 5, 7$ .

### 8.1.4 Darcy flows

**vergelijk met paper pedro!** The scalar Poisson problem can be extended with a non-uniform tensorial material property in the constitutive relation. In fluid dynamics these problems are known as Darcy flow problems, which model single phase incompressible flow in porous media. See Neuman [135] for a derivation of Darcy's law. These types of flows appear among others in groundwater dynamics, petroleum engineering and  $CO_2$  storage, [184]. Darcy flow problems are typically solved using either mimetic finite difference methods, [100], or mixed finite element methods, [183].

This two equation model consists of Darcy's law, a kinematic equation relating the flux  $\vec{w}$  to the gradient of pressure  $p$  weighted with a material coefficients tensor  $\mathbb{K}$

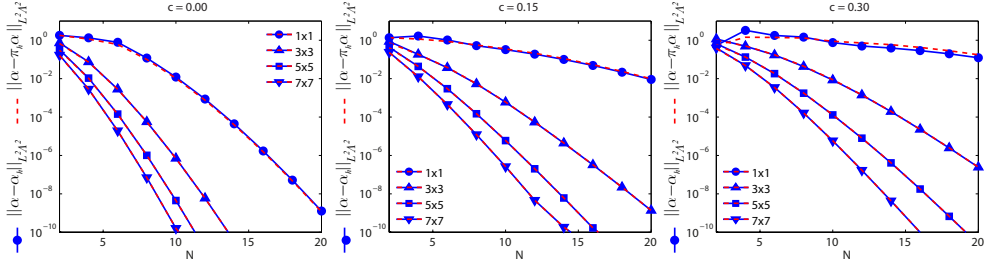


Figure 8.7:  $p$ -convergence potential for single grid approach, for  $M_x = M_y = 1, 3, 5, 7$ .

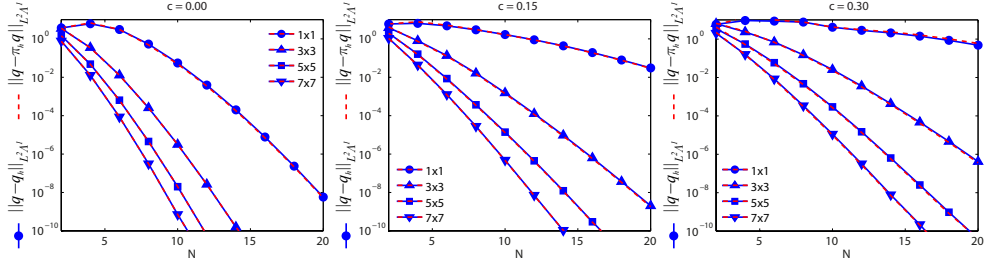


Figure 8.8:  $p$ -convergence flux for staggered and single grid approaches, for  $M_x = M_y = 1, 3, 5, 7$ .

representing the material permeability divided by the fluid kinematic viscosity, and a continuity equation,

$$\vec{w} = -\mathbb{K} \operatorname{grad} p, \quad (8.1.31a)$$

$$\operatorname{div} \vec{w} = f. \quad (8.1.31b)$$

Matrix  $\mathbb{K}$  is a symmetric, positive definite tensor, that is, for some  $0 < k_0 \leq k_1 < \infty$ ,

$$k_0 \xi^T \xi \leq \xi^T \mathbb{K}(\mathbf{x}) \xi \leq k_1 \xi^T \xi, \quad \forall \mathbf{x} \in \Omega, \forall \xi \in \mathbb{R}^n. \quad (8.1.32)$$

Note that the coefficients of matrix  $\mathbb{K}$  do not need to be smooth, but that the coefficients may also be discontinuous. In terms of differential forms Darcy's model as given in (8.1.31) becomes either

$$w^{(n-1)} = -\star_{\mathbb{K}} d \star p^{(n)} \quad \text{or} \quad w^{(n-1)} = d_{\mathbb{K}}^* p^{(n)} \quad (8.1.33)$$

$$dw^{(n-1)} = f^{(n)} \quad (8.1.34)$$

In this thesis we prefer to use the single grid approach and therefore use the system on the right. The codifferential  $d_{\mathbb{K}}^*$  is defined using the weighted  $L^2$  inner product as

$$(w^{(n-1)}, d_{\mathbb{K}}^* p^{(n)})_{\mathbb{K}^{-1}, \Omega} = (dw^{(n-1)}, p^{(n)})_{\Omega}.$$

The mixed formulation of Darcy's problem reads: find  $(w^{(n-1)}, p^{(n)}) \in \{H\Lambda^{n-1}(\Omega) \times L^2 \Lambda^n(\Omega)\}$ , given  $f^{(n)} \in L^2 \Lambda^n(\Omega)$  and  $\mathbb{K}$ , for all  $(v^{(n-1)}, q^{(n)}) \in \{H\Lambda^{n-1}(\Omega) \times L^2 \Lambda^n(\Omega)\}$

---

$L^2\Lambda^n(\Omega)\}$  such that

$$(v^{(n-1)}, w^{(n-1)})_{\mathbb{K}^{-1}, \Omega} - (\mathrm{d}v^{(n-1)}, p^{(n)})_{\Omega} = 0, \quad (8.1.35)$$

$$(q^{(n)}, \mathrm{d}w^{(n-1)})_{\Omega} = (q^{(n)}, f^{(n)})_{\Omega}. \quad (8.1.36)$$

### 8.1.5 Numerical test cases Darcy flow

We consider two different test cases. The first considers a full coefficient matrix with coefficients depending on the location. The second considers a discontinuous scalar material property.

**Smooth full tensor** This test case is adopted from [183], Example 2. The computational domain is obtained from a smooth mapping  $(x, y) = \Phi(\xi, \eta)$  from  $\widehat{\Omega} = [-1, 1]^2$  to  $\Omega$  given by

$$x = \frac{1}{2}(\xi + 1) + 0.03 \sin(\frac{3}{2}\pi\xi) \sin(32\pi\eta), \quad (8.1.37)$$

$$y = \frac{1}{2}(\eta + 1) - 0.04 \sin(32\pi\xi) \sin(32\pi\eta). \quad (8.1.38)$$

The analytic solution for the pressure is given by

$$p^{(2)} = (x^3y^4 + x^2 + \sin(xy) \cos(y)) \, dx \wedge dy,$$

and the full permeability tensor is given by

$$\mathbb{K} = \begin{bmatrix} k_{11} & k_{12} \\ k_{21} & k_{22} \end{bmatrix} = \begin{bmatrix} (x+1)^2 + y^2 & \sin(xy) \\ \sin(xy) & (x+1)^2 \end{bmatrix}.$$

Figure 8.9 shows a colorplot of the pressure field. The arrows indicate the direction and magnitude of the velocity flux. At the right,  $h$ -convergence results are shown for the pressure and velocity fields. It shows that also with a full, location dependent tensorial material property, optimal convergence rates are obtained for both quantities on curvilinear quadrilateral meshes.

**Discontinuous tensor** The second test case considers a diagonal tensor,  $\mathbb{K} = k\mathbb{I}$ , which has a discontinuous distribution throughout the domain, see the left illustration in Figure 8.10. This problem is also called a checkerboard problem. It considers a uniform inflow at the left and uniform pressure at the outflow boundary. No fluid is allowed to flow through the upper and lower boundaries. The color plot at the right of Figure 8.10 shows the velocity magnitude in the domain, with streamlines on top of it. The results were obtained on a  $15 \times 15$  equidistant mesh, where  $N = 4$  in each element. This test case shows three things: First that the method is capable of handling discontinuous permeabilities. Secondly, that the streamlines follow a path of least resistance, i.e., through the high permeability areas. Thirdly, the method can handle the high velocity peaks that appear at the intersection points where low permeability exists on one diagonal and high permeability on the other diagonal.

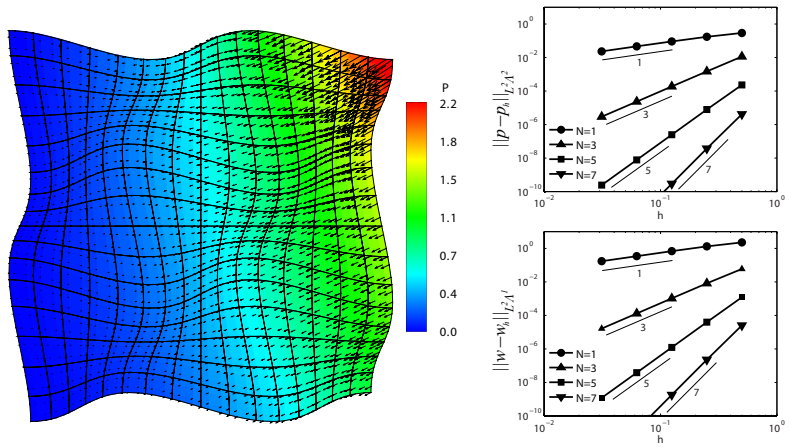


Figure 8.9: Left: a colorplot showing the pressure field with on top the velocity vectors. Right:  $h$ -convergence plots of the pressure and flux.

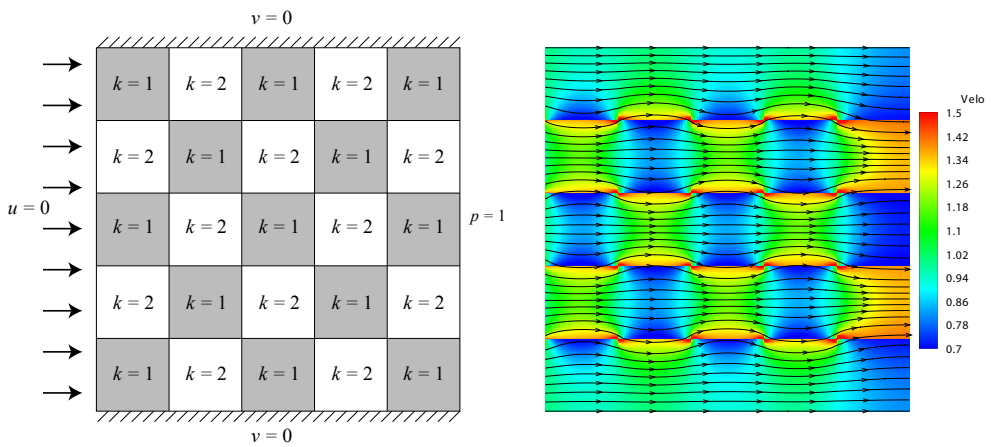


Figure 8.10: Right: Discontinuous coefficients and boundary conditions. Left: Magnitude of velocity field with streamlines on top.

### 8.1.6 Harmonic forms

**Deze sectie kan je overslaan**

The harmonic function for 0-forms is a constant. In case of Neumann boundary conditions  $\text{grad } u \cdot \vec{n} = 0$ , the constrained  $u \perp \mathcal{H}^0$  specifies a unique solution by requiring its average value to be zero.

## 8.2 Abstract Hodge-Laplacian problem

The previous section showed the basic steps in solving scalar Laplace problems. This section extends the discussion to the abstract Hodge-Laplacian that combines the scalar and vector Laplacians and higher dimensional variants. The focus of this section is somewhat more fundamental, whereas we try to find a proper variational formulation and proof discrete well-posedness. The basic ideas are largely based on the treatment of the abstract Hodge Laplacian in the extensive papers by Arnold, Falk and Winther, [6, 8], who generalized the ideas on mixed finite elements as described in e.g. [37]. Again this section comes with a range of numerical examples demonstrating the performance of the mimetic framework described in Part II.

### 8.2.1 Abstract Hodge-Laplacian

The Hodge-Laplace operator was given in Definition 24 as  $-\Delta := d^*d + dd^*$ . Then for  $u, f \in \Lambda^k(\Omega)$  and  $h \in \mathcal{H}^k$ , the abstract Hodge-Laplace problem or generalized Poisson problem is given by

$$dd^*u + d^*du = f - h, \quad \text{in } \Omega. \quad (8.2.1)$$

Specific cases of the abstract Hodge-Laplacian are found in many physical models, like the scalar Laplacian, vector Laplacian, curl-curl problems, div-curl problems or div-grad problems, which appear in fields like electromagnetism, solid mechanics and fluid dynamics.

In  $\Omega \subset \mathbb{R}^3$  we get four different kinds of problems. The analogue in terms of in vector calculus are listed below:

$$k = 0 : \quad -\text{div}^* \text{grad } u = f - h, \quad (8.2.2)$$

$$k = 1 : \quad \omega = -\text{div}^* \vec{u}, \quad \text{grad } \omega + \text{curl}^* \text{curl } \vec{u} = \vec{f} - \vec{h}, \quad (8.2.3)$$

$$k = 2 : \quad \vec{\omega} = \text{curl}^* \vec{u}, \quad \text{curl } \vec{\omega} - \text{grad}^* \text{div } \vec{u} = \vec{f} - \vec{h}, \quad (8.2.4)$$

$$k = 3 : \quad \vec{\omega} = -\text{grad}^* \vec{u}, \quad \text{div } \vec{\omega} = f. \quad (8.2.5)$$

In  $\Omega \subset \mathbb{R}^2$  the analogue problems in vector calculus appears in two different sets. The first is

$$k = 0 : \quad \text{rot}^* \text{curl } u = f - h, \quad (8.2.6)$$

$$k = 1 : \quad \omega = \text{rot}^* \vec{u}, \quad \text{curl } \omega - \text{grad}^* \text{div } \vec{u} = \vec{f} - \vec{h}, \quad (8.2.7)$$

$$k = 2 : \quad \vec{\omega} = -\text{grad}^* \vec{u}, \quad \text{div } \vec{\omega} = f, \quad (8.2.8)$$

---

where we make the following distinction between the curl acting on a scalar and on a vector,  $\text{rot } \vec{u} \stackrel{\text{2D}}{=} \frac{\partial u_2}{\partial x} - \frac{\partial u_1}{\partial y}$  and  $\text{curl } u \stackrel{\text{2D}}{=} (-\frac{\partial u}{\partial y}, \frac{\partial u}{\partial x})^T$ . The second is

$$k = 0 : \quad -\text{div}^* \text{grad } u = f - h, \quad (8.2.9)$$

$$k = 1 : \quad \omega = -\text{div}^* \vec{u}, \quad \text{grad } \omega + \text{curl}^* \text{rot } \vec{u} = \vec{f} - \vec{h}, \quad (8.2.10)$$

$$k = 2 : \quad \vec{\omega} = \text{curl}^* \vec{u}, \quad \text{rot } \vec{\omega} = f, \quad (8.2.11)$$

The reason there exists two sets of equations in 2D for vector calculus is the existence of two different Hilbert complexes, as given in (4.7.12). In terms of oriented variables, the first set corresponds to the outer oriented variables, while the second is referred to as the inner oriented variables.

## 8.2.2 Mixed formulation

For the moment we assume zero natural boundary conditions on  $\partial\Omega$ . A standard Galerkin approach to (8.2.1), using integration by parts (4.8.5), would give; find  $u \in H\Lambda^k(\Omega) \cap H^*\Lambda^k(\Omega)$  with  $\text{d}u \in L^2\Lambda^{k+1}(\Omega)$  and  $\text{d}^*u \in L^2\Lambda^{k-1}(\Omega)$ , given  $f \in L^2\Lambda^k(\Omega)$ , such that

$$(\text{d}^*v, \text{d}^*u)_\Omega + (\text{d}v, \text{d}u)_\Omega = (v, f)_\Omega, \quad \forall v \in H\Lambda^k(\Omega) \cap H^*\Lambda^k(\Omega). \quad (8.2.12)$$

It has a corresponding minimization problem for an energy functional over the space  $H^k\Lambda^k(\Omega) \cap H^*\Lambda^k(\Omega)$ . The standard Galerkin formulation is coercive, which immediately implies stability. Corresponding to this standard Galerkin formulation one usually chooses a  $H^1\Lambda^k(\Omega)$ -conforming approximation space. This could be a standard continuous piecewise polynomial vector space based on nodal interpolation.

However, in case of a nonconvex polyhedral or curvilinear or noncontractible domain  $\Omega$ , for allmost all  $f$ ,  $H\Lambda^k(\Omega) \cap H^*\Lambda^k(\Omega) \not\subset H^1\Lambda^k(\Omega)$ . Consequently, the solution will be stable but inconsistent in general, [47]. In other words the solution converges to the wrong solution. Unfortunately, it seems not possible to construct  $H\Lambda^k(\Omega) \cap H^*\Lambda^k(\Omega)$  conforming finite element spaces. Alternatively, one proposed to use *mixed formulations*, [37]. In contrast to standard Galerkin, the mixed formulation uses integration by parts (4.8.5) to express each codifferential in terms of an exterior derivative and suitable boundary conditions. Consequently, mixed formulations require only  $H\Lambda^k(\Omega)$ -conforming finite element spaces, which are much easier to construct. Therefore, in all cases mixed formulations do converge to the true solution. Mixed formulations correspond to saddle point problems instead of minimization problems.

For the mixed formulation, we slightly rewrite the abstract Hodge-Laplace problem by introducing an auxiliary variable,  $\omega = \text{d}^*u \in H\Lambda^{k-1}(\Omega)$ . Moreover we exclude any harmonic part of the solution  $u$  to make the solution unique, and introduce  $h \in \mathcal{H}^k$  to count for the harmonic part of the data, i.e  $h = f_{\mathcal{H}}$ , where  $f_{\mathcal{H}}$  is the harmonic part of  $f$ . Then  $(\omega, u, h) \in \Lambda^{k-1} \times \Lambda^k \times \mathcal{H}^k$  is a solution of

$$\omega = \text{d}^*u, \quad \text{d}\omega + \text{d}^*\text{d}u = f - h, \quad u \perp \mathcal{H}^k, \quad \text{in } \Omega, \quad (8.2.13)$$

with natural boundary conditions  $\text{tr } \star u = 0$ ,  $\text{tr } \star \text{d}u = 0$ , on  $\partial\Omega$ . The derivation of the mixed formulation of the Poisson problem consists of three steps:

- 
1. Introduce an auxiliary variable  $\omega = d^* u$  in  $H\Lambda^{k-1}$ ,
  2. multiply both equations by test functions  $(\tau, v) \in \{H\Lambda^{k-1} \times H\Lambda^k\}$  using  $L^2$  inner products,
  3. use integration by parts, as in (4.8.5), to express the remaining codifferentials in terms of the exterior derivatives and boundary integrals.

The resulting mixed formulation for the generalized Poisson problem for all  $0 \leq k \leq n$  becomes: find  $(\omega, u, h) \in H\Lambda^{k-1} \times H\Lambda^k \times \mathcal{H}^k$ , given  $f \in L^2\Lambda^k$ , for all  $(\tau, v, q) \in H\Lambda^{k-1} \times H\Lambda^k \times \mathcal{H}^k$  such that

$$(\tau, \omega)_\Omega - (d\tau, u)_\Omega = 0, \quad (8.2.14)$$

$$(v, d\omega)_\Omega + (dv, du)_\Omega + (v, h)_\Omega = (v, f)_\Omega \quad (8.2.15)$$

$$(u, q)_\Omega = 0 \quad (8.2.16)$$

Note that this formulation avoids the metric-dependent codifferential, it only consists of metric-free exterior derivatives and  $L^2$  inner products.

The Lagrange functional corresponding to the mixed formulation is,

$$\mathcal{J}(\tau, v, q) = \frac{1}{2}(\tau, \tau)_\Omega - (d\tau, v)_\Omega - \frac{1}{2}(dv, dv)_\Omega - (v, q)_\Omega + (v, f)_\Omega,$$

and the critical point of this functional,  $(\omega, u, h) \in H\Lambda^{k-1} \times H\Lambda^k \times \mathcal{H}^k$ , is a saddle point according to,

$$\mathcal{J}(\omega, v, q) \leq \mathcal{J}(\omega, u, h) \leq \mathcal{J}(\tau, u, h), \quad \forall (\tau, v, q) \in H\Lambda^{k-1} \times H\Lambda^k \times \mathcal{H}^k.$$

In case of essential boundary conditions,  $\text{tr } \omega = 0$ ,  $\text{tr } u = 0$  on  $\partial\Omega$ , the mixed Hodge-Laplace problem changes to; find  $(\omega, u, h) \in H_0\Lambda^{k-1} \times H_0\Lambda^k \times \mathcal{H}_0^k$  such that (8.2.13) holds with  $u \perp \mathcal{H}_0^k$ . The mixed formulation (8.2.14)-(8.2.16) does not change. Only the trial and test spaces slightly changes.

For well-posedness, the generalized mixed formulation of the Hodge-Laplacian has to satisfy the inf-sup condition. Therefore define the bounded bilinear form  $B : [H\Lambda^{k-1} \times H\Lambda^k \times \mathcal{H}^k] \times [H\Lambda^{k-1} \times H\Lambda^k \times \mathcal{H}^k] \rightarrow \mathbb{R}$  for the Hodge Laplacian given above,

$$B(\omega, u, h; \tau, v, q) = (\omega, \tau)_\Omega - (d\tau, u)_\Omega + (d\omega, v)_\Omega + (du, dv)_\Omega + (v, h)_\Omega - (u, q)_\Omega, \quad (8.2.17)$$

This bilinear form is not coercive, and therefore it requires somewhat more effort to show well-posedness. The well-posedness of the mixed formulation (8.2.14)-(8.2.16) relies on a closed Hilbert complex. Well-posedness is obtained using only the Hodge decomposition, (4.9.5), and the Poincaré inequality, Lemma 2. The first comes with the Hilbert complex. The latter requires a closed range  $\mathcal{B}^k \subset L^2\Lambda^k$ , so well-posedness is only obtained in case the Hilbert complex is closed.

**Theorem 5. (Well-posedness)** [6, 8] Let  $(L^2\Lambda, d)$  and  $(H\Lambda, d)$  be closed Hilbert complexes. There exists a constant  $\beta > 0$ , depending only on the Poincaré constant  $c_P$ , such that for any  $(\omega, u, h) \in H\Lambda^{k-1} \times H\Lambda^k \times \mathcal{H}^k$ , there exists  $(\tau, v, q) \in H\Lambda^{k-1} \times H\Lambda^k \times \mathcal{H}^k$  with

$$B(\omega, u, h; \tau, v, q) \geq \beta(\|\omega\|_{H\Lambda^{k-1}} + \|u\|_{H\Lambda^k} + \|h\|_{L^2\Lambda^k})(\|\tau\|_{H\Lambda^{k-1}} + \|v\|_{H\Lambda^k} + \|q\|_{L^2\Lambda^k}).$$

*Proof.* By the Hodge decomposition,  $u = u_{\mathcal{B}} + u_{\mathcal{H}} + u_{\perp}$ . Since  $u_{\mathcal{B}} \in \mathcal{B}^k$ ,  $u_{\mathcal{B}} = d\rho$  for some  $\rho \in \mathcal{Z}^{k-1, \perp}$ . Since  $u_{\perp} \in \mathcal{Z}^{k, \perp}$ ,  $du_{\perp} = du$ , we get using Poincaré's inequality that

$$\|\rho\|_{H\Lambda^{k-1}} \leq c_P \|u_{\mathcal{B}}\|_{L^2\Lambda^k}, \quad \|u_{\perp}\|_{H\Lambda^k} \leq c_P \|du\|_{L^2\Lambda^{k+1}}, \quad (8.2.18)$$

where  $c_P \geq 1$ . Choose

$$\tau = \omega - \frac{1}{c_P^2} \rho \in H\Lambda^{k-1}, \quad v = u + d\omega + h \in H\Lambda^k, \quad q = p - u_{\mathcal{H}} \in \mathcal{H}^k. \quad (8.2.19)$$

From the Poincaré inequalities and the orthogonality of the Hodge decomposition, we have

$$\begin{aligned} \|\tau\|_{H\Lambda^{k-1}} &\leq \|\omega\|_{H\Lambda^{k-1}} + \frac{1}{c_P^2} \|\rho\|_{H\Lambda^{k-1}} \leq \|\omega\|_{H\Lambda^{k-1}} + \|u_{\mathcal{B}}\| \leq \|\omega\|_{H\Lambda^{k-1}} + \|u\|_{H\Lambda^k}, \\ \|v\|_{H\Lambda^k} &\leq \|u\|_{H\Lambda^k} + \|d\omega\| + \|h\| \leq \|\omega\|_{H\Lambda^{k-1}} + \|u\|_{H\Lambda^k} + \|h\|, \\ \|q\|_{L^2\Lambda^k} &\leq \|u_{\mathcal{H}}\| + \|h\| \leq \|u\|_{H\Lambda^k} + \|h\|, \end{aligned}$$

which gives the following bound,

$$\|\tau\|_{H\Lambda^{k-1}} + \|v\|_{H\Lambda^k} + \|q\|_{L^2\Lambda^k} \leq C(\|\omega\|_{H\Lambda^{k-1}} + \|u\|_{H\Lambda^k} + \|p\|_{L^2\Lambda^k}), \quad (8.2.20)$$

In order to bound  $B(\omega, u, h; \tau, v, q)$ , let's substitute (8.2.19) in (8.2.17). We get

$$B(\omega, u, h; \tau, v, q) = \|\omega\|^2 + \|d\omega\|^2 + \|h\|^2 + \|u_{\mathcal{H}}\|^2 + \frac{1}{c_P^2} \|u_{\mathcal{B}}\|^2 + \|du\|^2 - \frac{1}{c_P^2} (\omega, \rho)_{\Omega}.$$

The last term can be bounded using Young's inequality and the first Poincaré inequality of (8.2.18),

$$\frac{1}{c_P^2} (\omega, \rho)_{\Omega} \leq \frac{1}{2} \|\omega\|^2 + \frac{1}{2c_P^4} \|\rho\|^2 \leq \frac{1}{2} \|\omega\|^2 + \frac{1}{2c_P^2} \|u_{\mathcal{B}}\|^2.$$

The  $H\Lambda^k$ -norm of  $u$  can be bounded using the second Poincaré inequality of (8.2.18),

$$\|u\|_{H\Lambda^k}^2 = \|u_{\mathcal{B}}\|^2 + \|u_{\mathcal{H}}\|^2 + \|u_{\perp}\|_{H\Lambda^k}^2 \leq \|u_{\mathcal{B}}\|^2 + \|u_{\mathcal{H}}\|^2 + c_P^2 \|du\|^2.$$

Substituting the previous two bounds in  $B(\omega, u, h; \tau, v, q)$  to show that it is bounded from below,

$$\begin{aligned} B(\omega, u, h; \tau, v, q) &\geq \frac{1}{2} \|\omega\|^2 + \|d\omega\|^2 + \|h\|^2 + \|u_{\mathcal{H}}\|^2 + \frac{1}{2c_P^2} \|u_{\mathcal{B}}\|^2 + \|du\|^2 \\ &\geq \frac{1}{2c_P^2} (\|\omega\|_{H\Lambda^{k-1}}^2 + \|u\|_{H\Lambda^k}^2 + \|h\|_{L^2\Lambda^k}^2). \end{aligned} \quad (8.2.21)$$

The theorem easily follows from the bounds (8.2.20) and (8.2.21). It shows that  $\beta$  only depends on the Poincaré constant  $c_P$ .  $\square$

**Corollary 18.** *Problem (8.2.13) is well-posed according to theorem 5 with a priori estimate*

$$\|\omega\|_{H\Lambda^{k-1}} + \|u\|_{H\Lambda^k} + \|h\|_{L^2\Lambda^k} \leq c \|f\|_{L^2\Lambda^k},$$

where  $c$  is a constant depending only on the Poincaré constant  $c_P$ .

### 8.2.3 Numerical stability

Since the bilinear form is not coercive, stability or discrete well-posedness of the approximate solution depends on the compatibility of the finite-dimensional spaces and the relationship between them.

The well-posedness of the finite dimensional problem relies on the subcomplex property and the existence of a bounded projection operator. From the subcomplex property we know that complex  $(\Lambda_h, d)$  also possesses a Hodge decomposition. The second ingredient required to obtain numerical stability is the discrete Poincaré inequality. Because the complexes  $(H\Lambda, d)$  and  $(\Lambda_h, d)$  are each others supercomplex and subcomplex, respectively, the discrete Poincaré inequality, as given in Lemma 7 (p. 108), is directly related to the Poincaré inequality in Lemma 2 (p. 63) and the bounded projection in Definitions 57 (p. 96) and 64 (p. 106). Then discrete well-posedness follows immediately from the subcomplex property and the bounded projection.

**Theorem 6 (Discrete well-posedness).** [8] Let  $(\Lambda_h, d)$  be a subcomplex of  $(H\Lambda, d)$ , admitting bounded projections. Then there exists a constant  $\beta_h > 0$ , depending only on  $c_{Ph}$ , such that for any  $(\omega_h, u_h, h_h) \in \Lambda_h^{k-1} \times \Lambda_h^k \times \mathcal{H}_h^k$ , there exists  $(\tau_h, v_h, q_h) \in \Lambda_h^{k-1} \times \Lambda_h^k \times \mathcal{H}_h^k$  with

$$B(\omega_h, u_h, p_h; \tau_h, v_h, q_h) \geq \beta_h (\|\omega_h\|_{H\Lambda^{k-1}} + \|u_h\|_{H\Lambda^k} + \|p_h\|_{L^2\Lambda^k}) (\|\tau_h\|_{H\Lambda^{k-1}} + \|v_h\|_{H\Lambda^k} + \|q_h\|_{L^2\Lambda^k}). \quad (8.2.22)$$

*Proof.* This is just Theorem 5 applied to the complex  $(\Lambda_h, d)$ , combined with the fact that the constant in the Poincaré inequality for  $\Lambda_h^k$  is  $c_{Ph}$  by Lemma 7.  $\square$

From consistency and stability in terms of the bounded projection and discrete well-posedness there follows convergence. A quasi-optimal error estimate is given in the following proposition.

**Proposition 32 (Convergence).** [6] Let  $(\omega, u, h) \in H\Lambda^{k-1}(\Omega) \times H\Lambda^k(\Omega) \times \mathcal{H}^k$  be the solution of system (8.2.14)-(8.2.16) and  $(\omega_h, u_h, h_h) \in \Lambda_h^{k-1}(\Omega) \times \Lambda_h^k(\Omega) \times \mathcal{H}_h^k$  be the solution of the finite dimensional problem, then quasi-optimal error estimate reads

$$\begin{aligned} & \|\omega - \omega_h\|_{H\Lambda^{k-1}} + \|u - u_h\|_{H\Lambda^k} + \|h - h_h\|_{L^2\Lambda^k} \\ & \leq C \left( \inf_{\tau_h \in \Lambda_h^{k-1}} \|\omega - \tau_h\|_{H\Lambda^{k-1}} + \inf_{v_h \in \Lambda_h^k} \|u - v_h\|_{H\Lambda^k} + \inf_{q_h \in \mathcal{H}_h^k} \|h - q\|_{L^2\Lambda^k} + \|P_{\mathcal{H}_h^k} u\|_{L^2\Lambda^k} \right), \end{aligned} \quad (8.2.23)$$

where  $P_{\mathcal{H}_h^k}$  is the  $L^2$ -projection of  $u$  into  $\mathcal{H}_h^k$ .

It is shown in [6] that the last term in (8.2.23) hardly contributes, because it converges twice as fast as the other terms. In [8] optimal error estimates were derived in  $L^2$ -norms. The theorem and proof of the optimal convergences estimates are too extensive to repeat here. Instead the results for the two and three dimensional Laplacian case are given here. For  $n = 2$  or  $n = 3$  and  $k = 0$ , we obtain,

$$\|u - u_h\|_{L^2\Lambda^0} = \mathcal{O}(h^{N+1}), \quad \|d(u - u_h)\|_{L^2\Lambda^1} = \mathcal{O}(h^N), \quad \|h - h_h\|_{L^2\Lambda^0} = \mathcal{O}(h^{N+1}). \quad (8.2.24)$$

For  $n = 2$  or  $n = 3$  and  $k \geq 1$ , we obtain,

$$\begin{aligned} \|\omega - \omega_h\|_{L^2\Lambda^{k-1}} &= \mathcal{O}(h^{N+s}), & \|d(\omega - \omega_h)\|_{L^2\Lambda^k} &= \mathcal{O}(h^N), \\ \|u - u_h\|_{L^2\Lambda^k} &= \mathcal{O}(h^N), & \|d(u - u_h)\|_{L^2\Lambda^{k+1}} &= \mathcal{O}(h^N), & \|h - h_h\|_{L^2\Lambda^k} &= \mathcal{O}(h^N). \end{aligned} \quad (8.2.25)$$

with  $s = 1$  if  $k = 1$  and  $s = 0$  if  $k > 1$ .

#### 8.2.4 Numerical test cases

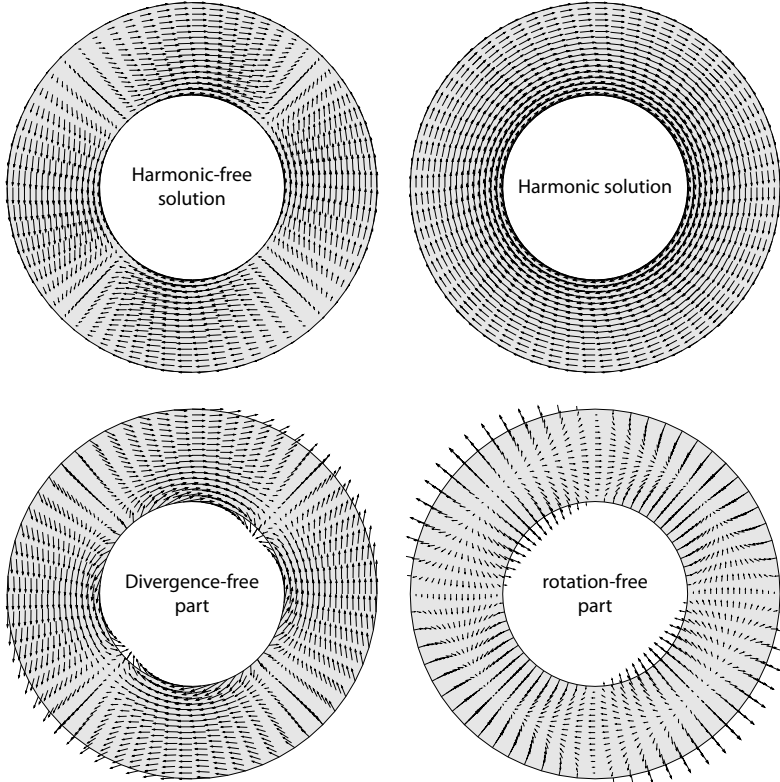


Figure 8.11: Hodge-decomposition of 1-form on an annulus.

Now that the compatible/mimetic spectral element method and its a priori error estimates are described, we perform a set of test problems to show optimal convergence behavior. Purpose of the test cases is to show convergence behavior in case of various boundary conditions and in case of curvilinear meshes. In all cases we show optimal convergence.

The first test case considers the vector Laplace or 1-form Hodge-Laplace on an annulus with radii  $\frac{1}{2}$  and 1, as is also discussed [8]. The forcing function we consider is  $\vec{f} = [0, x]^T$  or  $f^{(1)} = -x \, dx$ , where  $\omega^{(0)} \in H_0\Lambda^0$ ,  $u^{(1)} \in H_0\Lambda^1$  and  $f^{(1)} \in L^2\Lambda^1$  are outer-oriented 0- and 1-forms. We impose two essential boundary conditions, a zero

---

normal boundary condition  $\text{tr } u = 0$  and a non-rotating boundary condition  $\text{tr } \omega = \text{tr } d^*u = 0$ . The solution of the vector Laplace problem consists of the harmonic-free solution shown in Figure 8.11, modulo a multiplicity of the harmonic solution shown in the same figure. The harmonic-free solution consists of a divergence-free part and a rotation-free part through the Hodge decomposition. Both are shown at the bottom of Figure 8.11. Note that standard finite difference, finite volume and finite element methods only obtain the global harmonic solution, because these kind of methods lack a decent discrete Hodge decomposition.

The following two test cases originate from a recent paper by Arnold et. al. [5], where they show suboptimal convergence for normal velocity - tangential velocity boundary conditions in vector Laplace and Stokes problems, when using Raviart-Thomas elements [154]. Since Raviart-Thomas elements are the most popular  $H(\text{div})$  conforming elements, we compare our method to these results.

Figure 8.12 shows the result of the vector Poisson problem (8.2.1) on  $\Omega = [0, 1]^2$ , for a 1-form  $u \in H\Lambda^1(\Omega)$ , with tangential velocity - divergence-free boundary conditions ( $\text{tr } \star u = 0$ ,  $\text{tr } \star du = 0$ ). The corresponding solution is given by

$$\begin{aligned} u^{(1)} &= -v(\mathbf{x})dx + u(\mathbf{x})dy \\ &= -(2 \sin \pi x \cos \pi y)dx + (\cos \pi x \sin \pi y)dy. \end{aligned} \quad (8.2.26)$$

Both methods show optimal convergence rates. Figure 8.13 shows again the vector Poisson problem for a 1-form, but now supplemented with normal velocity - tangential velocity boundary conditions ( $\text{tr } u = 0$ ,  $\text{tr } \star u = 0$ ). The corresponding manufactured solution is

$$\begin{aligned} u^{(1)} &= -v(\mathbf{x})dx + u(\mathbf{x})dy \\ &= -(\sin \pi x \sin \pi y)dx + (\sin \pi x \sin \pi y)dy. \end{aligned} \quad (8.2.27)$$

The mimetic spectral element discretization again shows optimal convergence, as was expected from the above analysis. The Raviart-Thomas elements only show sub-optimal convergence in case of velocity boundary conditions. This sub-optimality was proven in [5]. Especially for  $\omega_h$  and  $d\omega_h$  the current method outperforms the Raviart-Thomas elements, with a difference in rate of convergence of  $\frac{3}{2}$ . All results were obtained on the same quadrilateral mesh of  $2^n \times 2^n$  subsquares,  $n = 1, 2, 3, 4, \dots$  as the RT solutions in [5].

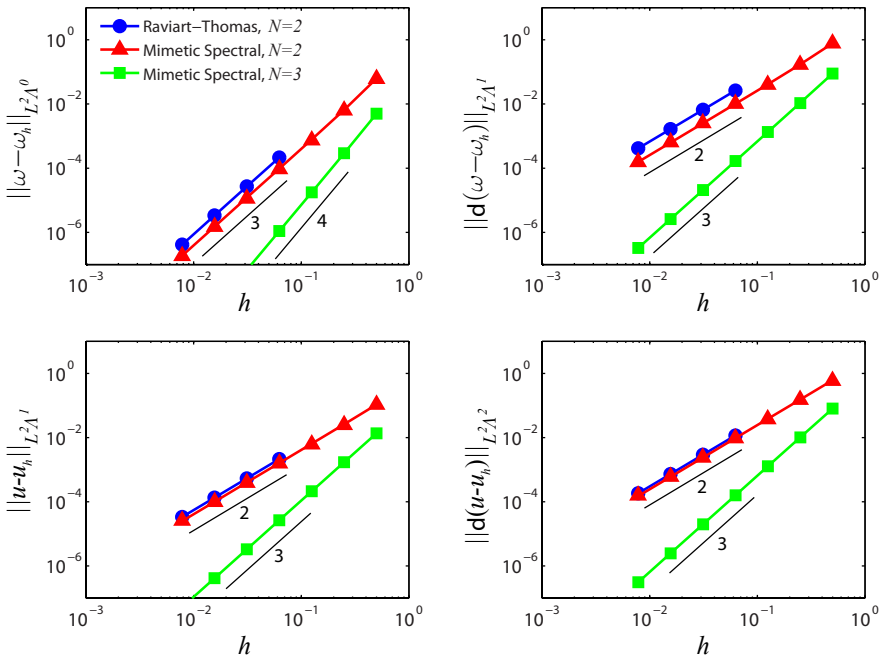


Figure 8.12: Comparison of the  $h$ -convergence between Raviart-Thomas and Mimetic spectral element projections for the 2D 1-form Poisson problem with tangential velocity - divergence-free boundary conditions.

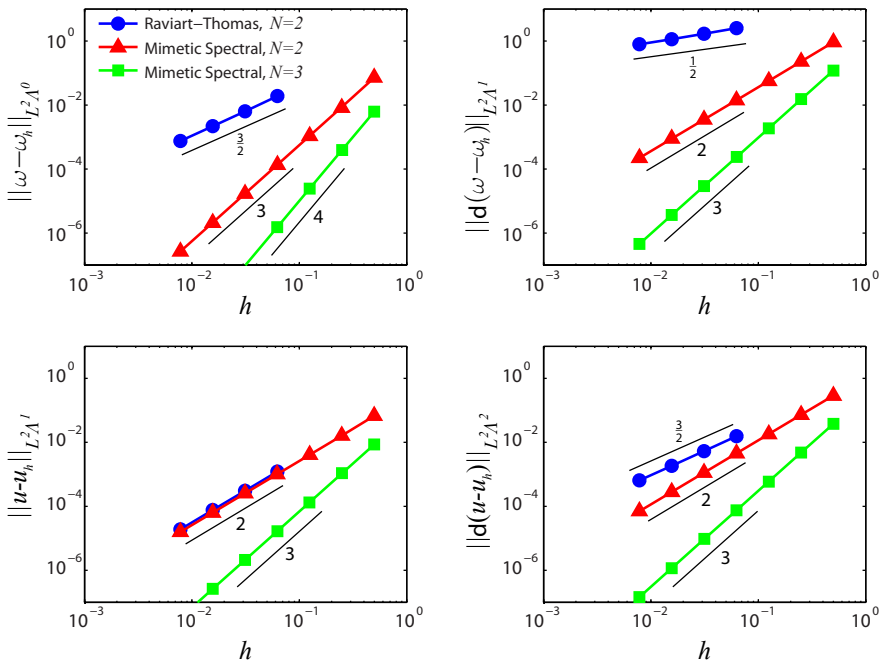


Figure 8.13: Comparison of the  $h$ -convergence between Raviart-Thomas and Mimetic spectral element projections for the 2D 1-form Poisson problem with tangential velocity - normal velocity boundary conditions.

## 8.3 Eigenvalue problem

In this section we discuss eigenvalue problems based on the Hodge-Laplacian. Eigenvalue problems appear in a wide range of applications, for example in the field of electromagnetism, [129]. Besides the possible applications of interest, eigenvalue problems also serve as a proof of operator convergence. While for source problems, discussed in the previous sections, we can only show and proof that the discrete operators converge in a weak sense, eigenvalue problems show that the discrete operators approximate the continuous operators in a strong sense. So every eigenvalue of the discrete problem should converge to the analytic eigenvalue. In that case we obtain also *operator convergence*. A nice overview on Laplace eigenvalue problems is found in [22].

The eigenvalue problem for the abstract Hodge-Laplacian is given by

$$-\Delta u^{(k)} = \lambda u^{(k)}, \quad \text{in } \Omega, \quad (8.3.1a)$$

$$\operatorname{tr} \star u^{(k)} = 0, \operatorname{tr} \star du^{(k)} = 0, \quad \text{on } \partial\Omega. \quad (8.3.1b)$$

Recall that  $-\Delta = dd^* + d^*d$  is a symmetric operator, it immediately follows that all nonzero eigenvalues are real and positive,

$$\lambda \|u^{(k)}\|^2 = \|du^{(k)}\|^2 + \|d^*u^{(k)}\|^2 \geq 0.$$

The nonzero real positive eigenvalues  $\lambda_i$  can have finite multiplicity, so

$$0 < \lambda_1 \leq \lambda_2 \leq \dots$$

For the mixed formulation corresponding to (8.3.1), we introduce the auxiliary variable  $\omega^{(k-1)} = d^*u^{(k)}$ . The mixed formulation reads: on a contractible domain, there exists an eigenvalue / eigenfunction pair  $(\lambda, u^{(k)}) \in \mathbb{R}^+ \times H\Lambda^k(\Omega)$  such that

$$(\tau^{(k-1)}, \omega^{(k)})_\Omega - (d\tau^{(k-1)}, u^{(k)})_\Omega = 0, \quad \forall \tau^{(k-1)} \in H\Lambda^{k-1}(\Omega), \quad (8.3.2a)$$

$$(v^{(k)}, d\omega^{(k-1)})_\Omega + (dv^{(k)}, du^{(k)})_\Omega = \lambda(v^{(k)}, u^{(k)})_\Omega, \quad \forall v^{(k)} \in H\Lambda^k(\Omega). \quad (8.3.2b)$$

### 8.3.1 Maxwell eigenvalue problem

The Maxwell eigenvalue problem considers the time-harmonic Maxwell problem with zero current density and zero charge density. It consists of the Ampère law and Faraday law. Then in a closed cavity  $\Omega$  with perfectly conducting boundary conditions on  $\partial\Omega$  we search for the resonance frequencies  $\omega \in \mathbb{R} \setminus \{0\}$  and the electromagnetic fields  $(\vec{E}, \vec{H})$  such that

$$\text{Ampère law :} \quad \operatorname{curl} \vec{E} = i\omega\mu\vec{H} \quad \text{in } \Omega, \quad (8.3.3a)$$

$$\text{Faraday law :} \quad \operatorname{curl} \vec{H} = -i\omega\epsilon\vec{E} \quad \text{in } \Omega, \quad (8.3.3b)$$

$$\text{Perfect conducting walls :} \quad \vec{E} \times \vec{n} = 0, \quad \vec{H} \cdot \vec{n} = 0, \quad \text{on } \partial\Omega. \quad (8.3.3c)$$

Since we are interested  $\omega \neq 0$  we get additional divergence constraints, also known as Gauss' law and the solenoidal constraint of the magnetic induction,

$$\operatorname{div} \epsilon\vec{E} = 0, \quad \text{in } \Omega, \quad (8.3.4)$$

$$\operatorname{div} \mu\vec{H} = 0, \quad \text{in } \Omega. \quad (8.3.5)$$

We refer to the book of Monk [129] how to obtain the time-harmonic problem from the full Maxwell problem. Alternatively to the electric and magnetic field intensities,  $\vec{E}$  and  $\vec{H}$ , we could have used the electric displacement  $\vec{D}$  and magnetic induction  $\vec{B}$ , since  $\vec{D} = \epsilon \vec{E}$  and  $\vec{B} = \mu \vec{H}$ . The material parameters  $\epsilon$  and  $\mu$  denote the dielectric permittivity and magnetic permeability.

In terms of differential forms we write the electromagnetic fields as  $\tilde{e}^{(1)}, \tilde{b}^{(2)}, h^{(n-2)}, d^{(n-1)}$ , where the first two correspond to inner-oriented manifolds and the latter two to outer-oriented manifolds. The relation between the two types of fields are given by,  $\tilde{b}^{(2)} = \star_\mu h^{(n-2)}$  and  $d^{(n-1)} = \star_\epsilon \tilde{e}^{(1)}$  as is illustrated in the diagram below.

$$\begin{array}{ccccc}
h^{(n-2)} & \xrightarrow{\frac{1}{i\omega}d} & d^{(n-1)} & \xrightarrow{d} & 0 (= j^{(n)}) \\
\downarrow \star_\mu & & \uparrow \star_\epsilon & & \\
0 & \xleftarrow{d} & \tilde{b}^{(2)} & \xleftarrow{\frac{1}{i\omega}d} & \tilde{e}^{(1)}.
\end{array}$$

Observe that the Hodge stars act in opposite direction. The time-harmonic Maxwell problem in differential forms becomes,

$$d\tilde{e}^{(1)} = i\omega \star_\mu h^{(n-2)}, \quad \text{in } \Omega, \quad (8.3.6a)$$

$$dh^{(n-2)} = -i\omega \star_\epsilon \tilde{e}^{(1)}, \quad \text{in } \Omega, \quad (8.3.6b)$$

$$\text{tr } \tilde{e}^{(1)} = 0, \text{ tr } \star_\mu h^{(n-2)} = 0, \quad \text{on } \partial\Omega, \quad (8.3.6c)$$

supplemented with the divergence constraints  $d \star_\mu h^{(n-2)} = 0$  and  $d \star_\epsilon e^{(1)} = 0$ . A second-order curl-curl problem is obtained by eliminating one of the two variables in (8.3.3) or (8.3.6). By means of the Hodge duality we can obtain a curl-curl problem for each of the four variables. Here we restrict ourselves to quantities associated with outer-oriented manifolds, so the magnetic field intensity  $h^{(n-2)}$  and the electric displacement  $d^{(n-1)}$  in this case. The second-order problems become

$$-\star_{\mu^{-1}} d \star_{\epsilon^{-1}} d h^{(n-2)} = \omega^2 h^{(n-2)}, \quad \Leftrightarrow \quad d^*_{\epsilon^{-1}, \mu^{-1}} d h^{(n-2)} = \omega^2 h^{(n-2)}, \quad (8.3.7a)$$

$$d \star_\mu h^{(n-2)} = 0, \quad \Leftrightarrow \quad d_\mu^* h^{(n-2)} = 0, \quad (8.3.7b)$$

with boundary condition  $\text{tr } \star_{\epsilon^{-1}} dh^{(n-2)} = 0$ , and

$$d \star_{\mu^{-1}} d \star_{\epsilon^{-1}} d^{(n-1)} = \omega^2 d^{(n-1)}, \quad \Leftrightarrow \quad dd^*_{\epsilon^{-1}, \mu^{-1}} d^{(n-1)} = \omega^2 d^{(n-1)}, \quad (8.3.8a)$$

$$d d^{(n-1)} = 0, \quad \Leftrightarrow \quad d d^{(n-1)} = 0, \quad (8.3.8b)$$

with boundary condition  $\text{tr } \star_{\epsilon^{-1}} d^{(n-1)} = 0$ . The first is the *Neumann curl-curl problem* and the second is the *Dirichlet curl-curl problem*. Both problems are special cases of the eigenvalue problem of the abstract Hodge Laplacian in (8.3.1).

For simplicity we only consider a homogeneous isentropic material. Using normalization both parameters reduce to an identity tensor,  $\epsilon = \mu = I$ . Note that in general the material parameters are tensors representing an anisotropic inhomogeneous material. The approach is similar to that of the Darcy flow case, and therefore not elaborated further in this section.

Furthermore, choose  $\lambda = \omega^2$ , then the variational formulations of the two Maxwell eigenvalue problems with natural boundary conditions become:

1. Neumann problem: seek  $(\lambda, h^{(n-2)}) \in \mathbb{R}^+ \times H\Lambda^{n-2}(\Omega) \setminus \{0\}$ , such that

$$(\mathrm{d}v^{(n-2)}, \mathrm{d}h^{(n-2)})_\Omega = \lambda(v^{(n-2)}, h^{(n-2)})_\Omega, \quad \forall v^{(n-2)} \in H\Lambda^{n-2}(\Omega). \quad (8.3.9)$$

2. Dirichlet problem: let  $\kappa^{(n-2)} = \mathrm{d}^* d^{(n-1)} \in H\Lambda^{n-2}(\Omega)$ , then seek  $(\lambda, d^{(n-1)}) \in \mathbb{R}^+ \times H\Lambda^{n-1}(\Omega) \setminus \{0\}$ , such that

$$(\tau^{(n-2)}, \kappa^{(n-2)})_\Omega - (\mathrm{d}\tau^{(n-2)}, d^{(n-1)})_\Omega = 0, \quad \forall \tau^{(n-2)} \in H\Lambda^{n-2}(\Omega), \quad (8.3.10a)$$

$$(v^{(n-1)}, \mathrm{d}\kappa^{(n-2)})_\Omega = \lambda(v^{(n-1)}, d^{(n-1)})_\Omega, \quad \forall v^{(n-1)} \in H\Lambda^{n-1}(\Omega). \quad (8.3.10b)$$

**Discretization** Define  $\Sigma = H\Lambda^{n-2}(\Omega)$  and  $V = H\Lambda^{n-1}(\Omega)$ . The discretization of the above two problems require a choice for compatible finite elements spaces  $\Sigma_h \subset \Sigma$  and  $V_h \subset V$ , where the range  $\mathcal{B}(\mathrm{d}; \Sigma_h)$  is in the nullspace of  $V_h$ , and since we assumed a contractible domain  $\Omega$  in this section, we actually want  $\mathcal{B}(\mathrm{d}; \Sigma_h) = \mathcal{Z}(\mathrm{d}; V_h)$ .  $\Sigma$  is better known as the  $H(\mathrm{curl}, \Omega)$ -space and  $V$  is also known as the  $H(\mathrm{div}, \Omega)$ -space.  $H(\mathrm{curl}, \Omega)$ -conforming finite elements are usually called *edge* finite elements, and the most often used edge elements are the Whitney forms developed by Bossavit [25, 153] and the Nédélec elements derived by Nédélec [133, 134]. Here we choose the mimetic spectral edge elements  $E_{i_1, \dots, i_n}^{n-2} \in \Lambda_h^{n-2}(\Omega; C_{n-2}) = \Sigma_h$  as given in Section 7.2.3 as the  $H(\mathrm{curl}, \Omega)$ -conforming finite elements, and the mimetic spectral surface elements  $S_{i_1, \dots, i_n}^{n-1} \in \Lambda_h^{n-1}(\Omega; C_{n-1}) = V_h$  as the  $H(\mathrm{div}, \Omega)$ -conforming elements. The finite dimensional problems are then given by:

1. Neumann problem: seek  $(\lambda_h, h_h^{(n-2)}) \in \mathbb{R}^+ \times \Sigma_h \setminus \{0\}$ , such that

$$(\mathrm{d}v_h^{(n-2)}, \mathrm{d}h_h^{(n-2)})_\Omega = \lambda_h(v_h^{(n-2)}, h_h^{(n-2)})_\Omega, \quad \forall v_h^{(n-2)} \in \Sigma_h. \quad (8.3.11)$$

2. Dirichlet problem: let  $\kappa_h^{(n-2)} = \mathrm{d}^* d_h^{(n-1)} \in \Sigma_h$ , then seek  $(\lambda, d_h^{(n-1)}) \in \mathbb{R}^+ \times V_h \setminus \{0\}$ , such that

$$(\tau_h^{(n-2)}, \kappa_h^{(n-2)})_\Omega - (\mathrm{d}\tau_h^{(n-2)}, d_h^{(n-1)})_\Omega = 0, \quad \forall \tau_h^{(n-2)} \in \Sigma_h, \quad (8.3.12a)$$

$$(v_h^{(n-1)}, \mathrm{d}\kappa_h^{(n-2)})_\Omega = \lambda(v_h^{(n-1)}, d_h^{(n-1)})_\Omega, \quad \forall v_h^{(n-1)} \in V_h. \quad (8.3.12b)$$

It is known that stability by means of the LBB conditions for linear saddle point systems are sufficient to guarantee convergence for the source problem, but are not sufficient to guarantee convergence of the corresponding eigenvalue problem. It can leads to spurious eigenvalues even if the problem is well-posed, [22]. Providing proofs on eigenvalue convergence is beyond the scope of this work, instead we refer to Boffi et. al. [20, 22, 23] and to Arnold et. al. [6, 8]. The two proofs differ from each other, whereas the former is based on the discrete compactness property and the Fortid property, while the latter relies on the subcomplex property and  $L^2$ -bounded projections. In that respect our method follows the latter approach, and therefore we refer to the mentioned references for proofs on stability and convergence of the eigenvalues and eigenfunctions.

---

For the eigenvalue problems in mixed formulation the order of approximation for the eigenvalues is double with respect to the order of approximation of the corresponding eigenfunctions. This is typical behavior of symmetric eigenvalue problems. For a polynomial degree  $p$ , the estimates for eigenfunction and eigenvalue convergence become

$$\|u_i^{(k)} - u_{h,i}^{(k)}\| = \mathcal{O}(h^p), \quad |\lambda_i - \lambda_{h,i}| = \mathcal{O}(h^{2p}). \quad (8.3.13)$$

### 8.3.2 Numerical test cases

The Maxwell eigenvalue problems are tested using two benchmark cases, a two-dimensional problem on a square domain and a three dimensional problem on Fichera's corner. For the first, analytic solutions of both the eigenvalues and eigenfunctions exists which allows to perform a convergence study. The second illustrates that the method is capable to deal with point and line singularities.

**Two-dimensional square domain** Before considering the two-dimensional problem, first consider a one dimensional problem on a domain  $\Omega = [0, \pi]$ . It is easily verified that for  $-u''(x) = \lambda u(x)$ , we find the following analytic solutions of the eigenvalues and eigenfunctions, for Dirichlet boundary conditions,  $u(0) = u(\pi) = 0$ ,

$$\lambda = r^2, \quad u(x) = \sin(r\pi x), \quad \text{with } r = 1, 2, 3, 4, \dots,$$

and for Neumann boundary conditions,  $u'(0) = u'(\pi) = 0$ ,

$$\lambda = r^2, \quad u(x) = \cos(r\pi x), \quad \text{with } r = 0, 1, 2, 3, 4, \dots.$$

Similar results are found for the two-dimensional problems. Let  $\Omega$  be a square  $[0, \pi]^2$ . It can easily be verified that the eigenvalues of (8.3.11) and (8.3.12) are given by  $\lambda_{r,s} = r^2 + s^2$ , with either  $r, s = 1, 2, 3, 4, \dots$  for the Dirichlet problem (8.3.12), or  $r, s = 0, 1, 2, 3, 4, \dots$  of the Neumann problem, (8.3.11). The eigenfunctions are now products of sine-waves or cosine-waves.

That stability does not automatically imply operator convergence was already shown in, among others, [19, 48]. Figure 8.14 shows reproduced results from [48]. This figure shows the resonant frequencies in an electromagnetic waveguide computed with standard  $H^1(\Omega)$ -conforming Lagrangian polynomial finite element method (left) and those computed with  $H(\text{div}, \Omega)$ -conforming Raviart-Thomas elements (right). While the classical finite element method completely misses the frequency pattern, the compatible finite element method nicely captures the zero modes that result from the divergence-free constraint on the electric displacement and obtains the correct multiplicity of the eigenvalues. The results in Figure 8.14 were obtained on an unstructured triangular mesh, but we obtained also spurious modes on curvilinear quadrilateral meshes for the Galerkin spectral element method, using Lagrangian polynomials. The mapping used is that of (8.1.30) with  $c = 0.2$ . These results are shown in Figure 8.15 where from left to right we see the exact nonzero eigenvalues, the nonzero eigenvalues obtained on an 20<sup>th</sup>-order single element mesh and on an 30<sup>th</sup>-order single element mesh. The spurious modes are indicated in red. The values of the spurious modes increase when increasing the order of approximation, but the number of spurious

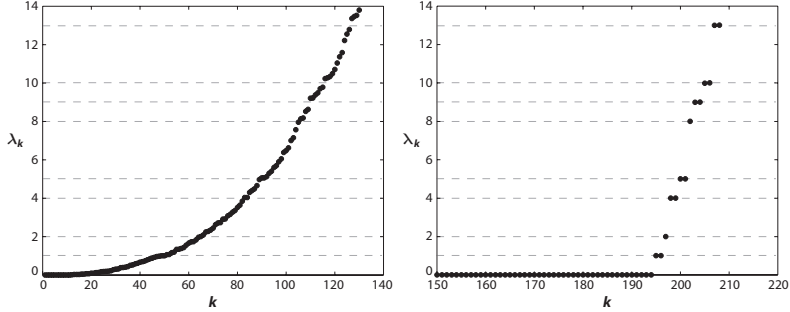


Figure 8.14: Eigenfrequencies for the Neumann resonant cavity problem using standard Lagrangian elements (left) and compatible Raviart-Thomas elements (right) on an unstructured triangular mesh (reproduced from [19, 48]).

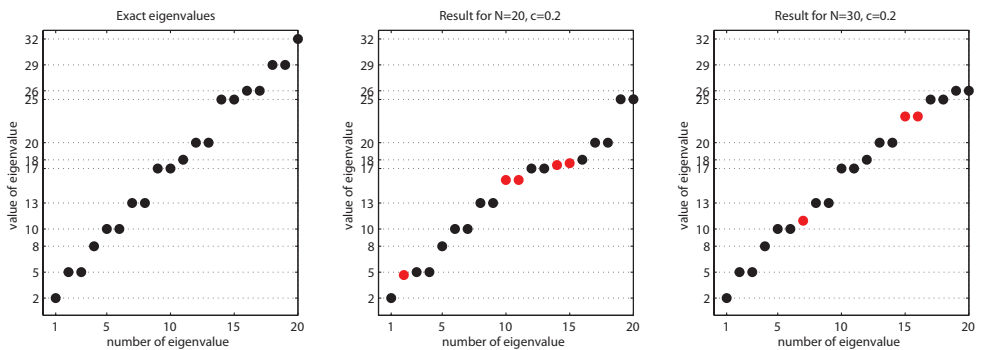


Figure 8.15: Eigenvalue approximation for the Dirichlet resonant-cavity problem using the Galerkin spectral element method with 20<sup>th</sup>- and 30<sup>th</sup>-order Lagrangian polynomials on a non-orthogonal mesh. The red dots indicate the spurious modes.

modes remains the same. Note that spurious modes on quadrilateral meshes were also reported in [48].

The  $h$ - and  $p$ -convergence results for the first ten nonzero eigenvalues obtained with the mixed mimetic spectral element method are shown in Figures 8.16 and 8.17. Since the mimetic spectral elements are compatible finite elements, there are no spurious modes and the correct eigenvalue multiplicity is found. Convergence results are found on a Cartesian mesh as well as on a curvilinear mesh. For the curvilinear mesh an equivalent mapping as in (8.1.30) is used which is scaled onto a  $[0, \pi]^2$  square and where we choose  $c = 0.2$  (see for example Figure 7.1). The  $h$ -convergence results were obtained on elements with  $N = 1$ ,  $N = 2$  and  $N = 4$ . Indeed it can be observed that the rate of convergence for the eigenvalues is  $\mathcal{O}(h^{2N})$ , and therefore optimal for both types of meshes. Having also optimal convergence on curvilinear meshes is what distinguishes the current approach to those using Nédélec and Raviart-Thomas quadrilateral elements, which are limited to affine mappings only.

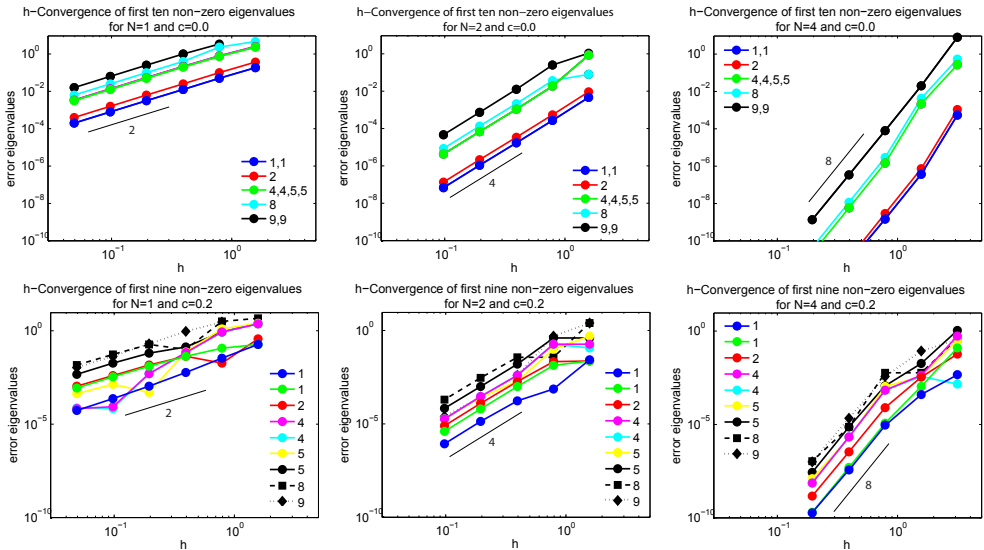


Figure 8.16:  $h$ -convergence of the Neumann curl-curl eigenvalue problem

Problems with Nédélec elements on non-uniform quadrilaterals have been reported in [3, 4, 22]. On distorted quadrilateral meshes, as shown for example in Figure 8.18, the lowest order Nédélec and Raviart-Thomas elements do not converge at all and higher-order versions converge suboptimal, see [24]. The same suboptimal convergence behavior is reported for BDM, BDFM and ABF elements. As alternative new elements were proposed by Arnold, Bozzo and Falk, [4]. These so-called ABF elements are Nédélec elements with additional internal degrees of freedom. Although these overdimensioned elements obtain the design convergence rates they still perform suboptimal. In contrast, the mimetic spectral edge elements has also optimal convergence on distorted meshes for all polynomial orders, including lowest order. The number of degrees of freedom are equal to those of the Nédélec elements and less than those of the ABF elements. The convergence results are shown in Figure 8.18 for first- and

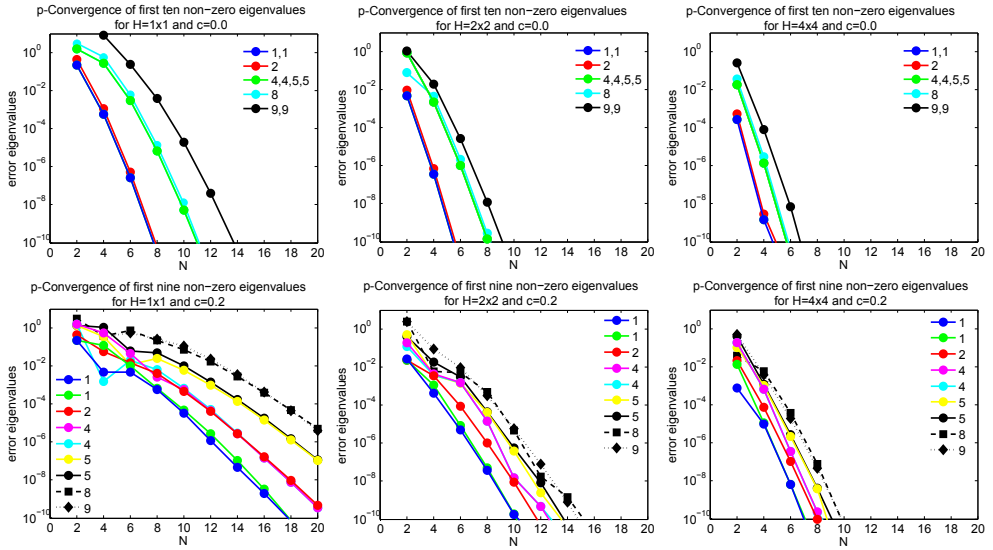


Figure 8.17:  $p$ -convergence Neumann curl-curl eigenvalue problem

third-order elements.

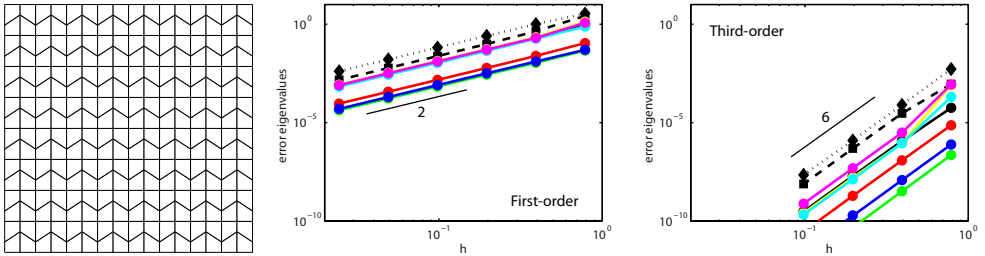
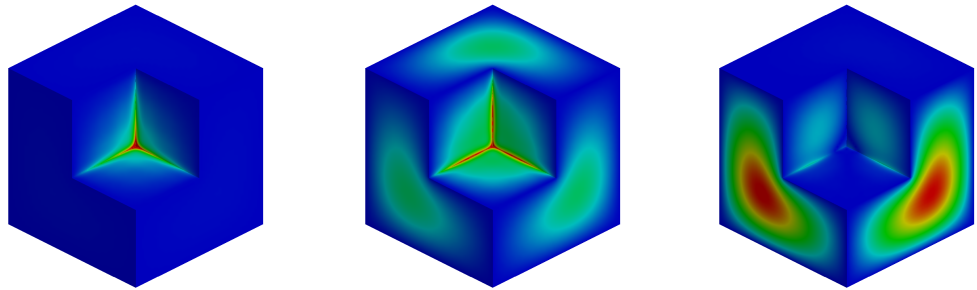


Figure 8.18: Eigenvalue convergence (middle and right) of the Neumann Maxwell eigenvalue problem on distorted quadrilateral meshes (left).

**Three dimensional Fichera corner** The domain of Fichera's corner is defined as  $\Omega = [-1, 1]^3 \setminus [0, 1]^3$ , that is, a cube minus a smaller cube. The Maxwell eigenvalue problem on Fichera's corner is a challenging case in that it contains both line and corner singularities. Both the Neumann and Dirichlet problem are subjected to Fichera's corner here. The first, fourth and fifth nonzero eigenfunctions are shown in Figure 8.19. The plots show both types of singularities in both problems. Table 8.1 shows the eigenvalues obtained with a 7 element mesh with  $N = 6$  and  $N = 12$ . We have chosen not to refine the mesh in the vicinity of the re-entrant corner. The rate of convergence is related to the smoothness of the corresponding eigenfunction. The error itself can be reduced by refining in the neighborhood of the singularity. *hp-adaptivity by means of mortar element method is treated in Chapter ??*. Because

---

Dirichlet boundary conditions



Neumann boundary conditions

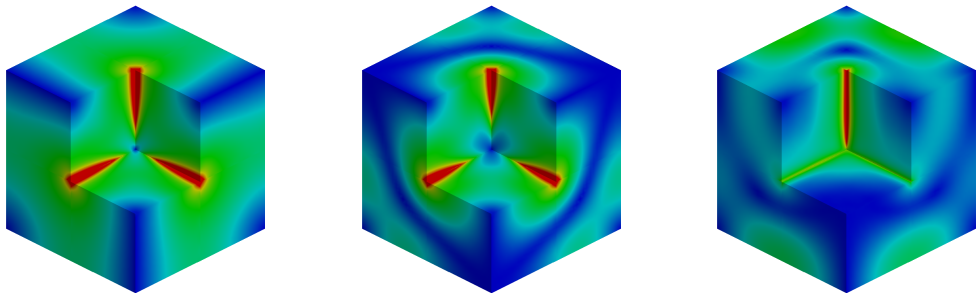


Figure 8.19: Colorplots of the first, fourth and fifth eigenfunction of Maxwell's eigenvalue problem on Fichera's corner using either Dirichlet or Neumann boundary conditions. The plots clearly show the corner and line singularities.

there does not exist good benchmark results, we compare our results to those obtained with other methods [40, 50, 186]. Note that these references choose to refine their mesh towards the singularities and therefore might have obtained better results with less degrees of freedom. Most important in this test case is that the present method captures the singularities well and that it converges towards the correct solution.

	Duruflé [50]	Zaglmayr [186]	Buffa [40]	MSEM $N = 6$	MSEM $N = 12$
1 <sup>st</sup> eigv.	3.2198740	3.2199938	3.2172044	3.2293194	3.2215174
2 <sup>nd</sup> eigv.	5.8804189	5.8804424	5.8805877	5.8797841	5.8803044
3 <sup>rd</sup> eigv.	5.8804189	5.8804552	5.8805877	5.8797841	5.8803044
4 <sup>th</sup> eigv.	10.685492	10.685663	10.688137	10.675488	10.683767
5 <sup>th</sup> eigv.	10.693782	10.693695	10.697915	10.678266	10.691113
6 <sup>th</sup> eigv.	10.693782	10.693728	10.697915	10.678266	10.691113
7 <sup>th</sup> eigv.	12.316520	12.316879	12.315929	12.319005	12.316929
8 <sup>th</sup> eigv.	12.316520	12.317690	12.315929	12.319005	12.316929

Table 8.1: First eight non-zero eigenvalues for the Dirichlet and Neumann curl-curl eigenvalue problems in Fichera's corner.

### 8.3.3 Remarks on conditioning

Some remarks can be made concerning the approximation behavior of the eigenvalues. For the lowest order approximations,  $N = 1, 2$ , using mimetic spectral edge elements on a uniform mesh all eigenvalues are approximated mainly from below, see for example Figure 8.20. For low order approximations on curvilinear or distorted meshes eigenvalues are approximated both from above as well as from below. When performing a spectral approximation using only one element, almost all eigenvalues are approximated from above for all mesh types. The  $\frac{2}{3}$  lowest eigenvalues are approximated accurately using the spectral method, while the  $\frac{1}{3}$  highest eigenvalues display really poor approximations, as is illustrated in Figure 8.20.

For  $N \rightarrow \infty$ , all eigenvalues do converge to the exact solution, but the  $\frac{2}{3} - \frac{1}{3}$  behavior is experienced for all  $N$ . The offset of the highest mode is a measure for the condition number of the system matrix. We find the following relation between the highest eigenvalue of the approximation and its corresponding exact eigenvalue,

$$|\lambda_{h,\text{highest}} - \lambda_{\text{exact}}| = N^S, \quad (8.3.14)$$

where the power  $S$  depends on the type of eigenvalue problem and the distortion of the mesh. For the Dirichlet and Neumann eigenvalue problems the power range is  $3 \lesssim S \lesssim 5$ , where the lower bound holds for uniform meshes and the upper bound for highly curved meshes, like (8.1.30) with  $c = 0.3$ , see also Figure 8.2. Other eigenvalue problems experience similar offsets for the highest eigenvalue.

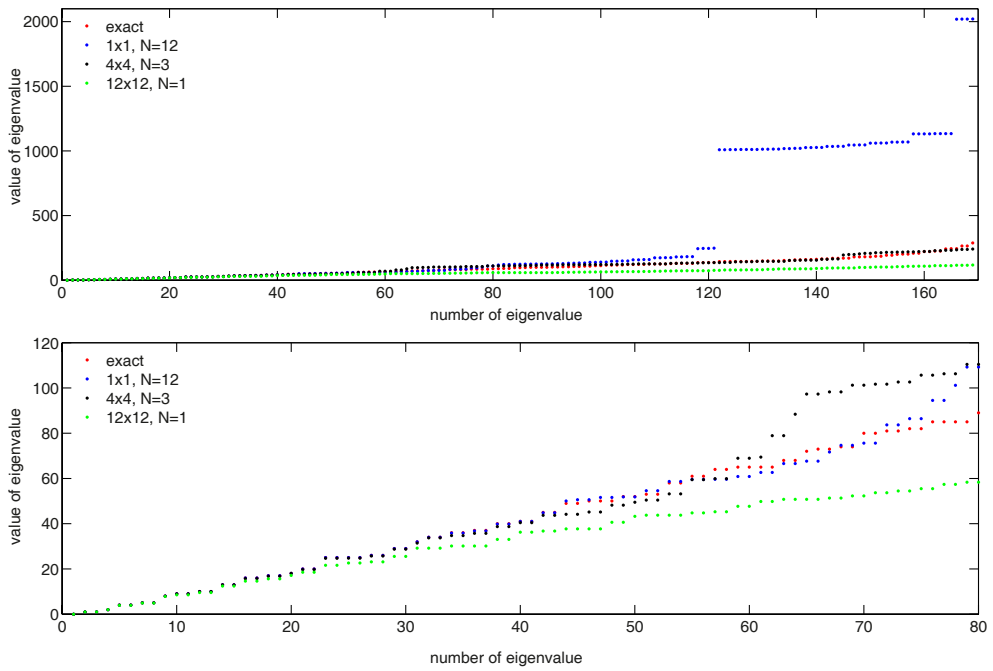


Figure 8.20: Eigenvalues of zero-form Laplacian on three topologically equivalent grids. Top figure shows all 169 nonzero eigenvalues. Bottom figure shows the first 80 nonzero eigenvalues.

# Chapter 9

## Mixed Mimetic Spectral Element Method for Stokes problem

This chapter is based on Kreeft and Gerritsma [111, 112, 113].

### 9.1 Introduction

In this chapter we consider Stokes flow, which models a viscous, incompressible fluid flow in which the inertial forces are negligible with respect to the viscous forces, i.e. when the Reynolds number is very small,  $Re \ll 1$ . Since  $Re = UL/\nu$ , small Reynolds numbers appear when either considering extremely small length scales, when dealing with a very viscous liquid or when one treats slow flows.

Let  $\Omega \subset \mathbb{R}^n$ ,  $n \geq 2$ , be a bounded domain with boundary  $\Gamma = \partial\Omega$ . On this domain we consider the Stokes problem, consisting of the equations for conservation of momentum and for conservation of mass. The Stokes problem is given by<sup>1</sup>

$$\nabla \cdot \sigma = \vec{f} \quad \text{on } \Omega, \tag{9.1.1a}$$

$$\operatorname{div} \vec{u} = g \quad \text{on } \Omega, \tag{9.1.1b}$$

where the stress tensor  $\sigma$  is given by

$$\sigma = -pI + \nu \nabla \vec{u}, \tag{9.1.2}$$

with  $\vec{u}$  the velocity vector,  $p$  the pressure,  $\vec{f}$  the forcing term,  $g$  the mass source and  $\nu$  the kinematic viscosity. System (9.1.1) slightly extends the Stokes model given in (2.3.1) by considering a possible mass source. For analysis purposes we choose  $\nu = 1$ . Although in most testcases we use  $g = 0$ , we leave the source term in for generality

<sup>1</sup>Remember from Chapter 2 that  $\operatorname{div}$  is the divergence operator acting on a vector, while  $\nabla \cdot$  is the divergence operator acting on a tensor. Idem for  $\operatorname{grad}$  and  $\nabla$ .

---

reasons. In some occasions we mention 'divergence-free', which refers to the most common case that  $g = 0$ .

The Stokes problem expressed in terms of vector operations only, instead of vector and tensor operations as in (9.1.1), is known as the *vorticity-velocity-pressure* (VVP) formulation, see also [16, 59]. The VVP formulation is obtained, by splitting the Laplace operator using the vector identity,  $-\Delta \vec{u} = \operatorname{curl} \operatorname{curl}^* \vec{u} - \operatorname{grad}^* \operatorname{div} \vec{u}$ , and by introducing vorticity as auxiliary variable,  $\vec{\omega} = \operatorname{curl}^* \vec{u}$ . The VVP formulation of the Stokes problem becomes

$$\vec{\omega} - \operatorname{curl}^* \vec{u} = 0, \quad \text{on } \Omega \quad (9.1.3a)$$

$$\operatorname{curl} \vec{\omega} - \operatorname{grad}^* \operatorname{div} \vec{u} + \operatorname{grad}^* p = \vec{f}, \quad \text{on } \Omega \quad (9.1.3b)$$

$$\operatorname{div} \vec{u} = g, \quad \text{on } \Omega. \quad (9.1.3c)$$

Following Section 2.3 and [16, 113], we make a distinction between the operators  $\operatorname{grad}$ ,  $\operatorname{curl}$  and  $\operatorname{div}$ , that correspond to the classical Newton-Leibniz, Stokes circulation and Gauss divergence theorems, and the operators  $-\operatorname{grad}^*$ ,  $\operatorname{curl}^*$  and  $-\operatorname{div}^*$  that are their formal Hilbert adjoints, (2.3.4). The distinction between the two types of differential operators is made explicitly, because the construction of our **conforming** finite element spaces relies on the generalized Stokes' theorem, while the mixed formulation relies on the formal Hilbert adjoint relations. While in vector calculus this distinction is not common, in differential geometry these structures naturally appear since they make a clear distinction between metric-free (topological) and metric-dependent operations.

Despite the simple appearance of Stokes flow model, there exists a large number of numerical methods to simulate Stokes flow. They all reduce to two classes of either circumventing the Ladyshenskaya-Babuška-Brezzi (LBB) stability condition or satisfying this condition, [70]. The first class can roughly be split into two subclasses, one is the group of stabilized methods, see e.g. [15, 97] and the references therein, the other the group of least-squares methods, see e.g. [17, 104].

The class that satisfies the LBB condition is the group of compatible methods. In compatible methods discrete vector spaces are constructed such that they satisfy the discrete LBB condition. Best known are divergence conforming Raviart-Thomas [154] and Brezzi-Douglas-Marini [36] spaces, and the curl conforming Nédélec space [133]. A subclass of compatible methods consists of *mimetic methods*. Mimetic methods do not solely search for appropriate vector spaces, but try to mimic structures and symmetries of the continuous problem, see [18, 33, 115, 122, 144, 172, 174]. As a consequence of this mimicking, mimetic methods intrinsically preserve structures of the continuous formulation.

The present study uses mimetic spectral element interpolation or basis functions on curvilinear quadrilaterals and hexahedrals of arbitrary order as described in Chapter 6 and in [73, 115]. The mixed mimetic spectral element method (MMSEM) satisfies the LBB condition and gives a *pointwise divergence-free solution for all mesh sizes*. This in contrast to nodal SEM methods, that are mostly used in combination with Galerkin (GSEM) [13, 106], and least-squares formulations (LSSEM) [148, 150]. The GSEM satisfies the LBB compatibility condition by lowering the polynomial degree of the pressure by two with respect to the velocity. This results in a method that is only weakly divergence-free, meaning that the divergence of the velocity field only

---

convergence to zero with mesh refinement. The LSSEM circumvents the LBB condition in order to be able to use equal order polynomials. The drawback of this method is the poor mass conservation property, [89, 107, 151].

The MMSEM is a compatible discretization method that relies on the construction of a bounded projection and a discrete Hodge-decomposition, which implies a discrete Poincaré inequality.

The MMSEM contains compatible finite elements that are compatible with all admissible types of boundary conditions for the Stokes problem in VVP formulation. We will show that the method obtains optimal rates of convergence for all variables on curvilinear meshes and for all admissible boundary conditions, i.e. standard and nonstandard. It is therefore extending the error estimates found in literature, which are often specifically constructed for certain types of boundary conditions, [1, 5, 17, 31, 60, 78, 96]. To show optimal convergence a priori error estimates are derived.

For compatible discretization methods that contain a **conforming** discrete Hodge decomposition, we derive optimal a priori error estimates which are valid for all admissible boundary conditions on both Cartesian and curvilinear meshes. These theoretical results are confirmed by numerical experiments using manufactured solution problems. These clearly show that the mimetic spectral elements outperform the commonly used  $H(\text{div})$ -compatible Raviart-Thomas elements. These are not compatible in case of no-slip boundary conditions and therefore lead to suboptimal convergence behavior, as was shown in [5, 60]. This non-compatibility results in a decrease in rate of convergence of maximal  $\frac{3}{2}$  order.

From a physical/fluid dynamics point-of-view the pointwise divergence-free and no-slip compatibility makes the MMSEM an attractive method.

This chapter is organized as follows: First the VVP Stokes problem is reformulated in terms of differential forms and boundary conditions are introduced. A break-down of the system is given based on the Hodge decomposition. In Section 9.3 the mixed formulation is given, well-posedness is proven and some remarks are made on the influence of given data on the flow variables. A proof for discrete well-posedness along with some remarks on discretization and implementation are given in Section 9.5. In Section 9.6 a first set of numerical results are discussed that qualitatively shows the performance of the mixed mimetic spectral element method. It considers Stokes flow problems that contain singularities in their solution and require non-affine mappings to mesh the computational domain. In order to obtain a quantitative measure a priori error estimates are developed in Section 9.7 that hold for all admissible types of boundary conditions. These theoretical results are confirmed in a second set of numerical results presented in Section 9.8. This chapter is closed with some concluding remarks.

[Link eventueel naar eerdere hoofdstukken](#)

## 9.2 Stokes problem in terms of differential forms

Consider again a bounded contractible domain  $\Omega \subset \mathbb{R}^n$ . The kind of form a variable has is directly related to the kind of submanifold this variable can be integrated over. This is motivated by physics. For example, from a physics point of view velocity is naturally integrated *along* a line (streamline), a 1-submanifold, indicating that velocity is a 1-form  $\tilde{u}^{(1)} \in \tilde{\Lambda}^1(\Omega)$ . So in  $\mathbb{R}^3$ , with  $\mathbf{x} := (x, y, z)$ , we can express

velocity as

$$\tilde{u}^{(1)} = u(\mathbf{x}) \, dx + v(\mathbf{x}) \, dy + w(\mathbf{x}) \, dz.$$

However, looking at conservation of mass (incompressibility constraint), velocity in incompressible (Navier)-Stokes equations is usually associated to a flux *through* a surface, indicating that velocity should be an  $(n-1)$ -form ( $n = \dim(\Omega)$ ). The two are directly related by the Hodge duality,  $u^{(n-1)} = \star \tilde{u}^{(1)}$ , see<sup>2</sup> (4.7.4). So alternatively, we can express velocity as

$$u^{(n-1)} = \star \tilde{u}^{(1)} \stackrel{n=3}{=} u(\mathbf{x}) \, dydz + v(\mathbf{x}) \, dzdx + w(\mathbf{x}) \, dx dy.$$

Although the Hodge star is an isomorphism, it changes the corresponding type of integration domain and type of orientation (from along a line = inner, to through a surface = outer). The Hodge star is usually combined with a constitutive relation. In that case the two variables have clearly a different meaning. In incompressible flow models, mass density plays the role of material property, so we actually have  $(\rho u)^{(n-1)} = \star_\rho \tilde{u}^{(1)}$ .

As for the velocity, also for pressure and vorticity there exists an inner and outer oriented version. The inner oriented variables are pressure,  $\tilde{p}^{(0)} \in \tilde{\Lambda}^0(\Omega)$ , associated to point values, and vorticity  $\tilde{\omega}^{(2)} \in \tilde{\Lambda}^2(\Omega)$ , associated to circulation in a surface. That is,

$$\begin{aligned} \tilde{p}^{(0)} &= p(\mathbf{x}), \\ \tilde{\omega}^{(2)} &= \omega_{xy}(\mathbf{x}) \, dx dy + \omega_{zx}(\mathbf{x}) \, dz dx + \omega_{yz}(\mathbf{x}) \, dy dz. \end{aligned}$$

Similarly, there exists the set of outer-oriented variables, being the pressure,  $p^{(n)} \in \Lambda^n(\Omega)$ , measured in a volume, and vorticity,  $\omega^{(n-2)} \in \Lambda^{n-2}(\Omega)$ , corresponding to circulation around a point in  $\mathbb{R}^2$  and around a line as in the Biot Savart law in  $\Omega \subset \mathbb{R}^3$ . Then

$$\begin{aligned} p^{(n)} &= \star \tilde{p}^{(0)} = p(\mathbf{x}) \, dx dy dz, \\ \omega^{(n-2)} &= \star \tilde{\omega}^{(2)} = \omega_{xy}(\mathbf{x}) \, dz + \omega_{zx}(\mathbf{x}) \, dy + \omega_{yz}(\mathbf{x}) \, dx. \end{aligned}$$

Both sets,  $(\tilde{p}^{(0)}, \tilde{u}^{(1)}, \tilde{\omega}^{(2)})$  and  $(\omega^{(n-2)}, u^{(n-1)}, p^{(n)})$  are used in literature to derive mixed formulations and numerical schemes. For the former see [1, 31] and for the latter see [12, 59, 60]. The two sets essentially result in the same system of equations, since the Hodge star is an isomorphism. It only leads to a different variational formulation and so to a different discretization.

To obtain an exact conservation of mass, i.e., a pointwise divergence-free solution in absence of a mass source, the incompressibility constraint is the dominant relation. Since we can perform exact discretization of the exterior derivative, see Chapter 6, the set of outer-oriented variables are used here, i.e.,  $(\omega^{(n-2)}, u^{(n-1)}, p^{(n)})$ , with forcing term  $f^{(n-1)}$  and mass source  $g^{(n)}$ . Then we get the following formulation of the Stokes

---

<sup>2</sup>With  $\tilde{\cdot}$  we indicate a variable associates with an inner oriented (sub)manifold and contained in the lower complex of (4.7.4).

problem:

$$\omega^{(n-2)} - d^* u^{(n-1)} = 0, \quad \text{on } \Omega, \quad (9.2.1a)$$

$$d\omega^{(n-2)} + d^* du^{(n-1)} + d^* p^{(n)} = f^{(n-1)}, \quad \text{on } \Omega, \quad (9.2.1b)$$

$$du^{(n-1)} = g^{(n)}, \quad \text{on } \Omega. \quad (9.2.1c)$$

Note the resemblance of this system with (9.1.3). System (9.2.1) is valid in  $\mathbb{R}^n$  for all  $n \geq 2$ . In the VVP formulation the pressure plus divergence of velocity in (9.2.1b) acts as a Lagrange multiplier for the constraint on velocity, (9.2.1c), whereas velocity in (9.2.1a) acts as a Lagrange multiplier for the constraint on vorticity in (9.2.1b). The former Lagrange multiplier is sometimes indicated as  $\Pi^{(n)} = p^{(n)} + du^{(n-1)}$ .

The actions of the exterior derivatives and codifferentials in this system are illustrated below for a two-dimensional domain.

**Example 34 (2D Stokes problem).** Let  $\Omega \subset \mathbb{R}^2$ , with Cartesian coordinates  $\mathbf{x} := (x, y)$ , and let the two-dimensional de Rham complex be equivalent to the second complex in (4.7.12). For  $n = 2$  the velocity flux is expressed as

$$u^{(n-1)} \stackrel{n=2}{=} -v(\mathbf{x})dx + u(\mathbf{x})dy.$$

Applying the exterior derivative gives us a 2-form, the divergence of velocity,

$$du^{(n-1)} \stackrel{n=2}{=} \left( \frac{\partial u}{\partial x} + \frac{\partial v}{\partial y} \right) dx \wedge dy.$$

Subsequently apply the codifferential gives,

$$d^* du^{(n-1)} \stackrel{n=2}{=} - \left( \frac{\partial^2 u}{\partial x \partial y} + \frac{\partial^2 v}{\partial y^2} \right) dx + \left( \frac{\partial^2 u}{\partial x^2} + \frac{\partial^2 v}{\partial y \partial x} \right) dy.$$

Vorticity is a 0-form,  $\omega^{(0)} = \omega(\mathbf{x}) \in \Lambda^0(\Omega)$ , and the curl of vorticity gives,

$$d\omega^{(n-2)} \stackrel{n=2}{=} \frac{\partial \omega}{\partial x} dx + \frac{\partial \omega}{\partial y} dy.$$

The gradient of pressure,  $p^{(2)} = p(\mathbf{x})dx \wedge dy \in \Lambda^2(\Omega)$ , is the action of the codifferential,

$$d^* p^{(n)} \stackrel{n=2}{=} -\frac{\partial p}{\partial y} dx + \frac{\partial p}{\partial x} dy.$$

Then the momentum equation follows,

$$-\left( \frac{\partial^2 u}{\partial x \partial y} + \frac{\partial^2 v}{\partial y^2} - \frac{\partial \omega}{\partial x} + \frac{\partial p}{\partial y} \right) dx + \left( \frac{\partial^2 u}{\partial x^2} + \frac{\partial^2 v}{\partial y \partial x} + \frac{\partial \omega}{\partial y} + \frac{\partial p}{\partial x} \right) dy = -f_y(x, y)dx + f_x(x, y)dy.$$

In a similar way the vorticity-velocity relation can be obtained.

Problem (9.2.1) needs to be supplemented with boundary conditions. Let  $\Gamma = \partial\Omega$  be the boundary of  $\Omega$ , where

$$\Gamma = \Gamma_\omega \cup \Gamma_t, \quad \Gamma_\omega \cap \Gamma_t = \emptyset, \quad \text{and} \quad \Gamma = \Gamma_n \cup \Gamma_\pi, \quad \Gamma_n \cap \Gamma_\pi = \emptyset.$$

---

We will impose the tangential vorticity and normal velocity as essential boundary conditions, and the tangential velocity and the pressure plus divergence of velocity as the natural boundary conditions:

$$\operatorname{tr} \omega^{(n-2)} = 0 \quad \text{on } \Gamma_\omega, \quad (9.2.2a)$$

$$\operatorname{tr} u^{(n-1)} = 0 \quad \text{on } \Gamma_n, \quad (9.2.2b)$$

$$\operatorname{tr} \star u^{(n-1)} = \tilde{u}_{b,t}^{(1)} \quad \text{on } \Gamma_t, \quad (9.2.2c)$$

$$\operatorname{tr} \star (p^{(n)} + du^{(n-1)}) = \tilde{\Pi}_b^{(0)} \quad \text{on } \Gamma_\pi. \quad (9.2.2d)$$

with  $\tilde{u}_{b,t}^{(1)} \in \tilde{\Lambda}^1(\Gamma_t)$  and with  $\tilde{\Pi}_b^{(0)} \in \tilde{\Lambda}^0(\Gamma_\pi)$ . Then the boundary  $\Gamma$  can be partitioned into four sections,  $\Gamma = \bigcup_{i=1}^4 \Gamma_i$ , with  $\Gamma_i \cap \Gamma_j = \emptyset$  for  $i \neq j$ , where

$$\Gamma_1 := \Gamma_t = \Gamma_n, \quad \Gamma_2 := \Gamma_t = \Gamma_\pi, \quad \Gamma_3 := \Gamma_\omega = \Gamma_n, \quad \Gamma_4 := \Gamma_\omega = \Gamma_\pi. \quad (9.2.3)$$

This decomposition, introduced before in [59, 96, 113], shows all admissible boundary conditions. It will also follow directly from the mixed formulation, see (9.3.4), Section 9.3. An overview is given in Table 9.1.

Name	Exterior Calculus	Vector Calculus	Type
Normal velocity tangential velocity	$\text{tr } u^{(n-1)} \Rightarrow \text{tr } v^{(n-1)} = 0$ $\text{tr } \star u^{(n-1)}$	$\vec{u} \cdot \vec{n} \Rightarrow \vec{v} \cdot \vec{n} = 0$ $\vec{u} \cdot \vec{t}$	essential natural
Tangential velocity pressure divergence of velocity	$\text{tr } \star u^{(n-1)}$ $\text{tr } \star (p^{(n)} + \text{d}u^{(n-1)})$	$\vec{u} \cdot \vec{t}$ $p + \text{div } \vec{u}$	natural natural
Tangential vorticity normal velocity	$\text{tr } \omega^{(n-2)} \Rightarrow \text{tr } \tau^{(n-2)} = 0$ $\text{tr } u^{(n-1)} \Rightarrow \text{tr } v^{(n-1)} = 0$	$\vec{\omega} \times \vec{t} \Rightarrow \vec{\tau} \times \vec{t} = \vec{0}$ $\vec{u} \cdot \vec{n} \Rightarrow \vec{v} \cdot \vec{n} = 0$	essential essential
Tangential vorticity pressure divergence of velocity	$\text{tr } \omega^{(n-2)} \Rightarrow \text{tr } \tau^{(n-2)} = 0$ $\text{tr } \star (p^{(n)} + \text{d}u^{(n-1)})$	$\vec{\omega} \times \vec{t} \Rightarrow \vec{\tau} \times \vec{t} = \vec{0}$ $p + \text{div } \vec{u}$	essential natural

Table 9.1: Admissible boundary conditions for the Stokes problem in vorticity-velocity-pressure formulation.

The VVP Stokes problem considers two singular cases with given boundary conditions. In case,  $\Gamma = \Gamma_1 \cap \Gamma_3$ ,  $\Gamma_2 \cup \Gamma_4 = \emptyset$ , no pressure boundary conditions are prescribed, and so the pressure is only determined up to an element  $\hat{p} \in \mathcal{Z}^{*,n}$ , i.e. up to a constant, so  $\mathcal{Z}^{*,n} = \mathbb{R}$ . As a post processing step either the pressure in a point in  $\Omega$  can be set, or a zero average pressure can be imposed; i.e.  $\int_{\Omega} \hat{p} = 0$ . In case  $\Gamma_4 \subseteq \Gamma$ , no velocity boundary conditions are prescribed, and so the solution of velocity is determined modulo a curl\*-free element, i.e. modulo a potential flow  $\hat{u} \in \mathcal{Z}^{*,n-1}$ . So there exists a flow potential  $\phi \in \Lambda^{n-2}(\Omega)$ , such that  $\hat{u} = d^* \phi$ . [Zijn harmonic spaces. Zie Stokes paper 2](#)

### 9.2.1 Hodge decomposition of the VVP Stokes problem

By means of the Hodge decomposition, we can unravel much of the structure of the VVP Stokes problem (9.2.1) and the effect of body force and source terms,  $f^{(n-1)}$  and  $g^{(n)}$ . Similar studies can be found in [79, 133], where they use variational statements instead of the Hodge decomposition.

The Hodge decomposition of  $k$ -form spaces in terms of their nullspace and orthogonal complement is given by  $\Lambda^k(\Omega) = \mathcal{Z}^k \oplus \mathcal{Z}^{k,\perp}$ . The momentum equation (9.2.1b) in the VVP Stokes problem is essentially the Hodge decomposition of the forcing function  $f^{(n-1)}$ ,

$$d\omega^{(n-2)} + d^*\Pi^{(n)} = f_{\mathcal{Z}}^{(n-1)} + f_{\perp}^{(n-1)}, \quad (9.2.4)$$

where  $\Pi^{(n)} = p^{(n)} + du^{(n-1)}$ ,  $f_{\mathcal{Z}}^{(n-1)} = d\omega^{(n-2)} \in \mathcal{Z}^{n-1}$ , and  $f_{\perp}^{(n-1)} = d^*\Pi^{(n)} \in \mathcal{Z}^{n-1,\perp}$ . The Hodge decomposition of a velocity field  $u^{(n-1)}$  is given by

$$\begin{aligned} u^{(n-1)} &= u_{\mathcal{Z}}^{(n-1)} + u_{\perp}^{(n-1)}, \\ &= d\psi^{(n-2)} + d^*\varphi^{(n)}, \end{aligned} \quad (9.2.5)$$

with  $\psi^{(n-2)} \in \Lambda^{n-2}(\Omega)$  and  $\varphi^{(n-2)} \in \Lambda^n(\Omega)$ . Substitution of the decomposition of velocity into the velocity-vorticity relation (9.2.1a) gives

$$\omega^{(n-2)} = d^*u^{(n-1)} = d^*u_{\mathcal{Z}}^{(n-1)} = d^*d\psi^{(n-2)}, \quad \Leftrightarrow \quad -\Delta\psi^{(n-2)} = \omega^{(n-2)}. \quad (9.2.6)$$

In (9.2.6) we recognize  $\psi^{(n-2)}$  as the stream function (2D) or stream vector (3D). Substitution of the velocity decomposition in the incompressibility constraint (9.2.1c) gives

$$du^{(n-1)} = du_{\perp}^{(n-1)} = dd^*\varphi^{(n)} = g^{(n)} \quad \Leftrightarrow \quad -\Delta\varphi^{(n)} = g^{(n)}. \quad (9.2.7)$$

In (9.2.7) we recognize  $\varphi^{(n)}$  as the velocity potential. Apply the exterior derivative and codifferential to the momentum equation (9.2.1b) gives,

$$dd^*\Pi^{(n)} = df_{\perp}^{(n-1)} \Leftrightarrow -\Delta P^{(n)} = df_{\perp}^{(n-1)}, \quad (9.2.8)$$

$$d^*d\omega^{(n-2)} = d^*f_{\mathcal{Z}}^{(n-1)} \Leftrightarrow -\Delta\omega^{(n-2)} = d^*f_{\mathcal{Z}}^{(n-1)}. \quad (9.2.9)$$

So we can break down the Stokes problem in a set of Laplace problems. It is clear that vorticity only depends on  $f_{\mathcal{Z}}^{(n-1)}$ , pressure only on  $f_{\perp}^{(n-1)}$ , and the two velocity components  $u_{\mathcal{Z}}^{(n-1)}$  and  $u_{\perp}^{(n-1)}$  depend only on  $f_{\mathcal{Z}}^{(n-1)}$  and  $g^{(n)}$ , respectively.

If we would add the space of harmonic forms, then we additionally get the terms  $u_{\mathcal{H}}^{(n-1)}$  and  $f_{\mathcal{H}}^{(n-1)}$ , and we write subscript  $\mathcal{B}$  instead of subscript  $\mathcal{Z}$  in the above analysis. It is easy to see that  $u_{\mathcal{H}}^{(n-1)}$  is completely determined by  $f_{\mathcal{H}}^{(n-1)}$ , i.e.,  $u_{\mathcal{H}}^{(n-1)} = f_{\mathcal{H}}^{(n-1)}$ , where  $u_{\mathcal{H}}^{(n-1)}$  is the harmonic part of a Darcy drag, as appears in Darcy-Stokes-Brinkman flow, see [66]. Usually  $f_{\mathcal{H}}^{(n-1)}$  is set to zero.

## 9.3 Mixed formulation

In the remainder of this chapter the superscripts indicating the kind of form are suppressed for the sake of readability. The kind of form will be indicated in the text and will also be clear from the context.

### 9.3.1 Mixed formulation of the Stokes problem

The use of a mixed formulation is based on the following reasoning: We know how to discretize exactly the metric-free exterior derivative  $d$  (see Lemma 6, Chapter 6, and the examples therein), but it is less obvious how to treat the codifferential operator  $d^*$ . Therefore we opt to perform integration by parts. A more extensive motivation was given in Section 8.2.2.

To obtain a unique solution for the corresponding mixed formulation, we define the following Hilbert spaces,

$$W := \{ \tau \in H\Lambda^{n-2}(\Omega) \mid \text{tr } \tau = 0 \text{ on } \Gamma_\omega \}, \quad (9.3.1)$$

$$V := \begin{cases} \{ v \in H\Lambda^{n-1}(\Omega) \mid \text{tr } v = 0 \text{ on } \Gamma_n \} & \text{if } \Gamma_4 = \emptyset, \\ \{ v \in H\Lambda^{n-1}(\Omega) \setminus \mathcal{Z}^{*,n-1}(\Omega) \mid \text{tr } v = 0 \text{ on } \Gamma_n \} & \text{if } \Gamma_4 \neq \emptyset, \end{cases} \quad (9.3.2)$$

$$Q := \begin{cases} q \in L^2\Lambda^n(\Omega), & \text{if } \Gamma_\pi \neq \emptyset, \\ q \in L^2\Lambda^n(\Omega) \setminus \mathcal{Z}^{*,n}, & \text{if } \Gamma_\pi = \emptyset, \end{cases} \quad (9.3.3)$$

with corresponding norms,  $\|\cdot\|_W$ ,  $\|\cdot\|_V$  and  $\|\cdot\|_Q$ , respectively. The derivation of the mixed formulation for the VVP Stokes problem consists of two steps:

1. multiply the three equations by test functions  $(\tau, v, q) \in \{W \times V \times Q\}$  using  $L^2$ -inner products,
2. perform integration by parts, as in (4.8.5), to express the remaining codifferentials in terms of the exterior derivatives and boundary integrals.

Then the mixed formulation of the VVP formulation reads: find  $(\omega, u, p) \in \{W \times V \times Q\}$ , for the given data  $f \in L^2\Lambda^{n-1}(\Omega)$ ,  $g \in L^2\Lambda^n(\Omega)$  and natural boundary conditions  $\tilde{u}_{b,t} \in H^{-\frac{1}{2}}\tilde{\Lambda}^1(\Gamma_t)$ ,  $\tilde{\Pi}_b \in H^{-\frac{1}{2}}\tilde{\Lambda}^0(\Gamma_\pi)$ , for all  $(\tau, v, q) \in \{W \times V \times Q\}$ , such that

$$(\tau, \omega)_\Omega - (d\tau, u)_\Omega = - \int_{\Gamma_1 \cup \Gamma_2} \text{tr } \tau \wedge \tilde{u}_{b,t}, \quad (9.3.4a)$$

$$(v, d\omega)_\Omega + (dv, du)_\Omega + (dv, p)_\Omega = (v, f)_\Omega + \int_{\Gamma_2 \cup \Gamma_4} \text{tr } v \wedge \tilde{\Pi}_b, \quad (9.3.4b)$$

$$(q, du)_\Omega = (q, g)_\Omega. \quad (9.3.4c)$$

---

**Proposition 33.** [12] Problems (9.2.1)-(9.2.2) and (9.3.4) are equivalent, in the sense that any triple  $(\omega, u, p) \in \{W \times V \times Q\}$  is a solution of problem (9.2.1)-(9.2.2) if and only if it is a solution of problem (9.3.4).

This mixed formulation is similar to those in [12, 59, 79].

### 9.3.2 Well-posedness of mixed formulation

First define the following nullspaces of  $W$ ,

$$\mathcal{Z}_W := \{ \tau \in W \mid d\tau = 0 \}, \quad (9.3.5a)$$

$$\mathcal{Z}_W^* := \{ \tau \in W \mid d^*\tau = 0 \}, \quad (9.3.5b)$$

and consider the following decompositions,  $W = \mathcal{Z}_W \oplus \mathcal{Z}_W^\perp$  and  $W = \mathcal{Z}_W^* \oplus \mathcal{Z}_W^{*,\perp}$ . Since vorticity is defined as  $\omega = d^*u$ , we have  $\omega \in \mathcal{Z}_W^*$ , and because we consider contractible domains only, it follows that  $\omega \in \mathcal{Z}_W^\perp$ . Note that for  $n = 2$ ,  $\mathcal{Z}_W^* \equiv W$ . A similar decomposition can be made for  $V$ . Define

$$\mathcal{Z}_V := \{ v \in V \mid dv = 0 \}, \quad (9.3.5c)$$

then  $V = \mathcal{Z}_V \oplus \mathcal{Z}_V^\perp$ . The velocity is decomposed as  $u = u_{\mathcal{Z}} + u_{\perp}$ , where  $u_{\mathcal{Z}} \in \mathcal{Z}_V$  and  $u_{\perp} \in \mathcal{Z}_V^\perp$ .

We can write the mixed formulation (9.3.4) in a more general representation, using four continuous bilinear forms,

$$\begin{aligned} \mathbf{a}(\cdot, \cdot) &:= (\cdot, \cdot)_\Omega : W \times W \rightarrow \mathbb{R}, & \mathbf{b}(\cdot, \cdot) &:= (d \cdot, \cdot)_\Omega : V \times Q \rightarrow \mathbb{R}, \\ \mathbf{c}(\cdot, \cdot) &:= (d \cdot, \cdot)_\Omega : W \times V \rightarrow \mathbb{R}, & \mathbf{e}(\cdot, \cdot) &:= (d \cdot, d \cdot)_\Omega : V \times V \rightarrow \mathbb{R}, \end{aligned}$$

and three continuous linear forms

$$\begin{aligned} \mathbf{f}(\cdot) &:= (\cdot, f)_\Omega + \int_{\Gamma_2 \cup \Gamma_4} \text{tr } \cdot \wedge \tilde{\Pi}_b : V \rightarrow \mathbb{R}, \\ \mathbf{g}(\cdot) &:= (\cdot, g)_\Omega : Q \rightarrow \mathbb{R}, & \mathbf{h}(\cdot) &:= - \int_{\Gamma_1 \cup \Gamma_2} \text{tr } \cdot \wedge \tilde{u}_{b,t} : W \rightarrow \mathbb{R}. \end{aligned}$$

The mixed formulation becomes

$$\mathbf{a}(\tau, \omega) - \mathbf{c}(\tau, u) = \mathbf{h}(\tau), \quad \forall \tau \in W, \quad (9.3.6a)$$

$$\mathbf{e}(v, u) + \mathbf{c}(\omega, v) + \mathbf{b}(v, p) = \mathbf{f}(v), \quad \forall v \in V, \quad (9.3.6b)$$

$$\mathbf{b}(u, q) = \mathbf{g}(q). \quad \forall q \in Q. \quad (9.3.6c)$$

There exist continuity constants  $0 < c_a, c_b, c_c, c_e < \infty$  such that

$$\begin{aligned} \mathbf{a}(\tau, \kappa) &\leq c_a \|\tau\|_W \|\kappa\|_W, & \mathbf{b}(v, q) &\leq c_b \|v\|_V \|q\|_Q, \\ \mathbf{c}(\tau, v) &\leq c_c \|\tau\|_W \|v\|_V, & \mathbf{e}(v, w) &\leq c_e \|v\|_V \|w\|_V. \end{aligned} \quad (9.3.7)$$

By Cauchy-Schwarz we know that  $c_a = 1$ , however we write  $c_a$  for generality. The continuous linear forms are bounded such that

$$\mathbf{f}(v) \leq \|f\| \|v\|_V, \quad \mathbf{g}(v) \leq \|g\| \|v\|_V, \quad \mathbf{h}(\tau) \leq \|h\| \|\tau\|_W. \quad (9.3.8)$$

First restrict to all  $v = v_{\mathcal{Z}} \in \mathcal{Z}_V$ . This gives the vorticity-velocity subproblem, which is a saddle point problem:

$$\mathbf{a}(\tau, \omega) - \mathbf{c}(\tau, u_{\mathcal{Z}}) = \mathbf{h}(\tau), \quad \forall \tau \in W, \quad (9.3.9a)$$

$$\mathbf{c}(v_{\mathcal{Z}}, \omega) = \mathbf{f}(v_{\mathcal{Z}}), \quad \forall v_{\mathcal{Z}} \in \mathcal{Z}_V. \quad (9.3.9b)$$

**Proposition 34.** [59] System (9.3.9) has a unique solution  $(\omega, u_{\mathcal{Z}}) \in \{W \times \mathcal{Z}_V\}$  if there exists positive constants  $\alpha, \gamma$ , such that we have coercivity in the kernel of  $W$ ,

$$\inf_{\tau_{\mathcal{Z}} \in \mathcal{Z}_W} \sup_{\kappa_{\mathcal{Z}} \in \mathcal{Z}_W} \frac{\mathbf{a}(\tau_{\mathcal{Z}}, \kappa_{\mathcal{Z}})}{\|\tau_{\mathcal{Z}}\|_W \|\kappa_{\mathcal{Z}}\|_W} \geq \alpha, \quad \inf_{\kappa_{\mathcal{Z}} \in \mathcal{Z}_W} \sup_{\tau_{\mathcal{Z}} \in \mathcal{Z}_W} \frac{\mathbf{a}(\tau_{\mathcal{Z}}, \kappa_{\mathcal{Z}})}{\|\tau_{\mathcal{Z}}\|_W \|\kappa_{\mathcal{Z}}\|_W} \geq \alpha, \quad (9.3.10)$$

and satisfies the following inf-sup condition for  $\mathbf{c}(\tau, v_{\mathcal{Z}})$ ,

$$\inf_{v_{\mathcal{Z}} \in \mathcal{Z}_V} \sup_{\tau \in W} \frac{\mathbf{c}(\tau, v_{\mathcal{Z}})}{\|\tau\|_W \|v_{\mathcal{Z}}\|_V} \geq \gamma, \quad (9.3.11)$$

*Proof.* The proof of (9.3.10) is straightforward, see e.g. [37]. For (9.3.11), we have  $\mathbf{c}(\tau, v_{\mathcal{Z}}) = (\mathbf{d}\tau, v_{\mathcal{Z}})_{\Omega}$ , where  $\mathbf{d} : \mathcal{Z}_W^{\perp} \rightarrow \mathcal{Z}_V$ . Thus, given  $v_{\mathcal{Z}} \in \mathcal{Z}_V$  there exists a unique  $\tau_v \in \mathcal{Z}_W^{\perp}$  such that  $\mathbf{d}\tau_v = v_{\mathcal{Z}}$  and  $\|\tau_v\|_W \leq c_P \|v_{\mathcal{Z}}\|_V$  by Lemma 2. Therefore

$$\sup_{\tau \in W} \frac{\mathbf{c}(\tau, v_{\mathcal{Z}})}{\|\tau\|_W} \geq \frac{\mathbf{c}(\tau_v, v_{\mathcal{Z}})}{\|\tau_v\|_W} = \frac{\|v_{\mathcal{Z}}\|_V^2}{\|\tau_v\|_W} \geq \frac{1}{c_P} \|v_{\mathcal{Z}}\|_V.$$

□

**Proposition 35.** The full problem (9.3.6) has a unique solution  $(\omega, u, p) \in \{W, V, Q\}$  if conditions (9.3.10) and (9.3.11) from Proposition 34 are satisfied and additionally is there exists positive constants  $\varepsilon, \beta$ , such that we have coercivity in the range of  $V$ ,

$$\inf_{v_{\perp} \in \mathcal{Z}_V^{\perp}} \sup_{w_{\perp} \in \mathcal{Z}_V^{\perp}} \frac{\mathbf{e}(v_{\perp}, w_{\perp})}{\|v_{\perp}\|_V \|w_{\perp}\|_V} \geq \varepsilon, \quad \inf_{w_{\perp} \in \mathcal{Z}_V^{\perp}} \sup_{v_{\perp} \in \mathcal{Z}_V^{\perp}} \frac{\mathbf{e}(v_{\perp}, w_{\perp})}{\|v_{\perp}\|_V \|w_{\perp}\|_V} \geq \varepsilon, \quad (9.3.12)$$

and satisfies the following inf-sup condition for  $\mathbf{b}(v, q)$ ,

$$\inf_{q \in Q} \sup_{v \in V} \frac{\mathbf{b}(v, q)}{\|v\|_V \|q\|_Q} \geq \beta > 0. \quad (9.3.13)$$

*Proof.* By Poincaré inequality,  $\|dw_{\perp}\|_{L^2 \Lambda^n} \geq \frac{1}{c_P^2} \|w_{\perp}\|_{H \Lambda^{n-1}}$ , it follows that  $\mathbf{e}(\cdot, \cdot)$  is coercive, which is an even stronger statement than (9.3.12). The proof of (9.3.13) is similar to that of Proposition 34. See also [14], Section 7.1. □

So well-posedness of the Stokes problem (9.3.4) relies only on the Hodge decomposition and the Poincaré inequality.

**Corollary 19.** [12, 59] Problem (9.3.4) is well-posed according to Propositions 34 and 35. That is, for any given data  $f \in L^2 \Lambda^{n-1}(\Omega)$  and  $g \in L^2 \Lambda^n(\Omega)$  and natural

---

boundary conditions  $\tilde{u}_{b,t} \in H^{-\frac{1}{2}}\tilde{\Lambda}^1(\Gamma_t)$  and  $\tilde{\Pi}_b \in H^{-\frac{1}{2}}\tilde{\Lambda}^0(\Gamma_\pi)$ , there exists a unique solution  $(\omega, u, p) \in W \times V \times Q$  satisfying (9.3.4). Moreover, this solution satisfies:

$$\|\omega\|_W + \|u\|_V + \|p\|_Q \leq C \left( \|f\|_{L^2\Lambda^{n-1}} + \|g\|_{L^2\Lambda^n} + \|\tilde{u}_{b,t}\|_{H^{-\frac{1}{2}}\tilde{\Lambda}^1} + \|\tilde{\Pi}_b\|_{H^{-\frac{1}{2}}\tilde{\Lambda}^0} \right), \quad (9.3.14)$$

where  $C$  is a constant depending only on the Poincaré constant  $c_P$  and the continuity constants.

Alternative proofs for the mixed formulation of the VVP Stokes problem can be found in [59, 79].

### 9.3.3 Influence of boundary terms

Continuing with the Hodge decomposition in Section 9.2.1, we can show the influence of the boundary terms on the flow variables using the mixed formulation.

The incompressibility constraint (9.2.1c) gives a global relation between the normal boundary condition  $\text{tr } u$  and source term  $g$ ,

$$\int_\Omega g = \int_\Omega \text{d}u_\perp = \int_{\partial\Omega} \text{tr } u_\perp. \quad (9.3.15)$$

Now choose  $v = v_Z = \text{d}\tau_\perp \in Z_V$ , where  $\tau_\perp \in Z_W^\perp$ , and substitute this in (9.3.4b) gives

$$(v_Z, \text{d}\omega)_\Omega = (v_Z, f_Z)_\Omega + \int_{\Gamma_2 \cup \Gamma_4} \text{tr } v_Z \wedge \tilde{\Pi}_b, \quad \forall v_Z \in Z_V. \quad (9.3.16)$$

This shows that  $\text{d}\omega$  only depends on  $f_Z$  and the boundary condition,  $\tilde{\Pi}_b$ . In case of normal velocity boundary condition,  $\text{d}\omega$  solely depends on the data  $f_Z$ . The relation between vorticity and velocity is given by substitution of  $\tau_\perp \in Z_W^\perp$  into (9.3.4a),

$$(\tau_\perp, \omega)_\Omega - (\text{d}\tau_\perp, u_Z)_\Omega + \int_{\Gamma_1 \cup \Gamma_2} \text{tr } \tau_\perp \wedge \tilde{u}_{b,t} = 0. \quad (9.3.17)$$

This shows that the solution of vorticity depends on the tangential velocity boundary condition,  $\tilde{u}_{b,t}$ , and on  $u_Z$ , but does not depend on  $u_\perp$ . Vice versa,  $u_Z$  is completely determined by the given tangential velocity boundary condition and the solution of vorticity, which by (9.3.16) depends on  $f_Z$  and  $\tilde{\Pi}_b$ . Finally, by choosing  $v = v_\perp \in Z_V^\perp$ , it can be shown that the pressure solely depends on the force function  $f_\perp$  and pressure boundary conditions  $\tilde{\Pi}_b$ ,

$$(\text{d}v_\perp, \Pi)_\Omega = (v_\perp, f_\perp)_\Omega + \int_{\Gamma_2 \cup \Gamma_4} \text{tr } v_\perp \wedge \tilde{\Pi}_b. \quad (9.3.18)$$

In case  $g = 0$  and  $\Gamma_2 \cup \Gamma_4 = \emptyset$ , the pressure is completely decoupled from the vorticity and velocity. As a consequence one could consider the vorticity-stream function formulation [64, 78], instead of vorticity-velocity-pressure formulations, where one chooses  $u = \text{d}\psi$  and  $v = \text{d}\tau$ . Note that  $\tau_Z \in Z_W$  has no contribution.

## 9.4 Issues on discretization and implementation

### 9.4.1 Pointwise divergence-free discretization

One of the most interesting properties of the mimetic method presented in this thesis, is that within the variational formulation, the divergence-free constraint is satisfied pointwise. This result follows from the three commuting properties with the exterior derivative, (6.1.4), (6.1.8) and (6.2.4), as was shown in Lemma 6. The corresponding commuting diagrams are repeated in the diagram below for the two dimensional case.

$$\begin{array}{ccccc}
 \Lambda_h^0(\mathcal{Q}; C_0) & \xrightarrow{\text{curl}} & \Lambda_h^1(\mathcal{Q}; C_1) & \xrightarrow{\text{div}} & \Lambda_h^2(\mathcal{Q}; C_2) \\
 \mathcal{R} \uparrow \mathcal{I} & & \mathcal{R} \uparrow \mathcal{I} & & \mathcal{R} \uparrow \mathcal{I} \\
 C^0(D) & \xrightarrow{\delta} & C^1(D) & \xrightarrow{\delta} & C^2(D)
 \end{array}$$

Note that by curl we refer to the two-dimensional variant, applied to a scalar, i.e.  $\text{curl } \omega = (\partial\omega/\partial y, -\partial\omega/\partial x)^T$ , see also Example 34.

In the following two examples we demonstrate the action of the exterior derivative on vorticity,  $\omega_h^{(0)} \in \Lambda_h^0(\widehat{Q}; C_0)$ , and on the velocity flux,  $u_h^{(1)} \in \Lambda_h^1(\widehat{Q}; C_1)$ , defined on a reference domain  $\widehat{Q} = [-1, 1]^2$ . Two dimensional reconstruction is based on tensor product construction of one dimensional reconstruction functions derived in Chapter 7.

**Example 35 (Curl operator).** Consider a flux  $z_h^{(1)} \in \Lambda_h^1(\widehat{Q}; C_1)$  with  $C_1$  outer-oriented, and where  $z_h^{(1)} = \text{d}\omega_h^{(0)}$ . Then  $\omega_h^{(0)}$  is expanded in the reference coordinates  $(\xi, \eta)$  as

$$\omega_h^{(0)} = \sum_{i=0}^N \sum_{j=0}^N \omega_{i,j} l_i(\xi) l_j(\eta). \quad (9.4.1)$$

Apply the exterior derivative in the same way as in Lemma 8, gives

$$\begin{aligned}
 z_h^{(1)} &= \text{d}\omega_h^{(0)} = \sum_{i=1}^N \sum_{j=0}^N (\omega_{i,j} - \omega_{i-1,j}) e_i(\xi) l_j(\eta) + \sum_{i=0}^N \sum_{j=1}^N (\omega_{i,j} - \omega_{i,j-1}) l_i(\xi) e_j(\eta), \\
 &= - \sum_{i=1}^N \sum_{j=0}^N z_{i,j}^\eta e_i(\xi) l_j(\eta) + \sum_{i=0}^N \sum_{j=1}^N z_{i,j}^\xi l_i(\xi) e_j(\eta),
 \end{aligned} \quad (9.4.2a)$$

where  $z_{i,j}^\xi = \omega_{i,j} - \omega_{i,j-1}$ , and  $z_{i,j}^\eta = \omega_{i-1,j} - \omega_{i,j}$  can be compactly written as  $\mathbf{z}^{(1)} = \delta\boldsymbol{\omega}^{(0)}$ , with  $\boldsymbol{\omega}^{(0)} \in C^0(D)$  and  $\mathbf{z}^{(1)} \in C^1(D)$ , or in matrix notation as  $\mathbf{z} = \mathbf{E}^{(1,0)}\boldsymbol{\omega}$ . This relation is exact, coordinate free and invariant under transformations.

**Example 36 (Divergence operator).** Let  $u_h^{(1)} \in \Lambda_h^1(\widehat{Q}; C_1)$  be the velocity flux defined as

$$u_h^{(1)} = - \sum_{i=1}^N \sum_{j=0}^N v_{i,j} e_i(\xi) l_j(\eta) + \sum_{i=0}^N \sum_{j=1}^N u_{i,j} l_i(\xi) e_j(\eta). \quad (9.4.3)$$

Compare this to the velocity flux in Example 34, p.177. Then the change of mass,  $m_h^{(2)} \in \Lambda_h^2(\widehat{Q}; C_2)$ , is equal to the exterior derivative of  $u_h^{(1)}$ ,

$$\begin{aligned} m_h^{(2)} &= d u_h^{(1)} = \sum_{i=1}^N \sum_{j=1}^N (u_{i,j} - u_{i-1,j} + v_{i,j} - v_{i,j-1}) e_i(\xi) e_j(\eta). \\ &= \sum_{i=1}^N \sum_{j=1}^N m_{i,j} e_i(\xi) e_j(\eta), \end{aligned} \quad (9.4.4)$$

where  $m_{i,j} = u_{i,j} - u_{i-1,j} + v_{i,j} - v_{i,j-1}$  can be compactly written as  $\mathbf{m}^{(2)} = \delta \mathbf{u}^{(1)}$ , with  $\mathbf{u}^{(1)} \in C^1(D)$  and  $\mathbf{m}^{(2)} \in C^2(D)$ , or in matrix notation as  $\mathbf{m} = \mathbf{E}^{(2,1)} \mathbf{u}$ . Note that if the mass production is zero, the incompressibility constraint is already satisfied at discrete/cochain level. Interpolation then results in a pointwise divergence-free solution.

Examples for  $\Omega \subset \mathbb{R}^3$  can be found in Section 7.3.

#### 9.4.2 Implementation

From the implementation point of view we would like to mention that the  $L^2$  inner products and boundary integrals are evaluated using Gauss-Lobatto quadrature, which is exact for polynomials up to order  $2N - 1$ , [42]. The resulting system matrix is a saddle point system that is given by,

$$\begin{bmatrix} \mathbf{M}^{(n-2)} & (\mathbf{E}^{(n-1,n-2)})^T \mathbf{M}^{(n-1)} & \emptyset \\ \mathbf{M}^{(n-1)} \mathbf{E}^{(n-1,n-2)} & (\mathbf{E}^{(n,n-1)})^T \mathbf{M}^{(n)} \mathbf{E}^{(n,n-1)} & (\mathbf{E}^{(n,n-1)})^T \mathbf{M}^{(n)} \\ \emptyset & \mathbf{M}^{(n)} \mathbf{E}^{(n,n-1)} & \mathbf{g}^{(n)} \end{bmatrix} \begin{bmatrix} \boldsymbol{\omega} \\ \mathbf{u} \\ \mathbf{p} \end{bmatrix} = \begin{bmatrix} -\mathbf{B}_1 \tilde{\mathbf{u}}_{b,t}^{(1)} \\ \mathbf{M}^{(n-1)} \mathbf{f}^{(n-1)} + \mathbf{B}_2 \tilde{\mathbf{\Pi}}_b^{(0)} \\ \emptyset \end{bmatrix} \quad (9.4.5)$$

The final system matrix is symmetric and only consists of  $L^2$  inner product matrices for  $k$ -forms,  $\mathbf{M}^{(k)}$  (also known as mass matrices), and incidence matrices,  $\mathbf{E}^{(k,k-1)}$ , that are directly obtained from the mesh topology, see p.80. Coordinate transformations imposed by the pullback operator appear in the  $L^2$  inner products as a standard change of basis, see also [30]. The matrices  $\mathbf{B}_1$  and  $\mathbf{B}_2$  represent the boundary integrals in (9.3.4a) and (9.3.4b), and  $\tilde{\mathbf{u}}_{b,t}^{(1)}$  and  $\tilde{\mathbf{\Pi}}_b^{(0)}$  are the tangential velocity and pressure plus divergence of velocity boundary conditions imposed. A discussion on efficient solvers for symmetric indefinite systems that follow from saddle point problems can be found in [11, 177].

#### 9.5 Numerical stability

Well-posedness of the Stokes problem in VVP formulation relied on the Hodge decomposition and the Poincaré inequality. For a compatible discretization, these properties need to be respected as well in the finite dimensional spaces. Key ingredient to obtain a discrete Hodge decomposition and discrete Poincaré inequality is the construction of a bounded projection operator that commutes with the exterior derivative.

---

The higher-order compatible discretization consists of three parts. First, the discrete structure is described in terms of chains and cochains from algebraic topology, the discrete counterpart of differential geometry. This discrete structure mimics many of the properties from differential geometry. Secondly, mimetic operators are introduced that relate the continuous formulation in terms of differential forms to the discrete representation based on cochains and finite dimensional differential forms. Thirdly, mimetic spectral element basis functions are described following the definitions of the mimetic operators. These result in a bounded projection. These topics were treated in Part II. What is left is the proof of well-posedness for the discrete numerical formulation. Moreover, interpolation error estimates are given.

The discrete problem is almost the same as the continuous problem, that is: find  $(\omega_h, u_h, p_h) \in \{W_h \times V_h \times Q_h\}$ , for given data  $f_h \in \Lambda_h^{n-1}$  and  $g_h \in \Lambda_h^n$  and natural boundary conditions  $\tilde{u}_{b,t,h} \in \tilde{\Lambda}_h^1(\Gamma_t)$  and  $\tilde{\Pi}_{b,h} \in \tilde{\Lambda}_h^0(\Gamma_\pi)$ , for all  $(\tau_h, v_h, q_h) \in \{W_h \times V_h \times Q_h\}$ , such that (9.3.4a)-(9.3.4c) hold.

Essential ingredients in proving numerical stability are the bounded projection, Definition 64, the discrete Hodge decomposition, (6.4.3), and the discrete Poincaré inequality, Lemma 7. It follows that the complexes  $(H\Lambda, d)$  and  $(\Lambda_h, d)$  are each others supercomplex and subcomplex, respectively. Having these properties, the discrete well-posedness follows.

**Theorem 7 (Discrete well-posedness).** *Let  $(\Lambda_h, d)$  be a subcomplex of the closed Hilbert complex  $(H\Lambda, d)$ . Then there exists constants  $\alpha_h, \beta_h, \gamma_h$ , depending only on  $c_{Ph}$ , such that for any  $(\tau_h, v_h, q_h) \in W_h \times V_h \times Q_h$ , there exists a stable finite dimensional solution  $(\omega_h, u_h, p_h) \in W_h \times V_h \times Q_h$  of the Stokes problem (9.3.4), with*

$$\alpha_h > \alpha > 0, \quad \beta_h > \beta > 0, \quad \gamma_h > \gamma > 0. \quad (9.5.1)$$

*Proof.* This is just Propositions 34 and 35 applied to the complex  $(\Lambda_h, d)$ , combined with the fact that the constant in the Poincaré inequality for  $\Lambda_h^k$  is  $c_{Ph} \leq c_P$  by Lemma 7.  $\square$

For the variables vorticity, velocity and pressure in the VVP formulation of the Stokes problem, the  $h$ -convergence rates of the interpolation errors become,

$$\begin{aligned} \|\omega - \pi_h \omega\|_{L^2 \Lambda^{n-2}} &= \mathcal{O}(h^{N+s}), & \|\omega - \pi_h \omega\|_{H\Lambda^{n-2}} &= \mathcal{O}(h^N), \\ \|u - \pi_h u\|_{L^2 \Lambda^{n-1}} &= \mathcal{O}(h^N), & \|u - \pi_h u\|_{H\Lambda^{n-1}} &= \mathcal{O}(h^N), \\ \|p - \pi_h p\|_{L^2 \Lambda^n} &= \mathcal{O}(h^N), \end{aligned} \quad (9.5.2)$$

where  $s = 1$  for  $n = 2$  and  $s = 0$  for  $n > 2$ , and with  $N$  defined as in Chapter 7. Because of (9.2.1c) and (6.2.4), we have for  $g = 0$ , that  $\|u - \pi_h u\|_{H\Lambda^{n-1}} = \|u - \pi_h u\|_{L^2 \Lambda^{n-1}}$ .

## 9.6 Numerical Results I

Now that the mixed mimetic spectral element method applied to the VVP Stokes problem is explained and the most important implementation issues are treated, we

can perform some test problems. The numerical results we obtain in this section are from well-known test cases. All testcases contain an additional difficulty, that is, either they contain singulaties in the solution or require non-affine mappings or both. In this first sequence of test-cases we show that it works. How well the method works is discussed in Section 9.8.

The first test case addresses the convergence for  $h$ - and  $p$ -refinement on a unit square with manufactured solution. The second test case consists of a series of lid-driven cavity flow problems on various domains, namely, inside a square and a triangle domain (both 2D) and inside a box (3D). The third test case consists of a Stokes flow around a cylinder moving with constant velocity inside a channel (2D).

### 9.6.1 Manufactured solution

The problem is defined on the unit square  $\Omega = [0, 1]^2$ , with Cartesian coordinates  $\mathbf{x} := (x, y)$ , with  $\nu = 1$ , without any mass source,  $g^{(2)} = 0$ , and with the body force  $f^{(1)} \in \Lambda^1(\Omega)$  given by

$$\begin{aligned} f^{(1)} &= -f_y(\mathbf{x}) dx + f_x(\mathbf{x}) dy, \\ &= -(\pi \sin(\pi x) \cos(\pi y) + 8\pi^2 \cos(2\pi x) \sin(2\pi y)) dx \\ &\quad + (\pi \cos(\pi x) \sin(\pi y) - 8\pi^2 \sin(2\pi x) \cos(2\pi y)) dy. \end{aligned} \quad (9.6.1a)$$

This right hand side results in an exact solution for the vorticity  $\omega^{(0)} \in \Lambda^0(\Omega)$ , velocity flux  $u^{(1)} \in \Lambda^1(\Omega)$ , and pressure  $p^{(2)} \in \Lambda^2(\Omega)$  components of the Stokes problem, given by

$$\omega^{(0)} = \omega(\mathbf{x}) = -4\pi \sin(2\pi x) \sin(2\pi y), \quad (9.6.1b)$$

$$\begin{aligned} u^{(1)} &= -v(\mathbf{x}) dx + u(\mathbf{x}) dy \\ &= -(\cos(2\pi x) \sin(2\pi y)) dx + (-\sin(2\pi x) \cos(2\pi y)) dy, \end{aligned} \quad (9.6.1c)$$

$$p^{(2)} = p(\mathbf{x}) dx \wedge dy = (\sin(\pi x) \sin(\pi y)) dx \wedge dy. \quad (9.6.1d)$$

This testcase was discussed before in [77, 150]. Calculations were performed on both a Cartesian as well as a curvilinear mesh as shown in Figure 9.1. The map,  $(x, y) = \Phi(\xi, \eta)$ , used for the curved mesh is given by

$$x(\xi, \eta) = \frac{1}{2} + \frac{1}{2} (\xi + \frac{1}{5} \sin(\pi\xi) \sin(\pi\eta)), \quad (9.6.2a)$$

$$y(\xi, \eta) = \frac{1}{2} + \frac{1}{2} (\eta + \frac{1}{5} \sin(\pi\xi) \sin(\pi\eta)). \quad (9.6.2b)$$

Figure 9.2 shows the  $h$ -convergence and Figure 9.3 shows the  $p$ -convergence of the vorticity  $\omega_h^{(0)} \in \Lambda_h^0(Q; C_0)$ , velocity  $u_h^{(1)} \in \Lambda_h^1(Q; C_1)$  and pressure  $p_h^{(2)} \in \Lambda_h^2(Q; C_2)$ . For both figures, the results of the top row are obtained on Cartesian meshes and the results depicted underneath are obtained on curvilinear meshes. The errors for the vorticity and velocity are both measured in the  $L^2\Lambda^k$ - and  $H\Lambda^k$ -norm, i.e.  $\|\omega - \omega_h\|_{L^2\Lambda^0}$ ,  $\|\omega - \omega_h\|_{H\Lambda^0}$ , and  $\|u - u_h\|_{L^2\Lambda^1}$ ,  $\|u - u_h\|_{H\Lambda^1}$ , respectively. Because the divergence-free constraint is satisfied pointwise, the norm  $\|d(u - u_h)\|_{L^2\Lambda^2}$  is zero or machine precision, see Figure 9.4, and so the  $H\Lambda^1$ -norm is equal to the  $L^2\Lambda^1$ -norm of

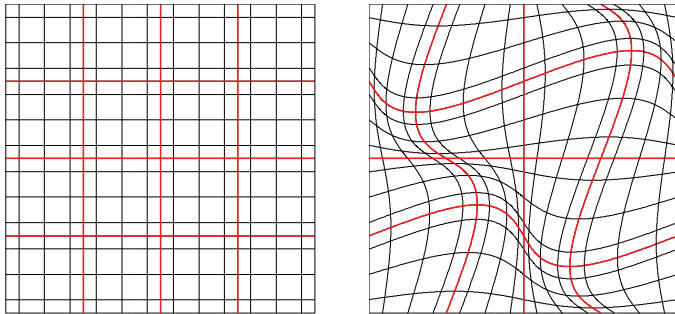


Figure 9.1: Examples of a Cartesian and a curvilinear mesh used in the convergence analysis. The meshes shown consist of  $4 \times 4$  spectral elements, with for each element,  $N = 4$ . The element boundaries are indicated in red.

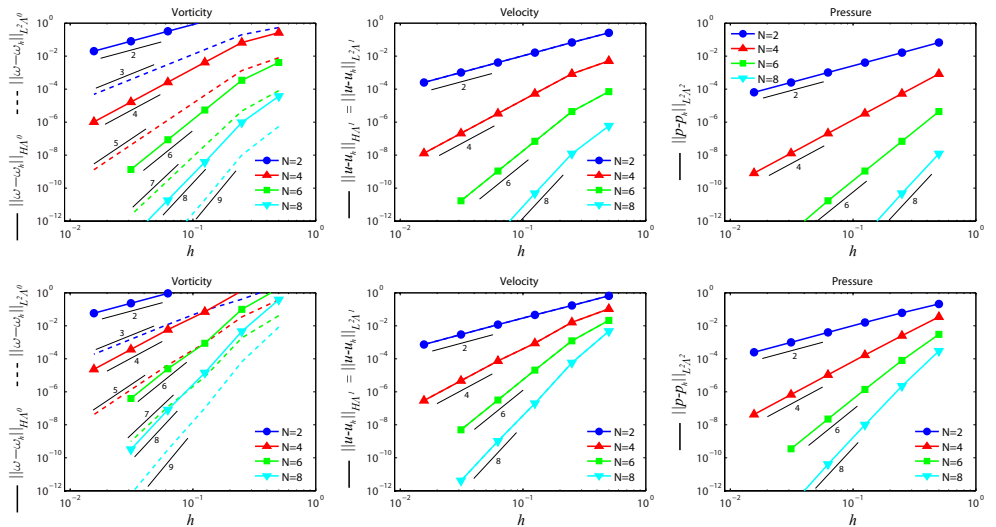


Figure 9.2: Vorticity, velocity and pressure  $h$ -convergence results of problem (9.6.1). Results in the top row correspond to Cartesian meshes, results in the bottom row are obtained on curvilinear meshes. All variables are tested on meshes with  $N = 2, 4, 6$  and  $8$ .

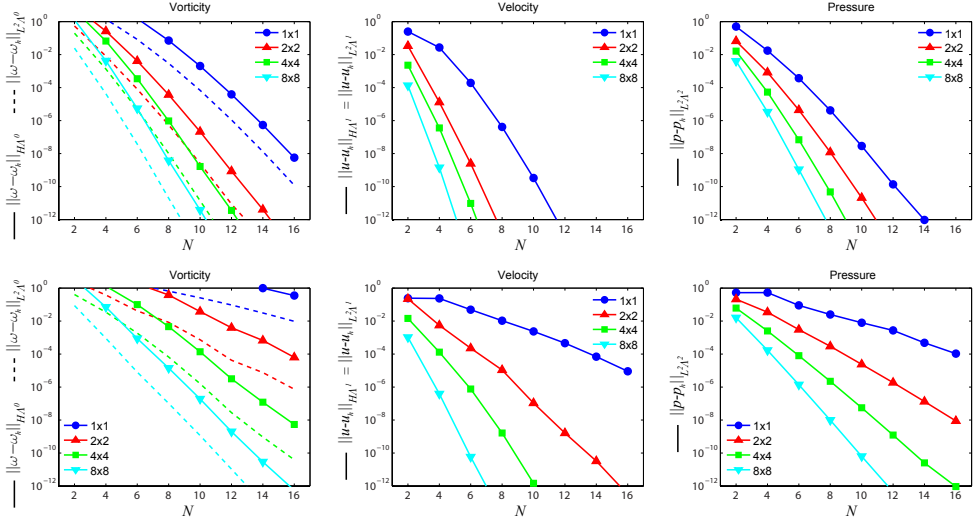


Figure 9.3: Vorticity, velocity and pressure  $p$ -convergence results of problem (9.6.1). Results in the top row correspond to Cartesian meshes, results in the bottom row are obtained on curvilinear meshes. All variables are tested on meshes with  $1 \times 1$ ,  $2 \times 2$ ,  $4 \times 4$  and  $8 \times 8$  spectral elements.

the velocity, i.e.,  $\|u - u_h\|_{H\Lambda^1} = \|u - u_h\|_{L^2\Lambda^1}$ . This does not hold for the vorticity, since  $d\omega^{(0)} \in \Lambda_h^1(\mathcal{Q}; C_1)$  is again a function of sine and cosine functions. The norm  $\|\mathbf{d}(\omega - \omega_h)\|_{L^2\Lambda^1}$  converges one order slower than  $\|\omega - \omega_h\|_{L^2\Lambda^0}$ . More details on the convergence behavior can be found in Section 9.7.

In Figure 9.2 the slope of the convergence rates are added which shows that  $h$ -convergence rates are equal to the  $h$ -convergence rates of the interpolation error (9.5), on both Cartesian as well as curvilinear meshes. Figure 9.3 shows that exponential convergence rates are obtained on both types of meshes.

## 9.6.2 Lid-driven cavity Stokes

For many years, the lid-driven cavity flow was considered as one of the classical benchmark cases for the assessment of numerical methods and the verification of incompressible (Navier)-Stokes codes. The standard lid-driven cavity test case deals with a flow in a unit-square box with three solid boundaries and moving lid as the top boundary, moving with constant velocity equal to one to the right. Because of the discontinuities of the velocity in the two upper corners, the solution becomes singular at these corners, where both vorticity and pressure become infinite. Especially these singularities make the lid-driven cavity problem a challenging test case. The body force  $f$  and source term  $g$  are zero here.

For this test case a non-uniform  $6 \times 6$  Cartesian spectral element mesh is used. Each spectral element consists of a Gauss-Lobatto mesh for  $N = 6$ , see Figure 9.5. The solutions of the vorticity, velocity, pressure and stream function are shown in

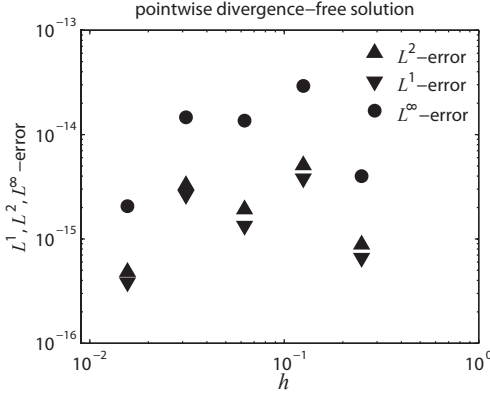


Figure 9.4:  $L^1$ ,  $L^2$  and  $L^\infty$ -error of  $\operatorname{div} u$  on the Cartesian mesh for discontinuous piecewise linear functions,  $N = 2$ .

Figure 9.5. Also shown in Figure 9.5 is a plot of the divergence of velocity. It confirms a pointwise divergence-free solution up to machine precision. The results are in perfect agreement with those in [159].

Because in the mixed mimetic spectral element method no velocity unknowns are located at the upper corners – only velocity flux *through* edges is considered –, no special treatment is needed for the corner singularities, in contrast to many nodal finite-difference, finite-element and spectral element methods, [29, 65, 147, 149]. This is due to the finite-volume like structure of the method, as explained in the Chapter 5 on algebraic topology.

In Figure 9.6 the centerline velocities are plotted. Three different configurations are used, based on the same cell complex consisting of  $9 \times 9$  2-cells:

- left:  $9 \times 9$  spectral elements with  $N = 1$ , resulting in piecewise constant approximations along the centerlines,
- middle:  $3 \times 3$  spectral elements with  $N = 3$ , resulting in piecewise quadratic approximations along the centerlines,
- right: One global spectral element with  $N = 9$ , resulting in 8<sup>th</sup> order polynomial approximations along the centerlines.

Despite the low resolution, all approximations are in good agreement with those in [159].

Because of the tensor-product construction of discrete unknowns and basis functions, an extension to three dimensions is straightforward. A 3D lid-driven cavity is of interest because it not only contains corner singularities, but also line singularities. The left plot in Figure 9.7 shows slices of the magnitude of the velocity field in a three dimensional lid-driven cavity Stokes problem, obtained on a  $2 \times 2 \times 2$  element mesh with  $N = 8$ . The slices are taken at 10%, 50% and 90% of the y-axis. The right plot in Figure 9.7 shows slices of divergence of the velocity field. The solution at the symmetry plane coincides with the 2D results in Figure 9.5. It confirms that also in

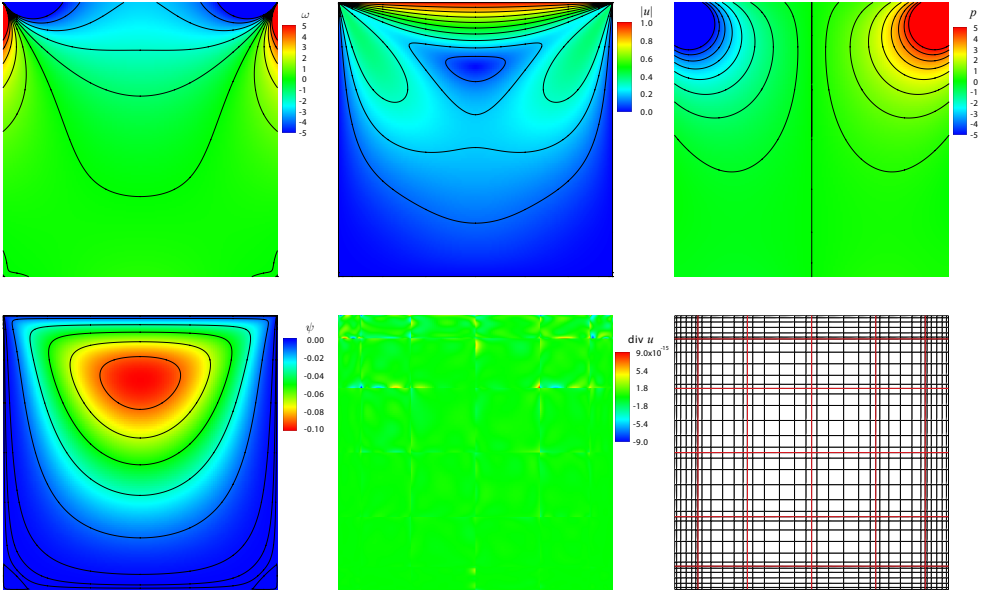


Figure 9.5: Lid-driven cavity Stokes problem results. The top row from left to right shows the solution of the vorticity, velocity magnitude and pressure fields. The bottom row shows from left to right the solution of the stream function, the divergence of the velocity field and the  $6 \times 6$ ,  $N = 6$  mesh.

three dimensions the mixed mimetic spectral element method leads to an accurate result with a pointwise divergence-free solution.

The corner singularities can be made even more severe by sharpening the corners, as happens for a lid-driven cavity problem in a triangle. Figure 9.8 shows the vorticity field and the velocity magnitude. On top of the velocity plot, stream function contours are plotted. The solutions are constructed on a 9 spectral element mesh with  $N = 9$ . A close-up of the stream function contours is shown in the rightmost plot in Figure 9.8. The stream function contours nicely show the first three Moffatt eddies [127].

### 9.6.3 Flow over a cylinder

This section considers the flow around a cylinder moving with constant velocity to the left, as defined in [43]. This testcase is mostly considered in the context of least-squares finite and spectral element methods, due to their moderate performance in case of large contraction regions, [43, 54, 151], mainly in terms of conservation of mass.

The cylinder moves with unit velocity along the centerline of a narrow channel. The computational domain is defined as a rectangular box minus the cylinder, as shown in Figure 9.9. Also visible in this figure are the 12 spectral elements in which the computational domain is divided. A transfinite mapping, [80], is used to define the curved elements around the cylinder. Velocity boundary conditions of  $(u, v) =$

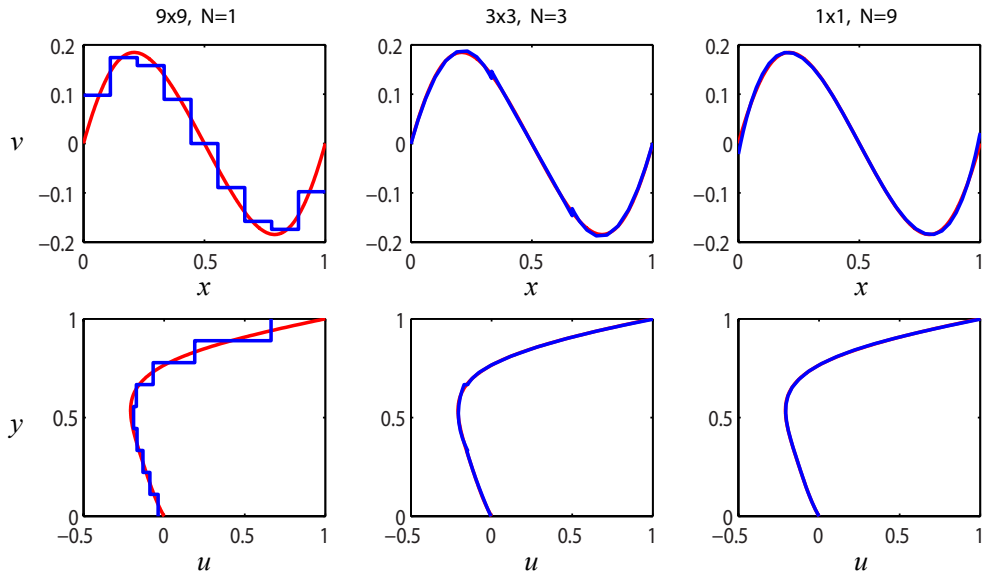


Figure 9.6: Horizontal (top) and vertical (bottom) centerline velocities are shown in blue for a very coarse mesh,  $9 \times 9$  2-cells. From left to right the  $9 \times 9$  2-cells are used in:  $9 \times 9$  zeroth-order elements,  $3 \times 3$  second-order elements and one eight-order element. In red the reference solution from [159].

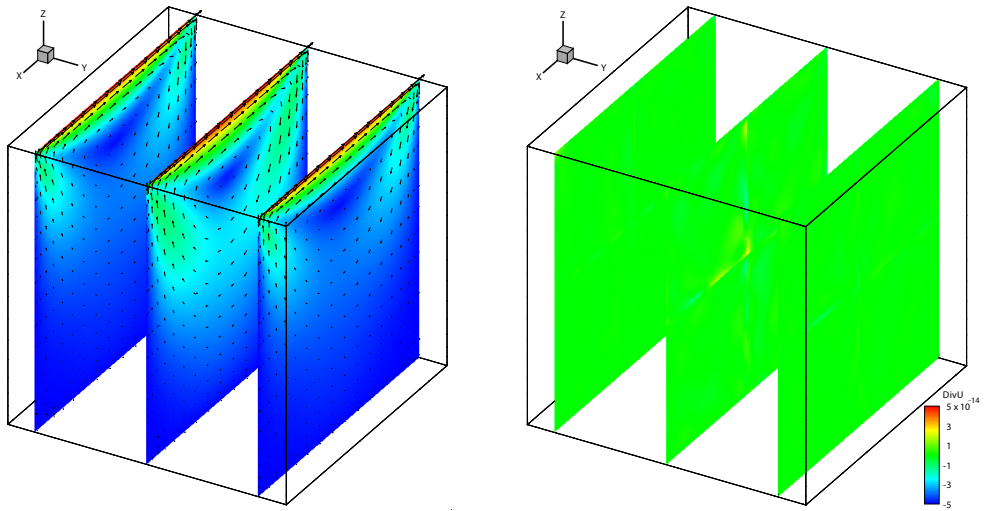


Figure 9.7: Left: slices of magnitude of the velocity field of a three dimensional lid-driven cavity Stokes problem obtained on a  $2 \times 2 \times 2$  element mesh with  $N = 8$ . Right: slices of the divergence of velocity. Is confirms a divergence-free velocity field.

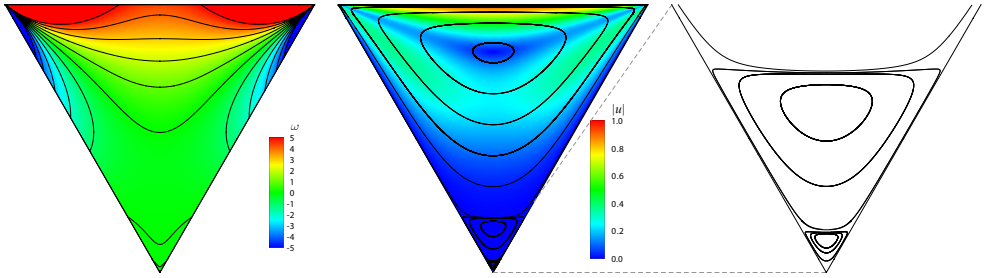


Figure 9.8: Lid-driven cavity Stokes flow in a triangle. Left the vorticity field, in the middle the velocity magnitude with stream function contours on top, and right the stream function contours of a close-up of the bottom corner, revealing the second and third Moffatt eddies.

$(1, 0)$  are prescribed on the outer boundary and no-slip,  $(u, v) = (0, 0)$ , is prescribed along the boundary of the cylinder. Solution of the vorticity, velocity magnitude and pressure, together with streamlines are shown in Figure 9.9. The results are in perfect agreement with the high resolution solutions obtained in [43, 107, 149]. At moderate resolution, as is used in Figure 9.9 the MMSEM solution outperforms the cited solutions, as will also be shown later in this section.

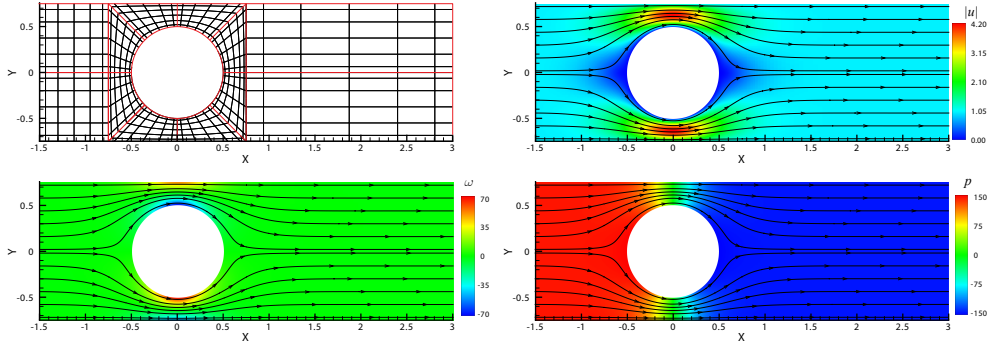


Figure 9.9: Spectral element mesh (top left), magnitude of velocity (top right), vorticity (bottom left) and pressure (bottom right) for flow around a moving cylinder, on a 12 element,  $N = 6$  mesh.

Next consider a control volume  $\Omega_c$  consisting of the 6 elements in the domain  $-1.5 \leq x \leq 0$ ,  $0.75 \leq y \leq 0.75$ . The control volume is chosen such that the ratio in size between inflow and outflow boundary is maximal. In this control volume conservation of mass should hold. Conservation of mass is expressed, by means of generalized Stokes theorem (4.6.4), in terms of a boundary integral as

$$0 = \int_{\Omega_c} du_h^{(1)} \stackrel{(4.6.4)}{=} \int_{\partial\Omega_c} u_h^{(1)}. \quad (9.6.3)$$

From Section 9.4.1 and the results of the previous test cases we know that the

solution of the velocity is divergence-free throughout the domain, independent of the chosen control volume. In Figure 9.10 a comparison is made for the horizontal velocity component  $u$  at the smallest cross-section above the cylinder, i.e.  $x = 0$ ,  $0.5 \leq y \leq 0.75$ , between the recently developed LSSCM, [107], and our MMSEM method for  $N = 3, 6, 12$ . Both methods use a similar mesh of 12 spectral elements. As can be seen from this figure, the MMSEM method performs already very well for  $N = 3$ , i.e. quadratic polynomial, where the LSSCM still fails for  $N = 6$ , i.e. sixth order polynomial. This is a direct consequence of the pointwise divergence-free discretization.

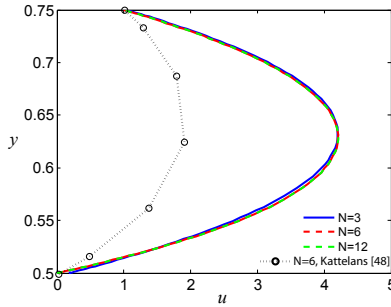


Figure 9.10: Horizontal velocity at smallest cross-section above the cylinder, on a 12 element mesh, for  $N = 3, 6, 12$ . **REFERENTIE LABEL IN FIGUUR OP HET LAATST PAS AANPASSEN!!!**

## 9.7 A priori error estimates for all admissible boundary conditions

The above obtained results show the qualitative performance of the MMSEM. Next we want to measure the quantitative performance of the method. This will be done in two stages. First, a priori error estimates will be derived. These estimates are valid for all admissible boundary conditions formulated in Section 9.2 and for both affine and non-affine mappings. Second, numerical results are performed to confirm the estimated optimal rates of convergence.

sectionError estimates Next consider the finite dimensional problem: find  $(\omega_h, u_h, p_h) \in \{W_h \times V_h \times Q_h\}$ , given  $f \in L^2 \Lambda^{n-1}(\Omega)$  and  $g \in L^2 \Lambda^n$  and boundary conditions in (9.2.2), for all  $(\tau_h, v_h, q_h) \in \{W_h \times V_h \times Q_h\}$ , such that

$$a(\tau_h, \omega_h) - c(\tau_h, u_h) = h(\tau_h), \quad \forall \tau_h \in W_h, \quad (9.7.1a)$$

$$e(v_h, u_h) + c(\omega_h, v_h) + b(v_h, p_h) = f(v_h), \quad \forall v_h \in V_h, \quad (9.7.1b)$$

$$b(u_h, q_h) = g(q_h). \quad \forall q_h \in Q_h. \quad (9.7.1c)$$

The following theorem gives the a priori error estimates of this problem when using the compatible spectral discretization method described in the previous section. Corollary 14 showed that we have  $Z_{W_h} \subset \mathcal{Z}_W$  and  $Z_{V_h} \subset \mathcal{Z}_V$ . From this it follows that we

have compatible finite dimensional subspaces:  $W_h \subset W$ ,  $V_h = dW_h \oplus d^*Q_h \subset V$  and  $Q_h = dV_h \subset Q$ . The derivations of the error estimates are based on the methodology of [37]. The proofs are given in the subsequent propositions.

**Theorem 8 (Error estimates).** *Let  $(\omega, u, p)$  be the solution of the continuous problem given in (9.3.4) or (9.3.6) and  $(\omega_h, u_h, p_h)$  the solution of the finite dimensional problem in (9.7.1). The continuous problem is well-posed by Propositions 34 and 35 and the finite dimensional problem is well-posed by Theorem 7 and Propositions 29 and 30. Furthermore, from Corollary 14 we have that for the compatible spectral discretization method,  $Z_{W_h} \subset \mathcal{Z}_W$  and  $Z_{V_h} \subset \mathcal{Z}_V$ . Then the following a priori error estimates for the VVP formulation of the Stokes problem hold:*

$$\|\omega - \omega_h\|_W \leq \left(1 + \frac{c_a}{\alpha_h}\right) \left(1 + \frac{c_c}{\gamma_h}\right) \inf_{\tau_h \in W_h} \|\omega - \tau_h\|_W, \quad (9.7.2)$$

$$\|u - u_h\|_V \leq \left(1 + \frac{c_c}{\gamma_h}\right) \left(1 + \frac{c_b}{\beta_h}\right) \inf_{v_h \in V_h} \|u - v_h\|_V + \frac{c_a}{\gamma_h} \left(1 + \frac{c_a}{\alpha_h}\right) \left(1 + \frac{c_c}{\gamma_h}\right) \inf_{\tau_h \in W_h} \|\omega - \tau_h\|_W, \quad (9.7.3)$$

$$\begin{aligned} \|p - p_h\|_Q &\leq \left(1 + \frac{c_b}{\beta_h}\right) \inf_{q_h \in Q_h} \|p - q_h\|_Q + \frac{c_e}{\beta_h} \left(1 + \frac{c_c}{\gamma_h}\right) \left(1 + \frac{c_b}{\beta_h}\right) \inf_{v_h \in V_h} \|u - v_h\|_V \\ &\quad + \left(\frac{c_a}{\gamma_h} + \frac{c_c}{\beta_h}\right) \left(1 + \frac{c_a}{\alpha_h}\right) \left(1 + \frac{c_c}{\gamma_h}\right) \inf_{\tau_h \in W_h} \|\omega - \tau_h\|_W. \end{aligned} \quad (9.7.4)$$

*Proof.* The proof of this Theorem will be given in a series of Propositions 36 to 39.  $\square$

**Proposition 36 (Vorticity error bound).** *Let  $\sigma_h \in Z_{W_h}^\perp$ , the error for vorticity is bounded by*

$$\|\omega - \omega_h\|_W \leq \left(1 + \frac{c_a}{\alpha_h}\right) \inf_{\sigma_h \in Z_{W_h}^\perp} \|\omega - \sigma_h\|_W. \quad (9.7.5)$$

*Proof.* Subtract the velocity-vorticity relation in the finite dimensional problem (9.7.1a) from that of the continuous problem (9.3.6a), we get

$$a(\tau_h, \omega - \omega_h) - c(\tau_h, u - u_h) = 0, \quad \forall \tau_h \in Z_{W_h} \subset \mathcal{Z}_W.$$

Bound  $\sigma_h - \omega_h \in Z_{W_h}$  using inf-sup condition (9.3.10), we get

$$\begin{aligned} \alpha_h \|\sigma_h - \omega_h\|_W &\leq \sup_{\tau_h \in Z_{W_h}} \frac{a(\tau_h, \sigma_h - \omega_h)}{\|\tau_h\|_W} \\ &= \sup_{\tau_h \in Z_{W_h}} \frac{a(\tau_h, \sigma_h - \omega) + a(\tau_h, \omega - \omega_h)}{\|\tau_h\|_W} \\ &= \sup_{\tau_h \in Z_{W_h}} \frac{a(\tau_h, \sigma_h - \omega) + c(\tau_h, u - u_h)}{\|\tau_h\|_W}. \end{aligned}$$

The last term vanishes since  $\tau_h \in Z_{W_h}$  and  $Z_{W_h} \subset \mathcal{Z}_W$ , hence  $\alpha_h \|\sigma_h - \omega_h\|_W \leq c_a \|\omega - \sigma_h\|_W$ . By the triangle inequality and the infimum over all  $\sigma_h \in Z_{W_h}^\perp$  we obtain (9.7.5).  $\square$

---

**Proposition 37 (Velocity error bound).** Let  $s_h \in Z_{V_h}^\perp$ , the error for velocity is bounded by

$$\|u - u_h\|_V \leq \left(1 + \frac{c_c}{\gamma_h}\right) \inf_{s_h \in Z_{V_h}^\perp} \|u - s_h\|_V + \frac{c_a}{\gamma_h} \left(1 + \frac{c_a}{\alpha_h}\right) \inf_{\sigma_h \in Z_{W_h}^\perp} \|\omega - \sigma_h\|_W. \quad (9.7.6)$$

*Proof.* Use the inf-sup condition (9.3.11) to bound  $s_h - u_h \in \mathcal{Z}_V$ ,

$$\begin{aligned} \gamma_h \|s_h - u_h\|_V &\leq \sup_{\tau_h \in \bar{Z}_{W_h}} \frac{c(\tau_h, s_h - u_h)}{\|\tau_h\|_W} \\ &= \sup_{\tau_h \in \bar{Z}_{W_h}} \frac{c(\tau_h, s_h - u) + c(\tau_h, u - u_h)}{\|\tau_h\|_W} \\ &= \sup_{\tau_h \in \bar{Z}_{W_h}} \frac{c(\tau_h, s_h - u) + a(\tau_h, \omega - \omega_h)}{\|\tau_h\|_W} \\ &\leq c_c \|u - s_h\|_V + c_a \|\omega - \omega_h\|_W. \end{aligned}$$

By triangle inequality, estimate (9.7.5) and the infimum over all  $s_h \in Z_{V_h}^\perp$ , we obtain (9.7.6).  $\square$

**Proposition 38 (Pressure error bound).** The error for pressure is bounded by

$$\begin{aligned} \|p - p_h\|_Q &\leq \left(1 + \frac{c_b}{\beta_h}\right) \inf_{q_h \in Q_h} \|p - q_h\|_Q + \frac{c_e}{\beta_h} \left(1 + \frac{c_c}{\gamma_h}\right) \inf_{s_h \in Z_{V_h}^\perp} \|u - s_h\|_V \\ &\quad + \left(\frac{c_a}{\gamma_h} + \frac{c_c}{\beta_h}\right) \left(1 + \frac{c_a}{\alpha_h}\right) \inf_{\sigma_h \in Z_{W_h}^\perp} \|\omega - \sigma_h\|_W. \end{aligned} \quad (9.7.7)$$

*Proof.* Subtract (9.7.1b) from (9.3.6b), we get

$$c(\omega - \omega_h, v_h) + e(v_h, u - u_h) + b(v_h, p - p_h) = 0, \quad \forall v_h \in V_h.$$

So for  $q_h \in Q_h$  we have

$$b(v_h, q_h - p_h) = -c(\omega - \omega_h, v_h) - e(v_h, u - u_h) - b(v_h, p - q_h).$$

Use this and the inf-sup condition (9.3.13) to bound  $q_h - p_h \in Q_h$ ,

$$\begin{aligned} \beta_h \|q_h - p_h\|_Q &\leq \sup_{v_h \in V_h} \frac{b(v_h, q_h - p_h)}{\|v_h\|_V} \\ &= \sup_{v_h \in V_h} \frac{-c(\omega - \omega_h, v_h) - e(v_h, u - u_h) - b(v_h, p - q_h)}{\|v_h\|_V} \\ &\leq c_c \|\omega - \omega_h\|_W + c_e \|u - u_h\|_V + c_b \|p - q_h\|_Q. \end{aligned}$$

By triangle inequality, estimates (9.7.5) and (9.7.6), and the infimum over all  $q_h \in Q_h$ , we obtain (9.7.7).  $\square$

Next we replace the infimums over  $\sigma_h \in Z_{W_h}^\perp$  and  $s_h \in Z_{V_h}^\perp$  by best approximation errors.

---

**Proposition 39.** *The terms  $\inf_{\sigma_h \in Z_{W_h}^\perp} \|\omega - \sigma_h\|_W$  and  $\inf_{s_h \in Z_{V_h}^\perp} \|u - s_h\|_V$  are bounded by the best approximation estimates  $\inf_{\tau_h \in W_h} \|\omega - \tau_h\|_W$  and  $\inf_{v_h \in V_h} \|u - v_h\|_V$ , using the inf-sup conditions (9.3.13) and (9.3.11), as*

$$\inf_{\sigma_h \in Z_{W_h}^\perp} \|\omega - \sigma_h\|_W \leq \left(1 + \frac{c_c}{\gamma_h}\right) \inf_{\tau_h \in W_h} \|\omega - \tau_h\|_W, \quad (9.7.8)$$

$$\inf_{s_h \in Z_{V_h}^\perp} \|u - s_h\|_V \leq \left(1 + \frac{c_b}{\beta_h}\right) \inf_{v_h \in V_h} \|u - v_h\|_V. \quad (9.7.9)$$

*Proof.* Take  $\tau_h \in W_h$ , then there exists a  $\kappa_h \in W_h$  such that

$$c(\kappa_h, v_{Z_h}) = c(\omega - \tau_h, v_{Z_h}), \quad \forall v_{Z_h} \in Z_{V_h}.$$

This is equivalent to

$$c(\kappa_h + \tau_h, v_{Z_h}) = c(\omega, v_{Z_h}) = f(v_{Z_h}), \quad \forall v_{Z_h} \in Z_{V_h},$$

which shows that  $\sigma_h = \kappa_h + \tau_h \in Z_{W_h}^\perp$ . We can bound  $\|\kappa_h\|_W$  using the discrete inf-sup condition as follows

$$\gamma_h \|\kappa_h\|_W \leq \sup_{v \in Z_{V_h}} \frac{c(\kappa_h, v)}{\|v\|_V} = \sup_{v \in Z_{V_h}} \frac{c(\omega - \tau_h, v)}{\|v\|_V} \leq c_c \|\omega - \tau_h\|_V.$$

By triangle inequality and since  $\tau_h \in W_h$  was arbitrary, we find (9.7.8). A similar proof holds for (9.7.9) (see also [37], Proposition 2.5).  $\square$

Additionally, following section 7.7.6 in [17], we have the following  $L^2 \Lambda^k(\Omega)$  error estimates for the curl of vorticity and divergence of velocity,

**Proposition 40.** *The errors of the curl of vorticity and divergence of velocity are bounded by their best approximation estimates,*

$$\|d(\omega - \omega_h)\|_{L^2 \Lambda^{n-1}} \leq \inf_{\tau_h \in W_h} \|d(\omega - \tau_h)\|_{L^2 \Lambda^{n-1}}, \quad (9.7.10)$$

$$\|d(u - u_h)\|_{L^2 \Lambda^n} \leq \inf_{v_h \in V_h} \|d(u - v_h)\|_{L^2 \Lambda^n}. \quad (9.7.11)$$

*Proof.* Choose  $v = v_{Z_h} \in Z_{V_h}$  in (9.3.6b) and (9.7.1b) and subtract these. Set  $v_{Z_h} = d\tau_h$ , this gives the orthogonality relation

$$(d(\omega - \omega_h), d\tau_h)_\Omega = 0, \quad \forall \tau_h \in W_h.$$

Substitute this into the following Cauchy-Schwarz inequality,

$$\begin{aligned} \|d(\omega - \omega_h)\|_{L^2 \Lambda^{n-1}}^2 &= (d(\omega - \omega_h), d(\omega - \tau_h))_\Omega \\ &\leq \|d(\omega - \omega_h)\|_{L^2 \Lambda^{n-1}} \|d(\omega - \tau_h)\|_{L^2 \Lambda^{n-1}}, \quad \forall \tau_h \in W_h, \end{aligned}$$

and (9.7.10) follows. Next choose  $q_h = dv_h \in Q_h$  in (9.3.6c) and (9.7.1c) and subtract these. Then (9.7.11) follows again from the Cauchy-Schwarz inequality.  $\square$

---

Because the projections of respectively  $\omega$ ,  $u$ , and  $p$ , belong to the finite dimensional subspaces  $W_h \subset W$ ,  $V_h \subset V$  and  $Q_h \subset Q$ , the best approximation errors can be bounded using the interpolation errors,

$$\inf_{\tau_h \in W_h} \|\omega - \tau_h\|_W \leq \|\omega - \pi_h \omega\|_W, \quad \inf_{v_h \in V_h} \|u - v_h\|_V \leq \|u - \pi_h u\|_V, \quad \inf_{q_h \in Q_h} \|p - q_h\|_Q \leq \|p - \pi_h p\|_Q,$$

and therefore we obtain the following optimal a priori error estimates,

$$\|\omega - \omega_h\|_W = \mathcal{O}(h^N), \quad \|u - u_h\|_V = \mathcal{O}(h^N), \quad \|p - p_h\|_Q = \mathcal{O}(h^N). \quad (9.7.12)$$

So the convergence rates for the approximations are equal to those of the interpolations, (??), (??), thus we obtained optimal convergence. The error estimates were obtained independent of the chosen types of boundary conditions.

**Remark 37.** *In contrast to [5, 60] and [17], Table 7.5, where Raviart-Thomas elements were used, the proposed compatible method has provable optimal convergence also with standard velocity boundary conditions and with non-affine mappings.*

## 9.8 Numerical Results II

Now that the higher-order compatible discretization method and its a priori error estimates are derived, we perform a series of test problems to show optimal convergence behavior of the mixed mimetic spectral element method. Additionally, we put emphasis on showing the convergence behavior in case of various boundary conditions and in case of curvilinear meshes. In all cases we obtain optimal convergence rates.

The first testcase originates from a recent paper by Arnold et. al. [5], where suboptimal convergence is shown for no-slip (normal velocity - tangential velocity) boundary conditions in Stokes problems, when using Raviart-Thomas elements [154]. Since Raviart-Thomas elements are the most popular  $H(\text{div}, \Omega)$  conforming elements, we compare our method to these results. Figure 9.11 shows the result of the Stokes problem on  $\Omega = [0, 1]^2$  with coordinates  $\mathbf{x} := (x, y)$ , where  $\Gamma = \Gamma_1$ , i.e. with normal velocity - tangential velocity boundary conditions. The velocity and pressure fields are given by

$$\begin{aligned} u^{(1)} &= -v(\mathbf{x}) dx + u(\mathbf{x}) dy \\ &= -(2y^2(y-1)^2 x(2x-1)(x-1)) dx + (-2x^2(x-1)^2 y(2y-1)(y-1)) dy, \end{aligned} \quad (9.8.1)$$

$$p^{(2)} = p(\mathbf{x}) dx \wedge dy = ((x - \frac{1}{2})^5 + (y - \frac{1}{2})^5) dx \wedge dy. \quad (9.8.2)$$

The mimetic spectral element discretization shows optimal convergence, as was expected from the analysis in the previous section. The Raviart-Thomas element discretization only obtains optimal convergence for the velocity, while the pressure and vorticity only shows suboptimal rates of convergence. For the pressure a difference of  $\frac{1}{2}$  is noticed in the rate of convergence and for vorticity and the curl of vorticity a difference in rate of convergence of  $\frac{3}{2}$  is revealed. This suboptimality was proven in [5]. This test case shows that the mimetic spectral elements outperforms the Raviart-Thomas elements on quadrilateral meshes with velocity boundary conditions. All

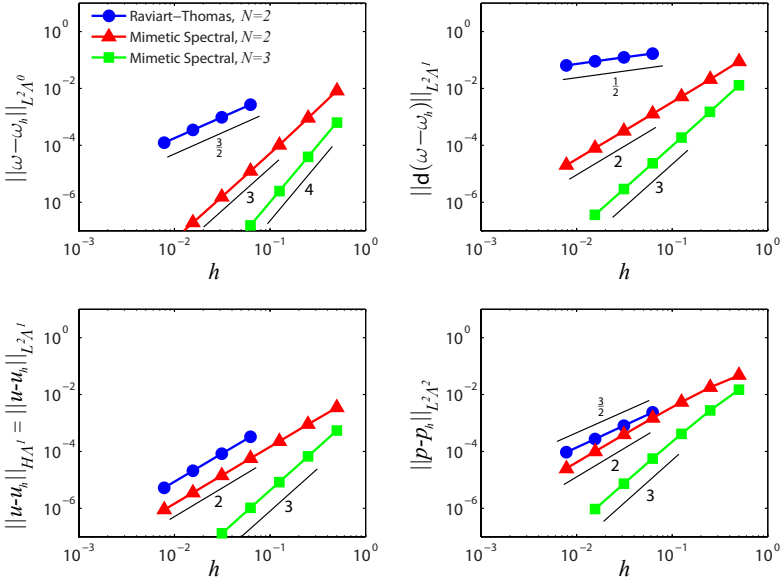


Figure 9.11: Comparison of the  $h$ -convergence between Raviart-Thomas and Mimetic spectral element projections for the 2D Stokes problem with normal velocity - tangential velocity boundary conditions.

results in this problem were obtained on the same quadrilateral mesh of  $2^n \times 2^n$  subsquares,  $n = 1, 2, 3, 4, \dots$  just like the reference solutions from [5]. The error in divergence of velocity is not shown here for the Stokes problem, because the method is pointwise divergence-free up to machine precision, as shown already in Section 9.6.

We would like to remark is that the results shown in Figure 9.11 are independent of the kind of boundary conditions used. Table 9.2 shows the results of vorticity for all types of admissible boundary conditions.

normal velocity tangential velocity	tangential velocity pressure	vorticity normal velocity	vorticity pressure	convergence rate
1.0280e-04	1.0109e-04	1.0030e-04	1.0035e-04	3.14
1.2445e-05	1.2410e-05	1.2364e-05	1.2375e-05	3.05
1.5424e-06	1.5426e-06	1.5399e-06	1.5416e-06	3.01
1.9238e-07	1.9247e-07	1.9230e-07	1.9255e-07	3.00
2.4035e-08	2.4042e-08	2.4032e-08	2.4065e-08	3.00

Table 9.2: This table shows the vorticity error  $\|\omega - \omega_h\|_{L^2\Lambda^0}$  obtained using the four types of boundary conditions given in (9.2.2). The results are obtained on an uniform Cartesian mesh with  $N = 2$  and  $h = \frac{1}{8}, \frac{1}{16}, \frac{1}{32}, \frac{1}{64}, \frac{1}{128}$ . All four cases show third order convergence.

The last test case reveals the optimal convergence in case of higher-order approximation on curvilinear quadrilateral meshes for all admissible types of boundary con-

---

ditions. The manufactured solution Stokes problem is given on a curvilinear domain, defined by the mapping  $(x, y) = \Phi(\xi, \eta)$ ,

$$x(\xi, \eta) = \frac{1}{2} + \frac{1}{2} (\xi + \frac{1}{10} \cos(2\pi\xi) \sin(2\pi\eta)), \quad (9.8.3a)$$

$$y(\xi, \eta) = \frac{1}{2} + \frac{1}{2} (\eta + \frac{1}{10} \sin(2\pi\xi) \cos(2\pi\eta)). \quad (9.8.3b)$$

A  $6 \times 6$  element  $N = 6$  mesh is show in Figure 9.12. Each side of the domain has a different type of boundary condition, so  $\Gamma = \Gamma_1 \cup \Gamma_2 \cup \Gamma_3 \cup \Gamma_4$ , as shown in the same figure and listed in (9.2.2). The solutions of vorticity  $\omega \in \Lambda^0(\Omega)$ , velocity  $u \in \Lambda^1(\Omega)$  and pressure  $p \in \Lambda^2(\Omega)$  are given by

$$\omega^{(0)} = \frac{3}{2}\pi \sin(\frac{3}{2}\pi x) \sin(\frac{3}{2}\pi y), \quad (9.8.4a)$$

$$u^{(1)} = -(\cos(\frac{3}{2}\pi x) \sin(\frac{3}{2}\pi y)) \, dx + (2 \sin(\frac{3}{2}\pi x) \cos(\frac{3}{2}\pi y)) \, dy, \quad (9.8.4b)$$

$$p^{(2)} = (\sin(\pi x) \sin(\pi y)) \, dx \wedge dy. \quad (9.8.4c)$$

They lead to nonzero body force  $f \in \Lambda^1(\Omega)$  and mass source  $g \in \Lambda^2(\Omega)$ . Figure 9.12 shows the convergence of the vorticity  $\omega_h \in \Lambda_h^0(Q; C_0)$ , velocity  $u_h \in \Lambda_h^1(Q; C_1)$  and pressure  $p_h \in \Lambda_h^2(Q; C_2)$ . The errors for the vorticity and velocity are measured in the  $H\Lambda^k$ -norm, i.e.  $\|\omega - \omega_h\|_{H\Lambda^0}$ , and  $\|u - u_h\|_{H\Lambda^1}$ , respectively, and the error of the pressure is given in the  $L^2\Lambda^2$ -norm. In Figure 9.12 convergence rates are added which show the *optimal h*-convergence behavior of the Stokes problem on a curvilinear domain with curvilinear grid and all four types of boundary conditions.

## 9.9 Conclusions and future aspects

In this thesis we presented the mixed mimetic spectral element method, applied to the vorticity-velocity-pressure formulation of Stokes model. At the heart lies the generalized Stokes theorem, which relates the boundary operator applied on an oriented geometric objects to the exterior derivative, resembling the vector operators grad, curl and div, and the recently developed higher-order mimetic discretization for quadrilaterals and hexadrals, [115]. The gradient, curl and divergence conforming method results in a point-wise divergence-free discretization of the Stokes problem, as was confirmed by a set of benchmark problems. These results also showed optimal convergence, independent of the type of boundary conditions on orthogonal and curved meshes. More on convergence behavior and error estimates is presented [111]. In the near future we plan to extend the method with structure-preserving *hp*-refinement based on a compatible mortar element method.

## 9.10 Concluding remark

Optimal approximation of the Stokes problem for all admissible boundary conditions essentially hinges on the construction of a conforming discrete Hodge decomposition,  $\Lambda_h^k = \mathcal{Z}_h^k \oplus \mathcal{Z}_h^{k,\perp}$  and a discrete Poicaré inequality, that are based on the bijection of

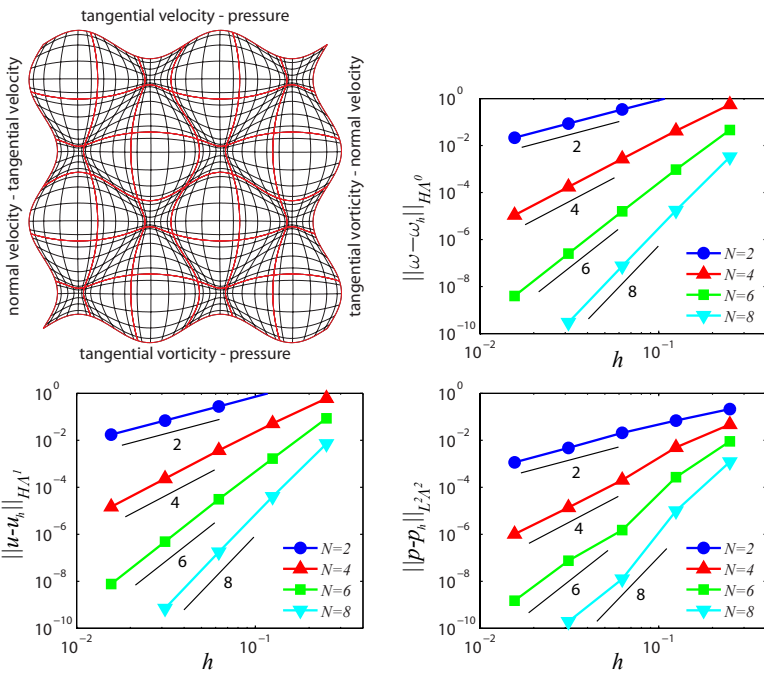


Figure 9.12: Upper left figure show the computational domain with a  $6 \times 6$  element mesh of  $N = 6$ . Furthermore the velocity, vorticity and pressure  $h$ -convergence results are shown of Stokes problem (9.8.4). All variables are tested on grids with  $N = 2, 4, 6$  and 8.

---

the exterior derivative on the conforming subspace,  $d : \mathcal{Z}_h^{k,\perp} \rightarrow \mathcal{B}_h^{k+1}$ . Ensuring these properties result in a compatible discretization method, and relied on the construction of a bounded projection operator,  $\pi_h : \Lambda^k(\Omega) \rightarrow \Lambda_h^k(\Omega; C_k)$ , that commutes with the exterior derivative,  $\pi_h d = \mathcal{I}\delta\mathcal{R} = d\pi_h$ . So the compatibility is based on the bijection of the coboundary operator,  $\delta : Z^{k,\perp} \rightarrow B^{k+1}$ , and the construction of interpolatory basis functions. From this it follows that,  $\mathcal{B}_h^{k+1} \subset \mathcal{B}^{k+1}$ ,  $\mathcal{Z}_h^k \subset \mathcal{Z}^k$  and  $\mathcal{Z}_h^{k,\perp} \subset \mathcal{Z}^{k,\perp}$ . From these properties the rest follows.

For piecewise sufficiently smooth mappings, the optimal convergence rates hold on curvilinear grids as well, since the pullback operator of the map from a curvilinear domain to the Cartesian frame commutes with the projection operator. Any projection (discretization) with these properties will yield similar results as described in this thesis.

To read: Journal of Scientific Computing, <http://www.springeronline.com/journal/10915>, Volume 52, Number 2, August 2012Local Mass Conservation of Stokes Finite Elements, D. Boffi, N. Cavallini, F. Gardini and L. Gastaldi, pp.383-400.



# Part IV

# Towards full Navier-Stokes



# Chapter 10

## Structure-Preserving Convection

### 10.1 Notes Evans

The most popular of these in the finite element community is the skew-symmetric representation [40]. Discretizations of the convection term using the skew-symmetric representation neither produce nor dissipate energy and hence lead to stable numerical methods. Unfortunately, these discretizations do not inherit the conservation structure of the Navier-Stokes equations. Alternatively, provably stable, convergent, and locally-conservative discontinuous Galerkin discretizations have been devised for the steady Navier-Stokes equations in [11, 12], but these discretizations are encumbered with a proliferation of degrees of freedom and are thus largely limited to two spatial dimensions. Hybrid technologies have recently been proposed with the aim of extending the applicability of discontinuous Galerkin methods to larger problem sizes [28, 29].

- 40 T A Zang. On the rotation and skew-symmetric forms for incompressible flow simulations. *Applied Numerical Mathematics*, 7:27-40, 1991.
- 28 R J Labeur and G N Wells. Energy stable and momentum conserving hybrid finite element method for the incompressible Navier-Stokes equations. *SIAM Journal on Scientific Computing*. To appear.
- 29 N C Nguyen, J Peraire, and B Cockburn. An implicit high-order hybridizable discontinuous Galerkin method for the incompressible Navier-Stokes equations. *Journal of Computational Physics*, 230:1147-1170, 2011.

### 10.2 Introduction

This article presents the pure convection model in the language of differential forms. Differential forms offer significant benefits regarding the construction of structure preserving spatial and space-time discretizations.

## 10.3 Convection in differential geometry

Although Chapter 4 showed the majority of notations, definitions and relations in differential geometry, it was limited to solve elliptic problems. In this section the discussion is continued with the introduction of vector fields, the interior product and the Lie derivative. Only the concepts from differential geometry which are relevant for convection will be explained here. Much more can be found in Frankel [71, Section 2.9]

### 10.3.1 Vector field

Let the velocity field  $\vec{v}$  be a smooth vector field defined pointwise tangent to an  $n$ -dimensional manifold  $\Omega$ . The velocity field  $\vec{v}$  is induced by the *flow function*  $\varphi_t(\mathbf{x}) \equiv \varphi(\mathbf{x}, t) : \Omega \times \mathbb{R}^+ \rightarrow \Omega$  that is varying with time  $t$ , a one-parameter group diffeomorphism. The instantaneous flow function represents the collection of flow lines on the manifold  $\Omega$ . The velocity field is related to the flow function by the following expression,

$$\frac{\partial \varphi_t(\mathbf{x})}{\partial t} = \vec{v}(\varphi_t(\mathbf{x})) \quad \text{with} \quad \varphi_0(\mathbf{x}) = \mathbf{x}. \quad (10.3.1)$$

Therefore for each  $t$  and any point in space  $\mathbf{x}$  there exists a *tangent space*,  $T_x\Omega$ , as defined in Section 4.1. That is, one can attach to every point  $\mathbf{x}$  of a differentiable manifold a tangent space, a real vector space which intuitively contains the possible ‘directions’ in which one can tangentially pass through  $\mathbf{x}$ . All the tangent spaces have the same dimension, equal to the dimension of the manifold.

Differential forms contract by the action of a vector field,  $\vec{v}(\mathbf{x}) \in V(\Omega)$ , where  $V(\Omega)$  is the tangent vector space  $V(\Omega) := T_{\mathbf{x}}\Omega$ . The tangent space  $T_{\mathbf{x}}\Omega$  has a dual, the cotangent space  $T_{\mathbf{x}}^*\Omega$ , which we also know as the space of one-forms,  $\Lambda^1(\Omega) := T_{\mathbf{x}}^*\Omega$ . On an  $n$ -dimensional manifold,  $\Omega$ , with coordinate system  $\mathbf{x} := (x^1, x^2, \dots, x^n)$ , we write a vector field  $\vec{v}$  as

$$\vec{v} = v^1(\mathbf{x}) \frac{\partial}{\partial x^1} + v^2(\mathbf{x}) \frac{\partial}{\partial x^2} + \cdots + v^n(\mathbf{x}) \frac{\partial}{\partial x^n}.$$

By the duality between the tangent space and cotangent space, there exists a direct relation between vector fields and 1-forms. This relation is given by the canonical isomorphisms flat,  $\flat$ , and sharp,  $\sharp$ , where  $\flat : T_{\mathbf{x}}\Omega \rightarrow T_{\mathbf{x}}^*\Omega$  or  $\flat : V(\Omega) \rightarrow \Lambda^1(\Omega)$ , and  $\sharp : T_{\mathbf{x}}^*\Omega \rightarrow T_{\mathbf{x}}\Omega$  or  $\sharp : \Lambda^1(\Omega) \rightarrow V(\Omega)$ . In general these isomorphisms depend on the metric tensor  $g$ ,

$$\left( \frac{\partial}{\partial x^i} \right)^{\flat} = \sum_j g_{ij} dx^j, \quad (dx^j)^{\sharp} = \sum_i g^{ij} \frac{\partial}{\partial x^i}. \quad (10.3.2)$$

However, since we only consider orthonormal coordinate systems in this thesis, the metric tensor reduces to the identity tensor, and so,  $\frac{\partial}{\partial x^i} dx^j = \delta_j^i$  where  $\delta_j^i$  is the Kronecker delta. The canonical isomorphisms are among others useful when relating the velocity vector field with the velocity 1-form.

**Example 37.** Given a velocity vector field,  $\vec{v} = \sum_i v_i \partial/\partial x^i \in V(\Omega)$ , and a velocity 1-form,  $\tilde{v}^{(1)} = \sum_j \tilde{v}_j dx^j \in \tilde{\Lambda}^1(\Omega)$ , then

$$(\tilde{v}^{(1)})^\sharp = \left( \sum_j \tilde{v}_j dx^j \right)^\sharp = \sum_i \left( \sum_j g^{ij} \tilde{v}_j \right) \frac{\partial}{\partial x^i} = \sum_i v^i \frac{\partial}{\partial x^i} = \vec{v},$$

$$\vec{v}^\flat = \left( \sum_i v^i \frac{\partial}{\partial x^i} \right)^\flat = \sum_j \left( \sum_i g_{ij} v^i \right) dx^j = \sum_j \tilde{v}_j dx^j = \tilde{v}^{(1)}.$$

Again, in most cases  $g_{ij} = g^{ij} = Id$ .

### 10.3.2 Interior product

Now consider a  $k$ -form  $a^{(k)} \in \Lambda^k(\Omega)$  and a  $k$ -dimensional submanifold  $\mathcal{S}$  (this could be for instance a  $k$ -cell). Then  $\mathcal{S} = \varphi_0(\mathcal{S})$ . The  $k$ -form  $a^{(k)}$ , which has a duality pairing with the submanifold  $\mathcal{S}$ , is convected by  $\vec{v}$  during a time  $t$ . The resultant submanifold is denoted by  $\mathcal{S}_t = \varphi_t(\mathcal{S})$ . The extrusion by  $\vec{v}$  of  $\mathcal{S}$  towards  $\mathcal{S}_t$  is a  $(k+1)$ -dimensional submanifold and is denoted by

$$E(\mathcal{S}, t) = \bigcup_{\tau=0}^t \varphi_\tau(\mathcal{S}). \quad (10.3.3)$$

Figure 10.3.2 shows an illustration of the displacement of  $k$ -dimensional submanifolds due to a velocity field. For  $k = 0, 1, 2$  the blue shaded areas show the extrusion. The

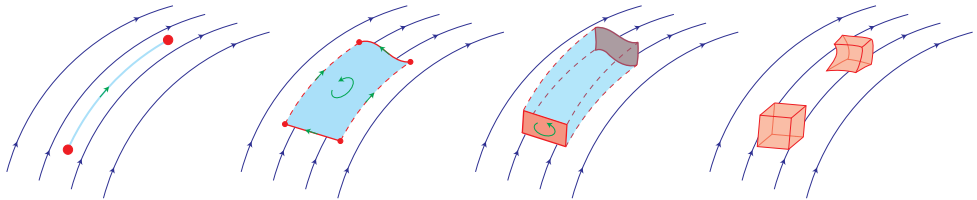


Figure 10.1: Illustration of extrusion

orientation of the extrusion is induced by its boundary, that is given by

$$\partial E(\mathcal{S}, t) = \varphi_t(\mathcal{S}) - \mathcal{S} - E(\partial \mathcal{S}, t). \quad (10.3.4)$$

The geometric definition of the *interior product* follows from the relation between flow and velocity, (10.3.1), and the definition of extrusion, (10.3.3).

**Definition 65 (Interior product).** The *interior product*,  $\iota_{\vec{v}} : \Lambda^k(\Omega) \times V(\Omega) \rightarrow \Lambda^{k-1}(\Omega)$ , is defined by the instantaneous change of a  $(k+1)$ -form  $\omega^{(k+1)}$  on the extrusion  $E(\mathcal{S}, t)$ . Let  $a^{(k)} = \iota_{\vec{v}} \omega^{(k+1)}$ , then

$$\int_{\mathcal{S}} \iota_{\vec{v}} \omega^{(k+1)} = \lim_{t \rightarrow 0} \frac{1}{t} \int_{E(\mathcal{S}, t)} \omega^{(k+1)}. \quad (10.3.5)$$

Alternatively, the interior product is defined as a contraction operator due to a vector field  $\vec{v}$ ,

$$(\iota_{\vec{v}}\omega^{(k+1)})(\vec{w}_1, \dots, \vec{w}_{k-1}) := \omega^{(k+1)}(\vec{v}, \vec{w}_1, \dots, \vec{w}_{k-1}). \quad (10.3.6)$$

Note that  $\iota_{\vec{v}}a^{(0)} = 0$ . Clearly  $\iota_{\vec{v}} + \iota_{\vec{w}} = \iota_{\vec{v}+\vec{w}}$  and  $\iota_{f\vec{v}} = f\iota_{\vec{v}}$  for some function  $f = f(\mathbf{x})$ .

**Example 38.** If  $\vec{v} = \sum_i v^i \partial/\partial x^i$  is a vector field and  $a^{(1)} = \sum_i a_i dx^i$  a one-form, then  $\iota_{\vec{v}}a^{(1)} = \sum_i a_i v^i$  in  $\Lambda^0(\Omega)$ .

**Example 39.** Let  $a^{(2)} = dx_1 \wedge dx_2$  be a two-form in  $\Omega \subset \mathbb{R}^2$  and  $\vec{v} = v^1 \partial/\partial x_1 + v^2 \partial/\partial x_2$ , then

$$(\iota_{\vec{v}}a^{(2)})(\vec{w}) = (dx^1 \wedge dx^2)(\vec{v}, \vec{w}) = \begin{vmatrix} v^1 & v^2 \\ dx^1(\vec{w}) & dx^2(\vec{w}) \end{vmatrix} = (-v_2 dx^1 + v_1 dx^2)(\vec{w}).$$

The interior product is linear, so for all  $\vec{v} \in V(\Omega)$ ,  $a^{(k)}, b^{(k)} \in \Lambda^k(\Omega)$ , it holds,

$$\iota_{\vec{v}}(a^{(k)} + b^{(k)}) = \iota_{\vec{v}}a^{(k)} + \iota_{\vec{v}}b^{(k)}, \quad (10.3.7)$$

and also possesses a Leibniz rule. Let  $a^{(k)} \in \Lambda^k(\Omega)$  and  $b^{(l)} \in \Lambda^l(\Omega)$ , then

$$\iota_{\vec{v}}(a^{(k)} \wedge b^{(l)}) = (\iota_{\vec{v}}a^{(k)}) \wedge b^{(l)} + (-1)^k a^{(k)} \wedge (\iota_{\vec{v}}b^{(l)}), \quad \text{for } 1 \leq k+l \leq n. \quad (10.3.8)$$

The interior product is a bounded map and is nilpotent, i.e.  $\iota_{\vec{v}}\iota_{\vec{v}}a^{(k)} = 0$ . It possesses the following sequence

$$0 \xleftarrow{\iota_{\vec{v}}} \Lambda^0(\Omega) \xleftarrow{\iota_{\vec{v}}} \cdots \xleftarrow{\iota_{\vec{v}}} \Lambda^{n-1}(\Omega) \xleftarrow{\iota_{\vec{v}}} \Lambda^n(\Omega) \leftrightarrow \mathbb{R}. \quad (10.3.9)$$

With the canonical isomorphisms, defined in the previous section, we can define the following adjoint relation. The interior product is adjoint of the wedge product with the flat of the velocity vector field. Then,

$$(\iota_{\vec{v}}a^{(k)}, b^{(k-1)}) = (a^{(k)}, \vec{v}^\flat \wedge b^{(k-1)}), \quad b^{(k-1)} \in \Lambda^{k-1}(\Omega). \quad (10.3.10)$$

The last property of the interior product involves the mapping  $\Phi : \widehat{\Omega} \rightarrow \Omega$ . For  $\vec{v} \in V(\widehat{\Omega})$ ,  $\Phi$  induces the pushforward map of vector fields,  $\Phi_* := V(\widehat{\Omega}) \rightarrow V(\Omega)$ . The pullback,  $\Lambda^k(\Omega) \rightarrow \Lambda^k(\widehat{\Omega})$ , of a contraction on a mapped domain can be related to the contraction on the reference domain as

$$\Phi^* \left( \iota_{\Phi_* \vec{v}} a^{(k)} \right) = \iota_{\vec{v}}(\Phi^* a^{(k)}), \quad \forall a \in \Lambda^k(\Omega). \quad (10.3.11)$$

### 10.3.3 Lie derivative

The flow function  $\varphi$  has a pullback  $\varphi_t^* : \Lambda^k(\mathcal{S}_t \subset \Omega) \rightarrow \Lambda^k(\mathcal{S} \subset \Omega)$  along the parameter  $t$ . The time rate of change of this mapping defines the Lie derivative.

**Definition 66 (Lie derivative).** The Lie derivative  $\mathcal{L}_{\vec{v}} : \Lambda^k(\Omega) \rightarrow \Lambda^k(\Omega)$  is defined as the rate of change of the pullback of a  $k$ -form  $a^{(k)}$ ,

$$\mathcal{L}_{\vec{v}}a^{(k)} := \frac{\partial \varphi_t^* a^{(k)}}{\partial t} \Big|_{t=0}. \quad (10.3.12)$$

---

This definition of the Lie-derivative is used in Heumann and Hiptmair, [86, 87, 88], for their semi-Lagrangian discretization method for advection. More commonly used to discretize is the Lie derivative expressed as a composition of the interior product (10.3.5) and the exterior derivative (??). This follows directly from definition (10.3.12) and is known as Cartans formula.

**Proposition 41 (Cartans formula).** *The Lie derivative can alternatively by expressed as a composition of the interior product with the exterior derivative. This is known as Cartans homotopy formula and is given by*

$$\mathcal{L}_{\vec{v}} a^{(k)} = \iota_{\vec{v}} da^{(k)} + d\iota_{\vec{v}} a^{(k)}. \quad (10.3.13)$$

*Proof.* Start by integrating (10.3.12) over  $\mathcal{S}$  and make use of (4.4.5),

$$\begin{aligned} \int_{\mathcal{S}} \mathcal{L}_{\vec{v}} a^{(k)} &= \lim_{t \rightarrow 0} \frac{1}{t} \int_{\mathcal{S}} \varphi_t^* a^{(k)} - a^{(k)} \\ &= \lim_{t \rightarrow 0} \frac{1}{t} \left( \int_{\varphi_t(\mathcal{S})} a^{(k)} - \int_{\mathcal{S}} a^{(k)} \right). \end{aligned}$$

Next, use the composition of the boundary of the extrusion (10.3.4), apply Stokes theorem (4.6.4) twice and substitute the definition of the interior product (10.3.5),

$$\begin{aligned} \int_{\mathcal{S}} \mathcal{L}_{\vec{v}} a^{(k)} &= \lim_{t \rightarrow 0} \frac{1}{t} \left( \int_{E(\mathcal{S}, t)} da^{(k)} + \int_{E(\partial\mathcal{S}, t)} a^{(k)} \right) \\ &= \int_{\mathcal{S}} \iota_{\vec{v}} da^{(k)} + \int_{\partial\mathcal{S}} \iota_{\vec{v}} a^{(k)} \\ &= \int_{\mathcal{S}} \iota_{\vec{v}} da^{(k)} + d\iota_{\vec{v}} a^{(k)}. \end{aligned} \quad (10.3.14)$$

□

The Lie derivative is linear, i.e., for all  $\vec{v} \in V(\Omega)$ ,  $a^{(k)}, b^{(k)} \in \Lambda^k(\Omega)$ , it holds,

$$\mathcal{L}_{\vec{v}}(a^{(k)} + b^{(k)}) = \mathcal{L}_{\vec{v}}a^{(k)} + \mathcal{L}_{\vec{v}}b^{(k)}, \quad (10.3.15)$$

and it possesses a Leibniz rule. For all  $\vec{v} \in V(\Omega)$ ,  $a^{(k)} \in \Lambda^k(\Omega)$  and  $b^{(l)} \in \Lambda^l(\Omega)$ ,

$$\mathcal{L}_{\vec{v}}(a^{(k)} \wedge b^{(l)}) = \mathcal{L}_{\vec{v}}a^{(k)} \wedge b^{(l)} + a^{(k)} \wedge \mathcal{L}_{\vec{v}}b^{(l)}. \quad (10.3.16)$$

Property (10.3.15) follows directly from Cartan's formula (10.3.13), and the linearity of the exterior derivative and the interior product (10.3.7). Property (10.3.16) is a consequence of (10.3.13) and the Leibniz rules of (4.6.2) and (10.3.8). From Cartan's formula and the nilpotency of the exterior derivative it follows that the Lie derivative commutes with the exterior derivative,

$$d\mathcal{L}_{\vec{v}} = \mathcal{L}_{\vec{v}}d. \quad (10.3.17)$$

---

**Remark 38 (Vector proxies).** The vector proxies of the Lie derivative of  $k$ -forms in  $\Omega \subset \mathbb{R}^3$  are given by

$$a \in \Lambda^0(\Omega) : \quad \mathcal{L}_{\vec{v}} a \stackrel{\text{v.p.}}{=} \vec{v} \cdot \operatorname{grad} a, \quad (10.3.18a)$$

$$a \in \Lambda^1(\Omega) : \quad \mathcal{L}_{\vec{v}} a \stackrel{\text{v.p.}}{=} \operatorname{grad}(\vec{v} \cdot \vec{a}) + \operatorname{curl} \vec{a} \times \vec{v}, \quad (10.3.18b)$$

$$a \in \Lambda^2(\Omega) : \quad \mathcal{L}_{\vec{v}} a \stackrel{\text{v.p.}}{=} \operatorname{curl}(\vec{v} \times \vec{a}) + \vec{v} \operatorname{div} \vec{a}, \quad (10.3.18c)$$

$$a \in \Lambda^3(\Omega) : \quad \mathcal{L}_{\vec{v}} a \stackrel{\text{v.p.}}{=} \operatorname{div}(\vec{v} a). \quad (10.3.18d)$$

So if we take the Lie-derivative of the velocity 1-form, we get

$$\begin{aligned} \mathcal{L}_{\vec{u}} u &\stackrel{\text{v.p.}}{=} \operatorname{grad}(\vec{u} \cdot \vec{u}) + \operatorname{curl} \vec{u} \times \vec{u} \\ &= (\vec{u} \cdot \nabla) \vec{u} + \frac{1}{2} \operatorname{grad} |\vec{u}|^2, \end{aligned}$$

or

$$\mathcal{L}_{\vec{u}} u - \frac{1}{2} d\iota_{\vec{v}} u \stackrel{\text{v.p.}}{=} (\vec{u} \cdot \nabla) \vec{u}. \quad (10.3.19)$$

Lie derivative and mapping

Lie derivative and projection

Gromeka-Lamb form:

$$\begin{aligned} (\vec{v} \cdot \nabla) \vec{u} &= \frac{1}{2} \operatorname{grad}(\vec{v}, \vec{u}) - \vec{v} \times \operatorname{curl} \vec{u} \\ \mathcal{L}_{\vec{v}} \tilde{u}^{(1)} &\stackrel{\text{v.p.}}{=} \operatorname{grad}(\vec{v}, \vec{u}) - \vec{v} \times \operatorname{curl} \vec{u} = (\vec{v} \cdot \nabla) \vec{u} + \frac{1}{2} \operatorname{grad}(\vec{v}, \vec{u}) \end{aligned}$$

### 10.3.4 Space-time notation

The domain  $\Omega$ , can be either an  $n$ -dimensional spatial manifold or a space-time manifold, e.g.  $(x^1, x^2, x^3, \dots) := (t, x, y, \dots)$ . In that case,  $v^1(\mathbf{x}) = 1$ .

$$\begin{aligned} \int_S \mathcal{D}_{\vec{v}} a^{(k)}(t) &:= \lim_{t \rightarrow 0} \int_S (\varphi_t^* a^{(k)}(t) - a^{(k)}(0)) \\ &= \lim_{t \rightarrow 0} \frac{1}{t} \int_S (\varphi_t^* a^{(k)}(t) - \varphi_t^* a^{(k)}(0)) + \lim_{t \rightarrow 0} \frac{1}{t} \int_S (\varphi_t^* a^{(k)}(0) - a^{(k)}(0)) \\ &= \int_S \left( \frac{\partial a^{(k)}}{\partial t} + \mathcal{L}_{\vec{v}} a^{(k)} \right). \\ D &= dt \wedge \frac{\partial}{\partial t} + d, \quad \vec{X} = \frac{\partial}{\partial t} + \vec{v} \\ \frac{d}{dt} \int_{V(t)} a^{(k)} &= \int_{V(t)} \frac{\partial a^{(k)}}{\partial t} + \mathcal{L}_{\vec{v}} a^{(k)} \\ \frac{\partial}{\partial t} \varphi_t^* a^{(k)} &= \varphi_t^* \left( \frac{\partial a^{(k)}}{\partial t} + \mathcal{L}_{\vec{v}} a^{(k)} \right) \end{aligned}$$

Vervolg example 10 (p. 54) (in feite hebben we  $r^{(3)} = \iota_{\vec{u}}(dt \wedge dx \wedge dy \wedge dz)$ , en conservation of mass is  $\mathcal{L}_{\vec{u}} M^{(4)} = 0$ , met  $M^{(4)} = \rho dt \wedge dx \wedge u dy \wedge dz$ . Refereer in het convectie hoofdstuk!!)

## 10.4 Skew-symmetric formulation

Consider the convection of a  $k$ -form,  $a \in \Lambda^k(\Omega)$ ,  $0 \leq k \leq n$ , due to the action of a vector field  $\vec{v} \in V(\Omega)$ . The convection operator acting on  $k$ -forms is the Lie-derivative,  $\mathcal{L}_{\vec{v}} : \Lambda^k(\Omega) \rightarrow \Lambda^k(\Omega)$ . The pure convection equation to be considered is given by

$$\mathcal{L}_{\vec{v}} a = 0. \quad (10.4.1)$$

Consider the weak formulation by wedge multiplying (10.4.1) by a test-function  $\star b \in \Lambda^{n-k}(\Omega)$ ,

$$\int_{\Omega} \mathcal{L}_{\vec{v}} a \wedge \star b = 0, \quad \forall b \in \Lambda^k(\Omega). \quad (10.4.2)$$

A first step to obtain a skew-symmetric formulation is to substitute Leibniz rule, (10.3.16), for half of (10.4.2). This gives

$$\frac{1}{2} \int_{\Omega} \mathcal{L}_{\vec{v}} a \wedge \star b - \frac{1}{2} \int_{\Omega} a \wedge \mathcal{L}_{\vec{v}} \star b + \frac{1}{2} \int_{\Omega} \mathcal{L}_{\vec{v}} (a \wedge \star b) = 0.$$

The third integral can be transformed into a boundary integral using Cartan's formula (10.3.13) and Stokes theorem (??). The obtained boundary integral can be split using Leibniz rule (10.3.8). So

$$\begin{aligned} \int_{\Omega} \mathcal{L}_{\vec{v}} (a \wedge \star b) &= \int_{\partial\Omega} \iota_{\vec{v}} (a \wedge \star b) \\ &= \int_{\partial\Omega} \iota_{\vec{v}} a \wedge \star b + (-1)^k \int_{\partial\Omega} a \wedge \iota_{\vec{v}} \star b. \end{aligned}$$

Then the skew-symmetric formulation for the convection equation of arbitrary  $k$ -forms (10.4.1) becomes: Find  $a \in \Lambda^k(\Omega)$ , given  $\vec{v} \in V(\Omega)$ , for all  $b \in \Lambda^k(\Omega)$ , such that

$$\frac{1}{2} \int_{\Omega} \mathcal{L}_{\vec{v}} a \wedge \star b - \frac{1}{2} \int_{\Omega} a \wedge \mathcal{L}_{\vec{v}} \star b + \frac{1}{2} \int_{\partial\Omega} \iota_{\vec{v}} a \wedge \star b + (-1)^k \frac{1}{2} \int_{\partial\Omega} a \wedge \iota_{\vec{v}} \star b = 0. \quad (10.4.3)$$

The first two terms show the skew symmetry of the domain part and the last two integrals give the skew symmetric formulation of the boundary part. The clear distinction at geometric level between boundary and domain integrals is discussed in [115]. Especially the skew-symmetric formulation of the boundary integral has often been an unresolved problem in skew-symmetric formulations, [?, ?, ?].

**Remark 39.** In general the Lie-derivative and Hodge- $\star$  do not commute, so  $\star \mathcal{L}_{\vec{v}} \neq \mathcal{L}_{\vec{v}} \star$ . As a result, the skew-symmetric formulation cannot be written in terms of  $L^2$ -inner products,

$$\frac{1}{2} (\mathcal{L}_{\vec{v}} a, b)_{\Omega} - \frac{1}{2} (a, \mathcal{L}_{\vec{v}} b)_{\Omega} \neq \frac{1}{2} \int_{\Omega} \mathcal{L}_{\vec{v}} a \wedge \star b - \frac{1}{2} \int_{\Omega} a \wedge \mathcal{L}_{\vec{v}} \star b.$$

This can be illustrated using the following example: Let  $f \in \Lambda^0(\Omega \subset \mathbb{R}^3)$ , then

$$\begin{aligned} \star \mathcal{L}_{\vec{v}} f &= \left( u \frac{\partial f}{\partial x} + v \frac{\partial f}{\partial y} + w \frac{\partial f}{\partial z} \right) dx dy dz, \\ \mathcal{L}_{\vec{v}} \star f &= \left( \frac{\partial u f}{\partial x} + \frac{\partial v f}{\partial y} + \frac{\partial w f}{\partial z} \right) dx dy dz. \end{aligned}$$

---

This can only be the same if we consider divergence-free vector fields. Similar result will be found for 3-forms. For 1-forms and 2-forms there does not even exist a condition such that it commutes.

What can I say about stability?

## 10.5 Incompressible Euler flow

### 10.5.1 Adjoint operators

As for the exterior derivative, which has the codifferential as its adjoint operator, we can also define adjoint operators for the interior product and the Lie derivative. These were already introduced by Heumann [85]. The formal adjoint of the interior derivative is

$$\star j_{\vec{v}} a^{(k)} = (-1)^k \iota_{\vec{v}} \star a^{(k)}, \quad \forall a^{(k)} \in \Lambda^k(\Omega), \quad (10.5.1)$$

and the formal adjoint of the Lie derivative is

$$\star L_{\vec{v}} = -\mathcal{L}_{\vec{v}} \star, \quad \forall a^{(k)} \in \Lambda^k(\Omega). \quad (10.5.2)$$

Following Cartans formula, the adjoint Lie derivative can be expressed as

$$L_{\vec{v}} = d^* j_{\vec{v}} + j_{\vec{v}} d^*, \quad (10.5.3)$$

and as a consequence of (10.3.17) it commutes with the codifferential,

$$d^* L_{\vec{v}} = L_{\vec{v}} d^*. \quad (10.5.4)$$

Integration by parts for the Lie derivative, as follows from the Leibniz rule and the definition of its adjoint, is given by

$$\int_{\partial\Omega} \text{tr } \iota_{\vec{v}} (a^{(k)} \wedge \star b^{(k)}) = (\mathcal{L}_{\vec{v}} a^{(k)}, b^{(k)})_{\Omega} - (a^{(k)}, \mathcal{L}_{\vec{v}} b^{(k)})_{\Omega}.$$

In case of the non-linear convection of velocity we get,

$$\begin{aligned} (\vec{u} \cdot \nabla) \vec{u} &\stackrel{\text{v.p.}}{=} \mathcal{L}_{\vec{u}} \tilde{u}^{(1)} - \frac{1}{2} d \iota_{\vec{u}} \tilde{u}^{(1)} \\ &= \star \left( (-1)^n L_{\vec{u}} u^{(n-1)} + \frac{1}{2} d^* j_{\vec{u}} u^{(n-1)} \right). \end{aligned}$$

### 10.5.2 Euler problem

The incompressible Euler problem represents an incompressible inviscid homogeneous fluid on a manifold  $\Omega$ . As we have seen for the Stokes flow problem in Section 2.3, also the Euler problem can be expressed either related to inner-oriented sub-manifolds or related to outer-oriented sub-manifolds, through the adjoint relations. By assuming a unit density, the inner-oriented expression of the Euler problem in terms of vector calculus becomes,

$$\frac{\partial \vec{u}}{\partial t} + (\vec{u} \cdot \nabla) \vec{u} = -\text{grad } p, \quad \text{div}^* \vec{u} = 0,$$

whereas the outer-oriented expression becomes,

$$\frac{\partial \vec{u}}{\partial t} + (\vec{u} \cdot \nabla^*) \vec{u} = -\text{grad}^* p, \quad \text{div } \vec{u} = 0.$$

Here the convection operator  $(\vec{u} \cdot \nabla^*)$  is the adjoint of  $(\vec{u} \cdot \nabla)$ , similar to relation (10.5.2).

In terms of differential forms, the Euler problem can be expressed either in inner-oriented variables  $(\tilde{u}^{(1)}, \tilde{p}^{(0)}) \in \{\tilde{\Lambda}^1(\Omega) \times \tilde{\Lambda}^0(\Omega)\}$  or in terms of outer-oriented variables  $(u^{(n-1)}, p^{(n)}) \in \{\Lambda^{n-1}(\Omega) \times \Lambda^n(\Omega)\}$ . This is due to the Hodge star duality, where  $u^{(n-1)} = \star \tilde{u}^{(1)}$  and  $p^{(n)} = \star \tilde{p}^{(0)}$ . This results in the following two expressions: for the inner-oriented variables,

$$\frac{\partial \tilde{u}^{(1)}}{\partial t} + \mathcal{L}_{\vec{u}} \tilde{u}^{(1)} = d\left(\frac{1}{2} \iota_{\vec{u}} \tilde{u}^{(1)} - \tilde{p}^{(0)}\right), \quad d^* \tilde{u}^{(1)} = 0, \quad (10.5.5)$$

or in terms of  $u^{(n-1)}$  and  $p^{(n)}$ , as

$$\frac{\partial u^{(n-1)}}{\partial t} + \mathsf{L}_{\vec{u}} u^{(n-1)} = d^*\left(\frac{1}{2} j_{\vec{u}} u^{(n-1)} - (-1)^n p^{(n)}\right), \quad du^{(n-1)} = 0. \quad (10.5.6)$$

The last expression will result in a pointwise divergence-free discretization of the velocity field.

Time:  $\star \mathsf{L}_{\partial/\partial_t} = -\mathcal{L}_{\partial/\partial_t} \star$

### 10.5.3 Advection of vorticity

The incompressible Euler model can alternatively be written in terms of a vorticity-stream function formulation, that results in an advection equation for vorticity and a Poisson equation for the stream function. Vorticity,  $\omega^{(n-2)} \in \Lambda^{n-2}(\Omega)$ , and stream function (stream vector in 3D),  $\psi^{(n-2)} \in \Lambda^{n-2}(\Omega)$ , are related to velocity as  $\omega^{(n-2)} = d^* u^{(n-1)}$  and  $u^{(n-1)} = d\psi^{(n-2)}$ . Therefore, if we apply the codifferential to the first equation in (10.5.6) we obtain an advection equation for the vorticity. Because of (10.5.4), we get

$$\frac{\partial \omega^{(n-2)}}{\partial t} + \mathsf{L}_{\vec{u}} \omega^{(n-2)} = 0, \quad (10.5.7a)$$

$$d^* d\psi^{(n-2)} = \omega^{(n-2)}. \quad (10.5.7b)$$

Skew-symmetric formulation:

$$\begin{aligned} & \left( \tau^{(n-2)}, \frac{\partial}{\partial t} \omega^{(n-2)} \right)_\Omega + \frac{1}{2} \int_\Omega \mathcal{L}_{\vec{u}} \tau^{(n-2)} \wedge \star \omega^{(n-2)} - \frac{1}{2} \int_\Omega \tau^{(n-2)} \wedge \mathcal{L}_{\vec{u}} \star \omega^{(n-2)} \\ & + \frac{1}{2} \int_{\partial\Omega} \text{tr } \iota_{\vec{u}} \tau^{(n-2)} \wedge \text{tr } \star \omega^{(n-2)} + (-1)^{n-2} \frac{1}{2} \int_{\partial\Omega} \text{tr } \tau^{(n-2)} \wedge \text{tr } \iota_{\vec{u}} \star \omega^{(n-2)} = 0 \end{aligned} \quad (10.5.8)$$

---

## 10.6 Discretization of Lie-derivative

## 10.7 Numerical Results

### 10.7.1 Testproblem 1

linear convection  $k$ -forms.

### 10.7.2 Testproblem 2

### 10.7.3 Incompressible Euler flow through advection of vorticity

This testcase considers the incompressible Euler flow on a manifold  $\Omega$ . The Euler problem in terms of vector calculus are given by,

$$\frac{\vec{v}}{\partial t} + (\vec{v} \cdot \nabla) \vec{v} = -\text{grad}^* p, \quad \text{div } \vec{v}. \quad (10.7.1)$$

In terms of differential geometry, the Euler problem is given as

$$\frac{\partial u^{(n-1)}}{\partial t} + \mathcal{L}_{\vec{v}} u^{(n-1)} = d^* \left( \frac{1}{2} \iota_{\vec{v}} u^{(n-1)} - p^{(n)} \right) \quad (10.7.2)$$

vortex problem with self-induced velocity field.

$$\begin{aligned} \frac{\partial \vec{v}}{\partial t} + (\vec{v} \cdot \nabla) \vec{v} + \nabla p &= 0 \\ \xrightarrow{\text{curl}} \\ \frac{\partial \omega}{\partial t} + \mathcal{L}_{\vec{v}} \omega &= 0 \\ \vec{v} &= u \frac{\partial}{\partial x} + v \frac{\partial}{\partial y} \end{aligned}$$

$\Omega = [-\pi, \pi]^2$  with periodic boundary conditions.

Initial condition is

$$\omega(\mathbf{x}) = \sum_{i=1}^2 \frac{U}{a} \left( 2 - \frac{(r(\mathbf{x}) - r_i)^2}{a^2} \right) \exp \left( \frac{1}{2} \left( 1 - \frac{(r(\mathbf{x}) - r_i)^2}{a^2} \right) \right)$$

with maximal tangential velocity,  $U = 1$ , core size  $a = 0.3$  and core centers  $r_i$  at  $(-0.4, 0)$  and  $(0.4, 0)$ .

$$\begin{aligned} \left( \frac{\partial \omega}{\partial t}, \psi \right)_\Omega + \frac{1}{2} \int_\Omega \mathcal{L}_{\vec{v}} \omega \wedge \star \psi - \frac{1}{2} \int_\Omega \omega \wedge \mathcal{L}_{\vec{v}} \star \psi \\ + \frac{1}{2} \int_{\partial\Omega} \iota_{\vec{v}} \omega \wedge \star \psi + \frac{1}{2} \int_{\partial\Omega} \omega \wedge \iota_{\vec{v}} \star \psi = 0 \end{aligned}$$

Because we consider non-linear convection, standard Gauss-Lobatto integration with order  $N$  is in general insufficient. However, in De Maerschalk and Gerritsma [53] it was shown that to obtain accurate result for smooth problems already slightly higher order Gauss-Lobatto integration than order  $N$  is sufficient.

## 10.8 Conclusions and future aspects

[http://differentialgeometry.org/#\[\[Lie%20derivative\]\]](http://differentialgeometry.org/#[[Lie%20derivative]])

The Lie derivative is the rate of change of any field perceived by an observer as she moves along a path with some velocity,  $\vec{v}$ . Basically, the field where she is going is pulled back and compared with the field where she's at. This description is extended to give the Lie derivative,  $\mathcal{L}_{\vec{v}}$ , with respect to a flow,  $\varphi_t$ , giving the rate of change of any field perceived by observers at every manifold point as they move according to the velocity field.

The Lie derivative of any field,  $\omega$ , is a *natural* operator defined as

$$\mathcal{L}_{\vec{v}}\omega = \frac{d}{dt}\varphi_t^*\omega = \frac{d}{dt}\omega(t) = \lim_{t \rightarrow 0} \frac{\varphi_t^*\omega - \omega}{t} = \lim_{t \rightarrow 0} \frac{(\varphi_{-t})_*\omega - \omega}{t}.$$

### 10.8.1 Curved meshes

$a \in \Lambda^k(\Omega)$ ,  $\vec{v} \in T(\Omega_0)$

$$\phi^*(\iota_{\phi_*\vec{v}}a) = \iota_{\vec{v}}\phi^*a$$

$$\vec{v}(\xi, \eta) = v_\xi(\xi, \eta) \frac{\partial}{\partial \xi} + v_\eta(\xi, \eta) \frac{\partial}{\partial \eta}$$

$$\begin{aligned} \frac{\partial}{\partial \xi} &= \frac{\partial x}{\partial \xi} \frac{\partial}{\partial x} + \frac{\partial y}{\partial \xi} \frac{\partial}{\partial y} \\ \frac{\partial}{\partial \eta} &= \frac{\partial x}{\partial \eta} \frac{\partial}{\partial x} + \frac{\partial y}{\partial \eta} \frac{\partial}{\partial y} \end{aligned}$$

$$(x, y) = \phi(\xi, \eta), \quad \vec{u}(x, y) = \phi_*\vec{v}(\xi, \eta)$$

$$\begin{aligned} \phi_*\vec{v}(\xi, \eta) &= v_\xi(x, y) \left( \frac{\partial x}{\partial \xi} \frac{\partial}{\partial x} + \frac{\partial y}{\partial \xi} \frac{\partial}{\partial y} \right) + v_\eta(x, y) \left( \frac{\partial x}{\partial \eta} \frac{\partial}{\partial x} + \frac{\partial y}{\partial \eta} \frac{\partial}{\partial y} \right) \\ &= \left( v_\xi(x, y) \frac{\partial x}{\partial \xi} + v_\eta(x, y) \frac{\partial x}{\partial \eta} \right) \frac{\partial}{\partial x} + \left( v_\xi(x, y) \frac{\partial y}{\partial \xi} + v_\eta(x, y) \frac{\partial y}{\partial \eta} \right) \frac{\partial}{\partial y} \\ &= u_x(x, y) \frac{\partial}{\partial x} + u_y(x, y) \frac{\partial}{\partial y} = \vec{u}(x, y) \end{aligned}$$

$$\begin{bmatrix} u_x \\ u_y \end{bmatrix} = \begin{bmatrix} \frac{\partial x}{\partial \xi} & \frac{\partial x}{\partial \eta} \\ \frac{\partial y}{\partial \xi} & \frac{\partial y}{\partial \eta} \end{bmatrix} \begin{bmatrix} v_\xi \\ v_\eta \end{bmatrix} \quad \Rightarrow \quad \begin{bmatrix} v_\xi \\ v_\eta \end{bmatrix} = \frac{1}{J} \begin{bmatrix} \frac{\partial y}{\partial \eta} & -\frac{\partial x}{\partial \eta} \\ -\frac{\partial y}{\partial \xi} & \frac{\partial x}{\partial \xi} \end{bmatrix} \begin{bmatrix} u_x \\ u_y \end{bmatrix}$$

with  $J = \frac{\partial x}{\partial \xi} \frac{\partial y}{\partial \eta} - \frac{\partial x}{\partial \eta} \frac{\partial y}{\partial \xi}$

$$\phi^*(\iota_{\phi_*\vec{v}}u) = \iota_{\vec{v}}\phi^*u$$

$$u = u_x dx + u_y dy, \quad \phi^*u = v = v_\xi d\xi + v_\eta d\eta$$

$$\vec{v} = v_\xi \frac{\partial}{\partial \xi} + v_\eta \frac{\partial}{\partial \eta}, \quad \phi_*\vec{v} = \vec{u} = u_x \frac{\partial}{\partial x} + u_y \frac{\partial}{\partial y}$$



# Chapter 11

## Discretization of Covector-Valued Differential Forms

Up till now, we considered differential  $k$ -forms, fully known as *real-valued* differential  $k$ -forms, that formed a generalization of scalar and vectors in vector calculus. The full Stokes and Navier-Stokes equations are tensor equations as we have seen in Chapter ???. The analoge in differential geometry of tensors in tensor calculus, that adds the favored geometric structure, are bundle-valued differential  $k$ -forms. For the Navier-Stokes equations we require *vector*-valued and *covector*-valued differential  $k$ -forms.

The theory of vector-valued differential  $k$ -forms is a relatively new field of mathematics and was first described by Frölicher and Nijenhuis in 1956, [72], in the journal of the Royal Dutch Mathematical Society. It was only recently mentioned in combination with computational methods for continuum mechanics, [105].

Verschil vector- en covector-valued forms

Kanso 2007 opzoeken met scopus, voor eventuele vervolg verhalen

see some Springer books

### 11.1 Calculus on (co)vector-valued differential $k$ -forms

Let  $E$  be a real rank- $n$  vector of the tangent space  $T\Omega$  of a smooth  $n$ -dimensional manifold  $\Omega$ . Then on the dual space  $T^*\Omega$  we consider a real rank- $n$  covector  $E^*$ .

**Definition 67** ((Co)vector-valued differential  $k$ -forms). *Let  $\mathbb{E}$  be either  $E$  or  $E^*$ . A differential  $k$ -form on  $\Omega$  with values in  $\mathbb{E}$  is a mapping,*

$$\vec{a}^{(k)} : T_p\Omega \times \cdots \times T_p\Omega \rightarrow \mathbb{E}_p. \quad (11.1.1)$$

*They can be written locally, with respect to coordinates  $\mathbf{x} := (x_1, \dots, x_n)$  in  $\Omega$ , a*

vector basis  $\{\partial_{x_1}, \dots, \partial_{x_n}\}$  in  $E$  and covector basis  $\{dx_1, \dots, dx_n\}$  in  $E^*$ , as

$$\vec{a}^{(k)} = \sum_I f_I(\mathbf{x}) dx^{i_1} \wedge \dots \wedge dx^{i_k} \otimes \partial_{x_I}, \quad (11.1.2)$$

$$\vec{a}^{(k)} = \sum_I f_I(\mathbf{x}) dx^{i_1} \wedge \dots \wedge dx^{i_k} \otimes dx_I, \quad (11.1.3)$$

where  $I = i_1, \dots, i_k$  with  $1 \leq i_1 < \dots < i_k \leq n$  and where  $f_I(\mathbf{x})$  is a sufficiently smooth function.

The space of  $k$ -forms on  $\Omega$  with values in either  $E$  or  $E^*$  will be denoted by  $\Lambda^k(\Omega, E)$  and  $\Lambda^k(\Omega, E^*)$ , respectively. Note that we write for real-valued differential  $k$ -forms  $\Lambda^k(\Omega, \mathbb{R})$  or simply  $\Lambda^k(\Omega)$ . We can write

$$\Lambda^k(\Omega; E) = \Lambda^k(\Omega; \mathbb{R}) \otimes E \quad \text{and} \quad \Lambda^k(\Omega; E^*) = \Lambda^k(\Omega; \mathbb{R}) \otimes E^*.$$

Some relevant examples of covector-valued differential forms are given below.

**Example 40.** Examples in  $\mathbb{R}^3$  with  $\mathbf{x} := (x, y, z)$ :

$$\begin{aligned} \text{Momentum : } \vec{m}^{(3)} &= m_{,x}(\mathbf{x}) dx \wedge dy \wedge dz \otimes dx \\ &\quad + m_{,y}(\mathbf{x}) dx \wedge dy \wedge dz \otimes dy \\ &\quad + m_{,z}(\mathbf{x}) dx \wedge dy \wedge dz \otimes dz. \end{aligned}$$

$$\begin{aligned} \text{Stress : } \vec{\sigma}^{(2)} &= (\sigma_{x,x}(\mathbf{x}) dy \wedge dz + \sigma_{y,x}(\mathbf{x}) dz \wedge dx + \sigma_{z,x}(\mathbf{x}) dx \wedge dy) \otimes dx \\ &\quad + (\sigma_{x,y}(\mathbf{x}) dy \wedge dz + \sigma_{y,y}(\mathbf{x}) dz \wedge dx + \sigma_{z,y}(\mathbf{x}) dx \wedge dy) \otimes dy \\ &\quad + (\sigma_{x,z}(\mathbf{x}) dy \wedge dz + \sigma_{y,z}(\mathbf{x}) dz \wedge dx + \sigma_{z,z}(\mathbf{x}) dx \wedge dy) \otimes dz. \end{aligned}$$

**Definition 68 (Wedge product).**

Frölicher-Nijenhuis bracket for product on (co)vector-valued differential forms.

**Definition 69 (Integration).**

$$\Lambda^k(\Omega; E) \wedge \Lambda^l(\Omega; E^*) \rightarrow \Lambda^{k+l}(\Omega; \mathbb{R})$$

### 11.1.1 Covariant derivative

$$\begin{aligned} d\vec{\sigma}^{(2)} &= \left( \frac{\partial \sigma_{x,x}}{\partial x} + \frac{\partial \sigma_{y,x}}{\partial y} + \frac{\partial \sigma_{z,x}}{\partial z} \right) dx \wedge dy \wedge dz \otimes dx \\ &\quad + \left( \frac{\partial \sigma_{x,y}}{\partial x} + \frac{\partial \sigma_{y,y}}{\partial y} + \frac{\partial \sigma_{z,y}}{\partial z} \right) dx \wedge dy \wedge dz \otimes dy \\ &\quad + \left( \frac{\partial \sigma_{x,z}}{\partial x} + \frac{\partial \sigma_{y,z}}{\partial y} + \frac{\partial \sigma_{z,z}}{\partial z} \right) dx \wedge dy \wedge dz \otimes dz. \end{aligned} \quad (11.1.4)$$

---

### 11.1.2 $L^2$ -inner product

### 11.1.3 Cohomology (Hodge decomposition)

### 11.1.4 Pullback

### 11.1.5 Lie-derivative

## 11.2 Inclusion and Trace

In incompressible Stokes and Navier-Stokes equations one often encounters the term pressure gradient,  $\text{grad } p$ . In compressible flow equations, one prefers to write everything in conservation form, and there one prefers to write  $\nabla \cdot (pI)$ . In this section we explain how to express one in terms of the other. For that we introduce the pressure force  $\Pi$  as follows to distinguish between both pressures,

$$\text{grad } p = \nabla \cdot (pI) = \nabla \cdot \Pi. \quad (11.2.1)$$

Pressure  $p$  is a real-valued  $n$ -form. In three dimensions, we have

$$p^{(3)} = p(\mathbf{x}) dx dy dz.$$

Pressure force  $\Pi$  is a covector-valued  $(n-1)$ -form. In three dimensions we have

$$\vec{\Pi}^{(n-1)} = p(\mathbf{x}) dy \wedge dz \otimes dx + p(\mathbf{x}) dz \wedge dx \otimes dy + p(\mathbf{x}) dx \wedge dy \otimes dz.$$

In (11.2.1) we have the operator  $I$ , transforming a scalar into a tensor. Here we introduce a similar operator.

**Definition 70 (Identity operator).** *The identity operator,  $\mathbb{I} : \Lambda^k(\Omega; \mathbb{R}) \rightarrow \Lambda^{k-1}(\Omega; E)$ , is an inclusion map from real-valued differential  $k$ -forms to covector-valued differential  $k-1$ -forms. The identity operator is given by*

$$\mathbb{I} = \frac{\partial}{\partial x_1} \otimes dx_1 + \frac{\partial}{\partial x_2} \otimes dx_2 + \dots + \frac{\partial}{\partial x_n} \otimes dx_n. \quad (11.2.2)$$

Ook in Frankel In case of pressure  $p^{(n)}$  and pressure force  $\vec{\Pi}^{(n-1)}$ , we get

$$\vec{\Pi}^{(n-1)} = \mathbb{I} p^{(n)} \stackrel{n=3}{=} p(\mathbf{x}) dy \wedge dz \otimes dx + p(\mathbf{x}) dz \wedge dx \otimes dy + p(\mathbf{x}) dx \wedge dy \otimes dz.$$

2D change of basis in case of mapping (for example for spectral elements),

$$\begin{aligned} \mathbb{I} &= \frac{\partial}{\partial x} \otimes dx + \frac{\partial}{\partial y} \otimes dy \\ &= \frac{1}{J} \left( \frac{\partial y}{\partial \eta} \frac{\partial}{\partial \xi} - \frac{\partial y}{\partial \xi} \frac{\partial}{\partial \eta} \right) \otimes dx + \frac{1}{J} \left( -\frac{\partial x}{\partial \eta} \frac{\partial}{\partial \xi} + \frac{\partial x}{\partial \xi} \frac{\partial}{\partial \eta} \right) \otimes dy. \end{aligned}$$

In the opposite direction, mapping covector-valued differential forms onto real-valued ones is the trace operator.

---

**Definition 71 (Trace).** *The trace operator  $\text{Tr} : \Lambda^{k-1}(\Omega; E) \rightarrow \Lambda^k(\Omega; \mathbb{R})$ , is the restriction of covector-valued differential  $(k-1)$ -forms into real-valued differential  $k$ -forms. The trace operator is the formal Hilbert adjoint of the identity operator. For all  $\vec{\kappa}^{(k+1)} \in \Lambda^{k+1}(\Omega; E)$  and  $q^{(k)} \in \Lambda^k(\Omega; \mathbb{R})$ , it holds*

$$(\text{Tr} \vec{\kappa}^{(k-1)}, q^{(k)})_{\Omega} := (\vec{\kappa}^{(k-1)}, \mathbb{I}q^{(k)})_{\Omega}. \quad (11.2.3)$$

The trace is linear.

One may ask, which quantities of a (co)vector-valued remain unchanged under coordinate transformations. One of them is their trace. The trace of a (co)vector-valued differential  $k$ -form is therefore an invariant. The best example is the trace of the viscous stress tensor for a Newtonian fluid, which is the divergence of the velocity field. Then for incompressible flow we find the invariant,  $\text{Tr} \vec{\tau}^{(n-1)} = \text{d}u^{(n-1)} = 0$ .

**Definition 72 (Co-identity and cotrace).** *We define two co-operators, the co-identity operator,  $\mathbb{I}^* : \Lambda^k(\Omega; \mathbb{R}) \rightarrow \Lambda^{k+1}(\Omega; E)$ , and cotrace operator,  $\text{Tr}^* : \Lambda^{k+1}(\Omega; E) \rightarrow \Lambda^k(\Omega; \mathbb{R})$ , as*

$$\star \mathbb{I}^* := \pm \mathbb{I} \star \Leftrightarrow \mathbb{I}^* := \pm \star \mathbb{I} \star, \quad (11.2.4)$$

$$\star \text{Tr}^* := \pm \text{Tr} \star \Leftrightarrow \text{Tr}^* := \pm \star \text{Tr} \star. \quad (11.2.5)$$

They are each others formal Hilbert adjoint, for all  $\vec{\kappa}^{(k+1)} \in \Lambda^{k+1}(\Omega; E)$  and  $q^{(k)} \in \Lambda^k(\Omega; \mathbb{R})$

$$(\mathbb{I}^* q^{(k)}, \vec{\kappa}^{(k+1)})_{\Omega} = (q^{(k)}, \text{Tr}^* \vec{\kappa}^{(k+1)})_{\Omega}. \quad (11.2.6)$$

Cotrace of (11.1.4),

$$\begin{aligned} \text{Tr}^* d\vec{\sigma}^{(2)} &= \left( \frac{\partial \sigma_{x,x}}{\partial x} + \frac{\partial \sigma_{y,x}}{\partial y} + \frac{\partial \sigma_{z,x}}{\partial z} \right) dy \wedge dz \\ &\quad + \left( \frac{\partial \sigma_{x,y}}{\partial x} + \frac{\partial \sigma_{y,y}}{\partial y} + \frac{\partial \sigma_{z,y}}{\partial z} \right) dz \wedge dx \\ &\quad + \left( \frac{\partial \sigma_{x,z}}{\partial x} + \frac{\partial \sigma_{y,z}}{\partial y} + \frac{\partial \sigma_{z,z}}{\partial z} \right) dx \wedge dy. \end{aligned} \quad (11.2.7)$$

### 11.2.1 Discretization

We proceed with the explanation in two dimensions. Expand the real-valued 2-form  $p$  on the primal grid in terms of edge functions, then  $p_h$  is a  $(N-1) \times (N-1)$  polynomial,

$$p_h^{(2)} = \sum_{i=1}^N \sum_{j=1}^N p_{i,j} e_i(x) e_j(y)$$

The function  $\pi_{1,h}(x, y)$  is a polynomial of degree  $((N+1) \times (N-1))$  and  $\pi_{2,h}(x, y)$  is a polynomial of degree  $(N-1) \times (N+1)$ , and therefore we have  $\pi_{1,h}(x, y) = p_h(x, y)$

and  $\pi_{2,h}(x, y) = p_h(x, y)$ . The expressions are as follows,

$$\begin{aligned}\pi_{1,h}(x, y) &= \sum_{i=0}^{N+1} \sum_{j=1}^N \left[ \sum_{k=1}^N p_{k,j} \varepsilon_k(\tilde{x}_i) \right] \tilde{h}_i(x) \varepsilon_j(y), \\ &= \sum_{i=0}^{N+1} \sum_{j=1}^N \pi_{i,j}^1 \tilde{h}_i(x) \varepsilon_j(y), \\ \pi_{2,h}(x, y) &= \sum_{i=1}^N \sum_{j=0}^{N+1} \left[ \sum_{l=1}^N p_{i,l} \varepsilon_l(\tilde{y}_j) \right] \varepsilon_i(x) \tilde{h}_j(y), \\ &= \sum_{i=1}^N \sum_{j=0}^{N+1} \pi_{i,j}^2 \varepsilon_i(x) \tilde{h}_j(y),\end{aligned}$$

where  $\tilde{\cdot}$  indicates the dual grid. The finite dimensional covector-valued 1-form for the pressure becomes

$$\Pi_h = \sum_{i=0}^{N+1} \sum_{j=1}^N \pi_{i,j}^1 \tilde{h}_i(x) e_j(y) \otimes dx + \sum_{i=1}^N \sum_{j=0}^{N+1} \pi_{i,j}^2 e_i(x) \tilde{h}_j(y) \otimes dy.$$

### 11.3 Velocity

Velocity in terms of real-valued differential forms can be written as either

$$u^{(n-1)} = u dy dz + v dz dx + w dx dy, \quad (11.3.1)$$

or

$$\tilde{u}^{(1)} = u dx + v dy + w dz. \quad (11.3.2)$$

Velocity in terms of a covector-valued 0-form should be written as

$$U = u \otimes dx + v \otimes dy + w \otimes dz \quad (11.3.3)$$

Then using (11.2.2) we find the relation

$$U = \mathbb{I} \tilde{u}. \quad (11.3.4)$$

The velocity gradient tensor now follows by applying the exterior derivative to the covector-valued 0-form  $U$ ,

$$dU = du \otimes dx + dv \otimes dy + dw \otimes dz \quad (11.3.5)$$

$$\begin{aligned}&= \left( \frac{\partial u}{\partial x} dx + \frac{\partial u}{\partial y} dy + \frac{\partial u}{\partial z} dz \right) \otimes dx \\ &\quad + \left( \frac{\partial v}{\partial x} dx + \frac{\partial v}{\partial y} dy + \frac{\partial v}{\partial z} dz \right) \otimes dy \\ &\quad + \left( \frac{\partial w}{\partial x} dx + \frac{\partial w}{\partial y} dy + \frac{\partial w}{\partial z} dz \right) \otimes dz.\end{aligned} \quad (11.3.6)$$

---

For the transpose of the velocity gradient tensor we need to introduce an additional operator  $\mathbb{T}$ . Again I don't know if such an operator exists, but it should act as follows,

$$\mathbb{T}(dx \otimes dy) = dy \otimes dx, \quad \mathbb{T}(dx \otimes dz) = dz \otimes dx, \quad \mathbb{T}(dy \otimes dz) = dz \otimes dy. \quad (11.3.7)$$

Then the transpose of the velocity gradient tensor is given by  $\mathbb{T} d\mathbb{I}\tilde{u}$ .

## 11.4 Conclusion

Finally, since  $u^{(n-1)} = \star\tilde{u}^{(1)}$ , we can write the Stokes problem as

$$d[-\mathbb{I}p + \star_\mu (d\mathbb{I} \star u + \mathbb{T} d\mathbb{I} \star u)] = F, \quad (11.4.1)$$

$$du = 0, \quad (11.4.2)$$

where the body force  $F$  is a covector-valued  $n$ -form.

### 11.4.1 Velocity and momentum

- velocity differential form:  $\tilde{u}^{(1)}$ ,
- velocity flux:  $(\rho u)^{(n-1)} = \star_\rho \tilde{u}^{(1)}$ ,
- momentum:  $\vec{m}^{(n)} = \rho^{(n)} \otimes \tilde{u}^{(1)}$
- momentum:  $\vec{m}^{(n)} = \mathbb{I}^*(\rho u)^{(n-1)}$ , and  $(\rho u)^{(n-1)} = \text{Tr}^* \vec{m} \wedge n$
- Viscous stress:  $\vec{\tau}^{(n-1)} = \star_\mu d_\nabla \mathbb{I} \tilde{v}^{(1)} = \star_\mu d_\nabla \star_\rho^{-1} \vec{m}^{(n)} = \star_\mu d_\nabla \star_{1/\rho} \vec{m}^{(n)} = d_{\nabla, \mu, \rho^{-1}}^* \vec{m}^{(n)}$

---

**The Stokes Problem:**

$$\nabla \cdot \boldsymbol{\sigma} = \vec{f}, \quad (11.4.3)$$

$$\operatorname{div} \vec{u} = 0, \quad (11.4.4)$$

with

$$\boldsymbol{\sigma} = -Ip + \boldsymbol{\tau}, \quad (11.4.5)$$

$$\boldsymbol{\tau} = \mu \nabla \vec{u}. \quad (11.4.6)$$

**Identity and trace operator:**

$$(\boldsymbol{\kappa}, Ip)_{\Omega} \stackrel{??}{=} (\operatorname{div} \vec{v}, p)_{\Omega} \quad (11.4.7)$$

**Definition 73.** The formal adjoint of the identity operator  $I : \Lambda^k(\Omega; \mathbb{R}) \rightarrow \Lambda^{k-1}(\Omega; E)$  is the trace operator  $\operatorname{Tr} : \Lambda^{k-1}(\Omega; E) \rightarrow \Lambda^k(\Omega; \mathbb{R})$ , defined as

$$(\boldsymbol{\kappa}, Iq)_{\Omega} = (\operatorname{Tr} \boldsymbol{\kappa}, q)_{\Omega}. \quad (11.4.8)$$

**Example 41.**

$$\operatorname{Tr} \boldsymbol{\sigma} = -3p + \mu \operatorname{div} \vec{u}$$

**Proposition 42.** Both the identity and trace operators possess a commuting diagram property with respect to differentiation:

$$d_{\nabla} \circ I = I \circ d, \quad (11.4.9)$$

$$\operatorname{Tr} \circ d_{\nabla} = d \circ \operatorname{Tr}. \quad (11.4.10)$$

So

$$(\boldsymbol{\kappa}, Ip)_{\Omega} = (\operatorname{Tr} \boldsymbol{\kappa}, p)_{\Omega} = ((\operatorname{Tr} \boldsymbol{\kappa})_{\mathcal{Z}}, p)_{\Omega} = (\operatorname{div} \vec{v}, p)_{\Omega}, \quad \forall \vec{v}, \boldsymbol{\kappa}. \quad (11.4.11)$$

**Weak formulations:**

(Standard) velocity-pressure formulation:

$$(\nabla \vec{v}, \mu \nabla \vec{u})_{\Omega} + (\operatorname{div} \vec{v}, p)_{\Omega} = (\vec{v}, \vec{f})_{\Omega}, \quad \forall \vec{v} \quad (11.4.12)$$

$$(q, \operatorname{div} \vec{u})_{\Omega} = 0, \quad \forall q \quad (11.4.13)$$

(Asymmetric) stress-velocity-pressure formulation:

$$(\vec{v}, \nabla \cdot \boldsymbol{\sigma})_{\Omega} = (\vec{v}, \vec{f})_{\Omega}, \quad \forall \vec{v}, \quad (11.4.14)$$

$$(\boldsymbol{\kappa}, \boldsymbol{\sigma})_{\Omega} + (\operatorname{Tr} \boldsymbol{\kappa}, p)_{\Omega} - (\nabla \cdot \boldsymbol{\kappa}, \vec{u})_{\Omega} = 0, \quad \forall \boldsymbol{\kappa}, \quad (11.4.15)$$

$$(q, \operatorname{div} \vec{u})_{\Omega} = 0, \quad \forall q. \quad (11.4.16)$$

(Symmetric) viscous stress-velocity-pressure formulation:

$$(\vec{v}, \nabla \cdot \boldsymbol{\tau})_{\Omega} + (\operatorname{div} \vec{v}, p)_{\Omega} = (\vec{v}, \vec{f})_{\Omega}, \quad \forall \vec{v}, \quad (11.4.17)$$

$$(\boldsymbol{\kappa}, \boldsymbol{\tau})_{\Omega} - (\nabla \cdot \boldsymbol{\kappa}, \vec{u})_{\Omega} = 0, \quad \forall \boldsymbol{\kappa}, \quad (11.4.18)$$

$$(q, \operatorname{div} \vec{u})_{\Omega} = 0, \quad \forall q. \quad (11.4.19)$$

---

## 11.5 Mail Marc

Jasper, Deepesh, Rene,

I did a search and the integration of  $E$ -valued differential  $k$ -forms is not well-defined. What one can do (must do) is take the wedge of a  $E$ -valued differential  $k$ -form with a  $E^*$ -valued differential  $m$ -form. This gives an ordinary  $(k+m)$ -form which can be integrated over a  $(k+m)$ -dimensional manifold. Duality aring between  $E$  and  $E^*$  is a metric-free operation which produces a real number.

Let  $a \in \Lambda^k(\Omega, E)$  and  $b \in \Lambda^m(\Omega, E^*)$ , then  $a \wedge b \in \Lambda^{(k+m)}(\Omega; \mathbb{R})$  and we have

$$d(a \wedge b) = \nabla a \wedge b \pm a \wedge \nabla b$$

where  $d$  is the ordinary exterior derivative and  $\nabla$  is the covariant differential.

So there exists something like integration by parts and we can produce a boundary integral, because

$$\int_{\Omega_{k+m+1}} \nabla a \wedge b = \mp \int_{\Omega_{k+m+1}} a \wedge \nabla b + \int_{\Omega_{k+m+1}} d(a \wedge b) = \mp \int_{\Omega_{k+m+1}} a \wedge \nabla b + \int_{\partial \Omega_{k+m+1}} (a \wedge b)$$

Momentum is a covector-valued 3-form, if we choose for the complemenatry space the space of vector-valued 0-forms, then  $p \in \Lambda^3(\Omega; TM^*)$  and  $b \in \Lambda^0(\Omega; TM)$ , we have that

$$p \wedge b \in \Lambda^3(\Omega; \mathbb{R})$$

So I think we need to wedge the whole momentum equation with an arbitary vector-valued 0-form and this equation needs to hold  $\forall b \in \Lambda^0(\Omega; TM)$ .

This approach has a certain 'finite-element'-flavor, where  $b$  plays the role of test function.

We repeatedly said that we should evaluate momentum component-wise and in fact multiplication by  $b$  is a way of extracting components from the covector. This extraction is metric-free and therefore independent of the curvature of space.

If the (weak form) of the momentum equation holds for all  $b$ , then it surely holds for  $b = v$ , where  $v$  is the velocity which is also a vector-valued 0-form.  $p \wedge v$  is twice the kinetic energy, so probably this approach will also allow us to conserve kinetic energy.

Just some thoughts, Marc

## 11.6 mathoverflow

For the trivial bundle  $M \times R^k$  - and with a fixed choice of trivialisation! - you can carry out the integral component by component, But if you change the trivialisation you will get a different answer. Moreover, you can change the trivialisation in a way that varies over the manifold, so there is no hope that the integral will just change by a linear map of  $R^k$ . You can see this behaviour even with ordinary functions. A function is a section of the trivialised rank 1 bundle. If you change the trivialisation, but insist on regarding ordinray  $p$ -forms as bundle valued, you multiply all your forms by a fixed nowhere vanishing function. This can change the integral over a  $p$ -cycle in a more-or-less arbitrary way.

---

What you can integrate  $E$ -valued forms against is  $E^*$ -valued ones. Given  $a \in \Omega^p(E)$  and  $b \in \Omega^q(E^*)$  their wedge product is an ordinary  $(p+q)$ -form which you can then integrate over a  $(p+q)$ -cycle. Now you have a version of Stokes theorem. If you have a connection  $A$  in  $E$  then you can check that

$$d(a \wedge b) = d_A(a) \wedge b \pm a \wedge d_A(b).$$

So Stokes theorem gives

$$\int_M d_A(a) \wedge b \pm a \wedge d_A(b) = \int_{\partial M} a \wedge b.$$

In the case when  $b$  is a covariant constant section of  $E$  and  $M$  has dimension one more than the degree of  $a$ , we get

$$\int_M \langle d_A(a), b \rangle = \int_{\partial M} \langle a, b \rangle$$

This is just the usual Stokes theorem, for the component of  $a$  in the direction  $b$ . Since  $b$  is covariant-constant,  $\langle d_A(a), b \rangle = d\langle a, b \rangle$ .



# **Part V**

## **Conclusions, Recommendations and Outlook**



# **Part VI**

# **Appendices**



# Appendix A

## From vectors and covectors to differential forms

This chapter is based on Gerritsma et al. [140].

### A.1 FORMS AND VECTORS

We emphasize here on the distinction between vectors, covectors and differential forms. Just like the vector field is an extension of the vector concept to manifolds, the 1-form is an extension of the covector to manifolds.

#### A.1.1 Tangent vectors and vector fields

Before introducing differential forms, we need to define vectors or – more precisely – *tangent vectors* in a domain  $\mathcal{M}$ . In general,  $\mathcal{M}$  is a differentiable manifold. Let  $\gamma(t)$  be a curve in  $\mathcal{M}$  parametrized by  $t \in (-\epsilon, \epsilon)$ ,  $\epsilon > 0$ , with  $p = \gamma(0) \in \mathcal{M}$ . The derivative  $\dot{\gamma}(0)$  is a *tangent vector* at the point  $p \in \mathcal{M}$ . Note that a vector will in general not lie in the manifold  $\mathcal{M}$  itself. So the conventional image of a vector as an arrow connecting two points in the domain  $\mathcal{M}$  is inadequate. For an  $n$ -dimensional manifold we can define  $n$  curves through the point  $p \in \mathcal{M}$  which produce  $n$  linear independent vectors. A collection of  $n$  linearly independent vectors,  $\vec{e}_1|_p, \dots, \vec{e}_n|_p$ , at the point  $p$  spans a linear vector space denoted by  $T_p\mathcal{M}$ . Any other vector at  $p$  can then be written as a linear combination of these basis vectors, i.e.

$$\vec{v}|_p = \sum_{i=1}^n a^i(p) \vec{e}_i|_p ,$$

where the expansion coefficients  $a^i(p)$  are associated to the point  $p$  and the particular basis  $\vec{e}_i|_p$ . If we introduce a local parametrization of the point  $p$ , we can use the

coordinate functions  $x^i$  for the curves which generate a basis at  $p$ . Such a basis is called a *coordinate basis* for the tangent space  $T_p\mathcal{M}$  and in this case the basis vectors are generally denoted by  $\partial/\partial x^i|_p$ , or briefly  $\partial_i|_p$ . For a coordinate basis a vector is represented as

$$\vec{v}|_p = \sum_{i=1}^n b^i(p) \frac{\partial}{\partial x^i}\Big|_p .$$

If we introduce another coordinate system in which to represent  $p$  locally, say  $(y^1, \dots, y^n)$ , we have

$$\vec{v}|_p = \sum_{i=1}^n \hat{b}^i(p) \frac{\partial}{\partial y^i}\Big|_p .$$

Since any  $y^i = y^i(x^1, \dots, x^n)$ , we have

$$\begin{aligned} \vec{v}|_p &= \sum_{i=1}^n b^i(p) \frac{\partial}{\partial x^i}\Big|_p \\ &= \sum_{i=1}^n \sum_{j=1}^n b^i(p) \frac{\partial y^j}{\partial x^i} \frac{\partial}{\partial y^j}\Big|_p \\ &= \sum_{i=1}^n \hat{b}^i(p) \frac{\partial}{\partial y^i}\Big|_p . \end{aligned}$$

So  $\hat{b}^i = (\partial y^i / \partial x^j) b^j$ . The fact that a change of coordinates is effectively the application of the chain rule for differentiation motivates the notation  $\partial_i$  for the coordinate basis.

The construction of a vector at a point  $p \in \mathcal{M}$  can be done for all points in  $\mathcal{M}$ , such that we smoothly associate with each point a vector. This construction generates vector fields. The collection of all tangent spaces is called the *tangent bundle*

$$T\mathcal{M} := \bigcup_{p \in \mathcal{M}} T_p\mathcal{M} .$$

### A.1.2 Covectors and 1-forms

With any linear vector space  $V$  we can associate the dual space  $V^*$  of linear functionals acting on  $V$ , i.e.

$$\forall \alpha \in V^* , \quad \alpha : V \rightarrow \mathbb{R} .$$

So with  $T_p\mathcal{M}$ , we can associate the dual space  $T_p^*\mathcal{M}$  of linear functionals acting on vector  $\vec{v} \in T_p\mathcal{M}$ .

$$\alpha : T_p\mathcal{M} \mapsto \mathbb{R} .$$

$$\alpha(a\vec{v} + b\vec{u}) = a\alpha(\vec{v}) + b\alpha(\vec{u}) , \quad \forall \vec{u}, \vec{v} \in T_p\mathcal{M} \text{ and } \alpha \in T_p^*\mathcal{M} .$$

The dual space itself becomes a linear vector space if we set

$$(a\alpha + b\beta)(\vec{v}) = a\alpha(\vec{v}) + b\beta(\vec{v}) , \quad \forall \vec{u}, \vec{v} \in T_p\mathcal{M} \text{ and } \alpha, \beta \in T_p^*\mathcal{M} .$$

The elements  $\alpha, \beta \in T_p^*\mathcal{M}$  are called *covectors at the point*  $p \in \mathcal{M}$ . The dimension of the cotangent space  $\dim T_p^*\mathcal{M} = \dim T_p\mathcal{M} = n$ .

Let  $\vec{e}_1|_p, \dots, \vec{e}_n|_p$  be a basis for the tangent space  $T_p\mathcal{M}$ , then a canonical basis for the cotangent space  $T_p^*\mathcal{M}$  is given by  $\vec{e}^1|_p, \dots, \vec{e}^n|_p$ , where the basis covectors satisfy

$$e^i(e_j) = \delta_j^i = \begin{cases} 1 & \text{if } i = j \\ 0 & \text{if } i \neq j \end{cases}.$$

In case the vectors are represented in a *coordinate basis*,  $\partial_i$ , the basis covectors are denoted by  $dx^j$ . In this case any covector at the point  $p$  can be represented as

$$\alpha = \alpha_1(p) dx^1|_p + \dots + \alpha_n(p) dx^n|_p.$$

Application of such a covector to a tangent vector at  $p$  then yields

$$\begin{aligned} \alpha(v) &= \sum_{i=1}^n \alpha_i(p) dx^i \left( \sum_{j=1}^n v^j(p) \frac{\partial}{\partial x^j} \right) \\ &= \sum_{i=1}^n \sum_{j=1}^n \alpha_i(p) v^j(p) dx^i \left( \frac{\partial}{\partial x^j} \right) \\ &= \sum_{i=1}^n \alpha_i(p) v^i(p). \end{aligned} \tag{A.1.1}$$

**Remark 40.** *In a given basis, application of a covector to a vector resembles the inner product in Euclidean space. However, an inner product depends on the metric tensor, whereas  $\alpha(v)$  is independent of the metric. Furthermore, an inner product is a bilinear form on a single vector space  $V$ , whereas application of a covector to a vector is an operation between two distinct spaces:  $V^* \times V \rightarrow \mathbb{R}$ . That these spaces are really different can be seen when we apply a change of coordinates. In this case vectors and covectors transform differently and should therefore be treated as different mathematical entities.*

**Remark 41.** *A pictorial representation of a vector is usually in terms of an arrow. Covectors can be represented by  $(n-1)$ -dimensional hyper-surfaces, (ordinary surfaces in 3D). Duality pairing between a covector and a vector then yields the number of times the arrow (vector) pierces the surfaces (covectors). For examples of these graphical representations, see Bossavit, [26], Burke, [41] and Misner, Thorne and Wheeler, [126]. The ultimate aim of this distinctive representation is to emphasize the difference between forms and vectors.*

**Remark 42.** *The cotangent space  $T_p^*\mathcal{M}$  is isomorphic to the tangent space  $T_p\mathcal{M}$ . But there is no canonical isomorphism which associates elements  $\alpha \in T_p^*\mathcal{M}$  to elements  $v \in T_p\mathcal{M}$ . It is physics which provides a unique connection between vectors and covectors.*

**Remark 43.** *We cannot 'see' a form, i.e. a linear functional, directly, but we can only assess its action on the elements of the primal space. The only knowledge we*

---

can obtain of a form  $\alpha$  is by applying  $\alpha$  to various elements  $v$  of the vector space. A similar thing happens for some physical variables: Nobody has seen 'force', but we only see the action of a force. We use scales and spring balances to measure force. The deflection of the hands on the scale or the extension of the spring are used to measure force. So we only have access to the work performed by the force,  $F(v)$ . It therefore seems obvious to represent certain physical variables by forms.

Just as we extended the tangent space in a point  $p \in \mathcal{M}$ , to all points in  $\mathcal{M}$  to form the tangent bundle, we can also consider the collection of cotangent spaces for all points in  $\mathcal{M}$ . This defines the cotangent bundle

$$T^*\mathcal{M} := \bigcup_{p \in \mathcal{M}} T_p^*\mathcal{M}.$$

An element (section) of  $T^*\mathcal{M}$  is then written as

$$\alpha^{(1)} = \sum_{k=1}^n \alpha_k(x^1, \dots, x^n) dx^k.$$

Such an element from the cotangent bundle is called a *differentiable 1-form* or a *1-form*. The space of differentiable 1-forms is also denoted by  $\Lambda^1(\mathcal{M})$ .

Application of a 1-form  $\alpha^{(1)}$  to a vector field  $v$  assigns to every point in  $\mathcal{M}$  a real number, i.e.  $\alpha^{(1)}(v)$  is a real-valued function on  $\mathcal{M}$ . We will denote the space of real-valued functions on  $\mathcal{M}$  by  $\Lambda^0(\mathcal{M})$ , the space of 0-forms on  $\mathcal{M}$ .

**Example 42.** Consider a 1-form  $\varphi^{(1)}(x^1, x^2) = \varphi_1(x^1, x^2)dx^1 + \varphi_2(x^1, x^2)dx^2$  and a curve  $\gamma(s) = (\gamma^1(s), \gamma^2(s))$ , such that:

$$\gamma : [0, 1] \mapsto \mathcal{M}$$

The tangent vectors along the curve are given, as usual, by:

$$\vec{g}(s) = \frac{d\gamma^1}{ds} \partial_1 + \frac{d\gamma^2}{ds} \partial_2$$

The action of  $\varphi^{(1)}$  on  $\vec{g}$  is then given by:

$$\varphi^{(1)}(\vec{g}) = \sum_{k=1}^n \varphi_k \frac{d\gamma^k}{ds} = w(s)$$

Where  $w(s)$  is a function of  $s$  and whose Lebesgue integral is:

$$\int_0^1 w(s) = W$$

**Remark 44.** Note that the less usual notation for Lebesgue integral was used. Typically the notation for Lebesgue integral shows the measure term, in this case  $ds$ , but that is optional. The Lebesgue measure was omitted since, by historical misfortune,  $ds$ , the Lebesgue measure has the same notation as a 1-form basis  $dx^1$ , nevertheless both are distinct mathematical objects. This overload of notation is the root of a common confusion between differentials and differential forms (a functional) and measures: A form changes sign under a change of orientation, whereas a measure remains positive.

---

**Remark 45.** As for the physical meaning of this example, consider  $\varphi^{(1)}$  as a force. Hence,  $W$  is the work done by this force along the path  $\gamma(s)$  and  $w(s)$  is a density of work along the path. The integral along a curve is a metric-free operation when the force is represented as a differential form. If the force were represented as a vector, as is the case in many elementary physics books, work would be a metric-dependent concept.

Now that we have defined the 0-forms on  $\mathcal{M}$  and the 1-forms on  $\mathcal{M}$ , we can proceed in different ways to define  $k$ -forms for  $k > 1$ . We can either define exterior powers of a vector space to produce  $k$ -vectors and then define  $k$ -forms as the elements of the dual space of the space of  $k$ -vectors. This approach is described in [174, 69, 41]. Alternatively, we can define a  $k$ -form as an alternating  $k$ -tensor on the tangent space which maps into the real numbers, [167]

$$\alpha^{(k)} : \underbrace{T_p \mathcal{M} \times \cdots \times T_p \mathcal{M}}_{k \text{ copies}} \rightarrow \mathbb{R},$$

with for  $v_i \in T_p \mathcal{M}$ , and  $i = 1, \dots, k$ , we have the following skew-symmetric property,

$$\alpha^{(k)}(\dots, v_i, \dots, v_j, \dots) = -\alpha^{(k)}(\dots, v_j, \dots, v_i, \dots).$$

Here we can define the *exterior product* or *wedge product* to inductively construct  $k$ -forms, for  $1 \leq k \leq n$ . Let  $\Lambda^k(\mathcal{M})$  and  $\Lambda^l(\mathcal{M})$  the space of  $k$ -forms and  $l$ -forms, respectively, with  $k + l \leq n$ , then the *wedge product*,  $\wedge$ , is a mapping:

$$\wedge : \Lambda^k(\mathcal{M}) \times \Lambda^l(\mathcal{M}) \rightarrow \Lambda^{k+l}(\mathcal{M}), \quad k + l \leq n.$$

Consider a sufficiently smooth bounded  $n$ -dimensional oriented manifold  $\mathcal{M} \subset \mathbb{R}^n$  and a coordinate system where points in the manifold,  $\mathbf{x} \in \mathcal{M}$ , are represented by an  $n$  tuple  $\mathbf{x} := (x^1, \dots, x^n)$ . Let  $\alpha^{(k)}$  denote a differential  $k$ -form,  $k \leq n$  and  $\Lambda^k(\mathcal{M})$  denote the space of *differential  $k$ -forms* or  *$k$ -forms*, then  $\alpha^{(k)} \in \Lambda^k(\mathcal{M})$ , can be written as

$$\alpha^{(k)} = \sum_I \alpha_I(\mathbf{x}) dx^{i_1} \wedge dx^{i_2} \wedge \cdots \wedge dx^{i_k},$$

where  $I = i_1, \dots, i_k$ , and  $1 \leq i_1 < \cdots < i_k \leq n$  and where  $\alpha_I(\mathbf{x})$  are continuously differentiable scalar functions.



# Appendix B

## Polynomial Expansions

In this chapter we discuss in more detail the polynomial expansions that are used for the reconstruction operator  $\mathcal{I}$ . Since every element is mapped to a reference element  $\widehat{\Omega} = [-1, 1]$ , using the pullback  $\Phi_m$  introduced in Section ??, the polynomial expansions can be discussed on this reference element. Polynomial expansions can differ due to physical and mathematical considerations. Moreover, different polynomial expansions will differ in orthogonality, conditioning, its approximation properties and its numerical efficiency. In this appendix we distinguish between two types of polynomial expansions, i.e., modal and interpolatory, respectively. Although only interpolatory polynomials have been used throughout the thesis, we also discuss the modal polynomials, since these are used to construct the interpolatory polynomials. We treat the interpolatory polynomials that are used on the primal grid as well as those that correspond to the dual grid.

Since we only use a tensor-based polynomial expansion, the discussion in this appendix is only in 1D. As for notation:  $\mathcal{P}_p$  indicates a  $p^{\text{th}}$  order polynomial space, and  $N$  is the number of volumes in a primal grid.

### B.1 Modal expansion

A modal expansion is a hierarschical expansion where an expansion set of order  $p - 1$  is contained within the expansion set of order  $p$ , then  $\mathcal{P}_{p-1} \subset \mathcal{P}_p$  holds. So higher-order expansion sets are built from the lower-order expansion sets. We will discuss two sets of modal expansions, i.e., the moment expansion and the expansion based on the class of Jacobi polynomials.

**Moment expansion** Moment expansion is the most basic modal expansion, where each order contributes an extra moment to the expansion. Mathematically it is defined as

$$\phi_p(\xi) = \xi^p, \quad p = 0, \dots, P. \quad (\text{B.1.1})$$

It is easy to see that if  $\mathcal{P}_2 = \{1, \xi, \xi^2\}$ , then  $\mathcal{P}_3 = \{1, \xi, \xi^2, \xi^3\} = \mathcal{P}_2 \cup \{\xi^3\}$ . This orthonormal expansion set has for an increasing polynomial order a **linearly/exponential** increasing condition number, see Karniadakis and Sherwin [106]. Although moment expansions are quite popular, and commonly used in the description of higher-order methods, this disadvantage makes it unsuitable for higher-order computations in practice, i.e.,  $p > 3$ .

**Jacobi Polynomials** Jacobi polynomials, denoted by  $\phi_p^{\alpha,\beta}(\xi)$ ,  $p = 0, \dots, P$ , represent the family of polynomial solutions to the singular Sturm-Liouville problem. An important feature of these polynomials is their orthogonality on the interval  $\xi \in [-1, 1]$  with respect to the function  $(1 - \xi)^\alpha(1 + \xi)^\beta$ ,  $(\alpha, \beta > -1)$ . The Sturm-Liouville problem is written as

$$\frac{d}{d\xi} \left[ (1 - \xi)^{1+\alpha}(1 + \xi)^{1+\beta} \frac{dy(\xi)}{d\xi} \right] = -\lambda_p (1 - \xi)^\alpha (1 + \xi)^\beta y(\xi), \quad (\text{B.1.2})$$

where

$$y(\xi) = \phi_p^{\alpha,\beta}(\xi), \quad \lambda_p = p(p + \alpha + \beta + 1).$$

Notice that  $p \in \mathbb{N} \cup \{0\}$  and  $\alpha, \beta > -1 \in \mathbb{R}$ . The Jacobi polynomial is given by Rodriguez formula

$$\phi_p^{\alpha,\beta}(\xi) = \frac{(-1)^p}{2^p p!} (1 - \xi)^{-\alpha} (1 + \xi)^{-\beta} \frac{d^p}{d\xi^p} [(1 - \xi)^{\alpha+p} (1 + \xi)^{\beta+p}]. \quad (\text{B.1.3})$$

An important relationship of these polynomials is their orthogonality

$$\int_{-1}^1 (1 - \xi)^\alpha (1 + \xi)^\beta \phi_p^{\alpha,\beta}(\xi) \phi_q^{\alpha,\beta}(\xi) d\xi = C \delta_{p,q}, \quad (\text{B.1.4})$$

where  $C$  is a constant depending only on  $\alpha, \beta, p, q$ . The polynomials can be constructed with a three term recursion relationship

$$\begin{aligned} \phi_0^{\alpha,\beta}(\xi) &= 1, \\ \phi_1^{\alpha,\beta}(\xi) &= \frac{1}{2}[\alpha - \beta + (\alpha + \beta + 2)\xi] \\ a_p^1 \phi_{p+1}^{\alpha,\beta}(\xi) &= (a_p^2 + a_p^3 \xi) \phi_p^{\alpha,\beta}(\xi) - a_p^4 \phi_{p-1}^{\alpha,\beta}(\xi), \end{aligned}$$

with

$$\begin{aligned} a_p^1 &= 2(p + 1)(p + \alpha + \beta + 1)(2p + \alpha + \beta), \\ a_p^2 &= (2p + \alpha + \beta + 1)(\alpha^2 - \beta^2), \\ a_p^3 &= (2p + \alpha + \beta)(2p + \alpha + \beta + 1)(2p + \alpha + \beta + 2) \\ a_p^4 &= 2(p + \alpha)(p + \beta)(2p + \alpha + \beta + 2). \end{aligned}$$

The derivative of the Jacobi polynomial is given by

$$\frac{d}{d\xi} \phi_p^{\alpha,\beta}(\xi) = \frac{1}{2}(\alpha + \beta + p + 1) \phi_{p-1}^{\alpha+1,\beta+1}(\xi). \quad (\text{B.1.5})$$

Some special values are  $\phi_p^{\alpha,\beta}(1) = \binom{p + \alpha}{p} = \frac{(p + \alpha)!}{\alpha! p!}$  and  $\phi_p^{\alpha,\beta}(-\xi) = (-1)^p \phi_p^{\beta,\alpha}(\xi)$ .

---

**Legendre Polynomials** A class of symmetric polynomials, known as the ultraspheric polynomials, correspond to the choice  $\alpha = \beta$ . Well known ultraspheric polynomials are the Legendre polynomials ( $\alpha = \beta = 0$ ) and the Chebyshev polynomials ( $\alpha = \beta = -\frac{1}{2}$ ). Here the Legendre polynomials,  $L_p(\xi)$ , are employed. The Sturm-Liouville problem for the Legendre polynomials is

$$\left( (1 - \xi^2) L'_p(\xi) \right)' + p(p+1)L_p(\xi) = 0, \quad \text{with } L_p(1) = 1. \quad (\text{B.1.6})$$

where

$$L_p(\xi) = \phi_p^{0,0}(\xi). \quad (\text{B.1.7})$$

The Rodriguez formula for the Legendre polynomials is

$$L_p(\xi) = \frac{(-1)^p}{2^p p!} \frac{d^p}{d\xi^p} (1 - \xi^2)^p. \quad (\text{B.1.8})$$

The special values are  $L_p(1) = 1$ ,  $L_p(-\xi) = (-1)^p L_p(\xi)$ . The derivative for the Legendre polynomials is

$$L'_p(\xi) = \frac{1}{2}(p+1)\phi_{p-1}^{1,1}(\xi). \quad (\text{B.1.9})$$

Some special values for the derivative are,

$$L'_p(\xi_j) = \begin{cases} \frac{(-1)^{p+1}}{2} p(p+1) & \text{for } j = 0, \\ 0 & \text{for } j = 1, \dots, p-1, \\ \frac{1}{2} p(p+1) & \text{for } j = p. \end{cases} \quad (\text{B.1.10})$$

Moreover, there exists the following recurrency relation to compute the derivative of the Legendre polynomial,

$$(\xi^2 - 1)L'_p(\xi) = p(\xi L_p(\xi) - L_{p-1}(\xi)). \quad (\text{B.1.11})$$

The orthogonality relation for the Legendre polynomials is

$$\int_{-1}^1 L_p(\xi) L_q(\xi) d\xi = c_p \delta_{p,q},$$

with  $c_p = \frac{2}{2p+1}$ . If we express some function  $u(\xi)$  in  $\widehat{\Omega} = [-1, 1]$  as

$$u(\xi) = \sum_{p=0}^{\infty} \mu_p L_p(\xi),$$

then we can use the concept of orthogonality to calculate the coefficients  $\mu_q$ .

Now we can use the concept of orthogonality. If we want to know the coefficient  $\mu_q$  we simply multiply the above expansion with  $L_q$ , integrate over the domain  $\Omega$  and divide by the constant  $c_q$

$$\frac{1}{c_q} \int_{-1}^1 u(\xi) L_q(\xi) d\xi = \frac{1}{c_q} \sum_{p=0}^{\infty} \mu_p \int_{-1}^1 L_p(\xi) L_q(\xi) d\xi = \mu_q. \quad (\text{B.1.12})$$

We are free to chose the first basis function, which will be  $L_0(\xi) = 1$ . From the orthogonality condition it follows that  $L_1(\xi) = \xi$ . Orthogonal polynomials obey a nice recurrence relation which for the Legendre polynomials is given by

$$(p+1)L_{p+1}(\xi) = (2p+1)\xi L_p(\xi) - pL_{p-1}(\xi). \quad (\text{B.1.13})$$

## B.2 Interpolatory polynomials

The second category of polynomials are the interpolatory polynomials, as are used in Chapter 7. Here we make use of tensor-products of nodal and edge polynomials to interpolate nodal, edge, surface and volume degrees of freedom. Since the edge polynomials are derived from the nodal interpolants, we mainly focus on nodal interpolatory polynomials in this section.

A nodal expansion is a non-hierarchical expansion, so  $\mathcal{P}_{N-1} \not\subset \mathcal{P}_N$ . It consists of  $N + 1$  polynomials  $l_i(\xi)$ ,  $i = 0, \dots, N$ , each of order  $N$ . Nodal expansions are based upon the Lagrange polynomials which are associated with a set of nodal points. The choice of the location of the points is free, but it plays an important role in the stability and conditioning of the system (see e.g. [106]). When equispaced nodal points are chosen, the condition number increases fast for higher-order polynomials. Moreover, convergence by increasing polynomial is not guaranteed. A convergent and well-conditioned nodal expansion is obtained when using the zeros of the Gauss (G) or Gauss-Lobatto (GL) polynomials are chosen as nodal points. In this section first the Lagrange polynomials are discussed. Next the Gauss-Lobatto polynomials and two types of Gauss polynomials, all based on Legendre polynomials, as specific types of Lagrange polynomials will be described. Finally the edge polynomials are discussed.

**Lagrange polynomials** Let the  $N + 1$  nodal points be denoted by  $\xi_i$ ,  $i = 0, \dots, N$ . The Lagrange polynomial, denoted by  $l_i(\xi)$ , is then the unique polynomial of order  $N$  which has a partition of unity, with the special case that it has an unit value at  $\xi_i$  and is zero at  $\xi_j$  ( $i \neq j$ ). These can be written as

$$\sum_{i=0}^N l_i(\xi) = 1, \quad l_i(\xi_j) = \delta_{i,j}, \quad (\text{B.2.1})$$

where  $\delta_{i,j}$  denotes the Kronecker delta. The Kronecker delta property makes the Lagrange polynomial useful as an interpolation basis. The Lagrange interpolant through the  $N + 1$  nodal points  $\xi_j$  is written as

$$u_h(\xi) = \sum_{i=0}^N u(\xi_i) l_i(\xi). \quad (\text{B.2.2})$$

The Lagrange polynomial can be written in product form as

$$l_i(\xi) = \frac{\prod_{j=0, j \neq i}^N (\xi - \xi_j)}{\prod_{j=0, j \neq i}^N (\xi_i - \xi_j)}. \quad (\text{B.2.3})$$

If  $g(\xi) \in \mathbb{P}_{N+1}(-1, 1)$  is a polynomial of order  $N + 1$  with zeros at the  $N + 1$  nodal points  $x_j \in [-1, 1]$ ,  $j = 0, \dots, N$ , so satisfying  $g(\xi_j) = 0$ , then  $l_i(\xi)$  can be written in more compact form as

$$l_i(\xi) = \frac{g(\xi)}{g'(\xi_i)(\xi - \xi_i)}, \quad \xi \in [-1, 1]. \quad (\text{B.2.4})$$

From this, we can set up a general formulation for the first derivative of the Lagrange polynomials, that is used to obtain the edge interpolatory polynomials. The first derivative reads

$$l'_i(\xi) = \frac{g'(\xi)(\xi - \xi_i) - g(\xi)}{g'(\xi_i)(\xi - \xi_i)^2}, \quad \xi \in [-1, 1]. \quad (\text{B.2.5})$$

From (B.2.4) it can be seen that problems occur when evaluating the Lagrange polynomial in its own point, so  $l_i(\xi_i)$ . Therefore we list the solution of some special cases, that either have the problem of  $\frac{0}{0}$ , or are especially useful for numerical integration. For the Lagrange polynomial evaluated in its own point, we find

$$l_i(\xi_i) = \lim_{\xi \rightarrow \xi_i} l_i(\xi) = \lim_{\xi \rightarrow \xi_i} \frac{g(\xi)}{g'(\xi_i)(\xi - \xi_i)} \stackrel{l'\text{hop}}{=} \lim_{\xi \rightarrow \xi_i} \frac{g'(\xi)}{g'(\xi_i)} = 1, \quad (\text{B.2.6})$$

and

$$l_i(\xi_j) = 0, \text{ since } g(\xi_j) = 0 \text{ for } i \neq j. \quad (\text{B.2.7})$$

These two results were already mentioned in (B.2.1). For the first derivative of Lagrange polynomials, we find the expression

$$\begin{aligned} l'_i(\xi_i) &= \lim_{\xi \rightarrow \xi_i} l'_i(\xi) = \lim_{\xi \rightarrow \xi_i} \frac{g'(\xi)(\xi - \xi_i) - g(\xi)}{g'(\xi_i)(\xi - \xi_i)^2} \\ &\stackrel{l'\text{hop}}{=} \lim_{\xi \rightarrow \xi_i} \frac{g''(\xi)(\xi - \xi_i)}{2g'(\xi_i)(\xi - \xi_i)} = \frac{g''(\xi_i)}{2g'(\xi_i)}. \end{aligned} \quad (\text{B.2.8})$$

and

$$l'_i(\xi_j) = \frac{g'(\xi_j)}{g'(\xi_i)} \frac{1}{\xi_j - \xi_i}. \quad (\text{B.2.9})$$

Next we will concentrate on specific distributions of the nodes, as formulated by the zeros of the function  $g(\xi)$ .

**Gauss-Lobatto-Legendre (GL-L) polynomials** As mentioned in Chapter 7, the zeros of the Gauss-Lobatto polynomial are used as the nodal points for the primal grid. The Gauss-Lobatto-Legendre zeros are given by the function

$$g(\xi) = (1 - \xi^2)L'_N(\xi). \quad (\text{B.2.10})$$

We repeat here the Sturm-Liouville differential equation for Legendre polynomials because it will be used many times below,

$$[(1 - \xi^2)L'_N(\xi)]' + N(N + 1)L_N(\xi) = 0$$

Above we saw that we need up to the second derivative of  $g(x)$ . Here we list them for the case of Legendre-Gauss-Lobatto. The first derivative is given by

$$g'(\xi) = -N(N + 1)L_N(\xi), \quad (\text{B.2.11})$$

The second derivative of  $g(\xi)$  is given by

$$g''(\xi) = -N(N + 1)L'_N(\xi), \quad (\text{B.2.12})$$

with special case

$$g''(\xi_j) = \begin{cases} \frac{(-1)^N}{2} N^2(N+1)^2 & \text{for } j=0, \\ 0 & \text{for } j=1, \dots, N-1, \\ \frac{-1}{2} N^2(N+1)^2 & \text{for } j=N. \end{cases} \quad (\text{B.2.13})$$

Given  $g(x)$  and its first and second derivative, we can express the Gauss-Lobatto-Legendre polynomials as,

$$l_i^{\text{gl}}(\xi) = -\frac{(1-\xi^2)L'_N(\xi)}{N(N+1)L_N(\xi_i)(\xi-\xi_i)}, \quad (\text{B.2.14})$$

with the trivial special case  $l_i^{\text{gl}}(\xi_j) = 0$ , and  $l_i^{\text{gl}}(\xi_i) = 1$ . The first derivative of the Gauss-Lobatto-Legendre polynomial becomes

$$l_i^{\text{gl}\prime}(\xi) = \frac{N(N+1)L_N(\xi)(\xi-\xi_i) + (1-\xi^2)L'_N(\xi)}{N(N+1)L_N(\xi_i)(\xi-\xi_i)^2} \quad (\text{B.2.15})$$

with for the evaluation in its own point

$$l_i^{\text{gl}\prime}(\xi_i) = \begin{cases} -\frac{N(N+1)}{4} & \text{for } i=0, \\ 0 & \text{for } i=1, \dots, N-1, \\ \frac{N(N+1)}{4} & \text{for } i=N. \end{cases} \quad (\text{B.2.16})$$

and for the evaluation in all other points,

$$l_i^{\text{gl}\prime}(\xi_j) = \frac{L_N(\xi_j)}{L_N(\xi_i)} \frac{1}{\xi_j - \xi_i}, \quad i \neq j \text{ and } i, j = 0, \dots, N. \quad (\text{B.2.17})$$

**Gauss-Legendre (G-L) polynomials** The Gauss and extended-Gauss polynomials are used for the dual grid. The zeros for the Gauss-Legendre polynomials are the zeros of the Legendre polynomial,

$$g(\xi) = L_N(\xi). \quad (\text{B.2.18})$$

Substitution in (??) gives the Gauss-Legendre Lagrange polynomial,  $l^{\text{g}}(\xi_i)$ , for  $i = 1, \dots, N$ ,

$$l_i^{\text{g}}(\xi) = \frac{L_N(\xi)}{L'_N(\xi_i)(\xi-\xi_i)}. \quad (\text{B.2.19})$$

The G-L polynomials have  $N$  zeros and are of polynomial order  $N-1$ , one lower than the GL-L polynomials. Its first derivative becomes,

$$l_i^{\text{g}\prime}(\xi) = \frac{L'_N(\xi)(\xi-\xi_i) - L_N(\xi)}{L'_N(\xi_i)(\xi-\xi_i)^2}, \quad (\text{B.2.20})$$

and has the special cases,

$$l_i^{\text{g}}(\xi_j) = \begin{cases} \frac{L'_N(\xi_j)}{L'_N(\xi_i)(\xi_j - \xi_i)}, & i \neq j, 0 \leq i, j \leq N-1, \\ \frac{\xi_i}{1-\xi_i^2}, & i=j. \end{cases} \quad (\text{B.2.21})$$

---

**Extended-Gauss-Legendre (EG-L) polynomials** The extended-Gauss polynomials are less known for Lagrange polynomials. They were first used in the context of spectral element methods in Bouman et al, [30]. They are used to interpolate the nodal values on the dual grid that includes the boundary values. The locations of the nodal points are based on the zeros of the Legendre polynomial, as in Gauss-Legendre polynomials, and the two end points  $\pm 1$ ,

$$g(\xi) = (\xi^2 - 1)L_N(\xi). \quad (\text{B.2.22})$$

The extended-Gauss-Legendre polynomials  $l_i^{\text{eg}}(\xi)$ , for  $i = 0, \dots, N + 1$ , is given by

$$l_i^{\text{eg}}(\xi) = \frac{(\xi^2 - 1)L_N(\xi)}{[(2\xi_i L_N(\xi_i) + (\xi_i^2 - 1)L'_N(\xi_i))(\xi - \xi_i)]}. \quad (\text{B.2.23})$$

The EG-L polynomials have  $N + 1$  zeros and are of polyoom order  $N + 1$ . The first derivative then becomes,

$$l_i^{\text{eg}}(\xi) = \frac{[2\xi L_N(\xi) + (\xi^2 - 1)L'_N(\xi)](\xi - \xi_i) - (\xi^2 - 1)L_N(\xi)}{[2\xi_i L_N(\xi_i) + (\xi_i^2 - 1)L'_N(\xi_i)](\xi - \xi_i)^2}, \quad (\text{B.2.24})$$

with special values,

$$l_i^{\text{eg}}'(\xi_j) = \begin{cases} \frac{2\xi_j L_N(\xi_j) + (\xi_j^2 - 1)L'_N(\xi_j)}{[2\xi_i L_N(\xi_i) + (\xi_i^2 - 1)L'_N(\xi_i)](\xi_j - \xi_i)}, & i \neq j, 0 \leq i, j \leq N + 1, \\ \frac{-\xi_i}{1 - \xi_i^2}, & 0 < i = j < N + 1, \\ -\frac{1}{2}(N(N + 1) + 1), & i = j = 0, \\ \frac{1}{2}(N(N + 1) + 1), & i = j = N + 1. \end{cases} \quad (\text{B.2.25})$$

**Edge Polynomials** ??????????????????????

### B.3 Numerical integration

The numerical integration or quadrature is closely related to the properties of the Lagrange polynomials. If we integrate a function  $u(\xi)$ , expanded in terms of an infinite Lagrange polynomial expansion, we get

$$\int_{-1}^1 u(\xi) d\xi = \sum_{i=0}^{\infty} \int_{-1}^1 u(\xi_i) l_i(\xi) d\xi = \sum_{i=0}^{\infty} w_i u(\xi_i),$$

where

$$w_i = \int_{-1}^1 l_i(\xi) d\xi \quad (\text{B.3.1})$$

are the integration weights corresponding to the Lagrange polynomial  $l_i(\xi)$ . In numerical integration we restrict ourselves to a finite set of quadrature points. Then

$$\int_{-1}^1 u(\xi) d\xi = \sum_{i=0}^N w_i u(\xi_i) + R(u),$$

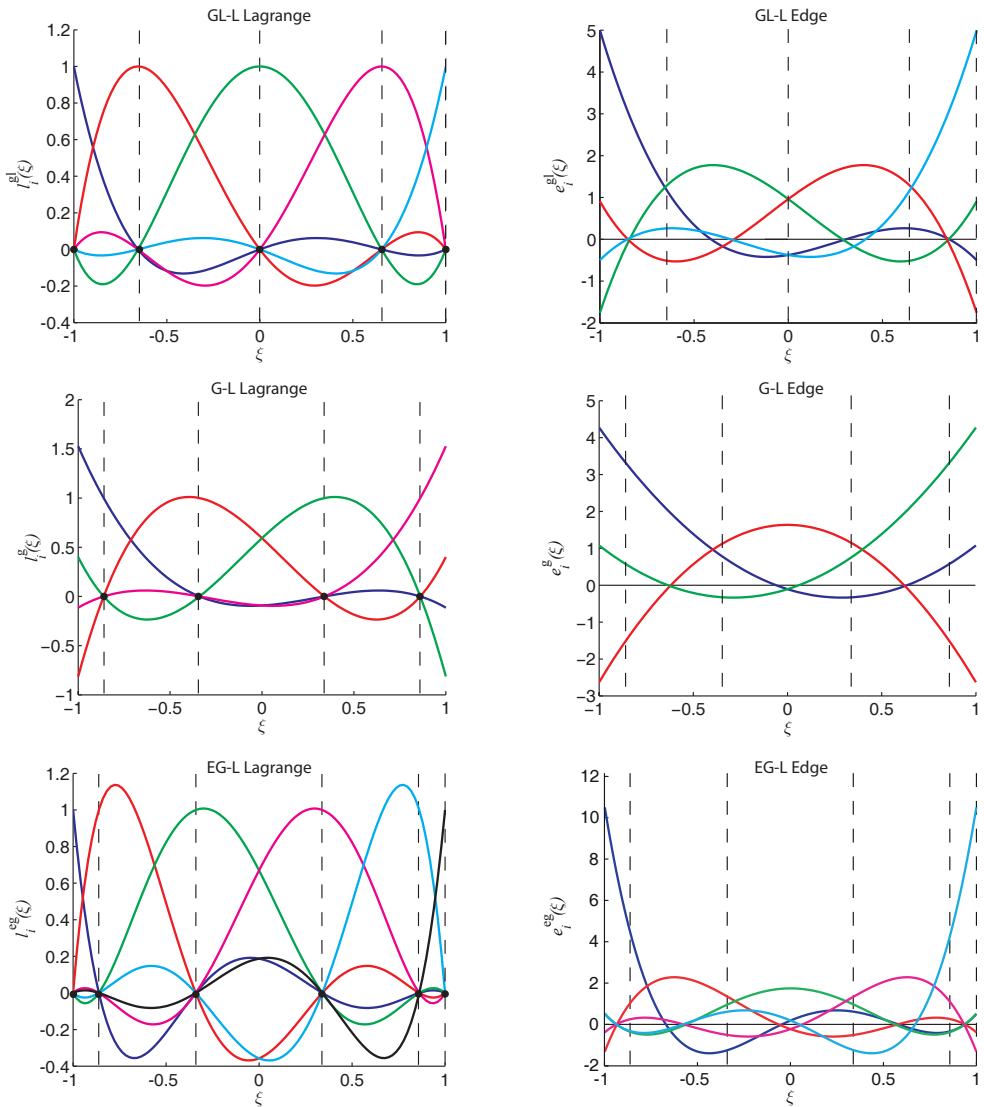


Figure B.1: Polynomial expansions of Gauss-Lobatto-Legendre (GL-L), Gauss-Legendre (G-L) and extended-Gauss-Legendre (EG-L) Lagrange and edge polynomials for  $N = 4$ .

---

where  $R(u)$  indicates a remainder term. In this work we only consider Gauss-Lobatto-Legendre, Gauss-Legendre and extended-Gauss-Legendre polynomials as Lagrange polynomials. The quadrature weights of the first two are given by,

$$w_i^{\text{gl}} = \frac{2}{N(N+1)[L_N(\xi_i)]^2}, \quad \text{for } i = 0, \dots, N, \quad (\text{B.3.2})$$

and

$$w_i^{\text{g}} = \frac{2}{(1-\xi_i^2)[L'_N(\xi_i)]^2}, \quad \text{for } i = 1, \dots, N. \quad (\text{B.3.3})$$

An interesting property of the EG-L quadrature weights is that with (B.3.1), we find that the weights of the additional two end-points are zero, while the weights of the interior points are equal to the G-L weights, so

$$w_i^{\text{eg}} = \begin{cases} w_i^{\text{g}} & i = 1, \dots, N, \\ 0 & i = 0 \text{ or } i = N+1. \end{cases} \quad (\text{B.3.4})$$

So even in the polynomial expansion and numerical integration we recognize the special role the boundary points play on the dual grid, with respect to the interior points.

In case  $u(\xi)$  is a polynomial of order  $2N - 1$  or less then the remainder  $R(u) = 0$  and so the numerical integration is exact. Therefore, evaluating an  $L^2$ -inner product of two edge functions, which are  $\varepsilon_i(\xi) \in \mathcal{P}_{N-1}$ , can be done exact with standard GL-L or G-L quadrature, while the  $L^2$ -inner product of two Lagrange polynomials,  $l_i(x) \in \mathcal{P}_N$ , is nearly exact. Examples for GL-L integration are given below,

$$(l_i^{\text{gl}}(\xi), l_j^{\text{gl}})_{\widehat{\Omega}} = \int_{-1}^1 l_i^{\text{gl}}(\xi) l_j^{\text{gl}}(\xi) d\xi \approx w_p^{\text{gl}}, \quad \text{with } p = i = j, \quad (\text{B.3.5})$$

$$(\varepsilon_i^{\text{gl}}(\xi), \varepsilon_j^{\text{gl}})_{\widehat{\Omega}} = \int_{-1}^1 \varepsilon_i^{\text{gl}}(\xi) \varepsilon_j^{\text{gl}}(\xi) d\xi = \sum_{p=0}^N w_p^{\text{gl}} \varepsilon_i^{\text{gl}}(\xi_p) \varepsilon_j^{\text{gl}}(\xi_p). \quad (\text{B.3.6})$$

Although in (B.3.5) the GL-quadrature is only nearly exact, the resultant matrix is a diagonal matrix instead of a full matrix. This has a main computational advantage.



# Bibliography

- [1] H. Abboud, F. E. Chami, and T. Sayah. A priori and a posteriori estimates for three-dimensional Stokes equations with nonstandard boundary conditions. *Numerical methods for partial differential equations*, 2011.
- [2] R. Abraham, J. Marsden, and T.Ratiu. *Manifolds, tensor analysis, and applications*, volume 75 of *Applied Mathematical Sciences*. Springer, second edition, 2001.
- [3] D. Arnold, D. Boffi, and R. Falk. Approximation by quadrilateral finite elements. *Mathematics of computation*, 71(239):909–922, 2002.
- [4] D. Arnold, D. Boffi, and R. Falk. Quadrilateral  $H(\text{div})$  finite elements. *SIAM journal of numerical analysis*, 42(6):2429–2451, 2005.
- [5] D. Arnold, R. Falk, and J. Gopalakrishnan. Mixed finite element approximation of the vector Laplacian with Dirichlet boundary conditions. *Mathematical Models & Methods in Applied Sciences*, 22(9), 2012.
- [6] D. Arnold, R. Falk, and R. Winther. Finite element exterior calculus, homological techniques, and applications. *Acta Numerica*, pages 1–155, 2006.
- [7] D. Arnold, R. Falk, and R. Winther. Geometric decomposition and local bases for spaces of finite element differential forms. *Computer methods in applied mechanics and engineering*, 198:1660–1672, 2009.
- [8] D. Arnold, R. Falk, and R. Winther. Finite element exterior calculus: from Hodge theory to numerical stability. *Bulletin of the American mathematical society*, 47:281–354, 2010.
- [9] K. Atkinson and W. Han. *Theoretical Numerical Analysis*, volume 39 of *Texts in Applied Mathematics*. Springer, 2009.
- [10] A. Back and E. Sonnendrücker. Spline discrete differential forms. Application to Maxwell’s equations. Technical report, IRMA, CNRS and Université de Strasbourg, 2011.

- 
- [11] M. Benzi, G. Golub, and J. Liesen. Numerical solution of saddle point problems. *Acta Numerica*, pages 1–137, 2005.
  - [12] C. Bernardi and N. Chorfi. Spectral discretization of the vorticity, velocity, and pressure formulation of the Stokes problem. *SIAM journal of numerical analysis*, 44(2):826–850, 2006.
  - [13] C. Bernardi and Y. Maday. *Approximations spectrale de problèmes aux limites elliptiques*. Springer-Verlag, 1992.
  - [14] P. Bochev. A discourse on variational and geometric aspects of stability of discretizations. Technical report, Sandia National Laboratories, 2003.
  - [15] P. Bochev, C. Dohrmann, and M. Gunzburger. Stabilization of low-order mixed finite elements for the Stokes equations. *SIAM Journal Numerical Analysis*, 44:82–101, 2006.
  - [16] P. Bochev and M. Gunzburger. A locally conservative mimetic least-squares finite element method for the Stokes equations. In I. Lirkov, S. Margenov, and J. Wasniewski, editors, *Proceedings of LSSC 2009*, volume 5910 of *Springer Lecture Notes in Computer Science*, page 637–644, 2009.
  - [17] P. Bochev and M. Gunzburger. *Least-Squares Finite Element Methods*, volume 166 of *Applied Mathematical Sciences*. Springer, 2009.
  - [18] P. Bochev and J. Hyman. Principles of mimetic discretizations of differential operators. In D. Arnold, P. Bochev, R. Lehoucq, R. Nicolaides, and M. Shashkov, editors, *Compatible Discretizations*, volume 142 of *IMA Volumes in Mathematics and its Applications*, pages 89–119. Springer, 2006.
  - [19] B. Boffi, P. Fernandes, L. Gastaldi, and I. Perugia. Computational models of electromagnetic resonators: analysis of edge element approximation. *SIAM Journal Numerical Analysis*, 36:1264–1290, 1999.
  - [20] D. Boffi. *Compatible Spatial Discretizations*, volume 142, chapter Compatible Discretizations for Eigenvalue Problems, pages 121–142. Springer, 2006.
  - [21] D. Boffi. *Numerical Mathematics and Advanced Applications 2009*, chapter Discrete Differential Forms, Approximation of Eigenvalue Problems, and Application to the  $p$  Version of Edge Finite Elements, pages 3–14. Springer, 2009.
  - [22] D. Boffi. Finite element approximation of eigenvalue problems. *Acta Numerica*, pages 1–120, 2010.
  - [23] D. Boffi, M. Costabel, M. Dauge, L. Demkowicz, and R. Hiptmair. Discrete compactness for the  $p$ -version of discrete differential forms. *SIAM Journal Numerical Analysis*, 49:135–158, 2011.
  - [24] D. Boffi and L. Gastaldi. Some remarks on quadrilateral mixed finite elements. *Computer and Structures*, 87(11-12):751 – 757, 2009.

- 
- [25] A. Bossavit. Whitney forms: A class of finite elements for three-dimensional computations in electromagnetism. In *Proc. IEE-A*, volume 135, pages 493–500, 1988.
  - [26] A. Bossavit. On the geometry of electromagnetism. *Journal of Japanese Society of applied electromagnetics and mechanics*, 6:17–28, 114–123, 233–240, 318–326, 1998.
  - [27] A. Bossavit. Computational electromagnetism and geometry. *Journal of Japanese Society of applied electromagnetics and mechanics*, 7, 1999, 2000.
  - [28] A. Bossavit. Generating Whitney forms of polynomial degree one higher degree. *IEEE Trans. Magn.*, 38:341–344, 2002.
  - [29] O. Botella and R. Peyret. Benchmark spectral results on the lid-driven cavity flow. *Computers & fluids*, 27(4):421–433, 1998.
  - [30] M. Bouman, A. Palha, J. Kreeft, and M. Gerritsma. A conservative spectral element method for arbitrary domains. In J. Hesthaven and E. Rønquist, editors, *Spectral and High Order Methods for Partial Differential Equations*, pages 111–120. Springer, 2011.
  - [31] J. Bramble and P. Lee. On variational formulations for the Stokes equations with nonstandard boundary conditions. *RAIRO modelisation mathematique et analyse numerique*, 28(7):903–919, 1994.
  - [32] S. Brenner and L. Scott. *The Mathematical Theory of Finite Element Methods*. Springer Verlag, 1994.
  - [33] F. Brezzi and A. Buffa. Innovative mimetic discretizations for electromagnetic problems. *Journal of computational and applied mathematics*, 234:1980–1987, 2010.
  - [34] F. Brezzi, A. Buffa, and K. Lipnikov. Mimetic finite differences for elliptic problems. *Mathematical Modelling and Numerical Analysis*, 43(2):277–296, 2009.
  - [35] F. Brezzi, J. Douglas, M. Fortin, and L. Marini. Efficient rectangular mixed finite elements in two and three space variables. *Mathematical Modelling and Numerical Analysis*, 21:581–604, 1987.
  - [36] F. Brezzi, J. Douglas, and L. Marini. Two families of mixed finite elements for second order elliptic problems. *Numerische Mathematik*, 47:217–235, 1985.
  - [37] F. Brezzi and M. Fortin. *Mixed and hybrid finite element methods, volume 15 of Springer Series in Computational Mathematics*. Springer-Verlag, New York, 1991.
  - [38] J. Brüning and M. Lesch. Hilbert complexes. *Journal of Functional Analysis*, 108:88–132, 1992.
  - [39] A. Buffa, C. de Falco, and G. Sangalli. Isogeometric analysis: stable elements for the 2D Stokes equation. *Int. J. Numer. Meth. Fluids*, 65:1407–1422, 2011.

- 
- [40] A. Buffa, J. Rivas, G. Sangalli, and R. Vazquez. Isogeometric discrete differential forms in three dimensions. *SIAM journal of numerical analysis*, 49:818–844, 2011.
  - [41] W. Burke. *Applied differential geometry*. Cambridge Univ Pr, 1985.
  - [42] C. Canuto, M. Hussaini, A. Quarteroni, and T. Zang. *Spectral Methods, fundamentals in single domains*. Springer, 2006.
  - [43] C. Chang and J. Nelson. Least-squares finite element method for the Stokes problem with zero residual of mass conservation. *SIAM journal of numerical analysis*, 34(2):480–489, 1997.
  - [44] Q. Chen, S. Chen, and G. Eyink. The joint cascade of energy and helicity in three dimensional turbulence. *Physics of fluids*, 15:361–374, 2003.
  - [45] S. Christiansen and R. Winther. Smoothed projections in finite element exterior calculus. *Mathematics of computation*, 77:813–829, 2008.
  - [46] P. Ciarlet and P.-A. Raviart. Interpolation theory over curved elements, with applications to finite element methods. *Comput. Methods Appl Mech. Engrg.*, 1:217–249, 1972.
  - [47] M. Costabel. A coercive bilinear form for Maxwell’s equations. *Journal of Mathematical Analysis and Applications*, 157:527–541, 1991.
  - [48] M. Costabel and M. Dauge. *Computation of resonance frequencies for Maxwell equations in non-smooth domains*, volume 31 of *Lecture Notes in Computational Science and Engineering*, chapter Topics in Computational Wave Propagation. Springer, 2003.
  - [49] J. Cottrell, T. Hughes, and Y. Bazilevs. *Isogeometric Analysis, Toward Integration of CAD and FEA*. Wiley, 2009.
  - [50] M. Dauge. Benchmark computations for Maxwell equations for the approximation of highly singular solutions.
  - [51] V. de Beauche and S. Sen. Discretizing geometry and preserving topology I: A discrete exterior calculus. 2004.
  - [52] C. de Boor. *A Practical Guide to Splines*. Springer, revised edition edition, 2001.
  - [53] B. de Maerschalck and M. Gerritsma. Higher-order Gauss-Lobatto Integration for Non-Linear Hyperbolic Equations. *Journal of Scientific Computing*, 27(1-3):201–214, 2006.
  - [54] J. Deang and M. Gunzburger. Issues related to least-squares finite element methods for the Stokes equations. *SIAM Journal Scientific Computing*, 20:878–906, 1998.

- 
- [55] M. Desbrun, A. Hirani, M. Leok, and J. Marsden. Discrete Exterior Calculus. *arXiv:math/0508341*, 2005.
  - [56] M. Desbrun, E. Kanso, and Y. Tong. *ACM SIGGRAPH Course Notes on Discrete Differential Geometry*, chapter Discrete differential forms for computational modeling. 2005.
  - [57] J. Dieudonné. *A History of Algebraic and Differential Topology, 1900 - 1960*. Birkhäuser, 1989.
  - [58] J. Dodziuk. Finite difference approach to the Hodge theory of harmonic functions. *American Journal of Mathematics*, 98(1):79–104, 1976.
  - [59] F. Dubois. Vorticity-velocity-pressure formulation for the Stokes problem. *Mathematical methods in the applied sciences*, 25:1091–1119, 2002.
  - [60] F. Dubois, M. Salaün, and S. Salmon. First vorticity-velocity-pressure numerical scheme for the Stokes problem. *Comput. Methods Appl Mech. Engrg.*, 192:4877–4907, 2003.
  - [61] S. Elcott, Y. Tong, E. Kanso, P. Schroder, and M. Desbrun. Stable, Circulation-Preserving, Simplicial Fluids. *ACM Transactions on Graphics*, 2007.
  - [62] P. Erdős and P. Vértesi. On the almost everywhere divergence of Lagrange interpolatory polynomials for arbitrary system of nodes. *Acta mathematica Academiae Scientiarum Hungaricae Tomus*, 36(1-2):71–89, 1980.
  - [63] A. Ern and J.-L. Guermond. *Theory and Practice of Finite Elements*, volume 159 of *Applied Mathematical Sciences*. Springer, 2004.
  - [64] A. Ern, J.-L. Guermond, and L. Quartapelle. Vorticity-velocity formulations of the Stokes problem in 3D. *Mathematical methods in the applied sciences*, 22:531–546, 1999.
  - [65] J. Evans. *Divergence-free B-spline discretizations for the Stokes and Navier-Stokes equations*. PhD thesis, University of Texas, 2011.
  - [66] J. Evans and T. Hughes. Isogeometric divergence-conforming B-splines for the Darcy-Stokes-Brinkman equations. Technical Report 12-03, ICES, 2012.
  - [67] L. Fejér. Bestimmung derjenigen Abszissen eines Intervalles, für welche die Quadratsumme der Grundfunktionen der Lagrangeschen Interpolation in Intervalle ein Möglichst kleines Maximum Besitzt. *Annali della Scuola Normale Superiore di Pisa, Classe di Scienze*, 3:263–267, 1932.
  - [68] R. Feynman, R. Leighton, and M. Sands. *Lecture notes in physics*, volume II. Addison-Wesley, Reading MA, 1963.
  - [69] H. Flanders. *Differential forms with applications to the physical sciences*. Dover publications, 1989.

- 
- [70] P. Franca and T. Hughes. Two classes of mixed finite element methods. *Comp. Meth. Appl. Mech. Eng.*, 69:89–129, 1988.
  - [71] T. Frankel. *The geometry of physics, an introduction*. Cambridge University Press, 2006.
  - [72] A. Frölicher and A. Nijenhuis. Theory of vector valued differential forms. part i. *Indagationes Mathematicae*, 18:338–359, 1956.
  - [73] M. Gerritsma. Edge functions for spectral element methods. In J. Hesthaven and E. Rønquist, editors, *Spectral and High Order Methods for Partial Differential Equations*, pages 199–208. Springer, 2011.
  - [74] M. Gerritsma. An introduction to a compatible spectral discretization method. *Mechanics of advanced materials and structures*, 19(1-3):48–67, 2012.
  - [75] M. Gerritsma, J. Kreeft, A. Palha, P. Rebelo, and R. Hiemstra. The geometric basis of mimetic spectral approximations. In *ECCOMAS*, 2012.
  - [76] M. Gerritsma and A. Palha. Least-squares spectral element method on a staggered grid. *Large scale scientific computing, Lecture notes on computer science*, 5910:659–666, 2010.
  - [77] M. Gerritsma and T. Phillips. Discontinuous spectral element approximations for the velocity-pressure-stress formulation of the Stokes problem. *Int. J. Numer. Meth. Eng.*, 43:1401–1419, 1998.
  - [78] V. Girault. Incompressible finite element methods for Navier-Stokes equations with nonstandard boundary conditions in  $\mathbb{R}^3$ . *Mathematics of computation*, 51(183):55–74, July 1988.
  - [79] V. Girault and P. Raviart. *Finite Element Methods for Navier-Stokes equations*. Springer-Verlag, 1986.
  - [80] W. Gordon and C. Hall. Transfinite element methods: blending-function interpolation over arbitrary curved element domains. *Numerische Mathematik*, 21(2):109–129, 1973.
  - [81] H. Gümral. Lagrangian description, symplectic structure, and invariants of 3d fluid flow. *Physics Letters A*, 232:417–424, 1997.
  - [82] F. Harlow and J. Welch. Numerical calculations of time dependent viscous incompressible flow of fluid with a free surface. *Physics of fluids*, 8(12):2182–2189, 1965.
  - [83] J. Harrison. geometric hodge star operator with applications to the theorems of Gauss and Green. In *Proceedings of the Cambridge Philosophical Society*, volume 139, 2006.
  - [84] A. Hatcher. *Algebraic topology*. Cambridge University Press, 2002.

- 
- [85] H. Heumann. *Eulerian and Semi-Lagrangian Methods for Advection-Diffusion of Differential Forms*. PhD thesis, ETH Zürich, 2011.
  - [86] H. Heumann and R. Hiptmair. Refined convergence theory for semi-Lagrangian schemes for pure advection. Technical report, ETH, 2011.
  - [87] H. Heumann, R. Hiptmair, K. Li, and J. Xu. Semi-Lagrangian methods for advection of differential forms. Technical report, ETH, 2011.
  - [88] H. Heumann, R. Hiptmair, and J. Xu. A semi-Lagrangian method for convection of differential forms. Technical report, ETH, 2009.
  - [89] J. Heys, E. Lee, T. Manteuffel, and S. McCormick. On mass-conserving least-squares methods. *SIAM Journal Scientific Computing*, 28(5):1675–1693, 2006.
  - [90] R. Hiemstra. Isogeometric mimetic methods. Master’s thesis, Delft University of Technology, 2011.
  - [91] D. Hilbert. Mathematical problems. *Bulletin of the American Mathematical Society*, 8(10):437–479, 1902.
  - [92] R. Hiptmair. Discrete Hodge operator. *Numerische Mathematik*, 90:265–289, 2001.
  - [93] R. Hiptmair. *PIER*, volume 42, chapter Higher order Whitney forms, pages 271–299. 2001.
  - [94] R. Hiptmair. Finite elements in computational electromagnetism. *Acta Numerica*, pages 237–339, 2002.
  - [95] A. Hirani. *Discrete Exterior Calculus*. PhD thesis, California Institute of Technology, 2003.
  - [96] T. Hughes and L. Franca. A new finite element formulation for computational fluid dynamics: VII. The Stokes problem with various well-posed boundary conditions: symmetric formulations that converge for all velocity/pressure spaces. *Comp. Meth. Appl. Mech. Eng.*, 65:85–96, 1987.
  - [97] T. Hughes, P. Franca, and M. Balestra. A new finite element formulation for computational fluid dynamics: V. Circumventing the Babuška-Brezzi condition: A stable Petrov-Galerkin formulation of the Stokes problem accomodating equal-order interpolations. *Comp. Meth. Appl. Mech. Eng.*, 59:85–99, 1986.
  - [98] J. Hyman, J. Morel, M. Shashkov, and S. Steinberg. Mimetic finite difference methods for diffusion equations. *Computational Geosciences*, 6(3-4):333–352, 2002.
  - [99] J. Hyman and J. Scovel. Deriving mimetic difference approximations to differential operators using algebraic topology. Technical report, Los Alamos National Laboratory, 1988.

- 
- [100] J. M. Hyman, M. Shashkov, and S. Steinberg. The numerical solution of diffusion problems in strongly heterogeneous non-isotropic materials. *Journal of Computational Physics*, 132:130–148, 1997.
  - [101] J. M. Hyman and S. Steinberg. The convergence of mimetic methods for rough grids. *Computers and Mathematics with applications*, 47(10-11):1565–1610, 2004.
  - [102] C. M. Institute. Millennium prize problems.
  - [103] C. Isham. *Modern differential geometry for physicists*. World scientific, 2001.
  - [104] B. Jiang. *The least-squares finite element method*. Springer, 1998.
  - [105] E. Kanso, M. Arroyo, Y. Tong, A. Yavari, J. Marsden, and M. Desbrun. On the geometric character of stress in continuum mechanics. *Z. angew. Math. Phys.*, 58:1–14, 2007.
  - [106] G. Karniadakis and S. Sherwin. *Spectral/hp element methods for CFD*. Numerical Mathematics and Scientific Computation. Oxford University Press, 1999.
  - [107] T. Kattelans and W. Heinrichs. Conservation of mass and momentum of the least-squares spectral collocation scheme for the Stokes problem. *Journal of Computational Physics*, 228:4649–4664, 2009.
  - [108] D. Kopriva. A conservative staggered-grid Chebyshev Multidomain method for compressible flows. II A semi-structured method. *Journal of Computational Physics*, 128:475–488, 1996.
  - [109] D. Kopriva. A staggered-grid multidomain method for the compressible Navier-Stokes equations. *Journal of Computational Physics*, 143:125–158, 1998.
  - [110] D. Kopriva and J. Kolias. A conservative staggered-grid Chebyshev Multidomain method for compressible flows. *Journal of Computational Physics*, 125:244–261, 1996.
  - [111] J. Kreeft and M. Gerritsma. A priori error estimates for compatible spectral discretization of the Stokes problem for all admissible boundary conditions. *submitted*, arXiv:1206.2812, 2012.
  - [112] J. Kreeft and M. Gerritsma. Higher-order compatible discretization on hexahedrals. In J. Hesthaven and E. Rønquist, editors, *Spectral and High Order Methods for Partial Differential Equations*, page to appear. Springer, 2013.
  - [113] J. Kreeft and M. Gerritsma. Mixed mimetic spectral element method for Stokes flow: a pointwise divergence-free solution. *Journal Computational Physics*, arXiv:1201.4409, 2013.
  - [114] J. Kreeft, A. Palha, and M. Gerritsma. Mimetic spectral element method for generalized convection-diffusion problems. In *Proceedings of ECCOMAS CFD*, 2010.

- 
- [115] J. Kreeft, A. Palha, and M. Gerritsma. Mimetic framework on curvilinear quadrilaterals of arbitrary order. *submitted*, arXiv:1111.4304, 2011.
  - [116] S. Kurz and B. Auchmann. Differential Forms and Boundary Integral Equations for Maxwell-Type Problems. In U. Langer, M. Schanz, O. Steinbach, and W. L. Wendland, editors, *Fast Boundary Element Methods in Engineering and Industrial Applications*, volume 63 of *Lecture Notes in Applied and Computational Mechanics*, pages 1–62. Springer, 2012.
  - [117] P. Lax and Richtmyer. Survey of the stability of linear finite difference equations. *Communications on pure and applied mathematics*, 9:267–293, 1956.
  - [118] D. Lilly. On the computational stability of numerical solutions of time-dependent nonlinear geophysical fluid dynamics problems. 93:11–26. *Mon. Weather Rev.*, 93:11–26, 1965.
  - [119] W. Massey. *Algebraic topology: an introduction*. Springer-Verlag, 1984.
  - [120] W. Massey. *A Basic Course in Algebraic Topology*. Springer, 1991.
  - [121] C. Mattiussi. An analysis of finite volume, finite element, and finite difference methods using some concepts from algebraic topology. *Journal of computational physics*, 133:289–309, 1997.
  - [122] C. Mattiussi. A reference discretization strategy for the numerical solution of physical field problems. *Advances in Imaging and Electron Physics*, 121:144–276, 2000.
  - [123] C. Mattiussi. The finite volume, finite element, and finite difference methods as numerical methods for physical field problems. *Advances in Imaging and Electron Physics*, 113:1–147, 2000.
  - [124] C. Mattiussi. *Advances in Imaging and Electron Physics*, volume 21. Academic Press, 2002.
  - [125] J. Maxwell. Remarks on the mathematical classification of physical quantities. *Proceedings of the London Mathematical Society*, III(34):224–232, 1871.
  - [126] C. Misner, K. Thorne, and J. Wheeler. *Gravitation*. WH Freeman, 1973.
  - [127] H. Moffatt. Viscous and resistive eddies near a sharp corner. *Journal of Fluid Mechanics*, 64:1–18, 1964.
  - [128] H. Moffatt and A. Tsinober. Helicity in laminar and turbulent flow. *Annual review of fluid mechanics*, 24:281–312, 1992.
  - [129] P. Monk. *Finite elements for Maxwell's equations*. Clarendon Press, 2008.
  - [130] S. Morita. *Geometry of differential forms*. American Mathematical Society, 2001.
  - [131] P. Mullen, K. Crane, D. Pavlov, Y. Tong, and M. Desbrun. Energy-preserving integrators for fluid animation. *ACM Transactions on Graphics*, 28(3), 2009.

- 
- [132] J. Munkres. *Elements of algebraic topology*. Westview Press, 1984.
  - [133] J. Nédélec. Mixed Finite Elements in  $\mathbb{R}^3$ . *Numerische Mathematik*, 35:315–341, 1980.
  - [134] J. Nédélec. A new family of mixed finite elements in  $\mathbb{R}^3$ . *Numerische Mathematik*, 50:57–81, 1986.
  - [135] S. Neuman. Theoretical derivation of Darcy’s law. *Acta Mechanica*, 25:153–170, 1977.
  - [136] M. Olshanskii and L. Rebholz. Note on helicity balance of the Galerkin method for the 3d Navier-Stokes equations. *Computer Methods in Applied Mechanics and Engineering*, 199:1032–1035, 2010.
  - [137] P. Olver. *Applications of Lie groups to differential equations*. Springer, 1998.
  - [138] A. Palha and M. Gerritsma. Mimetic least-squares spectral/hp finite element method for the Poisson equation. In I. Lirkov, S. Margenov, and J. Waśniewski, editors, *Large-Scale Scientific Computing*, volume 5910/2010 of *Lecture notes in Computer science*, pages 662–670, 2010.
  - [139] A. Palha and M. Gerritsma. Spectral element approximation of the Hodge- $\star$  operator in curved elements. In J. Hesthaven and E. Rønquist, editors, *Spectral and High Order Methods for Partial Differential Equations*, pages 283–292. Springer, 2011.
  - [140] A. Palha, P. P. Rebelo, R. Hiemstra, J. Kreeft, and M. Gerritsma. Physics-compatible discretization techniques on single and dual grids, with application to the poisson equation of volume forms. *Submitted to Journal Computational Physics*, 2012.
  - [141] D. Pavlov, P. Mullen, Y. Tong, E. Kanso, J. Marsden, and M. Desbrun. Structure-preserving discretization of incompressible fluids. *Physica D*, 2011.
  - [142] J. Perot, D. Vidovic, and P. Wesseling. *Compatible Spatial Discretizations*, volume 142 of *IMA Volumes in Mathematics and its Applications*, chapter Mimetic reconstruction of vectors, pages 173–188. Springer, 2006.
  - [143] J. B. Perot. Conservation properties of unstructured staggered mesh schemes. *Journal of Computational Physics*, 159(1):58–89, 2000.
  - [144] J. B. Perot. Discrete conservation properties of unstructured mesh schemes. *Annual review of fluid mechanics*, 43:299–318, 2011.
  - [145] J. B. Perot and V. Subramanian. A Discrete Calculus Analysis of the Keller Box Scheme and a Generalization of the Method to Arbitrary Meshes. *Journal of Computational Physics*, 226(1):494–508, 2007.
  - [146] J. B. Perot and V. Subramanian. Discrete calculus methods for diffusion. *Journal of Computational Physics*, 224(1):59–81, 2007.

- 
- [147] R. Peyret and T. Taylor. *Computational Methods for Fluid Flow*. Springer, 1983.
  - [148] J. Pontaza and J. Reddy. Spectral/hp least-squares finite element formulation for the Navier-Stokes equations. *Journal of Computational Physics*, 190:523–549, 2003.
  - [149] M. Proot. *The Least-Squares Spectral Element Method*. PhD thesis, Delft University of Technology, 2003.
  - [150] M. Proot and M. Gerritsma. Least-squares spectral elements applied to the Stokes problem. *Journal of Computational Physics*, 181:454–477, 2002.
  - [151] M. Proot and M. Gerritsma. Mass- and momentum conservation of the least-squares spectral element method for the Stokes problem. *Journal of scientific computing*, 27(1-3):389–401, 2006.
  - [152] F. Rapetti. High order edge elements on simplicial meshes. *ESIAM: Mathematical Modeling and Numerical Analysis*, 41(6):1001–1020, 2007.
  - [153] F. Rapetti and A. Bossavit. Whitney forms of higher degree. *SIAM journal of numerical analysis*, 47(3):2369–2386, 2009.
  - [154] P. Raviart and J. Thomas. A mixed finite element method for 2nd order elliptic problems. *Mathematical Aspects of the Finite Element Method, Lecture Notes in Mathematics*, 606:292–315, 1977.
  - [155] N. Robidoux. A New Method of Construction of Adjoint Gradients and Divergences on Logically Rectangular Smooth Grids. In F. Benkaldour and R. Vilmeier, editors, *Finite Volumes for Complex Applications: Problems and Perspectives*, pages 261–272. Éditions Hermès, 1996.
  - [156] N. Robidoux. *Numerical solution of the steady diffusion equation with discontinuous coefficients*. PhD thesis, University of New Mexico, Albuquerque, NM, USA, 2002.
  - [157] N. Robidoux. Polynomial Histogram, Superconvergent Degrees Of Freedom, And Pseudospectral Discrete Hodge Operators. *Unpublished: <http://www.cs.laurentian.ca/nrobidoux/prints/super/histogram.pdf>*, 2008.
  - [158] N. Robidoux and S. Steinberg. A discrete vector calculus in tensor grids. *Computational Methods in Applied Mathematics*, 1:1–44, 2011.
  - [159] M. Sahin and R. Owens. A novel fully implicit finite volume method applied to the lid-driven cavity problem - Part I: High Reynolds number flow calculations. *Int. J. Numer. Meth. Fluids*, 42:57–77, 2003.
  - [160] B. Sanderse. Energy-conserving Runge-Kutta methods for the incompressible Navier-Stokes equations. *Journal of Computational Physics*, 2012.
  - [161] L. Schumaker. *Spline Functions: Basic Theory*. Cambridge University Press, 3rd edition, 2007.

- 
- [162] B. Schutz. *Geometrical methods of mathematical physics*. Cambridge University Press, 1980.
  - [163] C. Scott.  $L^p$  Theory of differential forms on manifolds. *Transactions of the American Mathematical Society*, 347:2075–2096, 1995.
  - [164] M. Shashkov. *Conservative finite-difference methods on general grids*. CRC Press, Boca Raton, FL, USA, 1996.
  - [165] I. Singer and J. Thorpe. *Lecture notes on elementary topology and geometry*. Springer, 1976.
  - [166] S. Smale. Mathematical problems for the next century. *Mathematics: frontiers and perspectives*, page 271–294, 2000.
  - [167] M. Spivak. *Calculus on manifolds*. Perseus Books, 1998.
  - [168] S. Steinberg. A discrete calculus with applications of higher-order discretizations to boundary-value problems. *Computational Methods in Applied Mathematics*, 42:228–261, 2004.
  - [169] S. Steinberg and J. Zingano. Error estimates on arbitrary grids for 2nd-order mimetic discretization of Sturm-Liouville problems. *Computational Methods in Applied Mathematics*, 9:192–202, 2009.
  - [170] G. Strang. The fundamental theorem of linear algebra. *The American Mathematical Monthly*, 100(9):848–855, 1993.
  - [171] G. Strang. *Computational Science and Engineering*. Wellesley-Cambridge Press, 2007.
  - [172] V. Subramanian and J. Perot. Higher-order mimetic methods for unstructured meshes. *Journal of Computational Physics*, 219:68–85, 2006.
  - [173] T. Tarhasaari, L. Kettunen, and A. Bossavit. Some realizations of a discrete Hodge operator: A reinterpretation of finite element techniques. *IEEE Transactions on Magnetics*, 35(3):1494–1497, 1999.
  - [174] E. Tonti. On the formal structure of physical theories. *Monograph of the Italian National Research Council*, 1975.
  - [175] E. Tonti. *The Common Structure of Physical Theories*. Springer, to appear.
  - [176] L. Tu. *An Introduction to Manifolds*. Springer, 2008.
  - [177] M. ur Rehman, T. Geenen, C. Vuik, G. Segal, and S. MacLachlan. On iterative methods for the incompressible Stokes problem. *Int. J. Numer. Meth. Fluids*, 65:1180–1200, 2011.
  - [178] K. van der Zee. *Goal-adaptive discretization of fluid-structure interaction*. PhD thesis, Delft University of Technology, 2009.

- 
- [179] R. Verstappen and A. Veldman. Spectro-consistent discretization of navier-stokes: a challenge to rans and les. *Journal of Engineering Mechanics*, 34:163–179, 1998.
  - [180] R. Verstappen and A. Veldman. Symmetry-preserving discretization of turbulent flow. *Journal of Computational Physics*, 187:343–368, 2003.
  - [181] P. Wesseling. *Principles of Computational Fluid Dynamics*. Springer, 2001.
  - [182] P. Wesseling, A. Segal, and C. Kassels. Computing flows on general three-dimensional nonsmooth staggered grids. *Journal of Computational Physics*, 149:333–362, 1999.
  - [183] M. Wheeler, G. Xue, and I. Yotov. A multiscale mortar multipoint flux mixed finite element method. *ESIAM: M2AN*, 46:759–796, 2012.
  - [184] M. Wheeler, G. Xue, and I. Yotov. Local velocity postprocessing for multipoint flux methods on general hexahedra. *International Journal of Numerical Analysis and Modeling*, 9:607–627, 2012.
  - [185] H. Whitney. *Geometric Integration Theory*. Dover Publications, 1957.
  - [186] S. Zaglmayr. *High order finite element methods for electromagnetic field computation*. PhD thesis, Johannes Kepler University of Linz, 2006.
  - [187] E. Zeidler. *Nonlinear Functional Analysis and its Applications, Parts I-IV*. Springer, 1986-1990.
  - [188] X. Zhang, D. Schmidt, and B. Perot. Accuracy and conservation properties of a three-dimensional unstructured staggered mesh scheme for fluid dynamics. *Journal of Computational Physics*, 176:1–28, 2002.



# List of publications

## Journal papers

- J.J. Kreeft, M.I. Gerritsma, Mixed mimetic spectral element method for Stokes flow: a pointwise divergence-free solution, To appear in Journal of Computational Physics, 2012.
- J.J. Kreeft, M.I. Gerritsma, A priori error estimates for compatible spectral discretization of the Stokes problem for all admissible boundary conditions, Submitted, arXiv:1206.2812, 2012.
- A. Palha, P. Rebelo, R. Hiemstra, J.J. Kreeft, M.I. Gerritsma, Physics-compatible discretization techniques on single and dual grids, with application to the Poisson equation of volume forms, submitted, 2012.
- J.J. Kreeft, A. Palha, M.I. Gerritsma, Mimetic framework on curvilinear quadrilaterals of arbitrary order, Submitted, arXiv:1111.4304, 2011.
- J.J. Kreeft, B. Koren, A new formulation of Kapila's five equation model for compressible two-fluid flow, and its numerical treatment, Journal of Computational Physics, 229 (2010), 6220-6242.
- M.I. Gerritsma, J.J. Kreeft, Mimetic least-squares spectral element method for the Stokes problem, journal paper in preparation, 2013.
- J.J. Kreeft, A. van Zuijlen, M. Weghs, H. Bijl, Adaptive Multilevel Acceleration for Strongly Coupled Fluid Structure Interaction Computations, journal paper in preparation, 2013.

## Conference proceedings and contributed talks

- M.I. Gerritsma, J.J. Kreeft, A. Palha, P. Rebelo, R. Hiemstra, The geometric basis of mimetic spectral approximations, In proceedings of ECCOMAS 2012, Vienna (Austria).
- J.J. Kreeft, B. Koren, A new model and numerical method for compressible two-fluid flow, in proceedings of ECCOMAS 2012, Vienna (Austria).

- 
- J.J. Kreeft, M.I. Gerritsma, Higher-Order compatible finite elements for curvilinear quadrilaterals and hexahedrals, In proceedings of ICOSAHOM 2012, Tunis (Tunisia).
  - M.I. Gerritsma, J.J. Kreeft, A. Palha, Mimetic spectral element method, In proceedings of ICOSAHOM 2012, Tunis (Tunisia).
  - B. Koren, J.J. Kreeft, A new model and numerical method for compressible two-fluid Euler flow, HYP 2012, contributed talk, Padova (Italy).
  - J.J. Kreeft, M.I. Gerritsma, Higher-order Grad-, Curl- and Div-conforming discretization on curvilinear quadrilaterals, ACE2012 - 7th Workshop on Advanced Computational Electromagnetics, Karlsruhe, 2012.
  - J.J. Kreeft, M.I. Gerritsma, Mixed Mimetic Spectral Element Method the Stokes Equation, contributed talk at Finite Elements in Flow problems, FEF2011, Munchen.
  - J.J. Kreeft, A. Palha, M.I. Gerritsma, Higher-Order Grad-, Curl-, Div-conforming Discretization in Computational Electromagnetism, invited talk at Discontinuous Galerkin Methods in Computational Electromagnetics: A Workshop on recent developments in theory and applications, 2011, NLR, Amsterdam.
  - M. Bouwman, A. Palha, J.J. Kreeft, M. Gerritsma, A conservative spectral element method for curvilinear domains, in Lecture Notes in Computational Science and Engineering 2011, 76, 111-119.
  - J.J. Kreeft, M. Weghs, A.H. van Zuijlen, H. Bijl, Multi-level and Quasi-Newton Acceleration for Strongly Coupled Partitioned Fluid Structure Interaction, in proceedings of Coupled Problems 2011, Kos (Greece).
  - J.J. Kreeft, A. Palha, M.I. Gerritsma, Mimetic spectral element method for generalized convection-diffusion problems, in proceedings of ECCOMAS CFD 2010, Lisbon (Portugal).
  - A. Palha, J.J. Kreeft, M.I. Gerritsma, Numerical solution of convection-diffusion equations with the discretization of the Lie derivative, in proceedings of ECCOMAS CFD 2010, Lisbon (Portugal).
  - A. Palha, J.J. Kreeft, M.I. Gerritsma, Higher-order cochain interpolation, contributed talk, Non-Standard Numerical Methods for PDE's, Pavia (Italy), 2010.
  - J.J. Kreeft, A. Palha, M.I. Gerritsma, Higher-order discretization of the Laplace operator, Non-Standard Numerical Methods for PDE's, contributed talk, Pavia (Italy), 2010.
  - M.I. Gerritsma, J.J. Kreeft, A. Palha, Spectral Mimetic Methods on Quadrilaterals, contributed talk, Workshop for Compatible and Innovative Discretizations for PDE's, 2009, Oslo.

# Stellingen / Propositions

- Only if you're inspired you can excel

# Index

TEST, 3